Electroluminescent mis structures incorporating langmuir-blodgett films

J. Batey

ELECTROLUMINESCENT MIS STRUCTURES INCORPORATING LANGMUIR-BLODGETT FILMS

by

J. BATEY, B.Sc.

A Thesis submitted for the
Degree of Doctor of Philosophy
in the University of Durham
October 1983

DECLARATION

I hereby declare that the work reported in this thesis has not previously been submitted for any degree and is not being currently submitted in candidature for any other degree.

Signed _____

The work reported in this thesis was carried out by the candidate.

Signed _____

_____

Directors of Studies

_____

Candidate

ABSTRACT

The Langmuir-Blodgett (LB) technique provides an excellent method of depositing thin, uniform, insulating films of accurately defined thickness. They can therefore be used effectively in the investigation of metal/thin insulator/semiconductor electroluminescent structures where the insulator requirements are good dielectric properties allied to uniformity and an accurately defined thickness.

The insertion of a fatty acid LB film into the gold/n-type GaP system produces an increase in the effective barrier height of the device and also enables electroluminescence to be observed. The electroluminescent efficiency is shown to depend on the thickness of the organic film whereas the increase in the effective barrier height is relatively independent of this parameter. The optimum efficiency is obtained for a film thickness of approximately 27 nm, well above that predicted on the basis of direct quantum mechanical tunnelling. The increase in the effective barrier height is shown not to be due to an increased band bending in the semiconductor and a simple energy band model, which accounts for most of the experimental observations, is proposed. Measurements made on the diodes under illumination both support the proposed model and provide information about the mechanism of minority carrier injection. Diodes fabricated using phthalocyanine as the LB film exhibit very different characteristics, in particular the optimum thickness for EL efficiency is approximately 5.6 nm and the diodes appear to conform to the conventional tunnel injection theory. The prospects for commercial exploitation are quite promising in the case of the phthalocyanine-based diodes, particularly if the system can be extended to incorporate an efficient II-VI phosphor as the luminescent material. The results of preliminary experiments using ZnSe as the semiconductor are encouraging in this respect. Preliminary results for two other potential applications of LB films in metal/insulator/semiconductor devices are also described. The first of these concerns an attempt to invert the surface of p-type GaAs, with a view to producing an n-channel inversion mode field effect transistor, and the second describes the high field injection of charge into silicon dioxide, which has potential applications in the field of semiconductor memory devices.

ACKNOWLEDGEMENTS

Many people have helped to make this thesis possible and I would like to take this opportunity to thank them. I thank my friends and colleagues in the Department of Applied Physics and Electronics at the University of Durham for helping to make my time there both stimulating and enjoyable. In particular, I would like to express my gratitude to my supervisors, Professor G. G. Roberts and Dr. M. C. Petty, for their guidance, assistance and encouragement during the course of this research. I am indebted to Mr. S. Baker and all of the other members of the research group for contributing their help and expertise. The skills and expert knowledge of the workshop staff, headed by Mr. F. Spence, have been invaluable and greatly appreciated. I am grateful to Mrs. J. Smart for drawing the diagrams used in this thesis and I am indebted to Mrs. P. Morrell for her proficiency and patience in typing it.

The financial support provided by the SERC and RSRE, Malvern is gratefully acknowledged, and the provision of semiconductor substrates, by RSRE, Plessey and IBM is also greatly appreciated. I would also like to thank Dr. D. R. Wight (RSRE), Dr. G.Lidgard (Plessey) and Professor C. Hilsum (GEC) for valuable discussions and assistance during the course of this work.

Finally, I would like to thank my wife, Gillian, and also our parents, for their constant support and encouragement over the past years.

CONTENTS

CHAPTER 1

INTRODUCTION

Many electroluminescent (EL) devices depend on the introduction of minority carriers into the luminescent region of a semiconductor for their operation. In the majority of cases this is achieved using a forward biased p-n homojunction, in which the minority carrier injection ratio (γ) is inherently very high. However, many materials which have otherwise excellent properties from an EL viewpoint are poor amphoteric semiconductors, i.e. they are difficult to prepare in both n and p-type form. This is particularly true of the II-VI materials such as ZnS and ZnSe which are very efficient phosphors with wide, direct bandgaps, but can only be made n-type in low resistivity form. A great deal of effort has been expended in devising an alternative structure for such materials. One possibility is to use a metal-semiconductor (Schottky barrier) structure. However, in such a device γ is known to be small, typically of the order of 10^{-4}, which imposes severe constraints on the maximum EL efficiency possible using such a device. Fortunately, this value can be improved in a number of ways. For example, since γ is a sharp exponential function of the difference between the majority and minority carrier barrier heights, a significant improvement can be achieved by modifying the device in such a way as to increase the majority carrier barrier height. However, the largest increase can be achieved by the incorporation of a thin insulator between the semiconductor and the metal electrode. This increase is critically dependent on the insulator thickness and to achieve the optimum value of minority carrier injection ratio, fine control over both the thickness and uniformity of the insulating film is essential.

The Langmuir-Blodgett (LB) technique has received a good deal of attention in recent years as its potential for use in a variety of applications has been increasingly recognized. One of its attributes is that it provides an excellent method for depositing thin, uniform, insulating films of accurately defined

thickness, and in this respect is ideal for use in the investigation of MIS electroluminescent devices. In addition, there have been a number of recent reports concerning majority carrier barrier height modification using LB films, where the incorporation of the film is thought to increase the height of the Schottky barrier. The aim of this study was to attempt to capitalize on these interesting properties by investigating a 'model' LB film MIS EL system, based on well-characterised materials which, if successful, could be extended to incorporate other LB films and semiconductor materials. The system chosen for the initial investigation was gold/cadmium stearate/n-type gallium phosphide. GaP was chosen because it is a well-characterised semiconductor whose luminescent properties are well-understood. Furthermore, p-n junction devices fabricated from material with similar properties are readily available for comparison purposes. N-type material was chosen since the aim was to develop a system which could be extended to incorporate the (n-type only) II-VI materials ZnS and ZnSe. Cadmium stearate was chosen as the insulator because it is a particularly well-characterised LB film material and gold was used as the barrier electrode since it has a high work function, and hence is expected to form a relatively large Schottky barrier on n-type material. Gold also has the advantage of being easy to deposit as a continuous, semi-transparent evaporated electrode which is important from a light-extraction viewpoint. Since the work is concerned specifically with n-type semiconductors, the discussion in subsequent chapters makes the implicit assumption of an n-type material, although the arguments are equally valid for p-type material provided the necessary polarity changes are made.

The thesis begins with a general discussion concerning the physics of electroluminescent devices which is followed by a detailed account of the theory of Schottky barrier and thin-MIS diodes. These chapters establish the basic theory upon which much of the remainder of the thesis is based.

Chapter 4, which briefly reviews the technology of LB films, includes a description of the equipment used to deposit these films. In chapter 5 a description of the measuring equipment used, and the procedures adopted, in this work is given, together with an account of the device fabrication. Also included are the results of some basic, but nevertheless very important preliminary experiments concerned with device fabrication. The data for GaP Schottky barrier structures, explained in chapter 6, help to establish a standard by which the LB film MIS diodes may be judged. In addition, the extent and influence of the interfacial layer, which must inevitably be present between the LB film and the semiconductor surface, is assessed. Chapter 7 details the electrical and optical characteristics of the MIS devices and includes a detailed investigation into the effect of LB films on the Schottky barrier height. The significant effect of incorporating other LB films, in particular the very stable phthalocyanine material, is also considered; this chapter concludes with an assessment of the future prospects for MIS EL devices based on LB technology. The penultimate chapter describes the results of preliminary experiments aimed at extending the system to incorporate ZnSe as the luminescence material and also preliminary results for two other potential applications of LB films in MIS devices. The first of these concerns the use of LB films in MIS capacitors fabricated on p-type GaAs, in an attempt to invert the surface of this material with a view to producing an n-channel inversion mode FET. The second concerns the use of LB films in double insulator structures with a view to achieving high field charge injection into silicon dioxide at low voltages, which has potential applications in the field of memory devices.

The thesis concludes with a summary of the objectives achieved and some suggestions concerning the direction of future research in this field, with particular emphasis on the potential for commercial exploitation.

CHAPTER 2

THE PHYSICS OF ELECTROLUMINESCENT DEVICES

2.1 INTRODUCTION

The conversion of energy into photons can be achieved using a number of different techniques, one of which is electroluminescence (EL). This is defined as the direct conversion of electrical energy into light. It is important to be able to distinguish between EL and other, possibly concurrent processes such as thermoluminescence. This is often achieved by studying the spectral characteristics of the emitted light which, in the case of EL, contain relatively narrow ranges of wavelength.

The requirements for an EL device are essentially twofold. Firstly, the physical system involved must, when in an excited state, be able to relax through one or more different processes, of which at least one must be radiative. Secondly a means of exciting this system with electrical energy is required. In the vast majority of cases this involves the use of specially doped semiconducting material, with suitable electrodes to facilitate excitation, and the subsequent recombination of electron-hole pairs.

This chapter discusses both the excitation and recombination processes in some detail before describing a number of the structures used in EL devices. It concludes with more detailed comments relating to the specific materials used in this work.

2.2 EXCITATION PROCESSES

There are many different methods by which the population of free carriers in a semiconductor can be increased above the thermal equilibrium value. This section deals with those mechanisms pertaining to electroluminescence, i.e. electrical excitation processes.

2.2.1 Avalanche Multiplication

Rectifying structures, such as p-n junctions or Schottky diodes, are often employed to obtain avalanche EL. Inherent in these devices is a relatively thin, depletion region, across which most of the applied voltage is dropped. Under the influence of a reverse bias, the only current which can flow through these diodes is the relatively small, reverse saturation current. At low values of electric field (i.e. $\lesssim$ 10V/cm), the average electron energy is approximately equal to the equilibrium value of kT. As the field is increased, the average electron energy increases and the electrons are then said to be 'hot'. They are characterised by the temperature which would be required to excite these electrons by purely thermal means. If the field is high enough ($\gtrsim 10^5$V/cm), the electrons become sufficiently energetic to promote other electrons, bound to either lattice or impurity atoms, into the conduction band by impact ionization. An extra electron and hole are produced, each of which can in turn create another such pair. Thus an avalanche of carriers is produced by continuous ionization from the impact of hot carriers. This results in a large population of free carriers of both types in the depletion region and, provided the avalanche can be controlled so that catastrophic breakdown does not occur, then recombination will result. Methods by which the avalanche can be controlled are discussed in §2.4.4.

2.2.2 Internal Field Emission

Internal field emission is the term used to describe the creation of free carriers in a semiconductor by enhanced quantum mechanical tunnelling due to high electric fields. For example, fig. 2.1 shows a Schottky barrier structure to which a large reverse bias has been applied. When the band edges become so steep that the physical separation between bound electrons and the vacant states in the conduction band approaches tunnelling

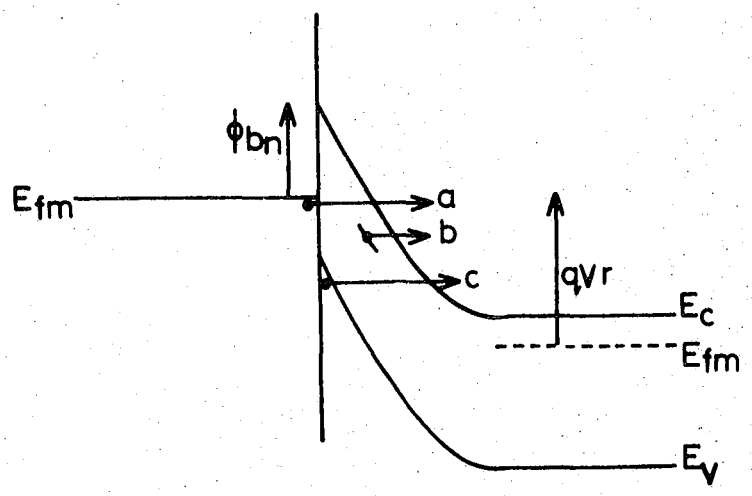

Figure 2.1 Internal field emission in a reverse-biased Schottky diode

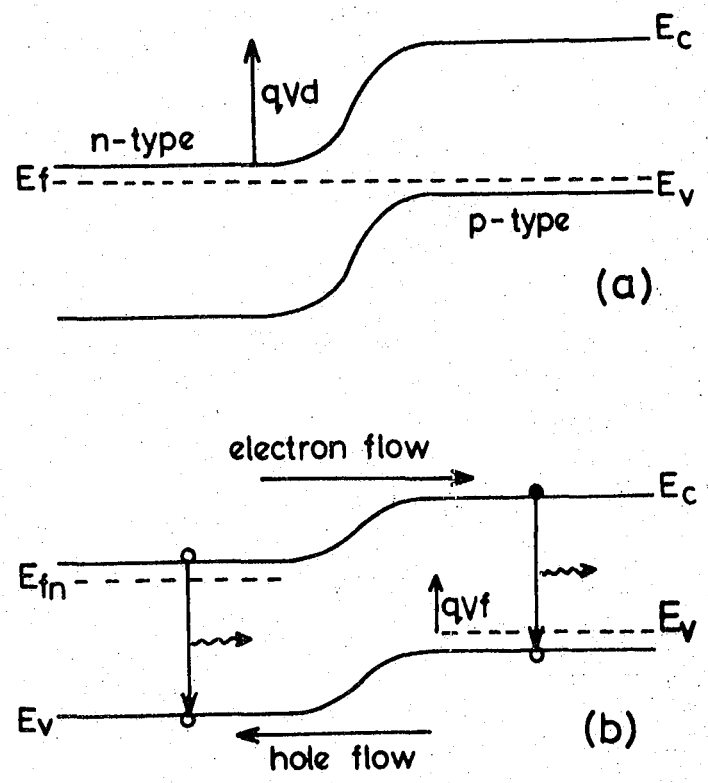

Figure 2.2 Energy band diagram of a p-n junction (a) in equilibrium and (b) under a small forward bias.

dimensions ($\lesssim$ 10nm), then the electrons are able to tunnel into the conduction band by one of the mechanisms illustrated. In process (a) the electrons are injected into the conduction band directly from the metal, process (b) involves the tunnelling of electrons bound to impurity atoms and (c), the so called "Zener effect" is the tunnelling of bound valence electrons into the conduction band. The result of one or more of these processes occurring is, as in the case of avalanche multiplication, a large population of free carriers in the high field region. These are able to diffuse into the semiconductor bulk and recombine, possibly radiatively.

The electric field required for the onset of either of these high field effects is a function of the particular system employed; it depends on the type of semiconductor, the impurity concentrations and the contact metal used. The onset of one process usually precludes the other and the system is often tailored to promote one mechanism in preference to the other.

2.2.3 Minority Carrier Injection

The two mechanisms described up to this point require high electric fields and consequently, relatively large operating voltages. However, in many instances an EL device whose operating voltage is low ($\lesssim$ 5 volts) is desirable. This can most easily be achieved by the process known as minority carrier injection. This concept is best understood by considering fig. 2.2. which shows the energy band diagrams of a p-n junction (a) in equilibrium and (b) under the application of a small forward bias. At equilibrium the inbuilt potential barrier, qVd, whose magnitude is just sufficient to align the Fermi levels in each material, prevents the flow of electric current. The small current due to minority carriers, created on either side of the junction, being swept away by the inbuilt electric field, is just balanced by the rate at which majority carriers surmount the

barrier by thermal means. If this delicate equilibrium is altered by the application of a forward bias, then the potential barrier is lowered and a current flows. The total current comprises a number of components, one of which is the diffusion current; electrons diffuse from the n-side to the p-side and vice-versa for holes. The carriers are said to be injected into the semiconductor bulk and since, once introduced into the opposite side of the junction, they are minority carriers, the process is termed 'minority carrier injection'. The result is a population of minority electrons and holes on either side of the junction which leads to the possibility of radiative recombination. This highly idealised treatment is useful in that it helps demonstrate the concept of carrier injection. The picture is, however, greatly complicated in practice by several factors, not least of which is the existence of alternative current mechanisms such as recombination via impurity levels in the depletion region.

The p-n junction is the structure most often utilized to achieve minority carrier injection and, indeed, it forms the basis of most commercial LEDs. However, there has been considerable recent interest in the use of Schottky barriers, or more correctly MIS diodes, as injection EL structures and these are the subject of this study. A thorough treatment of minority carrier injection in these devices is given in chapter 3.

2.2.4 Exciton Formation

It is possible for a free electron and a free hole to experience a Coulombic attraction since they are essentially a pair of opposite charges. In this situation the electron can be considered to be bound to the hole in a hydrogenic orbit. This entity is known as an exciton and since the energy associated with it is less than that of a free electron, excitonic states are located within the energy gap. In fact the exciton binding energies are small and consequently, the states are located very close to the conduction

band edge (usually within 0.1 eV). The salient feature of an exciton is its ability to move through the crystal lattice, as the energy involved is transferred from atom to atom, without an associated flow of current. Since the electron and hole are spatially associated, localization of one of the charges (at an impurity centre, for example) binds the exciton. Bound excitons play an important role in the efficient production of EL in many devices, particularly those fabricated from indirect bandgap semiconductors such as GaP (see § 2.6). Furthermore, excitonic transitions involve energies close to the bandgap energy which is important in the production of light with a high photon energy.

Electrons can enter exciton states in much the same manner as they enter other states, for example by tunnelling, thermal means or photo-excitation, and, once formed, have a certain lifetime before either recombination or dissociation occurs. From an EL viewpoint the rate of recombination via a radiative process must be favourable compared to the rate at which dissociation or non-radiative recombination occurs.

2.3 RECOMBINATION PROCESSES

This section describes qualitatively the various processes by which an excited carrier may lose its excess energy. It is intended as a description of the general mechanisms involved in most semiconductors and not as an exhaustive account of the subject. For a more quantitative treatment, the reader is referred to reference (1).

2.3.1 Radiative Recombination

Figure 2.3 shows the basic methods by which recombination can occur resulting in the production of light. These are now discussed in sequence:

(a) Interband Recombination

If a conduction electron encounters a valence band hole, then electron-hole annihilation occurs resulting in the production of a photon of light

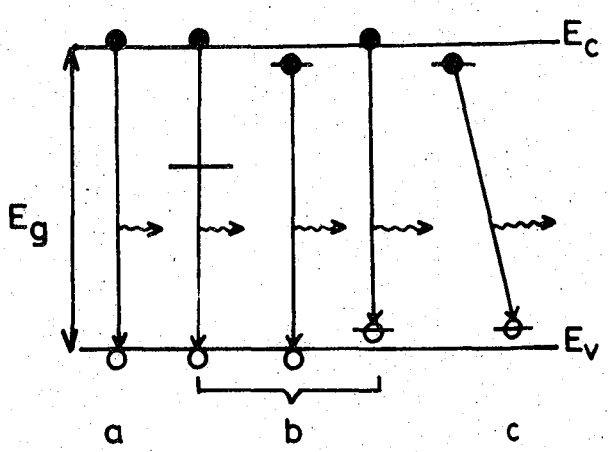

Figure 2.3 Radiative recombination processes (refer to text for description).

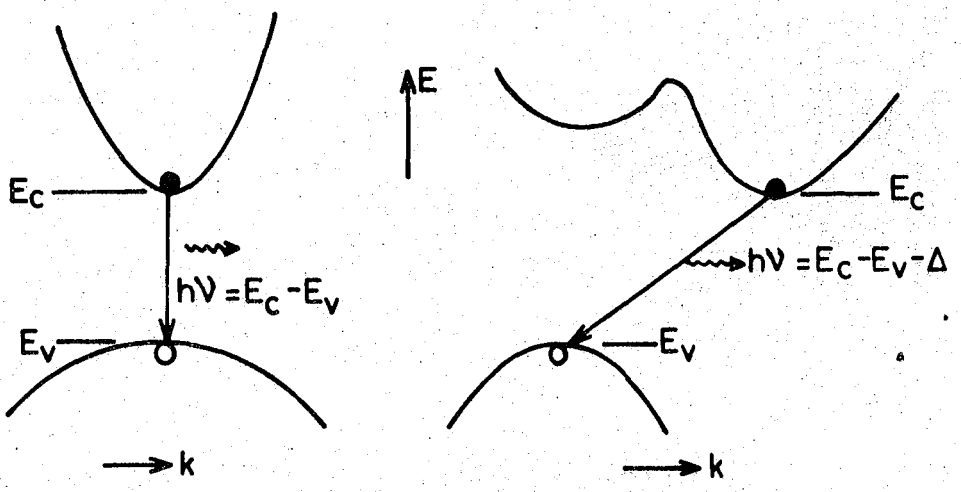

Figure 2.4 Simplified E-k diagrams, depicting recombination (a) in a direct bandgap material and (b) in an indirect bandgap material.

with energy, $h\nu \sim Eg$. Except at very high excitation levels and low temperatures[2], the radiative decay times are much longer than the scattering times of hot carriers by lattice vibrations. Consequently, recombination occurs between electrons and holes which are each in equilibrium with their respective populations. Thus most of the radiation produced by this process has an energy equal to Eg, although the thermal distribution of the carriers results in a broadening of the spectrum. In such a transition the nature of the bandgap (i.e. whether the positions, in k-space, of the valence band maximum and conduction band minimum result in a direct or indirect energy gap) is crucial. Fig. 2.4 shows a simple E-k diagram for (a) a direct energy gap and (b) an indirect gap. In the case of the direct gap, the probability of the transition from Ec to Ev is only significantly greater than zero if momentum and energy are conserved[3]. Since the momentum of a photon is negligible compared to that of an electron, such a transition must occur between states of equal momentum, i.e. vertically in fig. 2.4(a). In the case of the indirect gap, the transition is only allowed if the difference in momentum is accounted-for by interactions with the lattice vibrations, i.e. by the emission of a phonon with a specific energy. The resulting radiation has a photon energy which is less than Eg by an amount equal to the phonon energy, Δ.

(b) Recombination via Impurity Centres

Impurities, which give rise to allowed energy levels in the bandgap, are often used to activate EL. Usually the process involves the capture of at least one free carrier although there are exceptions (e.g. the well known manganese centre in ZnS is excited through impact ionisation). The impurity level involved may be shallow (i.e. situated close to one of the band edges), or located deeper in the energy gap. Usually the centre involved is relatively deep since carriers captured by shallower centres

are immobilised for only a short period of time which depends on the thermal activation rate, If this rate is larger than the radiative recombination rate, then the centre acts as a trap rather thar a recombination centre. Clearly, deeper centres are more likely to activate radiative recombination. Another important parameter is the density of these centres compared to the density of non-radiative centres. Both these factors play an important role in determining radiative efficiency and are discussed in more detail, specifically for nitrogen doped GaP, by Dapkus et al[4]. However, the actual mechanism is essentially the same irrespective of the concentration or the position of the impurity centre: An electron, in the vicinity of an ionized impurity, falls into the empty state - the energy involved usually being dissipated as heat. Providing the radiative recombination rate is greater than both the thermal activation rate and the non-radiative recombination rate, the electron will recombine with a hole in the valence band and the excess energy will be emitted as a photon of light. Clearly the use of deep centres to activate visible EL is restricted to semiconductors with relatively large bandgaps, such as ZnSe and GaP, since such a process necessarily results in a significant reduction in photon energy compared to interband mechanisms.

(c) Donor-Acceptor Pair Recombination

In semicondcutors where the doping densities are large, the Coulombic attraction between the donor and acceptor impurities tends to cause them to associate into pairs. Such a pair is capable of capturing an electron and a hole which may subsequently recombine radiatively. Since the capture of carriers is subject to the trapping kinetics discussed above, this type of EL is usually only important at temperatures low enough to quench thermal ionization ($\lesssim$ 150K in GaP). Low temperature study reveals a discrete line spectrum attributed to this kind of EL, each line being characteristic of a pair with a specific separation. Clearly, the greater the separation the

smaller the wavefunction overlap and hence the longer the decay time. In fact this time can be used effectively to study the spatial separation of these pairs. This separation is depicted in fig. 2.3 by using a diagonal line to represent the transition.

One mechanism, not illustrated in this figure, is the recombination of excitons. As mentioned previously, an electron in an exciton state is not free but is bound, albeit loosely, to an atom. One method by which the exciton may give up its excess energy is to recombine radiatively resulting in the production of a photon. If the exciton is bound to an impurity centre, then the momentum conservation constraints may be relaxed since the impurity can play a role in the conservation of momentum. This can be important in indirect gap semiconductors where the probability of radiative recombination is low. The specific case of excitons bound to nitrogen impurities in GaP is considered in detail in § 2.6.

2.3.2 Non-Radiative Processes

Mechanisms involving the recombination of charge carriers which do not produce light are also very important as they are in direct competition with those that do. In general, however, they are less well-understood due mainly to the difficulty experiencedin studying them (by their very nature they do not produce characteristic spectra). This section deals with the basic mechanisms by which non-radiative transitions occur, although there are differences in detail between various systems.

(a) Auger Recombination An electron in the conduction band, when falling into a lower energy state, can give up its energy by promoting a second free electron into a higher level in the continuum of states comprising the conduction band. This is Auger recombination, and it is non-radiative since the excited electron dissipates its energy as heat as it returns to the bottom of the conduction band. The process can also involve two holes and an electron and is particularly important when one carrier density is high and dominant.

(b) Multiphonon Emission. An electron may also lose energy by the simultaneous production of a number of phonons. However, interband transitions of this sort are unlikely in large bandgap materials since the number of phonons required is so large (e.g. in GaP, Eg = 2.25eV whereas the phonon energy is of the order of 0.05eV). Impurity or defect levels in the energy gap, particularly deep ones, can significantly increase the rate of these multiphonon transitions by dividing the required transition into two or more stages. Exciton states can also assist in this manner as an electron can cascade down the allowed exciton levels by successive production of phonons - the final transition occurring by an Auger or indeed multiphonon process. A similar 'cascade' mechanism has been proposed by Lax[5] who argued that a conduction band electron could fall into an excited energy level of an atom, from which it can decay to the ground state (via the allowed energy states associated with the impurity) by successive phonon emission.

Recombination in the vicinity of the semiconductor surface often represents a major loss mechanism. The perturbation of the crystal lattice by the surface gives rise to defect levels additional to those found in the bulk of the material, although the processes by which the excited electron decays are essentially the same as those described previously.

2.4 ELECTROLUMINESCENT STRUCTURES

In § 2.2 the various mechanisms by which a semiconductor could be excited in order to produce EL were discussed. Of these, minority carrier injection is by far the most common method used in commercial devices and the majority of this section deals with the structures used to facilitate this mechanism. Since the p-n homojunction is such a important device, it is considered in some detail in § 2.4.1. The following sections describe the Schottky barrier or, more correctly, the MIS diode which has

recently received a good deal of attention because of its potential as an alternative to the p-n junction for use with materials that are not good amphoteric semiconductors (e.g. many wide bandgap II-VI compounds). Since these structures are used exclusively in this work, chapter 3 is devoted to a discussion of the physics of these devices and therefore the treatment given at this stage is rather qualitative. The final section deals with other structures which can be used to excite EL, the majority of which do not involve minority carrier injection.

2.4.1 The p-n Homojunction

Figure 2.5 shows a schematic diagram of a p-n junction (a) in equilibrium, (b) under the application of a reverse bias and (c) under forward bias. When the junction is initially formed, electrons flow from the n-side to the p-side (and vice-versa for holes) until the Fermi levels on either side of the junction are aligned. No further net transfer of charge occurs. The electrostatic potential required to achieve this equilibrium is called the diffusion potential, Vd, and is supported by the space charge on either side of the junction. This space charge arises from the uncompensated ionized impurities in the region which is depleted of majority carriers - the so called 'depletion layer', W. The magnitude of the diffusion potential can be shown to be given by

$$Vd = \frac{kT}{q} \ln\left\{\frac{n_n}{n_p}\right\} = \frac{kT}{q} \ln\left\{\frac{p_p}{p_n}\right\} \qquad (2.1)$$

where n_p represents the density of electrons in the p-type material and n_n, p_p, p_n are defined using the same convention. The depletion region represents a layer $\sim$ 1μm thick which has a much higher resistivity than the bulk. This means that any bias applied to the diode will be dropped predominantly across this region causing a realignment of the band

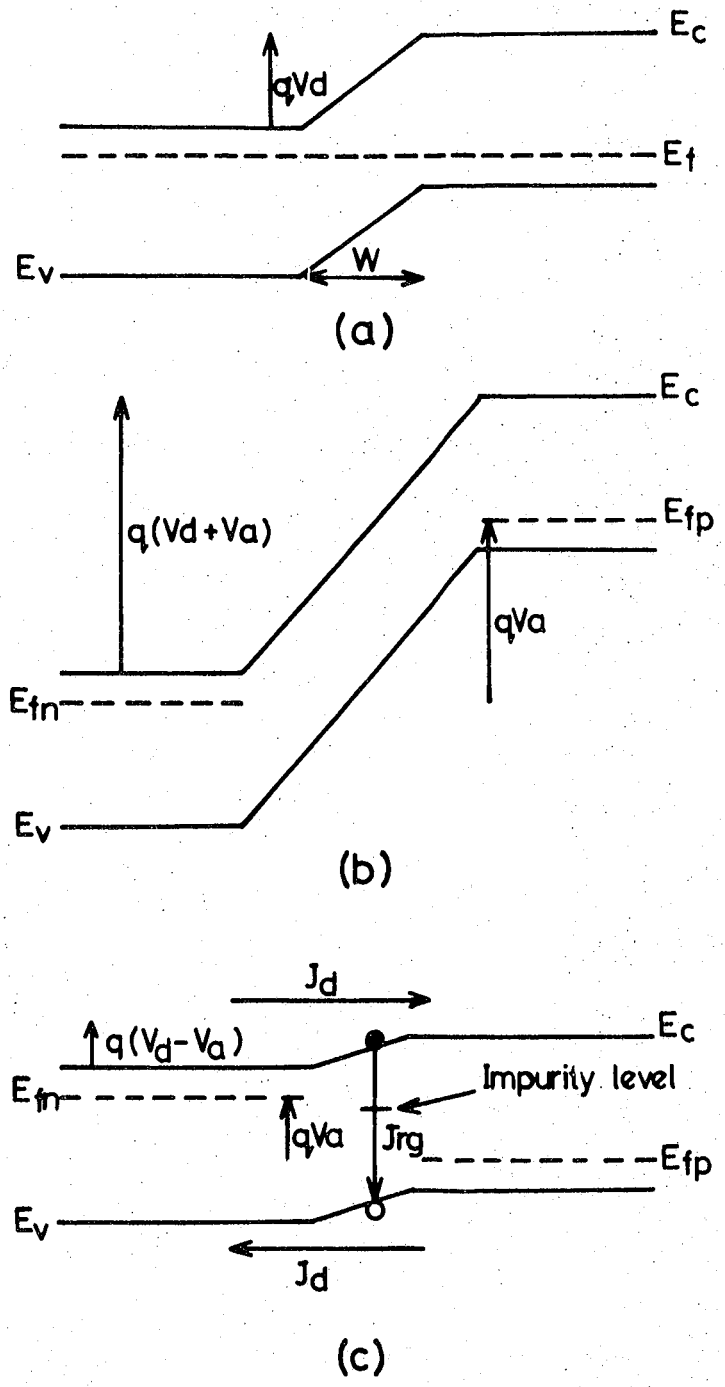

Figure 2.5 Schematic diagram of a p-n junction (a) in equilibrium, (b) under reverse bias and (c) under forward bias.

structure on either side of the junction, by an amount approximately equal to qVa, the applied voltage. The effect of both a reverse and a forward bias can be seen in figs. 2.5(b) and 2.5(c) respectively. It is possible to achieve relatively large electric fields in the depletion region for even modest values of reverse bias, and a reverse biased p-n junction has been used to obtain EL from a number of materials. In these cases the excitation mechanism is either avalanche multiplication or field emission. However, the forward biased p-n junction is by far the more important structure from a commercial viewpoint and the remainder of this section is devoted to a discussion of this particular structure. Under forward bias, the potential barrier to current flow is reduced by an amount approximately equal to the applied voltage. As a result a current, comprising a number of different processes, flows. Two such processes, J_d and J_{rg} are shown in fig. 2.5(c) and these represent the diffusion current and the net current due to recombination and generation in the depletion region respectively. These are now discussed in turn.

(a) The Diffusion Current. When the potential barrier is lowered, charge carriers diffuse into the material on the opposite side of the junction which represents an injection of minority carriers into both sides of the device. This is the most important current mechanism from an EL viewpoint as the injected minority carriers are able to recombine to produce light. On average, electrons on the p-side will have a lifetime, τ_n during which they will travel one diffusion length, L_n, before recombining. The parameter L_n is related to τ_n by the equation $L_n = (D_n \tau_n)^{\frac{1}{2}}$ where D_n is the electron diffusion coefficient (which is a function of the electron mobility). A similar relation, $L_p = (D_p \tau_p)^{\frac{1}{2}}$ is true for the holes injected into the n-side. The ideal current-voltage characteristic is given by the Schockley equation:

$$J = q(D_n n_{po}/L_n + D_p p_{no}/L_p) \quad (\exp. qV/kT - 1) \qquad (2.2)$$

where n_{po} and p_{no} are the equilibrium concentrations of electrons in the p-type, and holes in the n-type material respectively. Frequently in EL diodes, either the electron or the hole component of the diffusion current is made dominant. Usually, this is either because radiative recombination is more efficient on one side of the junction, or because of the problems involved in extracting light from both sides. In such a situation the minority carrier injection ratio, γ, (defined as the ratio of the minority carrier current to the total current) can be very large, indeed close to unity. As will be seen in § 2.5 (when EL efficiency is discussed) γ is a very important parameter.

(b) The Recombination Current. The recombination of minority carriers via impurity levels in the vicinity of the depletion region can often be an important current mechanism. This current is given by the approximate relationship

$$J_r \propto \exp (qV/nkT) \qquad (2.3)$$

where n is a constant, usually between 1 and 2. This process is particularly important from an EL viewpoint since it does not give rise to radiative recombination and is, therefore, in direct competition with the radiative mechanisms. Thus in practical diodes much care is exercised in order to minimise this 'loss' mechanism. This is usually achieved by careful control of the crystal growth conditions so that unwanted impurities, which are the main source of the recombination centres, are minimised.

The recombination current represents a deviation from the ideal current which is predicted by the Schockley equation (eq. (2.2)). There are a number of other such deviations, one of which is due to the effect of inter-band tunnelling. If the n and p-type materials are degenerately doped and the depletion region is very thin, a significant current can flow due to quantum mechanical tunnelling from the filled states in the conduction

band on the n-side to empty states in the valence band on the p-side. However, in most practical diodes this current is very small and not significant when compared to the other two mechanisms. Another deviation from eq. (2.2), which is particularly important in p-n junction laser devices, is the so called 'high injection condition'. In this case the electric field in the semiconductor bulk is appreciable and consequently, both drift and diffusion terms must be analysed. However, the current densities required to achieve this condition are very large, typically $\gtrsim 10^3 A/cm^2$. This is much higher than the current levels employed in a conventional LED and this mechanism is therefore not discussed further. One other deviation from ideality is mentioned, for completeness. This is the surface effect and it arises primarily because of ionic charges in the vicinity of the semiconductor surface which induce image charges in the semiconductor. These can give rise to surface depletion layer regions which lead to surface leakage currents. However, the effect is usually small and negligible compared to recombination in the depletion region.

2.4.2 The Schottky Barrier

In this section the Schottky diode is discussed qualitatively from the viewpoint of its use as an EL structure. Only the ideal case is considered, i.e. an intimate, abrupt metal-semiconductor interface which is free from the influence of interface states. Nevertheless it serves to illustrate some of the advantages of using such a structure and provides an introduction to chapter 3 in which the Schottky barrier and the tunnelling MIS diode are considered in detail.

Fig. 2.6 shows the band alignment in an idealized situation when a metal is brought into contact with an n-type semiconductor (a) before, and (b) after, contact has been made. For the particular case shown (i.e. the semiconductor electron affinity, χ_s, is less than the metal work function,

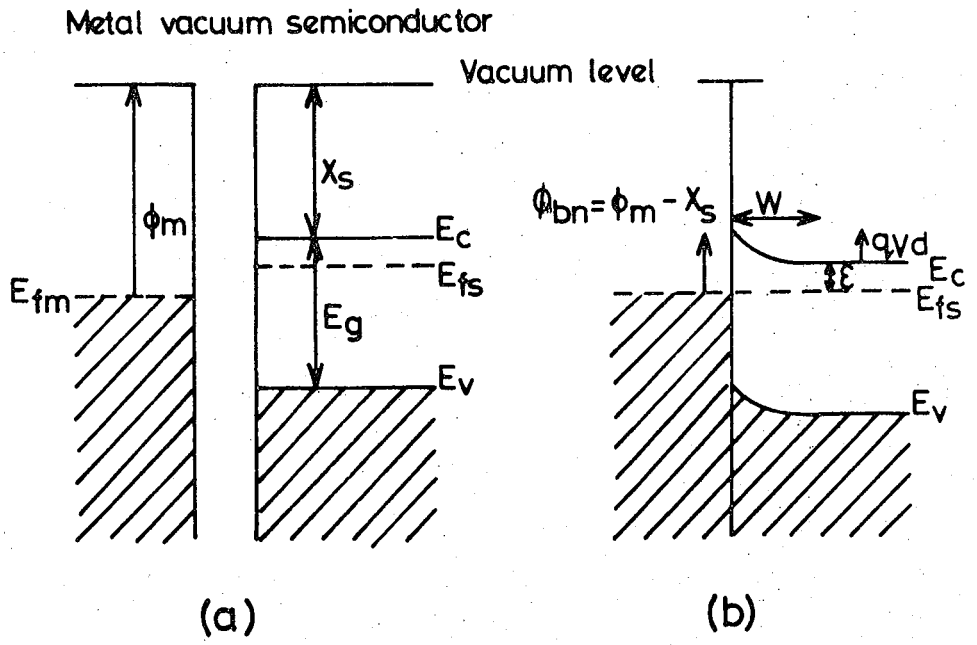

Figure 2.6 Simplified energy band diagrams depicting the formation of an ideal Schottky barrier (a) before, and (b) after, contact has been made.

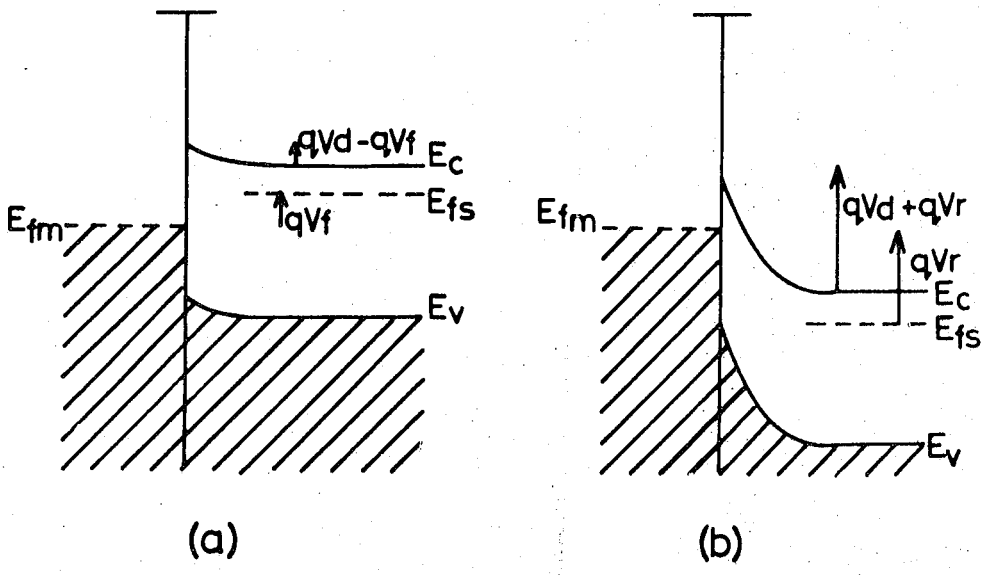

Figure 2.7 Energy band diagram of Schottky diode (a) under forward bias and (b) under reverse bias.

ϕ_m), charge flows from the semiconductor to the metal, once contact is made, until the Fermi levels in the two materials align and thermal equilibrium is established. This results in a build up of charge at the metal surface which is countered by an equal and opposite charge in the semiconductor. However, unlike the metal, the semiconductor is unable to accommodate this charge at its surface and consequently it is distributed along a length which is termed the depletion or space charge region. The barrier height of the junction ϕ_{bn}, is simply the difference between the metal work function and the semiconductor electron affinity, i.e. $\phi_{bn} = \phi_m - \chi_s$. This is the definitive barrier height although the barrier 'seen' by electrons in the conduction band is slightly less than this. It is given by the diffusion voltage, Vd, which represents the amount by which the semiconductor bands are bent. This is related to ϕ_{bn} by the relationship $Vd = \phi_{bn} - \varepsilon$, where ε is the difference between the Fermi level and the conduction band edge in the semiconductor bulk. Fig. 2.7 depicts the band structure (a) under forward bias (positive to the metal) and (b) under reverse bias. Under conditions of reverse bias, EL can be obtained as a result of either avalanche multiplication[6] or field emission as in a p-n junction. When a forward bias is applied, the degree of band bending in the semiconductor is reduced and a current flows. This current may comprise several components and these are discussed in detail in chapter 3. The important components from an EL viewpoint are the flow of majority electrons into the metal and the injection of minority holes into the semiconductor. More precisely, it is the minority carrier injection ratio, γ, which is important as this is directly related to the device efficiency (see §2.5). Unfortunately, in the vast majority of cases this device is essentially a unipolar (majority carrier) device (at least under low or moderate forward bias conditions). In fact in a typical Schottky barrier $\gamma \sim 10^{-4}$ which means that it is not practicable as an EL structure unless a substantial improvement in γ can be

achieved. Nevertheless these structures have received a good deal of attention recently as possible EL structures. One reason for this is the potential savings in processing time, and hence cost, that such a structure offers over the p-n junction. Another is the fact that the light in a Schottky barrier device is generated essentially at the surface of the device and consequently does not have to pass through the semiconductor in order to be extracted. (The only problem concerned with light extraction is involved with the obstruction due to the barrier electrode which must be made semi-transparent. Self-absorbtion in p-n junction diodes is a major source of inefficiency and requires a degree of 'device engineering' in order to reduce it to acceptable levels.) However, the greatest stimulus has been the advances made in crystal growth techniques, in particular, the growth of wide-bandgap II-VI semiconductors such as ZnS and ZnSe, which are extremely efficient phosphors and can, in principle, be suitably doped to emit light of virtually any wavelength in the visible spectrum. Indeed, a recent EL device, based on ZnS, has been reported which emits 'white' light[7]. Unfortunately, these materials are difficult, if not impossible to fabricate in low-resistivity p-type form, hence the interest in the Schottky barrier structure as an alternative to the p-n junction. Fortunately, the value of $\sim 10^{-4}$ quoted previously for γ can be improved upon in a number of ways. Most of these involve tailoring the system by varying the metal and/or the semiconductor properties and do not usually result in great improvements. However, for a given system a dramatic increase in γ can be achieved simply by incorporating a thin insulator, between the metal and the semiconductor, to form a metal-insulator-semiconductor (MIS) structure. This is considered in the following section

2.4.3. The MIS Diode

Figure 2.8 shows an exaggerated, idealised band diagram of an MIS diode (a) in equilibrium and (b) under the application of a forward bias. The insulator here is assumed to be ideal, i.e. there are no defect levels in the insulator bandgap and the conduction band edge is given by the vacuum level. It is also assumed, however, that the insulator is thin enough to allow direct quantum mechanical tunnelling to occur between the energy bands in the semiconductor and empty states in the metal. At equilibrium, a voltage, Δ_o, is developed across the insulator and, in the absence of interface states, the metal-semiconductor barrier height has been reduced from the Schottky barrier value to a value given by $\phi_{bn} = \phi_m - \chi_s - \Delta_o$. Under forward bias, a portion of the applied voltage is dropped across the insulator and the remainder across the semiconductor depletion region. The result is a reduced amount of band bending in the semiconductor (as in the Schottky barrier case) but also a relative shift between the metal Fermi level and the semiconductor band structure (fig. 2.8(b)). Electrons in the conduction band are able to tunnel into the metal but, more importantly, electrons in the valence band are also able to tunnel into empty states above the metal Fermi level. This represents an injection of holes (minority carriers) into the semiconductor, and an increase in the minority carrier injection ratio over the corresponding Schottky barrier level has been achieved. The real picture is, of course, much more complicated than this as several factors (not just the realignment of the band structure) have an important effect on the injection ratio. In particular, it will be shown that a real insulator can cause significant deviations from theory and the EL efficiency of the MIS diode can depend critically on the properties of the insulator and its associated interfaces.

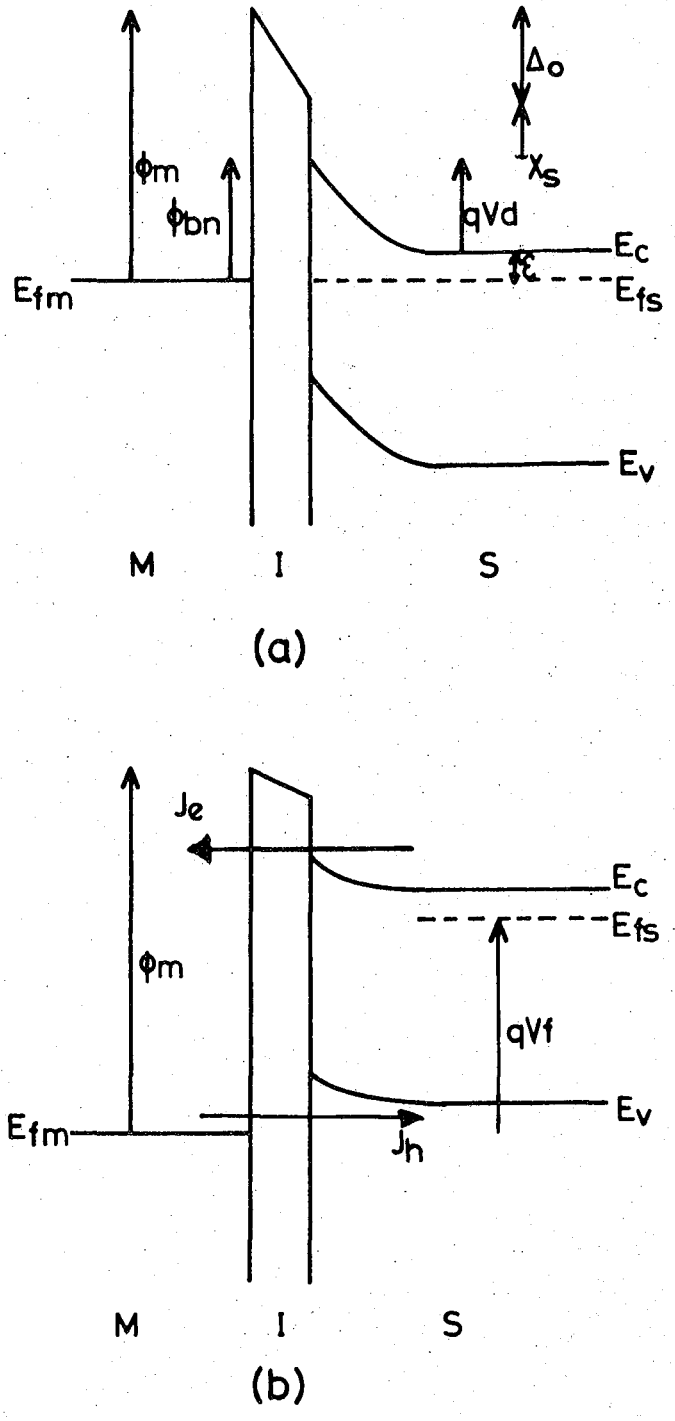

Figure 2.8 Exaggerated, idealised band diagram of a thin-MIS diode (a) in equilibrium and (b) under forward bias.

If the insulator in an MIS device is sufficiently thick to prevent any current flow between the metal and the semiconductor, then EL can often be observed under the application of an alternating voltage[8][9]. In this case the metal and semiconductor can be considered to be capacitively coupled and during the period when the voltage is negative (for an n-type material) a transient p-n junction is created at the surface. When the excitation voltage goes positive, the holes in the surface inversion region are 'injected' into the n-type bulk and radiative recombination can occur. However, the voltages required are relatively large and the external efficiencies are low, hence the structure is not particularly important from a commercial viewpoint.

2.4.4. Other Structures

This section deals with other structures, not previously mentioned, from which EL can be obtained. The majority is devoted to high field, large area structures which are designed specifically with flat panel displays in mind; however, another low field, injection structure is considered first - the heterojunction.

(a) The p-n Heterojunction. This is an alternative to the p-n homojunction, particularly suitable for use with non amphoteric semiconductors. In this respect it competes with the MIS diode as a possible structure for use with II-VI materials but suffers from several disadvantages, not least of which is the difficulty involved in fabrication. An excellent example of this type of structure is the ZnTe - ZnSe junction. ZnTe can only be made p-type in low resistivity form whereas ZnSe can only be made n-type and a p-n heterojunction can easily be fabricated. This system has been investigated as an EL structure[10, 11] and other structures studied include heterojunctions formed from Cu_2S - ZnS[12] and ZnTe - CdS[13]. Although these devices can, in principle, be formed from very different

materials, ideally the two should have similar structural properties, particularly their lattice constants. This minimises the stresses established at the interface and hence reduces the dislocation and interface state densities. Furthermore, in order to achieve a high minority carrier injection ratio, the source of minority carriers should be the material with the larger bandgap. Unfortunately in practical devices, at least those fabricated from II-VI materials, these conditions cannot be met, resulting in low, room-temperature quantum efficiencies with the light emitted predominately in the red.

(b) Large Area Structures. The recent increase in demand for large area EL displays has led to a great deal of interest in the II-VI compound phosphors. These structures are essentially high field devices and do not require low resistivity material since the EL is usually excited by impact ionization. The devices can be classified into AC or DC driven structures, the essential difference being that in the AC case the active phosphor is usually sandwiched between insulators and capacitively coupled to the excitation signal. Early work concentrated on the use of powdered phosphors dispersed in transparent dielectrics. Destriau[14] is first credited with discovering the phenomenon of intrinsic EL, using phosphor powder dispersed in caster oil to which a high alternating electric field was applied. More recently, however, attention has been focussed on the use of thin films of phosphor and particular success has been achieved with the production of AC driven panels. The research to date on thin film EL devices has been extensively reviewed recently[15, 16], as has the general field of EL panels[17]. Thus only some of the basic structures used in the production of these panels are discussed here. Fig. 2.9 (a) shows a schematic diagram of the thin film AC EL device. Typically, the metal electrode is aluminium, the insulator may be Y_2O_3, Si_3N_4 or Al_2O_3 and the phosphor is almost invariably ZnS which has been suitably doped to emit EL of the desired

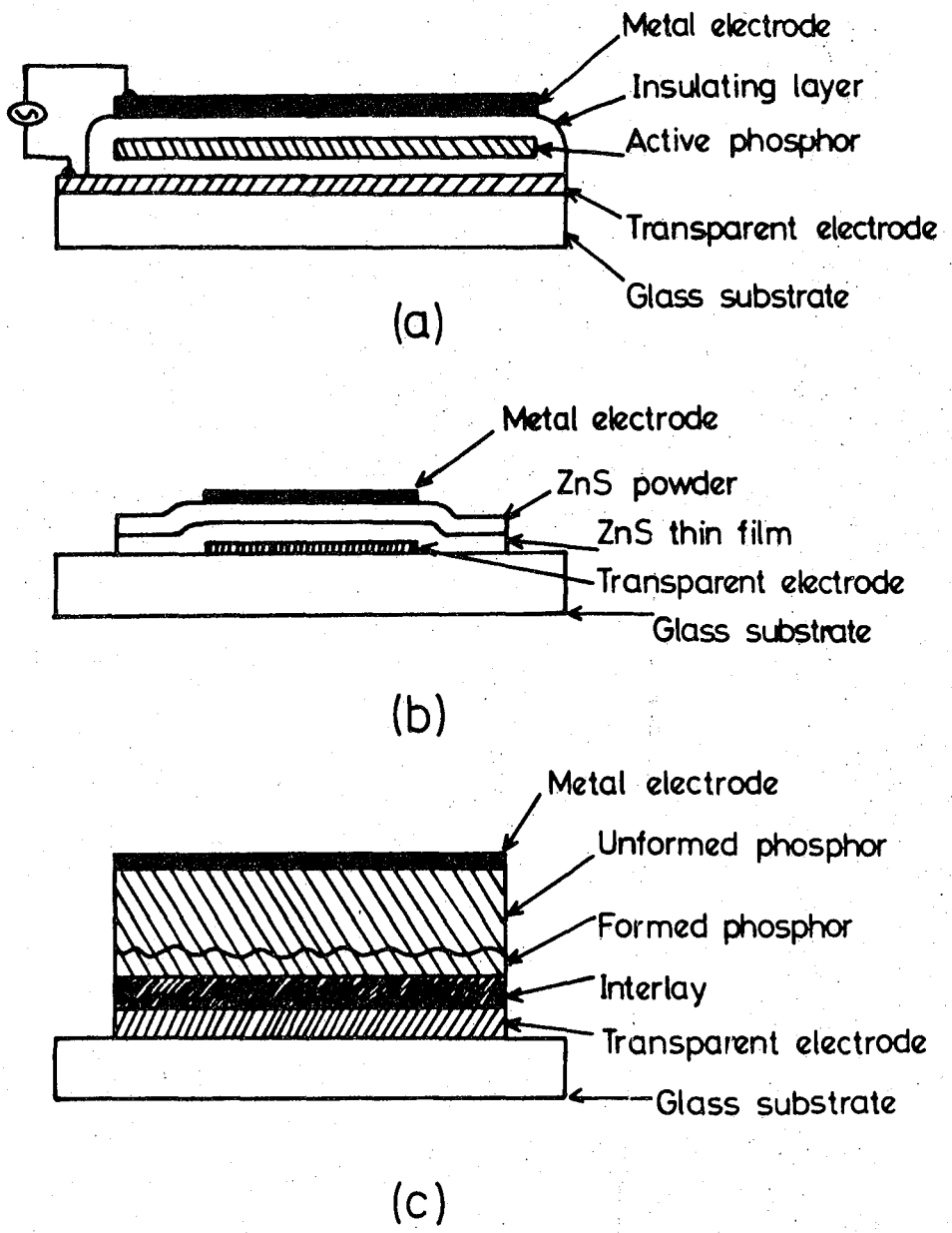

Figure 2.9 Schematic diagrams depicting various structures used in large area display devices; (a) A.C. driven device, (b) D.C. driven 'composite' device and (c) D.C. driven powder device.

wavelength. The design of DC driven cells is much more complex and indeed DC thin film panels have not yet reached a stage where they may be commercially produced. The main problem is due to the absence of the protective insulating layer, which is present in AC devices, leading to catastrophic failure at 'hot-spots'. Attempts to employ a current limiting film between the electrode and phosphor, in order to stabilize the device have had only limited success[18]. At present, the composite structure[19] shown in fig. 2.9 (b) appears to be most promising. Here the ZnS film is the active region and the powder serves to stabilize the structure by essentially separating the high field region from the active region. DC driven powder devices have enjoyed much more success and considerable progress has been made in the last decade. Fig. 2.9(c) shows a typical device. Unfortunately, these devices require an initial 'forming' process in order to produce the insulating, high field region necessary for their operation. This process must be carefully controlled as the panel is easily damaged by the heat dissipated during forming. The use of an interlayer as shown in (c) improves maintenance and reduces the forming power.

Typical operating voltages for these panels are of the order of 100v and this restricts their usefulness. Recently, however, progress has been made in reducing this value by a variety of means such as the use of dielectrics with ferroelectric properties[20] or thin films of single crystal phosphor material grown epitaxially onto semiconducting substrates[21].

EL has also been observed from organic materials, in particular from thin films of anthracene, formed by both evaporation and the LB technique[22]. In this case the geometry employed was a simple sandwich structure with the anthracene sandwiched between aluminium and gold electrodes. For applied fields greater than $\sim 5 \times 10^8$ Vm^{-1}, double injection effects gave rise to EL. Holes were injected from the gold contact and electrons from the aluminium contact.

2.5 ELECTROLUMINESCENT EFFICIENCY

There are several types of EL efficiency normally encountered in the literature and these are now discussed in sequence:

(a) The Visual Efficiency. This term is a photometric quantity and relates to the effectiveness of the emitted light in stimulating the human eye. It has units of lumen per watt and is the luminous flux produced by 1 watt of radiation. The human eye is most sensitive to light of wavelength $\sim$ 555 nm and at this wavelength the visual efficiency is unity with 1 watt of radiant energy being equivalent to 680 lumen. However, it falls to almost zero at the extremes of the eye's response (i.e. at 380 and 780 nm). This is an interesting parameter but not one which usually places constraints on LED design or fabrication.

(b) The Quantum Efficiency. This has units of photons per electron and is the ratio of the number of photons emitted per second to the number of electrons supplied to the diode per second. Care must be exercised when dealing with quantum efficiences as it is sometimes unclear whether the value quoted represents an external or an internal quantum efficiency. (The internal quantum efficiency is sometimes called the light generation efficiency to avoid confusion.) In fact the two parameters are related by the relationship;

$$\eta_q = \eta_i \ \eta_e \ \gamma \qquad (2.4)$$

where η_q is the external quantum efficiency, η_i is the internal or light generation efficiency, γ is the minority carrier injection ratio and η_e is the fraction of which escapes from the diode; (η_e is sometimes called the light extraction efficiency).

(c) The Power Conversion Efficiency. This is more conventional in that it is dimensionless and is simply the ratio of the total radiant flux

(in watts) to the input power supplied to the diode (in watts). For moderate bias levels the power conversion efficiency is approximately equal to the quantum efficiency since the applied voltage (multiplied by q) is comparable to the photon energy of the emitted light. In this work the efficiencies quoted are power conversion efficiencies. However, these values are likely to be significantly less than the true efficiency since they were calculated, not from the total radiant flux, but that fraction which was incident on the photodetector. This is quite acceptable for a comparative study such as this, although an estimate of the true efficiency was also attempted by 'calibrating' the measuring system using a standard p-n junction LED with a known external quantum efficiency.

The factor which limits the maximum attainable external quantum efficiency in an LED depends very much on the material used. For example, in green light emitting p-n junction diodes, the internal quantum efficiency is poor and this limits the theoretical maximum external efficiency to less than 1%; whereas in ZnS EL devices the internal efficiency is very high (up to $\sim$30%). However, in the former case, external efficiencies close to the theoretical maximum can be achieved due to efficient injection and light extraction processes, whereas in the latter, the maximum external efficiency claimed for an injection EL device is $\sim 10^{-4}$ which is a consequence of the poor injection and extraction efficiencies. An efficient injection structure for ZnS (or, indeed, other II-VI phosphors) is therefore highly desirable.

2.6 ELECTROLUMINESCENCE IN GaP

There are a number of important considerations when choosing materials for visible LEDs: The human eye is only sensitive to light with a photon energy of greater than approximately 1.8eV ($\lambda \sim 0.7\mu m$), which places a minimum constraint on the energy gap of the material to be used. Furthermore,

as discussed in § 2.3.1, the first-order nature of the radiative processes in a direct bandgap semiconductor means that such materials are preferable to those with indirect bandgaps. Another important factor is cost. The material must be economical to produce in high-quality, large area form with good control of the electrical characteristics. GaP satisfies two of these three requirements; it has a well-established growth technology and its bandgap of 2.25eV is very close to the photon energy at which the eye is most sensitive. However, since GaP has an indirect bandgap, only a minute fraction of the emitted light is due to interband recombination , the remainder has a photon energy of less than this, determined by the impurity content. By varying the growth conditions to incorporate varying concentrations of different impurities, EL with a range of different energies can be activated. The material used in this work was doped with nitrogen which is an isoelectronic impurity in GaP (see later) and most of the following discussion is devoted to this particular system. A comprehensive account of the other luminescence mechanisms in GaP can be found in reference (1).

2.6.1 The Isoelectronic Trap

An isoelectronic impurity atom is one which has replaced a host atom from the same group in the periodic table. Independent studies, on tellurium in CdS[23] and nitrogen in GaP[24] revealed that such impurities can lead to bound states in semiconductors. The work on GaP : N was soon extended and the nature of the transition elucidated[25]: Although the outer electronic structure of the impurity and host atoms are very similar, the structure of the electronic cores may be considerably different. In this case, a short range potential perturbation is produced in the lattice which can capture and bind a free carrier. The type of charge carrier trapped by the centre depends on the difference between the electronegativity of the

impurity and host atom[26]. Once a carrier of one type is bound, the centre becomes charged and the resulting long range Coulomb potential can then trap a carrier of the opposite type to form a bound exciton.

Nitrogen replaces phosphorus atoms when introduced into the GaP lattice and gives rise to an electron trap located very close to the conduction band edge. The short range potential which binds the electron is very different to the more usual Coulomb potential and the electron is highly localized at the nitrogen centre. Consequently, the electronic wave function is more extensive inmomentum (k) space which means that the exciton can undergo phonon-less recombination, thus emitting a photon of light with an energy very close to the bandgap of GaP. The extension of the wavefunction in k-space effectively relaxes the momentum conservation constraints usually encountered in indirect bandgap materials and results in a much shorter radiative lifetime for the impurity centre. This leads to a significant increase in the internal efficiency of the material when compared to non-nitrogen doped GaP. Another feature of using nitrogen, as an EL activator in GaP is that it can be introduced in very large concentrations ($> 10^{19} cm^{-3}$) without significantly affecting the concentration of free carriers. This is important since non-radiative Auger recombination, which is particularly significant in indirect semiconductors, is greatly enhanced as the carrier concentration is increased.

A different kind of isoelectronic trap is responsible for the efficient production of red EL in GaP - the so called 'molecular isoelectronic centre'. Here a Zn:O complex replaces a Ga:P pair and results in a trap very similar to the nitrogen centre but with a much greater binding energy ($\sim$ 0.3eV). This mechanism is not relevant to the work described here and is not discussed further.

2.6.2 Green Luminescence Mechanisms

The features of the isoelectronic nitrogen centre make it the only known method of producing relatively efficient, near-gap EL in GaP. In fact there is a total four processes which give rise to measurable amounts of near-gap EL in GaP; (a) the recombination of bound excitons at isolated nitrogen impurities[24], (b) the recombination of excitons bound to pairs of nitrogen impurities[25], (c) the recombination of free excitons[27] and (d) free to bound transitions[27], i.e. the recombination of free holes at neutral donors. However, only those processes involving the isoelectronic centre are significant from an LED viewpoint and, consequently, only they will be discussed here. A full account of the other mechanisms, and additional processes which are only important at very low temperatures can be found in reference (1).

Figure 2.10 shows the cathodoluminescence (CL) spectrum obtained from a GaP LED doped with nitrogen to a concentration of $\sim 10^{18}$ cm^{-3} [30]. The fine structure of the spectrum is revealed at 77 K. Three dominant processes are evident. The one corresponding to the highest energy transition is the well known 'A' line which is due to the recombination of excitons bound to isolated impurity atoms in the manner described previously. Several lower energy mechanisms can also be identified. These include phonon assisted recombination at isolated centres with both acoustic and optical modes being present. The strong A-O line is the first optical phonon replica. Also evident is the mechanism labelled NN_1: This is the result of phonon-less recombination of excitons bound to nearest neighbour nitrogen pairs. This becomes more significant as the nitrogen concentration is increased and as it is increased towards $\sim 10^{19} cm^{-3}$, the EL becomes progressively more yellow[29]. Again, the NN_1 feature is the principle line of a series, stretching down to almost 600nm ($\sim$2 eV). These can be attributed both to phonon assisted modes and to processes associated with pairs of nitrogen atoms at various separations.

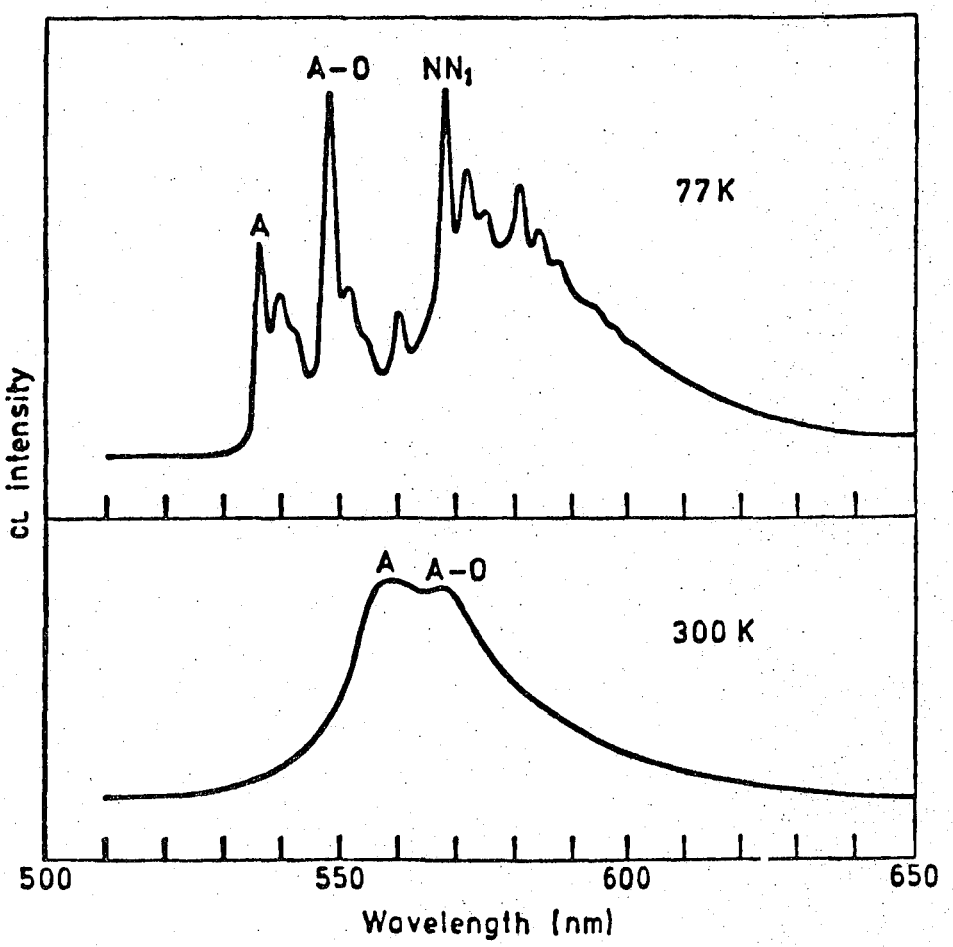

Figure 2.10 Cathodoluminescence spectra obtained from nitrogen-doped ($\sim 10^{18}$ cm^{-3}) GaP material. (after Wight et al[30]).

It should be noted that the spectra shown in fig. 2.10 are the result of CL studies. However, an excellent correlation has been demonstrated[30] between both spectral and efficiency properties as measured by CL and EL.

2.6.3 Loss Mechanisms

Loss mechanisms can be divided into two distinct groups: those which lead to a decrease in the internal quantum efficiency (i.e. those giving rise to competing, non-radiative mechanisms), and those which affect the light extraction efficiency. The former processes are an intrinsic feature of the semiconductor material and can only be improved by careful control of purity and crystallinity at the crystal growth stage. The other mechanisms are less fundamental and significant improvements can be achieved by employing a range of device engineering techniques.

(a) Internal Loss Mechanisms. It is instructive to define two lifetimes, τnr and τr, associated with the non-radiative and radiative processes respectively. Using these lifetimes, which represent transitions by all of the possible processes, one can define the internal efficiency as

$$\eta_i = \frac{\tau nr}{\tau r + \tau nr} \left[= \frac{Rr}{Rnr + Rr} \right] \qquad (2.5)$$

where Rr and Rnr are the corresponding recombination rates. It can be seen from this relationship that in order to increase η_i one must either decrease τr or increase τnr. A decrease of well over an order of magnitude in τr is achieved by incorporating nitrogen impurities, but even with the very high concentrations ($\sim 10^{20}$ cm^{-3}) possible in material grown by vapour phase epitaxy, τr cannot be decreased to values comparable with τnr (typically $\sim$100ns). A further improvement in τr can be achieved by increasing the concentration of free carriers since the creation of free and bound excitons depend on the carrier concentration. Unfortunately, when

the carrier concentration increases to $\sim 10^{18} cm^{-3}$, Auger recombination is enhanced and this counters the beneficial decrease in τr by decreasing τnr. It would therefore appear that the best chance of increasing η_i lies in the control of the factors that influence the non-radiative lifetime, τnr. As has been mentioned previously non-radiative processes are, in general, very difficult to study. In nitrogen-doped GaP this study has been facilitated by the fact that the exciton states involved in the EL processes are shallow when compared to the room temperature thermal energy. This means that the excited carriers can be assumed to be in equilibrium with the free carrier population and consequently, measurements of the EL (or CL) decay time can give information on the minority carrier lifetime in the material. Since the majority of the transitions in GaP are non-radiative, then the minority carrier lifetime is approximately equal to τnr. Indeed, the variation of η_i with τnr has been investigated by measuring CL decay times[31]. However, the study of the actual processes and associated levels through which non-radiative recombination occurs is much more difficult and, in general, these 'shunt-paths' are poorly understood. It is known that in GaP (at least in n-type material) the recombination processes are dominated by non radiative recombination via a deep hole trap located $\sim$ 0.75eV above the valence band. The precise origin of the trap is uncertain although there is good evidence to suppose that it may be due to a gallium vacancy complex[32]. The trap has been found to have an extremely large capture cross section ($\sim 10^{-13}$ cm^2) and has been measured in concentrations of up to $\sim 10^{15} cm^{-3}$. The mechanism by which recombination occurs via this centre is thought to be predominantly multiphonon emission although Auger recombination in GaP has also been observed[33]. Recombination at dislocations and at surface or interface states have also been demonstrated to occur in GaP although these processes are believed to be only minor sources of inefficiency in device grade

material. A discussion of these processes can be found in reference (34).

Despite the intense research carried out in this area over the past two decades, the best internal efficiencies achieved to date in green luminescent GaP are of the order of 1% which accounts for the low external efficiencies of green-emitting GaP LEDs.

(b) Light Extraction Inefficiencies. With such a low internal efficiency, LED device design becomes very important. The light extraction efficiency must be made as large as possible within the constraints imposed by economic considerations. This is primarily a technological concern and, consequently, only a brief description of the major losses and their minimisation is given here. The main source of loss is due to reabsorption in the semiconductor before the light can be extracted. The largest amount of reabsorption occurs in the heavily nitrogen-doped region although intrinsic processes in the bulk can also contribute. Methods of minimising this reabsorption have been extensively studied and these vary from simple design considerations (such as choosing the junction side with the lowest absorption coefficient to act as the LED window, and keeping this as thin as possible), to the design of complex encapsulant structures affording a higher probability of escape for the generated light. Such encapsulants improve the refractive index mismatch at the GaP/air boundary and as a result, the critical angle for escape can be increased. (Light incident on the boundary at an angle greater than this critical value is totally internally reflected.) Another major source of inefficiency is due to absorption at the Ohmic contacts. Often, a grid dielectric, interposed between the Ohmic contact and the substrate is used to reduce the surface area of the contact and hence the amount of absorption. However, a compromise is necessary as the dielectric results in a non-uniform current distribution and a higher series resistance.

Using techniques such as these it is possible to achieve large light extraction efficiencies and indeed green-emitting devices with external quantum efficiencies of almost 1% have been fabricated.

2.7 ELECTROLUMINESCENCE IN ZnSe

Zinc selenide, and indeed all of the II-VI phosphors, have a direct energy gap which means that radiative processes can compete efficiently with the alternative, non-radiative loss mechanisms. Consequently, it is possible to produce material with very high internal luminescence efficiencies. (For example, the ZnSe used in this work had an internal efficiency estimated to be approximately 30%[35].) Unfortunately, the growth of these wide-bandgap materials (possessing the desired properties) in a reproducible, controllable fasion is an exacting problem, and this has been a major factor in preventing the widespread exploitation of such materials in LED fabrication. Nevertheless, their importance for use in display devices in general has led to a great deal of research aimed at elucidating the mechanisms responsible for producing luminescence in these materials. These processes can be divided into two groups, namely edge emission and deep centre mechanisms.

(a) Edge Emission. Edge emission is the term used to describe emission resulting from transitions between levels located close to the band edges. The photon energy of the emitted light then corresponds quite closely (within a few tenths of an electron volt) to the bandgap energy. Edge emission in II-VI compounds in general has been attributed to a number of different processes. Photo- and cathodoluminescence studies have enabled free exciton, bound exciton and distant pair recombination, together with their phonon replicas, to be identified. These processes have been described previously and will therefore not be described here.

(b) Deep Centre Luminescence. These mechanisms can be divided into localized and non-localized categories. In the non-localized transitions, electrons or holes in the semiconductor bands make transitions to the impurity level itself (i.e. the process described in § 2.3.1). In localized transitions, the emission and absorption processes occur within the electronic structure of the impurity ion. Transition metal elements (e.g. manganese) or rare-earth ions give rise to this type of process. Such impurities are usually excited by impact ionization and, consequently, have little relevance to this work.

A wide range of impurities have been used to activate non-localised transitions in II-VI materials, including copper, aluminium and chlorine. Alternatively the emission may be self-activated with intrinsic defects such as vacancy complexes giving rise to radiative transitions.

The luminescence properties of the particular material vary greatly depending on the growth conditions and the concentration of unintentional impurities. In particular, it is often difficult to produce material in which the component due to edge emission is dominant. More often the luminescence properties are dominated by deep centre mechanisms resulting from the incorporation of extrinsic impurities or the formation of intrinsic defects. The ZnSe material used in this study (see chapter 5) has been shown to produce dominant near gap luminescence using favourable growth conditions[36], although deep centre mechanisms are also evident. In fact in some samples, particularly those grown on (111) oriented GaAs substrates, the luminescence properties were dominated by broad band, lower energy emission associated with copper impurities. The near-gap luminescence was identified to be due to both free exciton recombination and the recombination of excitons bound to neutral acceptors[35].

SUMMARY

This chapter has dealt, in a qualitative, manner with the physics of electroluminescent devices, beginning with a discussion of the general principles involved and progressing to a description of the specific mechanisms present in the material used in this work. The section on electroluminescent structures provided a general description of a number of device configurations used to obtain EL. In the following chapter, those structures of particular interest to this work, namely the Schottky barrier and the metal-thin insulator-semiconductor diode, are discussed in more detail.

CHAPTER 3

SCHOTTKY BARRIER AND METAL-THIN INSULATOR - SEMICONDUCTOR DIODE THEORY

3.1 INTRODUCTION

The first report of rectification between a metal (point) contact and a crystal dates back to 1874[1]. However, despite the intensive research carried out since then on first point, and then planar contact diodes, many aspects of metal-semiconductor barriers have yet to be fully explained. This is particularly true of the mechanism of formation of a Schottky barrier, although recent work has enabled a number of promising theories to be developed. The question of Schottky barrier formation is considered first in this chapter, beginning with a brief review of early theory and ending with a description of the more recent schools of thought. This is followed by a discussion on the properties of (and processes involved in) a ' near-ideal' Schottky diode, i.e. the situation which is usually achieved in normal, practical cases. The remainder of the chapter is devoted to the theory and applications of the metal-thin insulator-semiconductor (thin-MIS) diode. For the purposes of this discussion, the insulator is taken to be ideal. That is, to have band edges coincident with the vacuum level and no defect or impurity levels in the bandgap. It will be shown that while the inclusion of such an insulator into the Schottky barrier structure complicates the picture quite considerably, it can, under certain circumstances, be used to great advantage in a number of electronic devices. Particular emphasis is obviously placed on the use of the thin-MIS structure as an EL device and a descriptive review of the previous work in this field is given. This is followed by a brief description of the thin-MIS solar cell since there are certain similarities between their modes of operation. Practical evidence to support this view will be described in a later chapter.

3.2 SHOTTKY BARRIER FORMATION

3.2.1. Schottky-Mott Theory

In the previous chapter the formation of an ideal Schottky barrier was considered from the viewpoint of the flow of charge from the semiconductor to the metal as the two were brought into contact (fig. 2.6). The height of the barrier involved was described by Mott[2] as

$$\phi_{bn} = \phi_m - \chi_s \qquad (3.1)$$

where ϕ_m is the metal work function and χ_s is the electron affinity of the semiconductor. Schottky[3] [4] proposed that the uncompensated donors, which give rise to the space charge, are uniformly distributed up to the semiconductor surface. This uniform space charge gives rise to a linearly increasing electric field strength and hence a quadratically increasing electrostatic potential. The resulting parabolic barrier is known as a Schottky barrier (fig. 3.1). Mott[2], however, proposed a somewhat different model. He assumed the existence of a narrow region at the semiconductor surface, in which there are no donor impurities. This gives rise to the so-called 'Mott barrier', in which the electric field is constant throughout the depletion region yielding a linearly increasing electrostatic potential. The Mott barrier, although occasionally encountered in practice, is very rare and most practical contacts give rise to parabolic, Schottky barriers. The expression given in eq. (3.1) is sometimes called the Schottky-Mott relation.

The Schottky-Mott theory makes a number of somewhat gross assumptions. In particular, the assumption is made that the surface dipole contributions to ϕ_m and χ_s (or at least their difference) remains constant as the two materials are brought together. (The work functions of semiconductors and metals and the semiconductor electron affinities have, in general, surface

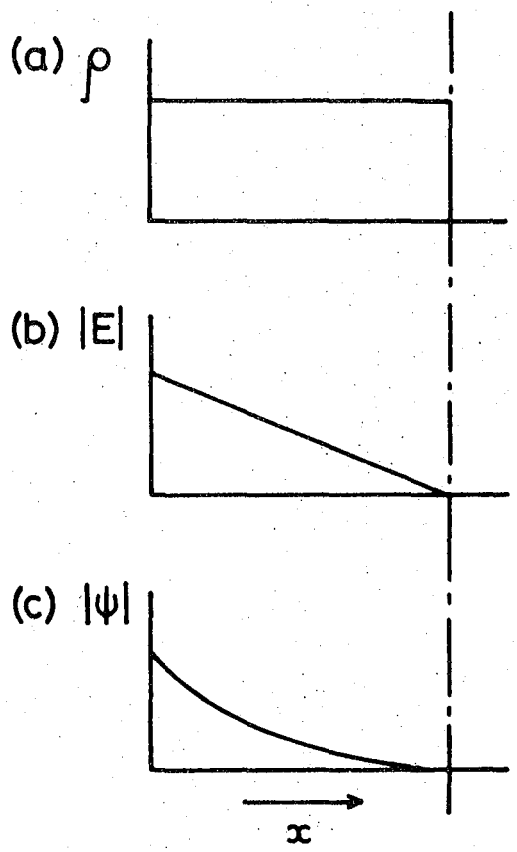

Figure 3.1 Depicting variation of (a) charge density, (b) electric field strength, and (c) electrostatic potential with distance for an ideal Schottky barrier.

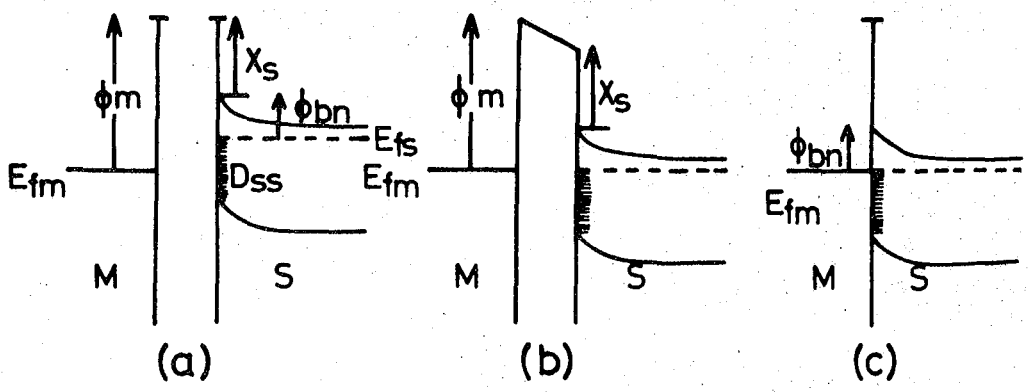

Figure 3.2 Sequence of energy band diagrams depicting Schottky barrier formation in the presence of a high density of surface states. (NB. The interfacial layer has been omitted for simplicity.)

and bulk contributions. The surface contribution arises from the distortion of the electron gas around the atoms at the surface, giving rise to an effective dipole layer which may not remain constant as the surface properties are altered.) This assumption is now acknowledged to be incorrect, and a wealth of experimental data[5] has shown that the linear dependence of ϕ_{bn} on ϕ_m, predicted by eq. 3.1 is not usually observed. (Although it is true that metals with higher work functions do tend to form larger Schottky barriers on n-type material.) Bardeen[6] was one of the first authors to propose an explanation for this observation and his model is now considered.

3.2.2 The Bardeen Model

Bardeen[6] proposed that the relative independence of ϕ_{bn} on ϕ_m could be explained by invoking the presence of interface (surface) states. Before proceeding to discuss the model it is instructive to examine the origins and properties of these states.

Surface States

The forbidden energy gap of a material arises because the solutions of the Schrodinger equation for an electron wave function in a periodic potential (i.e. the crystal lattice) are of a special form - the so-called 'Bloch functions'. These functions are themselves periodic and predict the band structure familiar to all solid-state scientists. (A detailed description of the theory of band structure can be found in reference (7).) Surface states are allowed solutions of the Schrodinger equation which relate to energy levels in the 'forbidden' gap. They become allowed if the perturbation of the crystal periodicity by the semiconductor surface is included in the analysis. In the simplest case they can be thought of, physically, in terms of a 'dangling bond' picture, where each surface atom has one unpaired electron associated with it in a localized orbit at

right angles to the surface plane. This is a dangling bond and it can be characterised as being either donor-like (positive when empty) or acceptor-like (negative when full). Distinct from these intrinsic surface states (i.e. those associated with a perfect free surface) are those due to the presence of defects or adsorbed foreign atoms at the surface. These are called extrinsic surface states. (It should be emphasised, however, that there is no conclusive evidence linking such states to specific defects.)

Bardeen[6] suggested that, if the density of these states is sufficiently high, then the space charge region in the semiconductor may be a property, not of the metal work function, but of the charge localized in the interface states. Furthermore, he introduced the concept of a neutral level, ϕ_o, for these states, defined as that level below which the states must be filled in order to achieve an electrically neutral surface. Fig. 3.2 shows a simplified sequence of energy band diagrams, depicting the formation of a Schottky barrier on an n-type semiconductor in which the density of surface states is assumed to be very high. When the metal and semiconductor are far removed (a), the surface states are in equilibrium with the semiconductor bulk (i.e. full to the level denoted by E_f) and the charge localized at the surface is balanced by an equal (and opposite) charge comprising the depletion region at the semiconductor surface. The bands are bent even though the metal and semiconductor are not in equilibrium. If the two materials are now electrically connected (b), alignment of the two Fermi levels occurs which results in an electric field being developed across the gap. Since the density of surface states is very high, then as the materials are brought into contact, the extra charge (associated with the field in the gap) can easily be accommodated by these states without affecting the position of E_f appreciably. The height of the barrier is then determined mainly by the properties of the semiconductor

surface and not the metal work function; the Fermi level has been 'pinned' relative to the band edges by the surface states and in the limit $D_s \rightarrow \infty$, ϕ_{bn} is given by

$$\phi_{bn} = Eg - \phi_o \qquad (3.2)$$

where Eg is the energy gap of the semiconductor.

In the general case, the barrier height is a function of both the charge in the interface states and the metal work function and, indeed, Cowley and Sze[8] extended the Bardeen model to derive a general expression for the barrier height. It is important to note the assumptions made in their analysis. These are: (a) the existence of an interfacial layer between the metal and the semiconductor, of the order of atomic dimensions, which is transparent to sufficiently energetic electrons, and (b) that the surface states are uniformly distributed across the energy gap and their density is a property only of the semiconductor surface and not of the metal. They showed that the barrier height could, in most practical cases, be given by the approximate expression

$$\phi_{bn} \simeq C_2(\phi_m - \chi_s) + (1 - C_2)(Eg - \phi_o) - \Delta\phi_{bn} \qquad (3.3)$$

$$\text{where } C_2 = \varepsilon_i/(\varepsilon_i + q\delta D_s) \qquad (3.4)$$

D_s is the density of surface states, ϕ_o is measured from the valance band edge, $\Delta\phi_{bn}$ is the image force barrier lowering (see §3.3.2), ε_i and δ are the permittivity and thickness of the interfacial layer respectively. (Fig. 3.3(a) shows the energy band diagram corresponding to this generalised expression for the barrier height.) The two limiting cases

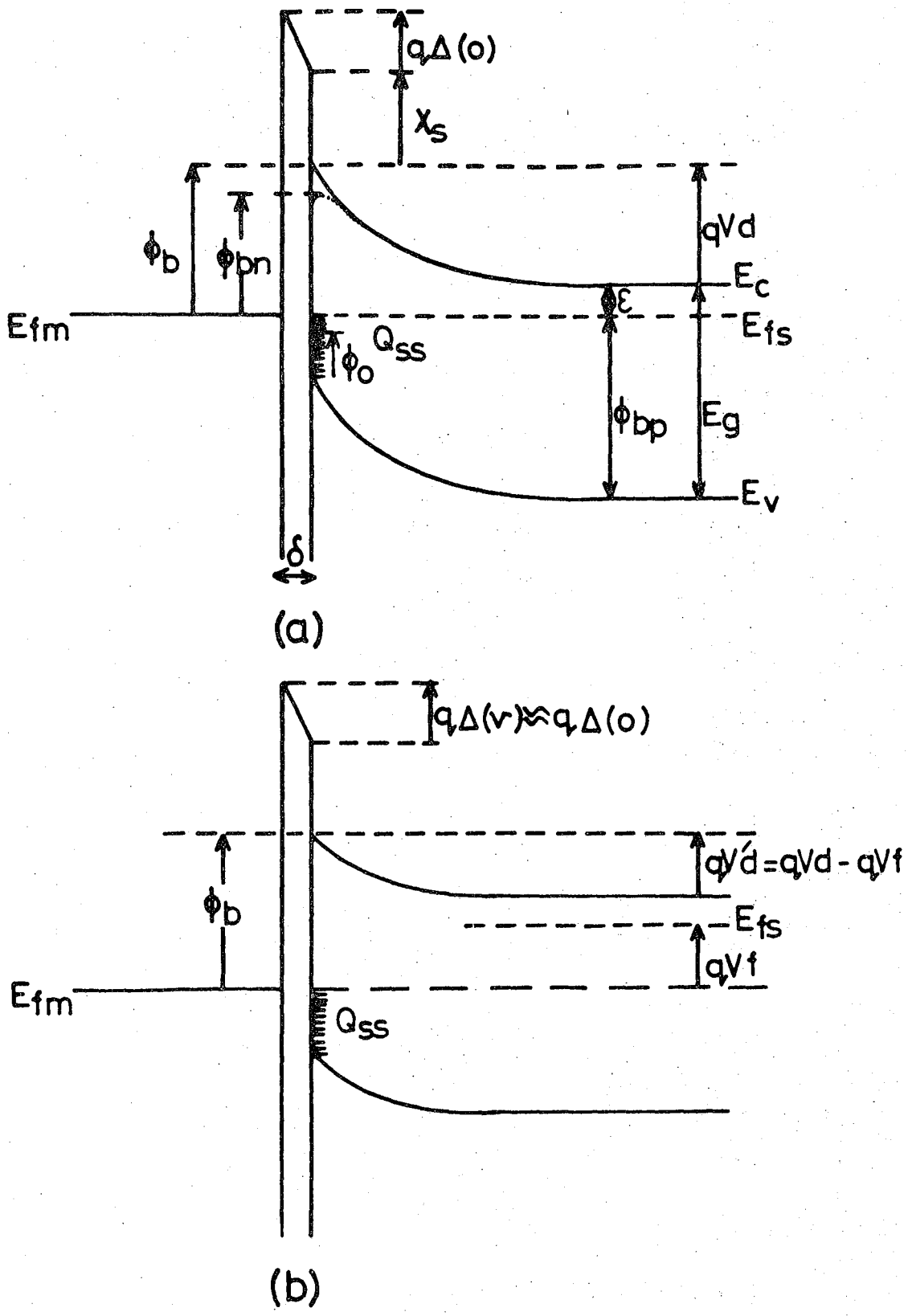

Figure 3.3 Energy band diagram of a Schottky barrier incorporating an interfacial layer of atomic dimensions (a) in equilibrium and (b) under the application of a forward bias.

(i.e. $D_s \sim 0$ and D_s is very high) can be identified from eq (3.3). If $D_s = 0$ then the expression reduces to the Schottky-Mott theory given in eq. (3.1). If, however, D_s is very large then eq. (3.3) approaches the Bardeen Limit, i.e. eq. (3.2). Cowley and Sze[8] also attempted to correlate eq. (3.3) with previously published results obtained for a number of semiconductors. They found that it gave a reasonable explanation of the data for Si, GaP and GaAs diodes (particularly so in the case of GaP), although, in general, there was a significant amount of scatter involved. In contrast, results for CdS appeared to conform to the Schottky-Mott theory and were thus inconsistent with their model.

It is now acknowledged that this model provides a reasonably accurate explanation for the variation of ϕ_{bn} with ϕ_m for many covalent semiconductors and has been widely used in the past to analyse Schottky barrier systems[9]. However, many do not conform to this theory (e.g. the more ionic semiconductors CdS and ZnS) and the model cannot be considered as universal. Indeed, more recently, a number of different theories have been proposed, some of which are essentially extensions of the Bardeen model; others are radically different. These developments are discussed in the following section.

3.2.3 Recent Developments

The Bardeen model is rather idealised, both in terms of the explicit assumptions mentioned earlier, and in terms of those implicit in the theory supporting the model. These include the assumption of abrupt interfacial boundaries, the use of point charges to represent interface states (whereas, in fact, they extend into the semiconductor to a distance of up to 1 nm[10]), and also the assumption that the metal, interfacial layer and semiconductor are all chemically inert. The fact that this last assumption may not always be valid was demonstrated by Andrews and Phillips[11]

who studied transition metal- silicide - silicon diodes. (These are now a well-established class of Schottky barriers in modern integrated circuits.) They found a high degree of correlation (up to 97%) between the Schottky barrier height and the heat of formation of the chemical reaction which occurs at the surface. This demonstrated, at least for this class of diodes, a definite link between Schottky barrier formation and metal reactivity. Our lack of understanding of Schottky barrier formation was aptly demonstrated by the fact that they found it necessary to distinguish four types of Schottky barrier each conforming to a different theory[11], one of which was their metal reactivity model. A more radical view was taken by Brillson[12] who, using a wide range of both reactive and non-reactive metals, presented evidence to show that in the case of CdS and CdSe, interface chemical reaction and local charge redistribution dominated the Schottky barrier properties. He proposed that these mechanisms may dominate Schottky barrier formation in general. The same effect was demonstrated for the Al/GaAs system[13] which is known to possess a relatively abrupt interface. Once again, microscopic charge rearrangement was proposed as the dominant mechanism in determining the macroscopic barrier height.

Spicer et al[14] proved that intrinsic surface states could not be used to explain Schottky barrier formation (at least in the III-V compounds) when they showed that, although the cleavage (110) face of these semiconductors does not possess intrinsic surface states in the energy gap, the position of the Fermi level could be pinned by much less than a monolayer coverage of metal - the pinned position showing little dependence on the metal species. They proposed the 'unified defect model' for Schottky barrier formation where the Fermi level is pinned by extrinsic interface states caused by lattice defects resulting from the adsorption of impurity (metal or oxygen) atoms. Although Spicer et al correlated the defect levels with missing column III or V elements,

there has recently been some contention of this point[15]. Williams et al[16], working independently, drew similar conclusions from their work on InP, thus providing strong support for the unified defect model. It should be noted, however, that this model does not contradict the previously mentioned results showing the influence of surface chemical reactions on Schottky barrier formation. Indeed, the relevance of this work to the unified defect model has been discussed by Spicer et al[17] where they suggest that it is the heat of condensation of the metal on the III-V materials which is responsible for the appearance of semiconductor material in the metal[14] and stress the importance of the development of interface (surface) thermodyanics and kinetics in order to provide a fuller understanding of the problem. (However, they also stress that they believe it is surface chemical interactions which are the determining factor and not the formation of bulk reaction products.)

Thus an elegant model, based on a wealth of experimental evidence, has been developed which can explain the problem of Schottky barrier formation in terms of extrinsic surface states and is therefore consistent with much of the Bardeen model. However, there remains considerable controversy and, indeed, Freeouf[18] has recently argued that the use of interface states to explain some of the experimental results for Schottky barriers is inconsistent with a number of other experimental observations; and, with Woodall[19], suggests an effective work function model as an alternative to the unified defect model. In this case the macroscopic barrier height is determined by the work functions of microclusters of one or more interface phases resulting from chemical reactions during formation. In addition to this, Lee et al[20] have proposed a metal-amorphous film-semiconductor configuration as the structure of a real Schottky barrier, and have used this model to explain many of the experimental observations traditionally attributed to interface states. Observations such as the difference in ϕ_{bn}

indicated by capacitance measurements compared to that measured by conductivity or photoemission techniques (§ 3.4.1); the variation in diode ideality factor (§ 3.3.3); the origin of Fermi-level pinning; and the difference in the interface behaviour between covalent and more ionic semiconductors. (These experiments were performed on diodes fabricated on chemically prepared semiconductor surfaces in comparison to much of the previously mentioned work which was performed, largely, using diodes fabricated on cleaved surfaces in UHV. This is certain to prove an important factor in determining the precise structure of the diodes.)

The work reviewed in this section has undoubtedly led to important advances in the understanding of the theory of Schottky barrier formation. However, the majority of practical diodes can be analysed quite successfully using the Bardeen model and, since this is used extensively in this thesis, the model is discussed in more detail in the subsequent section.

3.3 THE NEAR-IDEAL SCHOTTKY BARRIER

3.3.1 Introduction

A 'near-ideal' Schottky diode is defined here as one where the semiconductor (and hence the charge in the interface states) is separated from the metal by a very thin insulating layer of atomic dimensions. It is assumed to be essentially 'transparent' to electrons (i.e. readily traversed by quantum mehanical tunnelling) but nevertheless is able to withstand a potential. This interfacial layer is necessary from electrostatic considerations in order to analyse the diode according to the Bardeen model. (If the interfacial layer were absent, then the effect of the metal would be to 'screen' the interface states thus preventing them from affecting ϕ_m.) The band diagram for such a Schottky barrier is shown in fig. 3.3 (a) and is the model used by Cowley and Sze[8]

in their analysis. Since the interfacial layer is so thin, it is assumed to have a negligible affect on the Schottky barrier properties. In particular, a negligible proportion of any applied voltage is developed across this insulator and the degree of band bending in the semiconductor is approximately given by Vd + Va (where Va is the applied voltage). A consequence of this is that the position of the conduction and valence band edges (at the semiconductor surface) remain fixed with respect to the position of the metal Fermi level. This can be seen in fig. 3.3(b) which illustrates the situation under forward bias. An important consequence of this is that the charge localized in the interface states (which equilibrates with the metal Fermi level for such a thin insulator) is essentially fixed and independent of bias. This, together with the assumption that the effect of the insulator on the processes of current transport is negligible, enables the insulator to be omitted in much of the following discussion.

This near-ideal situation is close to that achieved in practice, when the semiconductor is carefully prepared chemically (before deposition of the metal electrode) with the intention of minimising the interfacial layer.

3.3.2 The Schottky Effect

The Schottky effect is the lowering of a potential barrier due to the existence of an image force between an electron and the surface of a metal. This originates from the fact that an electron, at a distance, x, from the metal surface, experiences an attractive force due to an induced positive charge on the metal surface. The effect on the metal-semiconductor barrier height is shown in fig. 3.4. The barrier height is lowered from ϕ_b to ϕ_{bn}, by an amount, $\Delta\phi_{bn}$. This barrier lowering is due to a combination of the electric field in the depletion region and the potential due to the image force. This force, F_i, is given by

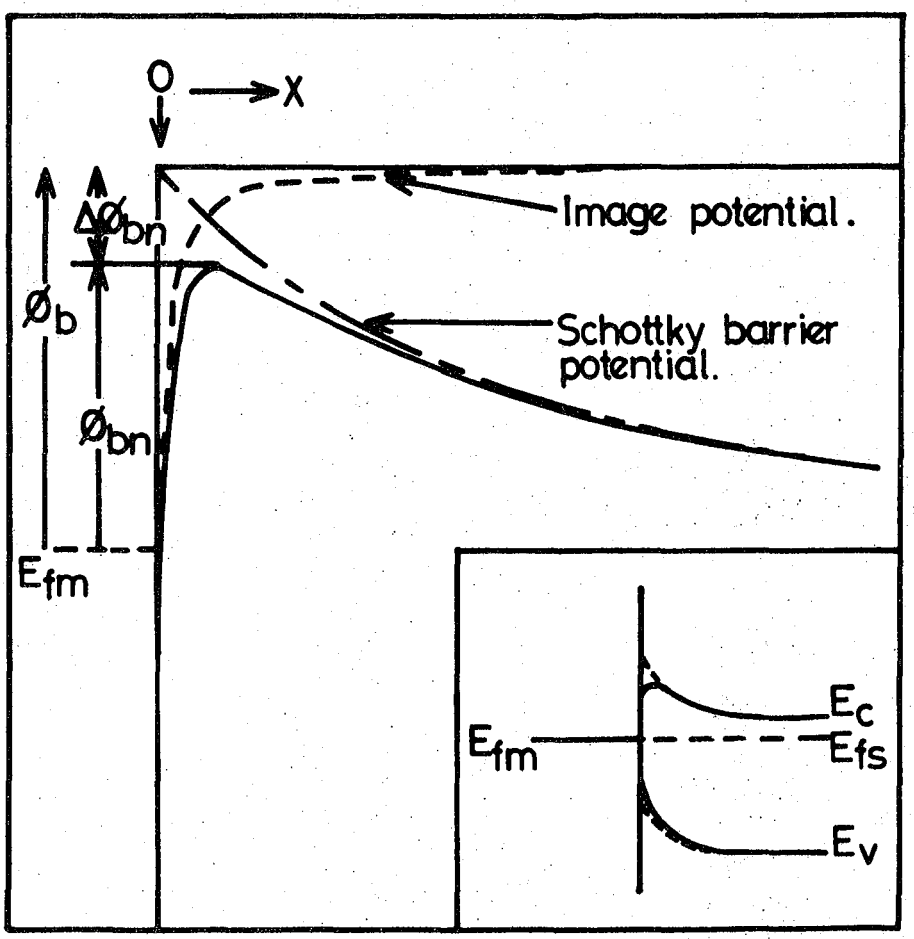

Figure 3.4 Image force lowering in a Schottky barrier. The inset illustrates the effect on both the conduction and valence bands.

$$F_i = - q^2/16\pi\varepsilon_s x^2 \qquad (3.5)$$

where ε_s is the permittivity of the semiconductor. The potential energy due to F_i is represented by the dashed line in fig. 3.4, and this, superimposed with the potential energy due to the Schottky barrier, gives the resulting barrier as shown. Since the image force is only significant in the vicinity of the interface, to a good approximation the field in the depletion region is constant and equal to E_{max}. Then the potential energy of an electron at a position, x is given by

$$X(x) = \int_{\infty}^{x} F_i dx + qEx = \left(\frac{q^2}{16\pi\varepsilon_s x}\right) + q E_{max} x \qquad (3.6)$$

This expression can be differentiated and equated to zero to yield.

$$x_{max} = \left(\frac{q}{16\pi\varepsilon_s E_{max}}\right)^{\frac{1}{2}} \qquad (3.7)$$

and $$\Delta\phi_{bn} = \left(\frac{q E_{max}}{4\pi\varepsilon_s}\right)^{\frac{1}{2}} \qquad (3.8)$$

Holes in the semiconductor valence band also experience an image force but in this case the effect on the band structure close to the semiconductor surface is to bend the valence band upwards, as shown in the inset to fig. 3.4.

Although the effect of this image force lowering is small ($\sim$0.04eV), it can have a significant effect on the Schottky barrier properties, particularly the current transport processes since the current depends exponentially on ϕ_{bn}. Furthermore, the amount by which the barrier is

lowered depends on E_{max} and hence on the applied bias - an effect discussed in the following section.

3.3.3 Current transport processes

There are several processes by which current may flow in a Schottky barrier under the influence of an applied bias. These are shown schematically in fig. 3.5 and are illustrated for the case of an applied forward bias (positive to the metal). Under reverse bias the exact inverse processes occur. These mechanisms are; (a) the emission of electrons over the top of the barrier, (b) quantum mechanical tunnelling through the barrier, (c) recombination in the depletion region and (d) recombination in the semiconductor bulk. Processes (c) and (d) are the result of minority carrier injection into the semiconductor with (d) being the true injection of interest in this work as it can lead to radiative recombination in the semiconductor. However, it is well known that, in the vast majority of cases, the minority carrier current in a Schottky barrier represents only a small fraction of the total current[21] and the Schottky barrier is predominantly a majority carrier device. Consequently, processes (c) and (d) are very small, as is (b) unless the material is very heavily doped or at a low temperature. This means that emission over the barrier (process (a)) is the dominant current mechanism in most Schottky barriers. However, before the carriers can be emitted over the barrier, they must be transported from the semiconductor bulk to the interface region. This occurs by the normal processes of diffusion and drift and is in series with the actual emission over the barrier. Wagner[22] and then Schottky and Spenke[4] proposed that the diffusion process limited and hence determined the current flow in the diode, whereas Bethe[23] proposed thermionic emission as the limiting process. It is now acknowledged that in the vast majority of cases (even in those semiconductors, like GaP, with relatively

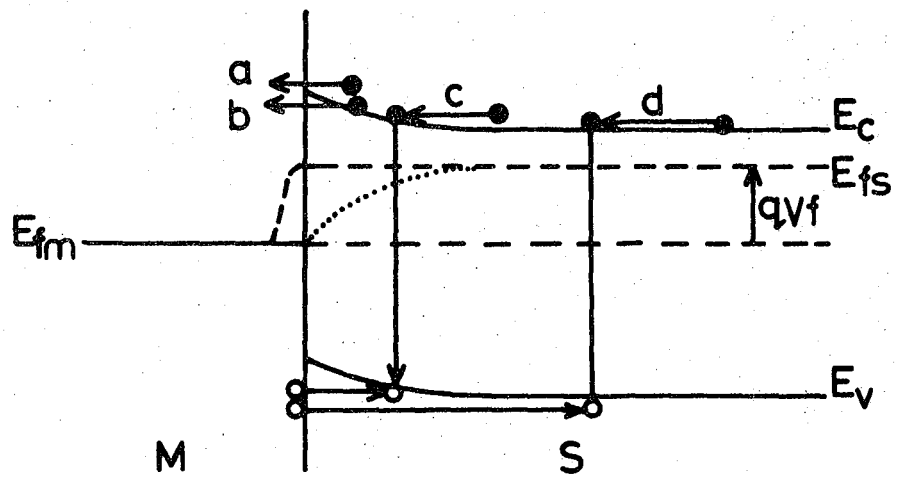

Figure 3.5 Schematic diagram depicting basic current transport processes in an MIS diode under forward bias.

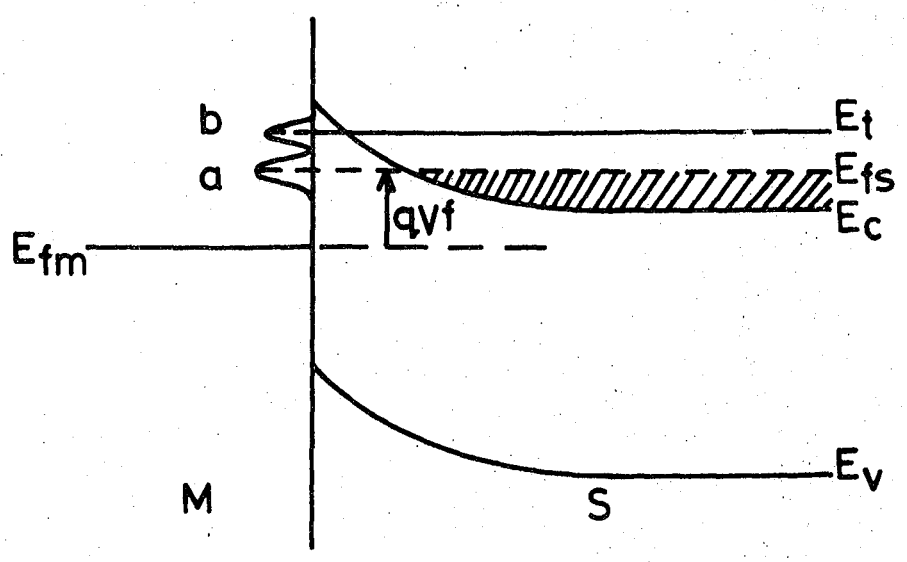

Figure 3.6 Field and thermionic field emission in a degenerately doped Schottky barrier structure.

low mobilities), the current-voltage characteristics are best described by the thermionic emission theory and this is discussed next in some detail.

(a) Emission Over the Barrier

(i) Thermionic Emission Theory. Since, under non-equilibrium conditions, the change in the quasi-Fermi level with distance is indicative of the 'driving force' behind the carrier flow (see appendix A), then this theory is tantamount to assuming that the electron quasi-Fermi level is flat throughout the depletion region and coincident with the Fermi level in the semiconductor bulk. (In order to account for the discontinuity of the Fermi level at the surface, one must either assign the energetic electrons which enter the metal their own quasi-Fermi level, as shown in fig. 3.5, or assume that thermal equilibrium is established at the metal-semiconductor plane.) It follows that the electron concentration in the semiconductor, at the interface, is given by

$$n = N_c \exp. \{ -q (\phi_{bn} - V)/kT \} \qquad (3.9)$$

where N_c is the effective density of states in the conduction band and V is the applied voltage. For a semiconductor in which the electrons have an isotropic velocity distribution (i.e. spherical constant energy surfaces), the number of electrons impinging on unit area of the interface per second can be shown (by kinetic theory) to be $n\bar{v}/4$, where $\bar{v}$ is the average electron thermal velocity. Thus, the current density passing from the semiconductor to the metal, J_{sm} is given by

$$J_{sm} = \frac{qN_c\bar{v}}{4} \left\{ \exp [-q (\phi_{bn} - V)/kT] \right\} \qquad (3.10)$$

Since there is a flow of electrons into the metal even at zero bias, there must be an equal and opposite flow from the metal which is governed by the value of ϕ_{bn} and is thus independent of bias. The total current is given by

$$J = \frac{N_c \bar{v}}{4} \exp (-q\phi_{bn}/kT) \{ \exp (qV/kT) - 1 \} \qquad (3.11)$$

Since for a maxwellian velocity distribution $\bar{v} = (8kT/\pi m^*)^{\frac{1}{2}}$, then J is given by

$$J = A^* T^2 \exp (-q\phi_{bn}/kT) \{\exp (qV/kT) - 1\} \qquad (3.12)$$

where $A^* = 4\pi m^* qk^2/h^3$; m^* is the electron effective mass and h is Planck's constant. The term A^* is the effective Richardson constant which accounts for the electron effective mass, but neglects the effect of optical phonon scattering and quantum mechanical reflection[24]. Eq. (3.12) is often written in the form

$$J = J_o \{\exp (qV/kT) - 1\} \qquad (3.13)$$

where the reverse saturation current density, J_o, is given by

$$J_o = A^* T^2 \exp (-q \phi_{bn}/kT) \qquad (3.14)$$

These equations represent the thermionic emission theory for current flow in an ideal Schottky diode.

(ii) The Diffusion Theory. In contrast to the thermionic emission theory, the assumptions inherent in the diffusion theory are the equivalent of assuming that the electrons in the semiconductor, at the interface,

are in equilibrium with the metal. This implies that the electron quasi-Fermi level (as shown by the dotted line in fig. 3.5) is not flat throughout the depletion region, indicating that the processes of drift and diffusion in this region represent the main impediment to current flow. Beginning with the general equation for the current flow in the depletion region i.e.

$$J = qn\ \mu_n E + q D_n \left(\frac{dn}{dx}\right) \tag{3.15}$$

(where μ_n is the electron mobility; D_n is the electron diffusion coefficient) and assuming that E, the electric field in the barrier, is constant and equal to E_{max}, it can be shown[25] that the current density is given by

$$J = q N_c \mu_n E_{max} \exp(-q \phi_{bn}/kT) \{\exp(qV/kT) - 1\} \tag{3.16}$$

$$\text{or} \quad J = J_d \{\exp(qV/kT) - 1\} \tag{3.17}$$

In this case, however, J_d is not a saturation current since E_{max} is a function of bias which causes J_d to increase with the applied voltage.

(iii) The Thermionic Emission - Diffusion Theory. In the most general case, the current will be determined by a combination of the two limiting theories. Such a combination has been derived by Crowell and Sze[24] in which the current density is given by the expression

$$J = \left(\frac{qN_c v_r}{1 + v_r/v_d}\right) \exp(-q \phi_{bn}/kT) \{\exp(qV/kT) - 1\} \tag{3.18}$$

where v_r is an effective recombination velocity at the potential energy maximum, and v_d is an effective diffusion velocity for the transport of

electrons from the edge of the depletion region to the potential energy maximum.

However, it has been shown theoretically[26] that diodes fabricated on reasonably high mobility semiconductors should behave according to the thermionic emission theory. This has been confirmed experimentally for the vast majority of Schottky diodes, even those with relatively low mobilities. Nevertheless, practical diodes invariably deviate from the ideal behaviour predicted by eq. (3.13). In particular, graphs of ln J versus V (which should be linear for $V \gtrsim 3kT/q$) do not exhibit the predicted slope of q/kT. Instead they can be described by the relation

$$J = J_o \exp (qV/nkT) \qquad (3.19)$$

for $V \gtrsim 3kT/q$. The parameter 'n' is known as the ideality factor and has a value greater than, or equal to, the ideal value of unity. The most common cause of this departure from ideality is due to the bias-dependence of the barrier height which arises primarily from the presence of an interfacial layer (see § 3.4). However, even in the absence of such a layer, the barrier height is still bias-dependent because of the effect of the image force, which itself depends on the applied bias. The value of n depends critically on the diode preparation procedure and, with care, values very close to unity can be repeatedly obtained using normal laboratory techniques.

Reverse Characteristics

Eq. (3.13) predicts a reverse current density which saturates at the value of J_o given by eq. (3.14). This is due to the thermionic emission of electrons from the metal over the barrier and into the semiconductor. However, any bias-dependence of the barrier height will prevent the

reverse current from saturating. The magnitude of this effect is governed by the same factors which influence the ideality factor of the forward bias characteristics.

(b) Quantum Mechanical Tunnelling Through the Barrier

In heavily doped materials at low temperature, it is possible for an appreciable current to flow due to electrons, with energies less than the barrier height, traversing the barrier by quantum mechanical tunnelling. This has been studied extensively[27, 28] and both field emission and thermionic-field emission have been identified. The tunnelling current is a function of the transmission coefficient, the occupancy of the states in the semiconductor, and the available states in the metal. Consequently, in a degenerate semiconductor at very low temperatures (under forward bias), the energy distribution of the tunnelling electrons is centred around the semiconductor Fermi energy. This is field emission and is depicted by process (a) in fig. 3.6. If the temperature is increased, the excited electrons 'see' a narrower (and lower) potential barrier and a second distribution, centred around E_t (the Fermi energy plus the thermal energy), is evident. This is thermionic field emission, i.e. process (b) in fig.3.6.

The forward bias current density - voltage characteristic is described by[27]

$$J = J_s \exp (V/E_o) \qquad (3.20)$$

where $E_o = E_{oo} \coth (q E_{oo}/kT)$ and $E_{oo} = \frac{h}{4\pi} \left(\frac{Nd}{m^* \varepsilon_s} \right)^{\frac{1}{2}}$

The term J_s is a function of both the temperature and the barrier height[28].

Reverse Characteristics

Tunnelling from the metal into the semiconductor is much more dominant a process than in the corresponding forward bias case. This is due to the

fact that, under reverse bias the electrons, at a given energy in the metal, 'see' a narrower barrier (see § 2.2.2). It represents a further departure from the ideal reverse bias characteristic and is a common cause of its non-saturation in practical devices.

(c) Recombination in the Depletion Region

This process has previously been discussed when it was considered as a non-radiative recombination path for injected minority carriers. The importance of this mechanism when compared to the other processes depends critically on the particular system investigated. It can, in some cases, significantly affect the forward current-voltage characteristic[29]. This current can be analysed[29] using Schockley-Read-Hall statistics by assuming that recombination proceeds via a centre located approximately mid-gap. Then the current density is given by

$$J = J_r \exp (qV/2kT) \qquad (3.21)$$

where $J_r = q\, n_i\, W/\tau$, n_i is the intrinsic carrier concentration, W is the width of the depletion region and τ is the lifetime in the depletion region. This process can affect both the ideality factor, n, and the saturation current density, J_o, of eq. 3.13 and is particularly evident at low temperatures when the thermionic emission process is much reduced.

Reverse Characteristics

Under reverse bias conditions, the opposite process occurs, namely, generation in the depletion region. Electron-hole pairs thus formed are separated and swept away by the electric field which gives rise to an additional current component. This is proportional to the width of the depletion region and consequently increases with reverse bias thus preventing current saturation.

3.3.4 The Capacitance of a Schottky Barrier

The capacitance of a Schottky barrier arises from the charge due to ionised donors in the depletion region and an equal, opposite charge on the surface of the metal. Since the width of the depletion region varies with applied bias then the capacitance is also a function of bias. The depletion approximation can be employed to simplify the analysis. This states that the charge density is constant and equal to qN_d up to the edge of the depletion region and equal to zero past this position. Then the charge in the depletion region is given by Gauss's law as

$$Q_d = (2\varepsilon_s q N_d V_d)^{\frac{1}{2}} \qquad (3.22)$$

when Nd is the donor density and Vd is the diffusion voltage. This is the case for zero bias; under the application of a reverse bias, Vd is replaced by $V_d' = V_d + V_r$ which is a measure of the degree of band bending in the semiconductor. The capacitance is usually measured by superimposing a small alternating voltage onto the D.C. bias and, consequently, it is the response of the charge distribution to the AC signal which gives rise to the capacitance; i.e. the differential capacitance is measured. This capacitance (per unit area) is given by

$$C = \frac{dQ_d}{dV} = \left(\frac{q\varepsilon_s N_d}{2(V_d+V_r)} \right)^{\frac{1}{2}} \qquad (3.23)$$

A more rigorous analysis, allowing for the effect of a non-abrupt depletion region, yields

$$C = \left\{ \frac{q\ \varepsilon_s\ N_d}{2(V_d + V_r - kT/q)} \right\}^{\frac{1}{2}} \qquad (3.24)$$

An assumption, inherent in the above analysis, is that the charge in the semiconductor is due solely to ionised donors. This is incorrect if there is an appreciable concentration of holes at the semiconductor surface, as would be the case if the surface were inverted. In such a situation the charge due to the holes must be subtracted from Qd and this complicates the theory considerably[30]. The effect is essentially to replace Vd in eq. (3.24) with a bias dependent voltage, and this results in a non-linear C^{-2} - Vr relationship (see § 3.3.5).

Practical Schottky diodes contain deep traps, due to unintentional impurities or defects, which may be filled or emptied according to external stimuli and consequently affect the capacitance. In fact this forms the basis of a wide range of capacitance spectroscopy techniques, a good account of which can be found in ref. (31).

3.3.5 Measurement of Barrier Height

There are a number of methods by which the Schottky barrier height, ϕ_{bn}, may be deduced. These are now discussed in sequence.

(a) Current-Voltage Measurements

The forward bias current density-voltage characteristic of a near-ideal Schottky diode is given by the thermionic emission theory as

$$J = J_o \exp.(qV/nkT) \text{ for } V \gtrsim 3kT \quad \text{i.e. eq. (3,19)}$$

where $J_o = A^* T^2 \exp.(-q\phi_{bn}/kT)$

Consequently, a plot of ln(J) against V can be used to determine both the ideality factor and the Schottky barrier height according to the following equations.

$$\text{Slope} \equiv \frac{d(\ln J)}{dV} = \left(\frac{q}{kT}\right) \cdot \left(\frac{1}{n}\right)$$

$$\text{i.e. } n = \left(\frac{d(\ln J)}{dV}\right)^{-1} \times \frac{q}{kT} \qquad (3.25)$$

and intercept $\ln J_o = \ln A^* T^2 \exp(-q\phi_{bn}/kT)$

$$\text{i.e. } \phi_{bn} = \left\{\frac{kT}{q} \ln\left(\frac{A^* T^2}{J_o}\right)\right\} \qquad (3.26)$$

It should be noted that the value of J_o, determined from the intercept, is only strictly accurate if the ideality factor is equal to unity. In practice the condition $n \lesssim 1.2$ is often taken as the requirement for an accurate determination of ϕ_{bn}, although it will be demonstrated later in this thesis that this criterion is not always valid.

In a real diode there is a resistance associated with the semiconductor bulk and near-Ohmic back contact which is in series with the surface barrier. This has the effect that for large values of applied bias, eq. (3.19) is no longer valid, since the current begins to be limited by this series resistance. For sufficiently large bias, the characteristic is dominated by the series resistance and the curve may obey Ohm's law. This so-called 'far-forward bias' regime has been used by some authors to estimate the diffusion potential and hence the barrier height[32]. The technique assumes that in this regime the applied voltage is divided according to the relation

$$Va \simeq Vd + IRs \qquad (3.27)$$

where Rs is the diode series resistance and I is the current. (i.e. Voltage in excess of that required to flatten the bands in the semiconductor is dropped across the series resistance.) Consequently, a plot of I against Va is, to a first approximation, linear with an intercept on the voltage axis equal to the diffusion voltage.

Reverse Characteristics

The barrier height may also be determined from the reverse current since the thermionic emission theory predicts that this characteristic should saturate at a value given by J_o. In this situation ϕ_{bn} can be determined using eq. (3.26). However, the fact that in practical diodes the reverse current rarely saturates (due to one or more of the processes discussed in § 3.3.3), limits the usefulness of this technique. Furthermore, if the barrier height is large, then the reverse current is often undetectable which has been the case in most of the diodes studied in this work.

If either the active device area, Aa, or the relevant value of A^* is unknown, then an activation energy plot can be used to determine ϕ_{bn}. For example, a graph of $\ln (I_o/T^2)$ versus $1/T$ should give a slope of $-q\phi_{bn}/kT$ and an intercept on the vertical axis of $\ln(A^* Aa)$. In addition, there are a number of modified versions of this technique which have been developed to overcome specific problems. For example, one such modification[33] enables ϕ_{bn} to be measured even in the presence of a large series resistance, which would prevent its measurement from the usual J-V characteristic. All of these techniques suffer from the disadvantage of being tedious to employ and are therefore only used when the more straightforward methods fail.

(b) Photoelectric Measurement

The photoelectric determination of the Schottky barrier height involves shining monochromatic light, of varying wavelength, onto the metal barrier

electrode and monitoring the current due to photoexcited electrons in the metal which surmount the barrier and are collected by the electric field in the depletion region. Fowler[34] studied the photoresponse of clean metal surfaces to monochromatic light and developed the theory upon which this technique is based. The photocurrent per absorbed photon R is given by the Fowler theory[34] as

$$R \sim \frac{T^2}{(Es-h\nu)^{\frac{1}{2}}} \left\{ \frac{x^2}{2} + \frac{\pi^2}{6} - \left(e^{-x} - \frac{e^{-2x}}{4} + \frac{e^{-3x}}{9} - \frac{e^{-4x}}{16} + \ldots \right) \right\} \quad (3.28)$$

$$\text{for } x \geq 0; \quad \text{where } x = h(\nu - \nu_o)/kT \quad (3.29)$$

The term $h\nu_o$ represents the Schottky barrier height, ϕ_{bn}, and Es is equal to the sum of ϕ_{bn} and the Fermi energy (measured from the bottom of the metal conduction band). Provided Es >> $h\nu$ (a condition which is almost always valid) and $h\nu - h\nu_o \gtrsim 3kT$, then to a good approximation eq. (3.28) reduces to

$$R = C(h\nu - h\nu_o)^2 \quad (3.30)$$

where C is a constant. Thus, a plot of $R^{\frac{1}{2}}$ versus $h\nu$ is linear over a certain range of energy and the intersection of this linear region with the energy axis gives a direct measurement of the barrier height. The range over which eq. (3.30) is valid is determined, at low energy, by the requirement $x \gtrsim 3$, and at high energy by the condition that Es >> $h\nu$. In practice, however, the high energy limitation is usually due to the generation of free carriers in the depletion region as $h\nu$ approaches the value of Eg. This effect can be reduced by employing a relatively thick top electrode in order to reduce the amount of light being transmitted to the semiconductor. Since the mean free path of a photoexcited

electron in a metal can be quite large[35] ($\sim$ 75 nm in gold), electrodes which are almost opaque can be used effectively. The same technique has been used to eliminate non-linearities in these 'Fowler' plots due to the photoexcitation of carriers from surface states by light of energy, $h\nu < Eg$[36]. However this is usually a problem only when there is a significant interfacial layer present (see § 3.4).

(c) Capacitance Measurements

The differential capacitance associated with the Schottky barrier depletion region is given by eq. (3.24) which may be written as

$$C^{-2} = 2(Vd - kT/q + Vr)/q\varepsilon_s Nd \qquad (3.31)$$

Thus, a plot of C^{-2} against Vr should be linear (provided Nd is constant in the depletion region) with an intercept, V_o, on the voltage axis given by

$$V_o = Vd - \frac{kT}{q} \equiv \phi_{bn} - \varepsilon - \frac{kT}{q} \qquad (3.32)$$

where ε is the difference between the conduction band edge and the Fermi level in the semiconductor bulk (as shown in fig. 3.3(a)). That this technique should measure Vd (and not ϕ_{bn}) results from the fact that extrapolating to the voltage at which $C^{-2} = 0$, i.e. the capacitance is infinity, indicates the voltage at which the band-bending is eliminated, i.e. Vd. Furthermore, since the technique does not involve the idea of charge carriers approaching the barrier (and consequently the concept of image charge), then the value of ϕ_{bn} deduced from such a measurement does not include the effect of Schottky barrier lowering. The term 'ε' is given by

$$\varepsilon = kT/q \ln (Nc/Nd) \qquad (3.33)$$

which can easily be computed since the value of Nd can be inferred from the slope of the C^{-2} - V plot.

Of the techniques described previously for the determination of the barrier height, the capacitance method is the least direct. Both the J-V and photoelectric techniques involve processes whereby carriers actually surmount the barrier, and therefore include the effect of processes such as image force lowering. Furthermore, the capacitance technique is, in general, the most unreliable and inaccurate since it is highly susceptible to the presence of an interfacial layer[37]. Nevertheless, for the near-ideal diodes considered in this section, good agreement can be expected using the various techniques.

The photoelectric method is the most accurate, since it directly measures the minimum energy required by an electron in order to surmount the barrier. It is generally regarded to be the definitive measurement and to provide the only irrefutable value for ϕ_{bn}. However, new results for GaP described in chapter 7 cast some doubt on its general applicability.

3.3.6 Minority Carrier Injection

The minority carrier injection ratio , γ, is defined as the ratio of the minority carrier current, Jp, to the total current.

i. e.
$$\gamma = \frac{Jp}{Jp + Jn} \simeq \frac{Jp}{Jn} \qquad (3.34)$$

provided the majority carrier current, Jn >> Jp (i.e. assuming low injection conditions). Rhoderick[38] has shown that, in addition to assuming an electron quasi-Fermi level that is flat in the depletion region, the hole quasi-Fermi level can be assumed flat throughout this region and coincident with the metal Fermi level at the interface (see Appendix A). This indicates that for the hole current, the limiting

mechanism is not emission over the barrier but rather the processes of drift and diffusion in the semiconductor bulk. If the applied bias is assumed to be sufficiently low so that diffusion is the dominant mechanism, then the hole current density can be expressed using p-n junction theory as

$$Jp = \frac{qD_p}{L}\,(p(w) - p_{no}) = \frac{qD_p\,p_{no}}{L}\left(\exp(qV/kT) - 1\right) \qquad (3.35)$$

where L is the width of the quasi-neutral region in the semiconductor (assumed to be less than the minority carrier diffusion length), p_{no} is the equilibrium concentration of holes and p(W) is the concentration at the edge of the depletion region. Then γ is given by eq. (3.34) as

$$\gamma = \frac{q\,D_p\,n_i^2}{Nd\,L\,A^*T^2\exp(-\phi_{bn}/kT)} \qquad (3.36)$$

This expression has been verified experimentally[29] for low injection conditions in silicon diodes. Using typical values for gold/(n)Si diodes, eq. (3.36) yields a γ value of the order of 10^{-5}. It is for this reason that the near-ideal Schottky diode is often termed a majority carrier device. Scharfetter[21] has considered the effect of including the drift component in the analysis and showed that for current densities greater than a critical value, J_c, the injection ratio increases linearly from that predicted by eq. (3.36). This critical current density is given by

$$J_c = q\,D_n\,Nd/L \qquad (3.37)$$

above which γ is given by

$$\gamma = \frac{n_i^2 J}{bNd^2 J_o} \qquad (3.38)$$

where b is the mobility ratio. This increase has been demonstrated experimentally[29], although only over a limited range and, in fact, the theory has been extended by Green and Schewchun[39] who predict a limit to the increase in γ due to both a limit in the supply of holes (by thermionic emission over the hole barrier at the surface), and the fact that Jp becomes comparable with Jn.

The value of J_c is typically of the order of 100 A cm^{-2} which is much larger than the current densities employed in this study and the effect is not significant in the LED work described in this thesis.

3.4 THE METAL - THIN INSULATOR - SEMICONDUCTOR DIODE

In this section, the inclusion of an insulator which has an appreciable effect on the device properties is considered. In this situation the insulator can no longer be considered as transparent to tunnelling electrons and represents a significant additional barrier to carrier transport. The band diagram for the MIS diode (a) in equilibrium and (b) under conditions of forward bias are shown in fig. 3.7. It can be seen that the applied voltage, V_f, is developed partially across the semiconductor depletion region, ΔVd, and partially across the interfacial layer, ΔV_i. A consequence of this is that the interface state charge is not fixed, it is bias dependent and, depending on the properties of the interfacial layer, may be determined by interactions with either the metal or the semiconductor. Under conditions of forward bias, the relative shift between the metal Fermi level and the semiconductor band structure, which gives rise to both the change in interface state charge and a bias dependent barrier height, can be seen in fig. 3.7. This is in contrast to the near-ideal situation depicted in fig. 3.3

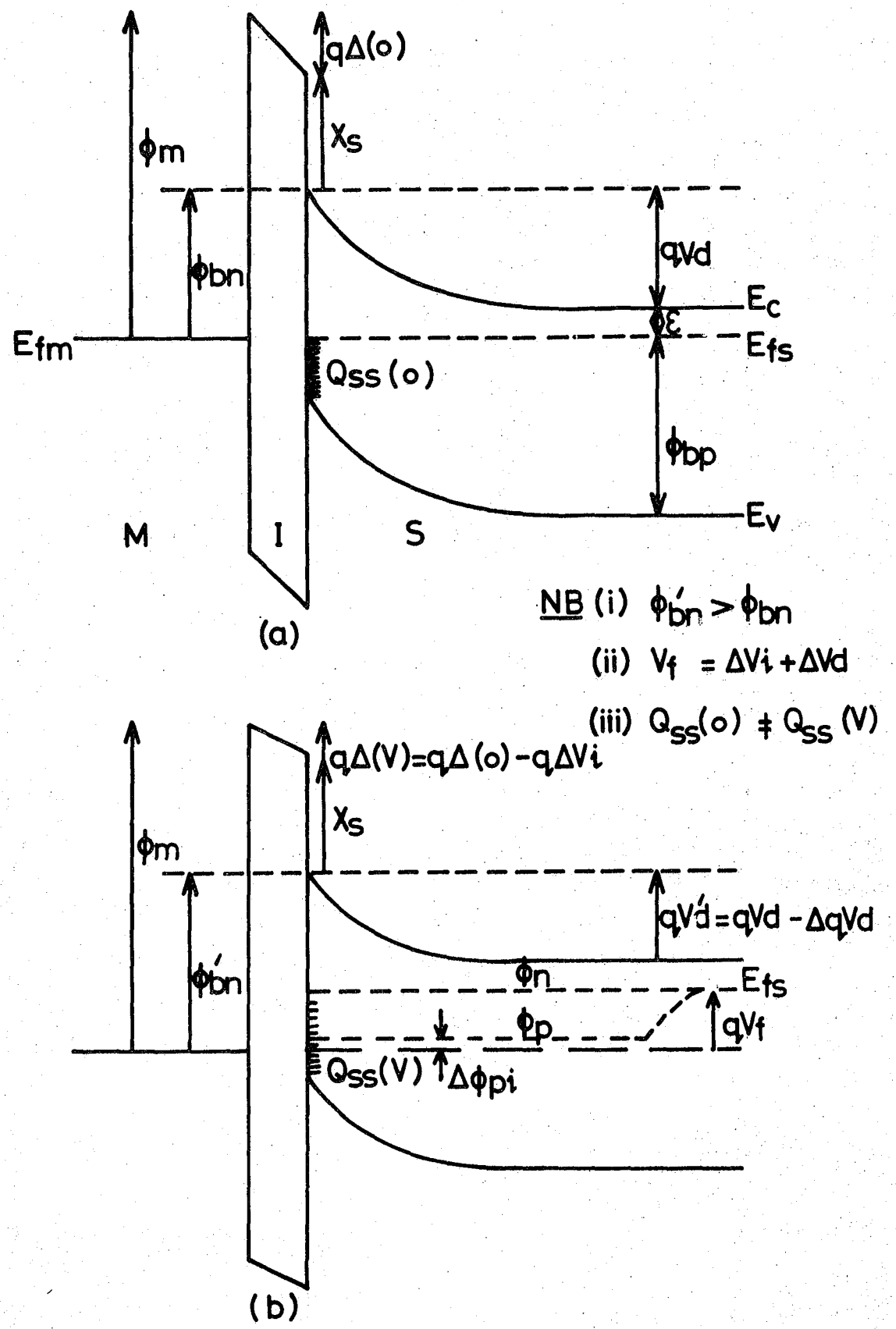

Figure 3.7 Energy band diagram of an MIS diode, (a) in equilibrium and (b) under forward bias showing the behaviour of the quasi-Fermi levels.

where ΔV_i was assumed to be negligible and the band edges at the surface were ' pinned' relative to the position of the metal Fermi level.

3.4.1 Modifications to Schottky Barrier Theory

The modifications to the theory discussed in §3.3 (which are necessary to account for the effects on an appreciable insulating layer) are now discussed.

(a) Current-Voltage Characteristics

The effect of such an insulator on the J-V characteristics has been considered by Card and Rhoderick[40]. They divided the interface states into two groups, one of which communicates more easily with the metal, the other with the bands in the semiconductor. The relative densities of these two groups is determined essentially by the thickness of the interfacial layer. By making a number of assumptions[40] they were able to show that the main effect of the layer was to alter the pre-exponential, J_o, term in eq. (3.19) to give

$$J = J_{oo} \exp (qV/nkT) \tag{3.39}$$

where $J_{oo} = J_o \exp (-\chi^{\frac{1}{2}}\delta) = A^*T^2 \exp (-\chi^{\frac{1}{2}}\delta) \exp (-q\phi_{bn}/kT)$ (3.40)

χ is the mean barrier height (in eV) presented by the energy gap of the insulating layer and δ is its thickness in Angstrom units. (In fact there is a constant with units of $(eV^{-\frac{1}{2}} \text{Å}^{-1})$ and a value of very close to unity which has been omitted from the term $(-\chi^{\frac{1}{2}}\delta)$ for simplicity.) In addition to this effect, the ideality factor is also affected by the presence of the insulator. It is governed predominantly by the bias-dependence of ϕ_{bn} which originates from a combination of the voltage drop in the insulator and the subsequent change in the interface state charge density. In this case the ideality factor is given by[40]

$$n = 1 + \frac{(\delta/\varepsilon_i)\,(\varepsilon_s/W + q\,Dsb)}{1 + (\delta/\varepsilon_i)\,q\,Dsa} \qquad (3.41)$$

where Dsa and Dsb are the density of interface states which communicate with the metal and semiconductor respectively. For very thin insulators Dsa >> Dsb; eq. (3.41) reduces to

$$n \simeq 1 + \frac{\delta\,\varepsilon_s}{W(\varepsilon_i + \delta q Dsa)} \qquad (3.42)$$

Conversely, for thicker insulators, Dsb >> Dsa and n is given by

$$n \simeq 1 + \frac{\delta}{\varepsilon_i}\left\{\frac{\varepsilon_s}{W} + qDsb\right\} \qquad (3.43)$$

A third limiting case exists, namely when the density of interface states, of either group, is very low then eq.(3.41) reduces to

$$n \simeq 1 + \frac{\delta\varepsilon_s}{W\varepsilon_i} \qquad (3.44)$$

Eq. (3.42) is the result derived by Crowell & Sze[24] who had earlier approached this problem by assuming that the interface states were all in equilibrium with the metal Fermi level.

Reverse Characteristics

The main effect of the insulator on the reverse characteristics is to prevent the current from saturating with increasing reverse bias. This,

again, is a consequence of the bias-dependence of ϕ_{bn}, but in this case ϕ_b decreases with bias. It is similar to the effect of the image force (see §3.3.3) in this respect but is much more pronounced and therefore usually dominates.

It is clear from the above discussion that the analysis of the J-V curves from MIS diodes is much more difficult than in the Schottky barrier case. In particular, the value of $(\chi^{\frac{1}{2}}\delta)$ is almost impossible to predict since it must represent an average term due to the fact that both χ and δ are likely to vary over the area of the electrode. This point was stressed by Card and Rhoderick who showed that experimentally-determined values of $(\chi^{\frac{1}{2}}\delta)$ differed greatly from those predicted using the relevant bulk values. It is often assumed that the condition $n \lesssim 1.2$ is justification for assuming that the diode is near ideal and thus employing eqs. (3.19) and (3.14) to evaluate ϕ_{bn}. The general validity of this assumption must be questionable as it is possible to envisage situations where the interfacial layer has only a small effect on n but a significant effect on J_o. Indeed, in chapters 6 and 7, results will be presented which show ideality factors of close to unity even though the insulating layer is thick and has a pronounced effect on the other diode characteristics.

(b) Capacitance - Voltage Characteristics

The use of C^{-2} -V characteristics to determine Vd, and hence ϕ_{bn}, has been discussed previously. However, in many practical cases the barrier height calculated from such a plot far exceeds that measured by the photoelectric or J-V techniques[37]. Goodman[41] has studied many different parameters which may influence these characteristics and showed that the intercept, V_o, of the C^{-2}-V plot is always greater than Vd when there is an interfacial layer present. Cowley[37] extended this analysis to include the effect of both the insulator and the bias-dependent interface states. He developed a number of models in an attempt to obtain some

quantitative agreement with his experimental data, obtained for diodes fabricated on GaP. His results have been widely used in the literature to analyse non-ideal C^{-2} -V plots and more recently[42] the same approach was used to derive a general expression (for C^{-2} as a function of V) where the interface states were divided into the two groups Dsa and Dsb described previously. The approach which was used can most easily understood by considering first an MIS diode without interface states:

In terms of the energies defined in fig. 3.7(a), ϕ_{ms} can be defined as

$$\phi_{ms} = \phi_m - (\chi_s + \varepsilon) \qquad (3.45)$$

$$\text{i.e. } \phi_{ms} = Vd + \Delta(o) \qquad (3.46)$$

Using Gauss' law to relate the charge in the depletion region, Qd, to the potential, $\Delta(o)$, yields (using the depletion approximation)

$$\Delta(o) = (\delta/\varepsilon_i)\,(2q\,\varepsilon_s\,Nd\,Vd)^{\frac{1}{2}}$$

$$\text{or } \Delta(o) = V_1^{\frac{1}{2}}\,Vd^{\frac{1}{2}} \qquad (3.47)$$

$$\text{where } V_1 = 2q\,\varepsilon_s\,Nd\,\delta^2/\varepsilon_i^2 \qquad (3.48)$$

Under the application of a reverse bias, $\Delta(v)$ replaces $\Delta(o)$ and Vd' replaces Vd. Then eqs. (3.46) and (3.47) can be written as

$$\phi_{ms} + V = Vd' + \Delta(v)$$

$$\text{and } \Delta(v) = V_1^{\frac{1}{2}}\,Vd'^{\frac{1}{2}}$$

Eliminating $\Delta(v)$ from these equations yields

$$\phi_{ms} + V = Vd' + V_1^{\frac{1}{2}}\,Vd'^{\frac{1}{2}} \qquad (3.49)$$

The semiconductor space charge is given by Gauss' law as

$Qd = (2q\varepsilon_s\ Nd\ Vd')^{\frac{1}{2}}$, and hence the differential capacitance is given by

$$C = \frac{dQd}{dV} = (2q\ \varepsilon_s\ Nd)^{\frac{1}{2}} \left\{ \frac{d(Vd'^{\frac{1}{2}})}{dV} \right\} \qquad (3.50)$$

The quadratic equation (3.49) can be solved and substituted into eq. (3.50) to yield

$$C = (2/q\ \varepsilon_s\ Nd)^{\frac{1}{2}}\ (\phi_{ms} + V + V_1/4)^{-\frac{1}{2}}$$

$$\text{i.e. } C^{-2} = (2/q\ \varepsilon_s\ Nd)\ (V + Vd + V_1/4 + V_1^{\frac{1}{2}}\ Vd^{\frac{1}{2}}) \qquad (3.51)$$

Thus a graph of C^{-2} against V is linear with a slope equal to that of the simple Schottky barrier case but an intercept which is significantly larger.

If the effect of interface states is included, the analysis is somewhat more complicated: Assuming that both type (a) and (b) interface states are uniformly distributed, i.e. Dsa and Dsb are both constant as a function of energy, then the change in the interface state charge, under the application of a bias can be shown to be

$$\Delta Qss = qDsbV - qDsb\ \Delta V_i - qDsa\ \Delta V_i \qquad (3.52)$$

Also $\Delta(o)$ and $\Delta(v)$ are now given by the modified expressions

$$\Delta(o) = V_1^{\frac{1}{2}}\ Vd^{\frac{1}{2}} + \delta/\varepsilon_i\ Qss(o)$$

and $$\Delta(v) = V_1^{\frac{1}{2}}\ Vd'^{\frac{1}{2}} + \delta/\varepsilon_i\ Qss(v)$$

$$\text{i.e } \Delta V_i = V_1^{\frac{1}{2}}\ (Vd'^{\frac{1}{2}} - Vd^{\frac{1}{2}}) + \delta/\varepsilon_i\ \Delta Qss \qquad (3.53)$$

The approach used initially by Cowley[37], and later followed in ref (42), was to substitute eq. (3.52) into (3.53), solve for $Vd'^{\frac{1}{2}}$ and to use eq. (3.50) to determine C. The following expression is obtained

$$C^{-2} = 2\frac{(1+\alpha_1+\alpha_2)}{q\varepsilon_s Nd(1+\alpha_1)}\left\{\frac{V_1 \quad V_1}{4(1+\alpha_1+\alpha_2)(1+\alpha_1)} + \frac{V_1^{\frac{1}{2}} Vd^{\frac{1}{2}}}{(1+\alpha_1)} + \right.$$

$$\left. \frac{Vd\,(1+\alpha_1+\alpha_2)}{(1+\alpha_1)} + V \right\} \qquad (3.54)$$

where $\alpha_1 = qDsa\delta/\varepsilon_i$ and $\alpha_2 = qDsb\,\delta/\varepsilon_i$.

Very recently, however, Fonash[43] has re-examined the problem and pointed to a flaw in the argument used by Cowley and in subsequent analyses. This concerns the use of eq. (3.53), which is essentially a quasistatic relationship derived simply by the summation of potentials, in the equation (3.50) for the <u>differential</u> capacitance. The point being that, if the charge in the interface states (in group (a) or (b)) can not respond to the high frequency measuring signal, then the quasistatic expression for Vd' (obtained from eq. (3.50)) does not accurately describe the variation of Vd' in response to this signal. It in fact describes the variation in Vd' with respect to the applied d.c. bias. Fonash[43] has used the correct (a.c.) variation of Vd' to analyse several models and has predicted that in only two cases is the slope of the C^{-2} -V plot constant with bias. These are, the simple case of Dsa = Dsb = 0 (eq. (3.51)) and the situation when all of the interface states communicate with the metal, i.e. Dsb = 0, and can follow the applied signal. In this latter case, the expression derived by Fonash[43] is

$$C^{-2} = \frac{2}{e\,\varepsilon_s\,Nd}\left\{\frac{V_1}{4(1+\alpha_1)^2} + \frac{V_1^{\frac{1}{2}}\,Vd^{\frac{1}{2}}}{(1+\alpha_1)} + Vd + V\right\} \qquad (3.55)$$

In all of the other cases, Fonash[43] predicts a non-linear C^{-2} -V plot even for a uniform density of states. It is interesting to note that the characteristics observed consistently in this, and other studies (of highly linear C^{-2} -V curves whose slope and intercept increase with film thickness) is not predicted by any of the models analysed by Fonash. This will be considered in more detail in chapter 7 when the C-V data are analysed.

Before proceeding, it is useful to reconsider the original analysis of Cowley[37]. In that work, the aim was to develop a model which agreed quantitatively with the data obtained using GaP MIS diodes incorporating interfacial 'oxides' resulting from the fabrication procedure. In order to achieve this, Cowley essentially chose an arbitrary function to relate the change in the interface state charge (with bias) to the thickness of the interfacial layer and hence, despite the flaw in his argument, the final model gave a good description of his experimental results. Since the 'non-ideal' diodes described in this work in chapter 6 also contained an interfacial 'oxide' resulting from the fabrication procedure, the model developed by Cowley is used later in this thesis to infer an approximate value for the thickness of the interfacial layer. Such a value can only be considered as very approximate since it must be assumed that the two interfacial layers possess similar properties.

The interpretation of the C-V characteristics of thin-MIS diodes is clearly a very complex problem and due consideration must be given when attempting such an analysis. In particular, the intercept on the

voltage axis of the C^{-2} -V curve cannot, in general, be considered as an accurate measurement of the diffusion voltage.

(c) The Photoelectric Measurement of Barrier Height

The direct measurement of metal-semiconductor barrier heights in MIS diodes has been the subject of a number of studies (see for example, ref. (36) and references contained therein). However, in most cases the measurement is hampered by the presence of non-linearities in the Fowler plots which make the extrapolation to zero photoresponse very difficult. The problem has been shown to increase with increasing insulator thickness and has been attributed to the photoexcitation of carriers from interface states: If a diode is illuminated from the front surface and the barrier electrode is reasonably thin, and hence transparent, then the light may not all be absorbed by the metal and can therefore promote electrons trapped in interface states into the semiconductor conduction band. This generates an additional current, in parallel to the photoexcitation of carriers from the metal, which does not conform to the Fowler theory. In a near-ideal diode this additional current is swamped by the relevant response, since the photoexcited electrons in the metal can readily tunnel through the interfacial layer. As the insulator thickness is increased, its transmission coefficient is decreased and the unwanted, parallel component becomes appreciable. Arora et al[36] have shown that such anomalies can be largely eliminated by using a thick ($\sim$ 50nm) barrier electrode. In this case most of the light is absorbed with $\sim$ 15 nm of the free surface and hence does not pass through to the interface. However, the photoexcited carriers can have mean free paths in excess of 50nm ($\sim$ 75nm in gold films[35]) and can therefore easily reach the metal-insulator interface.

3.4.2 Minority Carrier Injection

The effect of an interfacial layer on minority carrier injection has been analysed by Card and Rhoderick[44] who approached the problem theoretically and found qualitative agreement with their experimental results. The enhancement of minority carrier injection in MIS structures was described briefly in § 2.4.3 and from that discussion it is clear that both the insulator thickness and the degree of band realignment between the metal Fermi level and the semiconductor band structure are the important parameters: The insulator must be sufficiently thick so that a significant degree of band realignemnt may occur, but not too thick to prevent the minority carriers from tunnelling into the semiconductor with relative ease. It is convenient to discuss, separately, the effect of thin and thicker insulators.

(a) Thin Insulators

Since tunnelling can take place relatively easily through very thin insulators, the minority carrier current is limited by the rate of diffusion into the bulk (as in the case of a p-n junction) and not by the barrier presented by the insulator. For extremely thin insulators, the hole current is well described by eq. (3.35), i.e.

$$Jp = \frac{qD_p p_{no}}{L} \{ \exp (qV/kT) - 1 \}$$

since $\Delta\phi_{pi}$, the change in the hole quasi-Fermi level across the insulator, is very small and negligible when compared to the total change, which is approximately equal to the applied voltage (see fig. 3.7(a)). In this situation, the degree of band realignment is negligible and any increase in γ is expected to be small. As the insulator thickness is increased, $\Delta\phi_{pi}$ becomes significant and, although the hole quasi-Fermi level can still be considered as horizontal (see appendix A), its position at the

surface is given by Efm + $\Delta\phi_{pi}$ (as shown in fig. 3.7(b)). Eq. (3.35) must now be modified to include $\Delta\phi_{pi}$; then Jp is given by

$$Jp \simeq \frac{qD_p p_{no}}{L} \{ \exp. (qV - \Delta\phi_{pi})/kT - 1 \} \qquad (3.56)$$

However, as δ is increased still further, $\Delta\phi_{pi}$ increases and the bias dependence of Jp is reduced. Following the example of Card and Rhoderick[44], eq. (3.56) is now rewritten as

$$Jp \simeq \frac{qD_p p_{no}}{L} \{ \exp (qV/n_h kT) - 1 \} \qquad (3.57)$$

where n_h is an 'ideality factor' for the hole current. (This assumes that $\Delta\phi_{pi}$ is proportional to the applied voltage, which is valid over a limited range). The minority carrier injection ratio, for the general case of a thin insulator, where significant band realignment does not occur, is given by

$$\gamma \simeq Jp/Jn \simeq \frac{qD_p Nv}{LA^*T^2} \exp (\chi_n^{\frac{1}{2}} \delta) \exp \{q(Vd-\phi_{bp})/kT\}$$

$$\exp \{qV \left(\frac{1}{n_h} - \frac{1}{n_e} \right) /kT\} \qquad (3.58)$$

$$\text{since } p_{no} = Nv \exp (-q\phi_{bp}/kT) \qquad (3.59)$$

where Nv is the effective density of states in the valence band and ϕ_{bp} is the barrier height to holes (as shown in fig. 3.7(a)).

(b) Thicker Insulators

When the insulator is sufficiently thick, the minority carrier current is limited by the tunnelling transmission coefficient of the insulator bandgap. The determination of the hole current is much more complicated than in the diffusion limited case. Indeed it has been shown[44] that the expression for Jp includes an integral which cannot be solved in closed form. However, for such thick insulators a significant degree of band realignment occurs under forward bias and Card and Rhoderick[44] have determined Jp for three different cases. These are (i) the case when the bias voltage is less than that required to align the metal Fermi level, Efm, and the edge of the semiconductor valence band edge, Evo, (i.e. $V \lesssim \phi_{bp}$); (ii) the case when Efm $\simeq$ Evo (i.e $V \simeq \phi_{bp}$); (iii) the case when Efm > Evo (i.e. $V \gtrsim \phi_{bp}$). Only the third of these cases is particularly relative to this work and is considered here. In this situation, the hole current is given by[44]

$$Jp \simeq (2\pi m_p^* q^3/h^3) \exp(-\chi_p^{\frac{1}{2}} \delta)(V - \phi_{bp})^2 \qquad (3.60)$$

where m_p^* is the effective mass of holes in the valence band and χ_p is the mean height of the barrier presented to these holes by the insulator bandgap. Consequently, the minority carrier injection ratio is given by

$$\gamma \simeq m_p^*/2m_n^* (q/kT)^2 \exp(\chi_n^{\frac{1}{2}}\delta_n - \chi_p^{\frac{1}{2}}\delta_p) \exp(q\phi_{bn}/kT)(V - \phi_{bp})^2 \qquad (3.61)$$

where χ_p, χ_p, δ_n, δ_p are effective values of χ and δ pertaining either to electrons (subscript n) or holes (subscript p). Card and Rhoderick[44] were able to obtain a good agreement between the theoretical predictions and their experimental results. They showed that, under the application of a forward bias, γ could be increased from 10^{-4} to over 10^{-1}, in

Au : S_iO_2 : (n)Si diodes, by using an insulator of the optimum thickness. This optimum was found to vary quite significantly depending on the method used to prepare the oxide: Those produced by thermal means gave an optimum of $\delta \sim 3$nm, whereas those prepared by r.f.sputtering showed less dependency on thickness and gave an optimum of $\delta \sim$ 8nm. The weak dependency was attributed to a 'forming' process in the poorer quality sputtered oxide.

It should be stressed at this point that the above discussion assumes that the transport process across the oxide is quantum mechanical tunnelling, and this accounts for the appearance of the transmission coefficients in eq. (3.61). If, however, an alternative transport process is responsible for the injection of minority carriers, then eq. (3.61) cannot be applied although, qualitatively, the same argument is valid. An alternative current path of this kind would tend to increase the optimum insulator thickness for minority carrier injection. This, presumably, is the effect observed by Card and Rhoderick[44] in the case of r.f. sputtered oxides where, above a certain threshold, a 'shunt' path was produced or 'formed'. For such 'imperfect' insulators, the impediment to current flow (due to the insulator) is less than in the ideal case. Furthermore, the proportion of the applied voltage which is developed across the insulator may also be less. Since these considerations define the thickness at which γ is optimised, it follows that an ideal insulator will exhibit a smaller optimum thickness than an imperfect one.

3.4.3. The MIS Light Emitting Diode : A Brief Review

In the preceding section it was shown how, by careful control of the insulator thickness in an MIS device, it is possible to achieve a considerable increase in the minority carrier injection ratio under the application of a forward bias. Since the EL efficiency of an LED is directly proportional

to this parameter (see § 2.5), then a corresponding increase is possible over the EL efficiency of a simple Schottky diode. The possibility of using the MIS structure as an alternative to the p-n junction for LED design has been the focus of much attention in recent years, particularly from the viewpoint of its use with the II-VI compounds such as ZnS and ZnSe. These materials are very efficient phosphors with large bandgaps and in this respect are ideally suited as LED materials. However, they are poor amphoteric semiconductors and are very difficult, if not impossible, to produce in low resistivity p-type form. Conversely, the high intrinsic luminescence efficiency of these materials means, for example, that an ZnSe MIS diode emitting in the Yellow and operating at a 10% injection ratio would be significantly more efficient than a p-n junction GaP LED and, of course, much cheaper to manufacture. The rewards of finding a configuration in which this level of injection is possible promise to be extremely lucrative and the MIS structure has been extensively studied for this purpose.

Long before Card and Rhoderick[44] delineated, quantitatively, the effect of an interfacial layer on γ, enhanced minority carrier injection was well established as a method of obtaining measurable quantities of light from semiconductors. The first reports of tunnel-injection EL were on CdS[45, 46]. Jaklevic et al[46] obtained EL for applied voltages as low as 1.3V and proposed the tunnel-injection of minority carriers to explain the phenomenon. Since then, and in particular after the details concerning the electrical characteristics of the MIS diode had been elucidated in the early 1970s, there have been many other reports of thin MIS diodes fabricated on a variety of semiconductors[47-53]. All of these reports employed the concept of enhanced minority carrier injection to explain the experimental observations. The research carried out on diodes fabricated from GaP[47-49], and ZnS[50] are particularly relevant to this work and will therefore be discussed in more detail.

Tunnel-Injection EL in GaP

Card and Smith[47] have measured the optimum insulator thickness for EL in Au-SiO_2 - (n) GaP diodes to be approximately 4nm. The SiO_2 was deposited by the decomposition of tetraethoxysilane and a power output approximately 10% of that achieved using a comparable p-n junction LED was claimed. The density of the excitation current, however, seems to have been very large (> 200 A cm^{-2}) and no indication of the device lifetime or efficiency was given. A comprehensive study of MIS LEDs formed on GaP was subsequently carried out by Haeri and Rhoderick[48]. They employed a variety of insulators (native 'oxide', sputtered SiO_2 and sputtered Si_3N_4) and found that the best results were obtained with a native oxide $\sim$ 5nm thick. In this case a quantum efficiency of $\sim 5 \times 10^{-3}$% was achieved from which they inferred an injection ratio of approximately 10%. For insulator thicknesses greater than 6 nm, forming occurred which resulted in a drastic fall in EL efficiency. There was evidence that, if insulator forming could have been prevented, a further increase in efficiency would have been possible and this would have resulted in an optimum thickness in excess of 5 nm. For the sputtered SiO_2 insulators, forming was observed for all thicknesses between 2 and 60 nm with a correspondingly low EL efficiency. The diodes fabricated with Si_3N_4 as the insulator exhibited no forming effects although the efficiency was low (10^{-4}% for the optimum thickness of 8 nm), a result attributed to the transport process through the insulator which was not tunnelling and was thought to be Poole Frenkel emission. Chybicki[49] also encountered insulator forming problems when using polymer films as the insulator on GaP.

MIS EL in II-VI Compounds

Walker and Pratt[50], working on ZnS and using NaI as the insulator, obtained green and blue EL from their diodes with an external quantum

efficiency of $\sim 10^{-5}$ for the best devices. These were fabricated with average insulator thicknesses of 59Å which was the minimum thickness achieved. Their results were attributed to the tunnel injection of minority carriers and were analysed using the theory developed by Card and Rhoderick[44]. The observed trend, of increasing efficiency with decreasing film thickness, led them to conclude that the optimum insulator thickness was less than 59Å.

In addition to these results, several workers, investigating forward biased MIS LEDs fabricated from II-VI compounds[54-57], have reported observations which can not be explained using conventional tunnel injection theory. The peculiar features of these devices are that, although the turn on voltage is low (less than the photon energy of the emitted light), the efficiency is relatively independent of insulator thickness. For example, Livingstone et al[54] found that over the range 0 to 50 nm, the quantum efficiency increased by over four orders of magnitude, but was essentially independent of thickness over the range 50 to 200 nm. Their variation of quantum efficiency with insulator thickness is shown reproduced in fig. 3.8. Clearly quantum mechanical tunnelling cannot be the mechanism by which the minority carriers are injected into the semiconductor bulk and an alternative mechanism must be responsible. The explanation which is currently most favoured is that, first proposed by Fischer[58], and subsequently by Watanabe et al[59]. This involves a two stage process which is shown schematically in fig. 3.9. (N.B. In this figure the insulator is depicted, as having the same bandgap as the semiconductor. This is due to the fact that in many cases the same material, but with different doping levels, is used as both the insulator and the semiconductor - see, for example, reference (55). This is not a necessary requirement[56] but it is used here in order to simply the discussion). Under the application of a forward bias, electrons arrive at

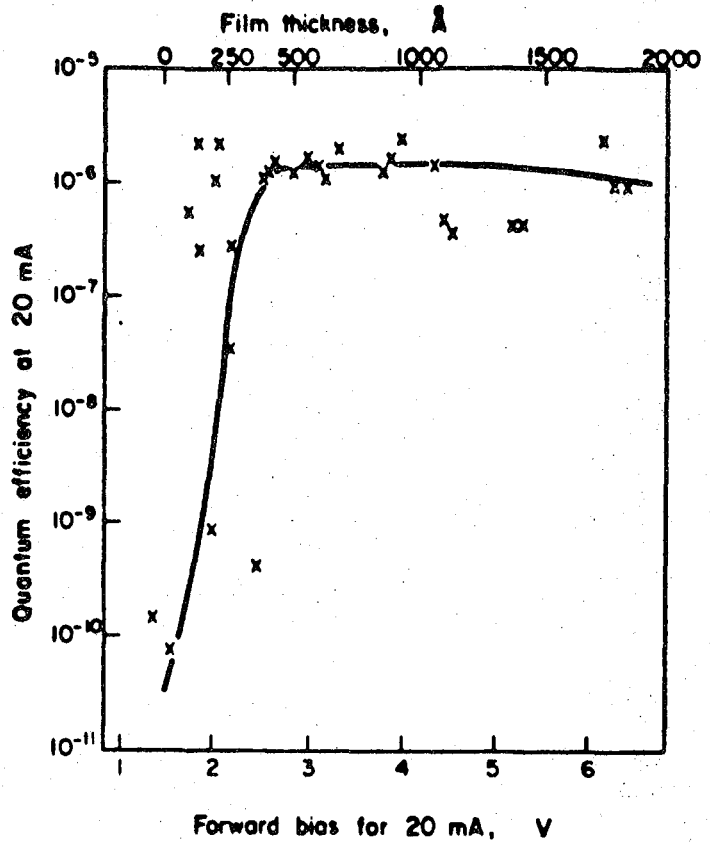

Figure 3.8 Variation of EL quantum efficiency with insulator thickness in ZnSe MIS diodes (after Livingstone et al[54]).

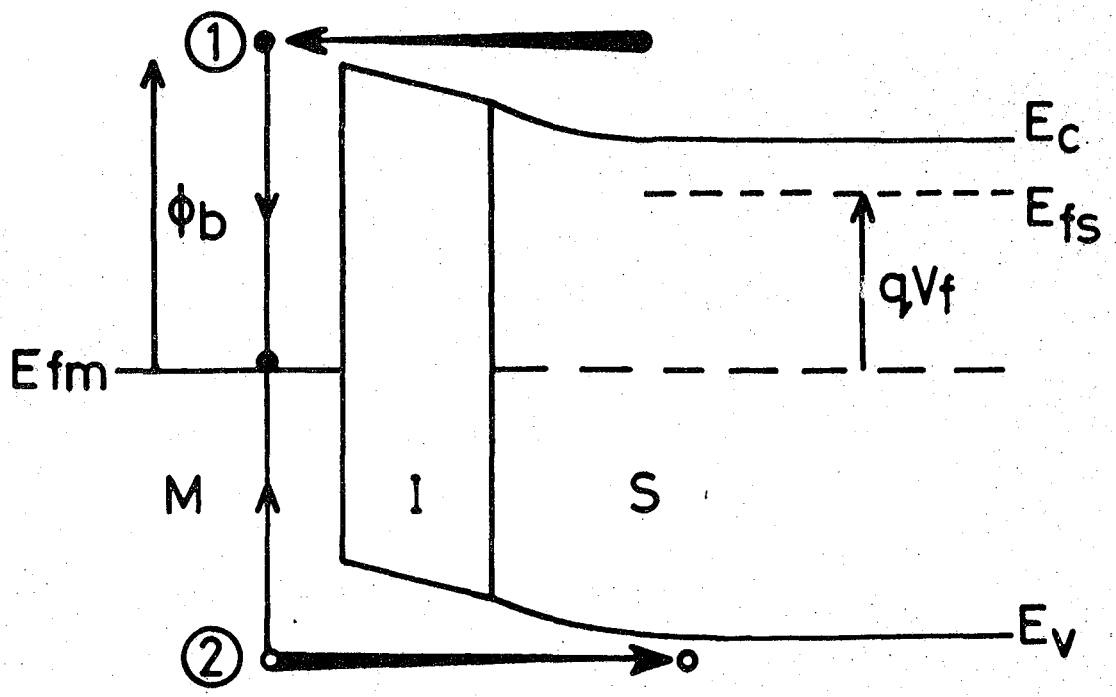

Figure 3.9 Minority carrier injection by two stage Auger recombination process (refer to text for explanation).

the metal with energies given by Efm + ϕ_b (stage 1). It is believed that these 'hot' electrons recombine in an Auger fashion, creating an energetic hole which may now surmount the hole barrier ϕ_{bp} and enter the semiconductor where radiative recombination may occur (stage 2). This model explains the relative independence of EL efficiency on insulator thickness. The fact that plasma radiation from hot electrons in the metal has been detected in inefficient MS diodes[55] has been used to support the model. Furthermore, it has recently been shown[60] that by using polymeric sulphur nitride $(SN)_x$, instead of the metal electrode, an increase of up to 100 can be achieved over the EL efficiency of diodes fabricated with gold top electrodes. This is attributed to the fact that the values of ϕ_{bn} achieved using $(SN)_x$ are $\sim$ 0.75 eV higher than those achieved with gold, and consequently the electrons entering the metal in stage 1 do so with significantly higher energies. However, this Auger mechanism is thought to be an inherently inefficient one and this may well explain why the efficiencies achieved to date ($\sim 10^{-4}$) fall disappointingly short of the theoretical maximum. The limitation, therefore, appears to be the inefficient injection mechanism and it is possible that a much higher efficiency could be achieved if a system, based on the more conventional injection theory, could be developed. The problem is essentially the lack of a good quality insulator, with suitable properties, which can be readily deposited with an accurately defined thickness.

3.4.4. Photovoltaic Properties of the MIS Diode

There are certain similarities between the physics of an MIS LED and that of an MIS solar cell. For instance, both are dependent upon minority carrier flow in their operation. In both cases the minority carriers are required to traverse the insulator with relative ease for efficient operation. In view of these similarities it was envisaged that measurements made on the diodes while under illumination might provide valuable

information on the minority carrier transport process. In this section the photovoltaic properties of the MIS diode are briefly described in order to establish the basic principles which will be referred to in later discussions. It is not intended as a comprehensive account and is somewhat qualitative in its approach. For a more rigorous analysis the reader is referred to the book by Fonash[61] and the references contained therein.

The main source of photovoltaic action in a Schottky barrier or MIS solar cell is the depletion region. For simplicity the Schottky barrier structure is considered first. Figure 3.10 shows the various processes which occur in an illuminated Schottky barrier. The photogenerated electron - hole pairs are separated by the field in the depletion region and the holes are collected by the metal electrode. The electrons, however, must pass through the semiconductor bulk before being collected, and if this distance is greater than the diffusion length, then the photocurrent due to the electron flow is very small. Consequently, the photocurrent is predominantly a minority carrier current. These photogenerated minority carriers can be 'lost' by a number of processes, labelled 1 to 4 in fig. 3.10, which all represent sources of inefficiency. Process 1 represents recombination in either the bulk or the depletion region, 2 represents losses at the Ohmic contact, 3 is recombination via interface states and process 4 represents the thermionic emission of majority carriers over the barrier. Those holes which are not lost are available to do work in an external load and constitute the photocurrent. These carriers are collected by the metal simply by arriving at the interface - there is no barrier to hole extraction in this simple case. Alternatively, the holes may be trapped at the interface and subsequently tunnel into the metal (process 5 in fig. 3.10). In most Schottky barrier solar cells, it is process 4, namely the thermionic emission of majority carriers from the

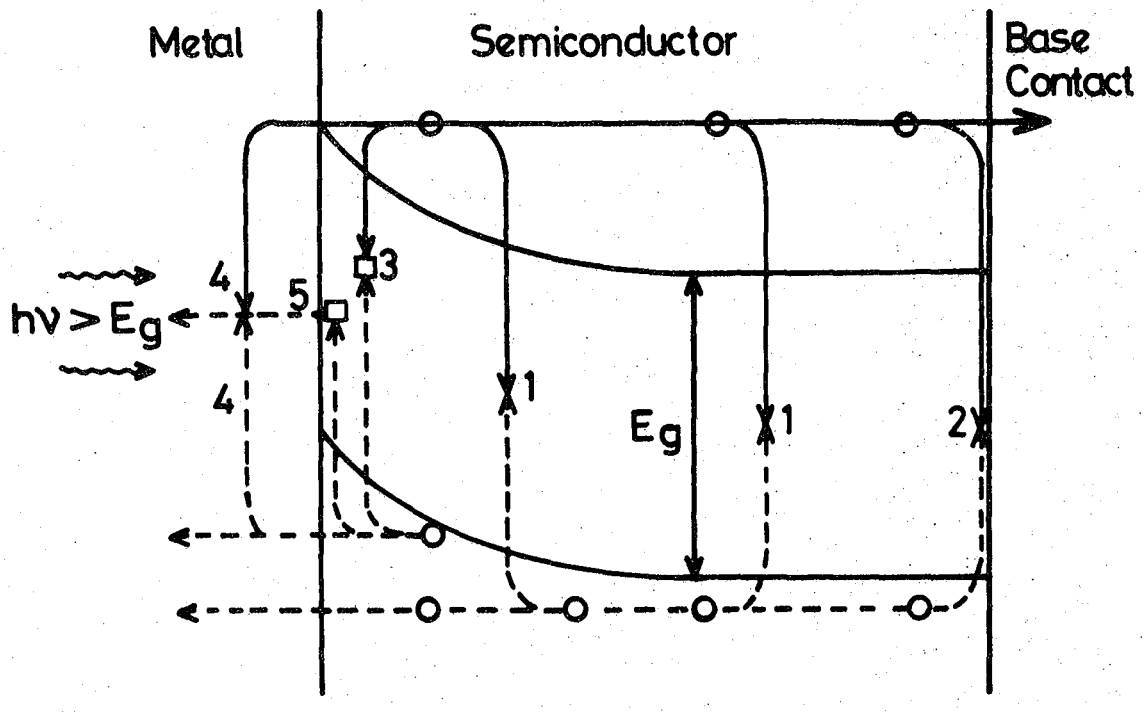

Figure 3.10 Various processes which can occur in an illuminated Schottky barrier solar cell.

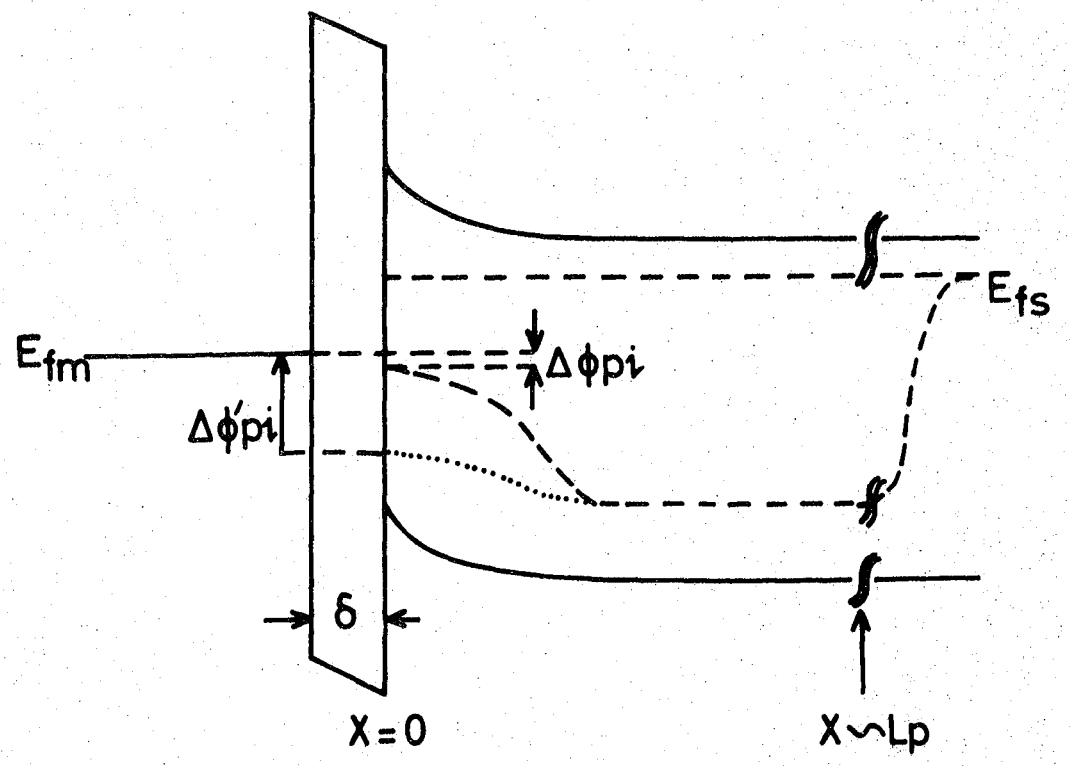

Figure 3.11 Band diagram of an MIS diode under illumination with an external load connected, depicting the behaviour of the quasi-Fermi levels.

semiconductor to the metal, which is the dominant loss mechanism. This emission is in the opposite sense to the photocurrent, and thus cancels part of it. Such a loss can be significantly reduced by inserting a suitable insulator to form an MIS solar cell. The incorporation of such an insulator can have a number of advantageous effects. For example, it can reduce the density of interface states both by satisfying the dangling bonds and minimising the formation of extrinsic interface states. However, the most important effect is the reduction that is possible in the thermionic emission loss mechanism. There are two main causes of this: The presence of fixed charge, of suitable polarity, in the insulator can increase the Schottky barrier height, ϕ_{bn}, by increasing the size of the depletion region. Also, the presence of the insulator represents another barrier in series with the semiconductor depletion region which must be surmounted. There have been many recent studies of MIS solar cells from which it has become clear that the result of incorporating a suitable insulator into a Schottky barrier solar cell is to increase, quite significantly, the open circuit voltage without affecting the magnitude of the short circuit current[62]. It is not at first obvious how it is possible to introduce a tunnellable insulator which consequently decreases the dark (majority carrier) current, by the amount exp $(-\chi^{\frac{1}{2}}\delta)$, but which has no significant effect on the minority carrier photocurrent. Card[63] has considered this theoretically with particular emphasis on the Au - SiO_2 - (n)Si system. He used essentially the same theory that was developed to describe minority carrier injection in MIS structures[44] and this is considered next.

Mode of Operation

The apparent anomaly is explained using a similar argument as that employed to explain the effect of enhanced minority carrier injection. In an MIS device, both electrons in the conduction band and holes in the

valence band experience essentially two current processes in series. Namely, the normal process of drift and diffusion (catagorised here as one mechanism for simplicity) in the semiconductor and a barrier limited process (which for holes is the barrier due solely to the insulator bandgap, and for electrons is that due to the depletion region in series with the insulator). Since the concentration of electrons in the conduction band is large then carriers can readily be removed or supplied to the interface. The largest impediment to electron flow is the barrier at the surface. However, in the case of the holes in the valence band the concentration is much less, the hole flow is limited, not by the insulator barrier but by the rate at which holes are supplied from the bulk. (The difference is further compounded by the fact that $\mu_n > \mu_p$.) Thus the insulator has a much more significant effect on the majority carriers than on the minority carriers. As the insulator thickness is increased, the impediment to hole flow, due to the insulator barrier, increases until it is comparable to the impediment due to the processes of drift and diffusion. At this critical thickness, δc, the short circuit photocurrent will begin to be reduced by an increase in insulator thickness. This is illustrated diagrammatically in fig. 3.11 which shows the band diagram of an MIS diode under illumination with an external load connected. The dashed lines indicate the positions of ϕ_p and ϕ_n for the case of a thin oxide ($\delta < \delta c$), and the dotted line represents ϕ_n in the case a thicker oxide ($\delta > \delta c$). Remembering that the change in quasi Fermi level with distance represents a 'driving force', it is clear that in the former case the largest impediment to hole flow is due to processes in the semiconductor, whereas in the latter case it is due to the barrier presented by the insulator. Card[63] has equated these two current processes for holes and used the criterion $\Delta\phi_{pi} \sim kT$ in order to evaluate δc. His predicted value of 20Å for the Au - SiO_2 - (n) Si system agrees well with that found experimentally.

Under illumination the total current is given by:

$$J = J_{s/c} - J_o' \exp(-\chi^{\frac{1}{2}}\delta) \exp\left(\frac{qV}{n'kT}\right) \qquad (3.62)$$

neglecting the recombination current.

An expression for the open circuit voltage can be found by setting $J = 0$ which yields;

$$V_{o/c} = n'\left(\frac{kT}{q}\right) \ln\left\{\frac{J_{s/c}}{J_o' \exp(-\chi^{\frac{1}{2}}\delta)}\right\} = n'\left(\frac{kT}{q}\right)\left\{\ln\left(\frac{J_{s/c}}{J_o'}\right) + \chi^{\frac{1}{2}}\delta\right\} \qquad (3.63)$$

The term J_o' represents the saturation current, as defined by eq.(3.14), but with ϕ_{bn} replaced with the barrier height under illumination ϕ_{bn}'. Similary n' represents the ideality factor under illumination. These terms may be different from their corresponding dark values. Since the illumination can alter the charge localised at the interface by photo-ionization processes.

SUMMARY

This chapter has described the physics of the Schottky barrier and the thin-MIS diode in some detail. A review of the current theories concerned with Schottky barrier formation was given first and this was followed by an analysis of the near-ideal Schottky diode, as defined in § 3.3.1, which was based essentially on the Bardeen model. This near-ideal situation is that usually achieved using normal (laboratory) preparation techniques and the theory described in § 3.3 will be used in chapter 6 to analyse the GaP Schottky barrier devices. This theory was extended to account for the incorporation of a thin insulator into the structure and the effect of this insulator on the device properties was

discussed. In particular, it was shown how the MIS structure could be used to obtain EL due to the phenomenon of minority carrier enhancement. A brief review of previous MIS LED work was given and from that it is clear that the main problem preventing the commercial realisation of MIS LEDs, is concerned with the insulator. Langmuir-Blodgett insulating films possess many of the features which are desirable from the viewpoint of MIS LEDs and in the next chapter, a brief description of the technology of LB films is given.

CHAPTER 4

LANGMUIR BLODGETT FILM TECHNOLOGY

4.1 INTRODUCTION

This chapter deals with the technology of Langmuir-Blodgett (LB) films. A Langmuir film is formed by spreading a small quantity of material onto the surface of a liquid subphase, and subsequently compressing this material so that a solid sheet, one molecule thick is produced. Generally, the liquid used for the subphase is ultra-pure water. In addition, it is common to dissolve the material in a solvent, and spread this solution onto the water surface, in order to aid dispersion. Once spread, the solvent evaporates, thereby leaving the film material on the water surface. Under certain conditions, the film may be transferred onto a suitable substrate; this is achieved by passing the substrate through the film on the surface of the water. Subsequent traversals of the monolayer-subphase interface enable multilayer structures to be built up. A film transferred in this manner is termed a Langmuir-Blodgett film.

In this chapter specific details concerning the LB technique are described. A brief historical introduction is given first and this is followed by a description of the Langmuir trough used to deposit the films described in this study. Materials which are used to produce LB films are discussed in § 4.3 which is followed by a general discussion concerning film deposition. The chapter is concluded with a discussion of some potential applications for LB films.

An Historical Introduction

The earliest reports of scientific experiments with 'Langmuir' films involved observations concerning the behaviour of oil films on water; in 1774 Franklin[1] described the spreading of a small quantity of oil over

a large area of water. However, it was not until 1891 that Pockels[2] described the first methods for manipulating these films using a very crude trough and in 1899 Rayleigh[3] proposed that they were only one molecule thick. Subsequently, Irving Langmuir[4] showed that films consisting of long chain fatty acids gave the same value of cross-sectional area per molecule, irrespective of the chain length. This classic work led to the first detailed description of the structure of these films. Langmuir concluded not only that they were, indeed, one monolayer thick, but also that the individual molecules were oriented nearly vertically on the water surface and hence the film thickness was equal to the molecular length. Some years later, working with Katherine Blodgett[5], Langmuir developed the process to control and transfer these films onto substrates which still forms the basis of modern LB film technology.

The trough used by Langmuir and Blodgett in their early work consisted of a metal container, which had been coated with paraffin wax in order to make it hydrophobic, filled to the brim with water. A control 'barrier', also rendered hydrophobic, was used both to define the effective area of the trough and to clean the surface of the water, simply by passing it across the surface thus forcing surfactant material into the unused region behind the control barrier. The material to be used to form the LB film was compressed using an oil piston, the oil being separated from the material by a waxed, silk thread floating on the water and fastened to the trough on each side. The substrates were raised and lowered through the film by means of a simple hand-winder, the oil piston maintaining a constant surface pressure as the material was deposited.

There have been many developments since these early, pioneering experiments, a full account of which (up to 1966) can be found in the book by Gaines[7]. Modern troughs, although based on the principles

described above, are much more sophisticated, both in mechanical construction and in the instrumentation used to control the procedure. The troughs employed to deposit the films used in this work are of an advanced design, and a description of one of them is given in the following section.

4.2 THE LANGMUIR TROUGH

4.2.1 Mechanical Construction

A photograph of one of the troughs used in Durham is shown in fig.4.1. It employs a constant perimeter, variable area compression system[6] using a PTFE-coated glass-fibre belt, located on PTFE rollers, as the barrier (marked 'A' in fig. 4.1). The use of a belt eliminates the need for a trough filled to the brim and allows a water level which is variable, within the limits imposed by the depth of the belt. The actual trough itself is made of glass (B) and is located in a metal frame onto which the beams (C), which support the barrier, are mounted. These beams are, in turn, supported by V-shaped rollers located on stainless steel rods, and are motor driven via a toothed belt (D). The dipping head (E) consists of a supported overbeam, to which a motor-driven micrometer screw is attached. The substrate is attached to the micrometer by a pressure clamp, and can be raised and lowered smoothly at a controlled speed. Microswitches are located at the extremes of the micrometer movement and adjustable trip rods can be set to give the desired dipping range. Alternatively, a linear potentiometer can be used instead of the microswitches and trip rods, to enable remote control of the dipping range.

Wherever possible, stainless steel or PTFE was used in the construction of the trough, and when this was not possible (e.g. for the large metal frame and overbeams), the metal was either chrome-plated or anodized. This was not only important from the viewpoint of avoiding contamination, but

also increased the time interval between major overhauls. The complete trough structure was housed in a glass-doored cabinet which was fitted with an extractor fan to aid in the removal of solvent vapour. The microbalance head, with which the surface pressure was monitored, was located on top of the cabinet, immediately above the dipping area of the trough. A piece of filter paper of known dimensions was used as a Wilhelmy plate. This was suspended by a thread from one part of the microbalance and enabled the surface pressure of the film to be measured. This was deduced directly from the force exerted on the plate by the compressed monolayer.

4.2.2. Instrumentation

A range of peripheral equipment is associated with the Langmuir trough: The surface pressure of the monolayer was monitored using a Beckman LM 600 microbalance, the output of which was fed directly to a Bryans 2900 X-Y chart recorder which was used to plot compression isotherms (see § 4.4.2). In addition, the surface pressure and the area enclosed by the barrier were monitored continuously, throughout the dipping procedure using a Bryans 312, 2 channel Y-t chart recorder. The pH of the subphase was monitored using a Pye-Unicam PW9409 pH meter. A purpose-built control box enabled several of the functions of the Langmuir trough to be automated. This box afforded the user full control over both barrier movement and dipping head functions. It enabled the dipping operation to be controlled manually or automatically. In the latter mode, the number of 'dips' required could be pre-programmed and, with the limit switches defining the dipping range and the dipping speed set to the required value, the rest of the procedure was automated. The barrier could be closed (and hence the film compressed) at a variable speed, or reversed at high speed. In addition, a third barrier function,

i.e. 'control' enabled the surface pressure to be maintained constant throughout the dipping procedure. The output from the Beckman balance, which was proportional to the actual surface pressure, was compared by a differential amplifier with a preset voltage corresponding to the desired surface pressure. The output from the comparator was fed back to the barrier control circuit so that fluctuations in the surface pressure could be compensated by variations in the area enclosed by the barrier. In particular, the loss of material from the monolayer, due to deposition onto a substrate, was automatically compensated by a decrease in the area enclosed by the barriers, thereby maintaing a constant surface pressure. The introduction of this feedback circuit into the Langmuir trough design[8, 9] represented an important advance in Langmuir trough technology, and today is acknowledged as essential for the repeatable production of high quality LB films.

As in any device processing technology, cleanliness is of paramount importance, and for this reason the troughs in Durham are housed in a microelectronics, class 10000 clean room. Furthermore, a thorough weekly cleaning procedure was adopted which involved cleaning all removable parts of the trough (in particular the components of the barrier mechanism), changing the subphase and Wilhelmy plate, and also recalibration of the instrumentation. The ultrapure water subphase was supplied to the trough via high purity polypropylene tubing. The water was purified by double ionization, activated charcoal organic removal, and 0.2 μm filtration. The resistivity of the final water, used for both the subphase and cleaning procedures, was approximately 10 MΩcm. A fine glass vacuum nozzle, attached to a water driven pump, was used to clean the subphase surface before spreading the film material. This also enabled the unused monolayer to be removed once the deposition was complete.

4.3 MATERIALS FOR LANGMUIR-BLODGETT FILMS

For the purposes of this discussion, the range of LB film materials have been classified into 'classical' and 'novel' materials. Classical materials have been taken to be the long chain fatty acids and alcohols, on which much of the pioneering work was performed, and also other materials with a similar long chain structure. The novel materials are those which differ in some significant way to the classical structure. The majority of these have been specially synthesised and have only recently been used to form LB films. The discussion is not intended to be exhaustive and only those materials used in this work are described in any detail. A comprehensive review of the field up to 1980 can be found in ref. (10).

4.3.1 Classical Materials

A material which is to be suitable for the formation of a Langmuir film must possess certain features. In the simplest case it should consist of a hydrophilic end to the molecule (usually an acid or alcohol group) to which is attached a hydrophobic region (usually a hydrocarbon chain). On the surface of the water the polar group will tend to encourage the molecule to dissolve, whereas the hydrocarbon chain will tend to prevent this. In fact the solubility of the material is essentially determined by the length of this chain. In practice the chain length must be fairly long ($\sim$20 carbons)to be completely insoluble, and this is important since in monomolecular form, the area in contact with the water is very large when compared to the volume of the material. Fig. 4.2(a) shows the chemical structure of stearic acid which is the fatty acid used in much of this study. It has eighteen carbons in the aliphatic chain and is referred to as C18 fatty acid. In practice, it is advantageous to introduce a divalent metal ion (usually in the form of a chloride) into the subphase. This can replace the

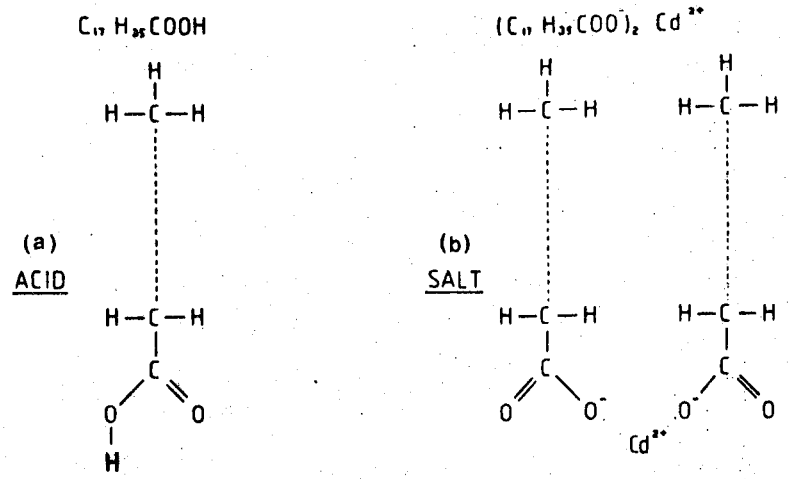

Figure 4.2 Chemical structure of (a) stearic acid and (b) its cadmium salt, cadmium stearate.

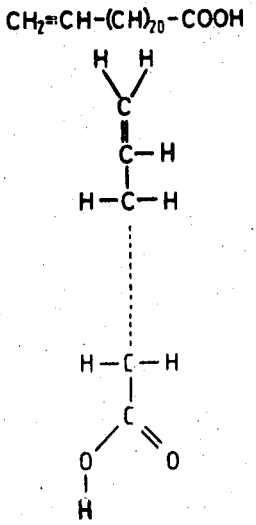

Figure 4.3 Chemical structure of ω-tricosenoic acid (ω-TA).

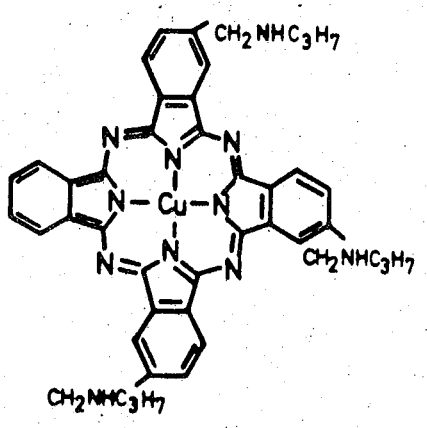

Figure 4.4 Chemical structure of the lightly substituted phthalocyanine material used in this study.

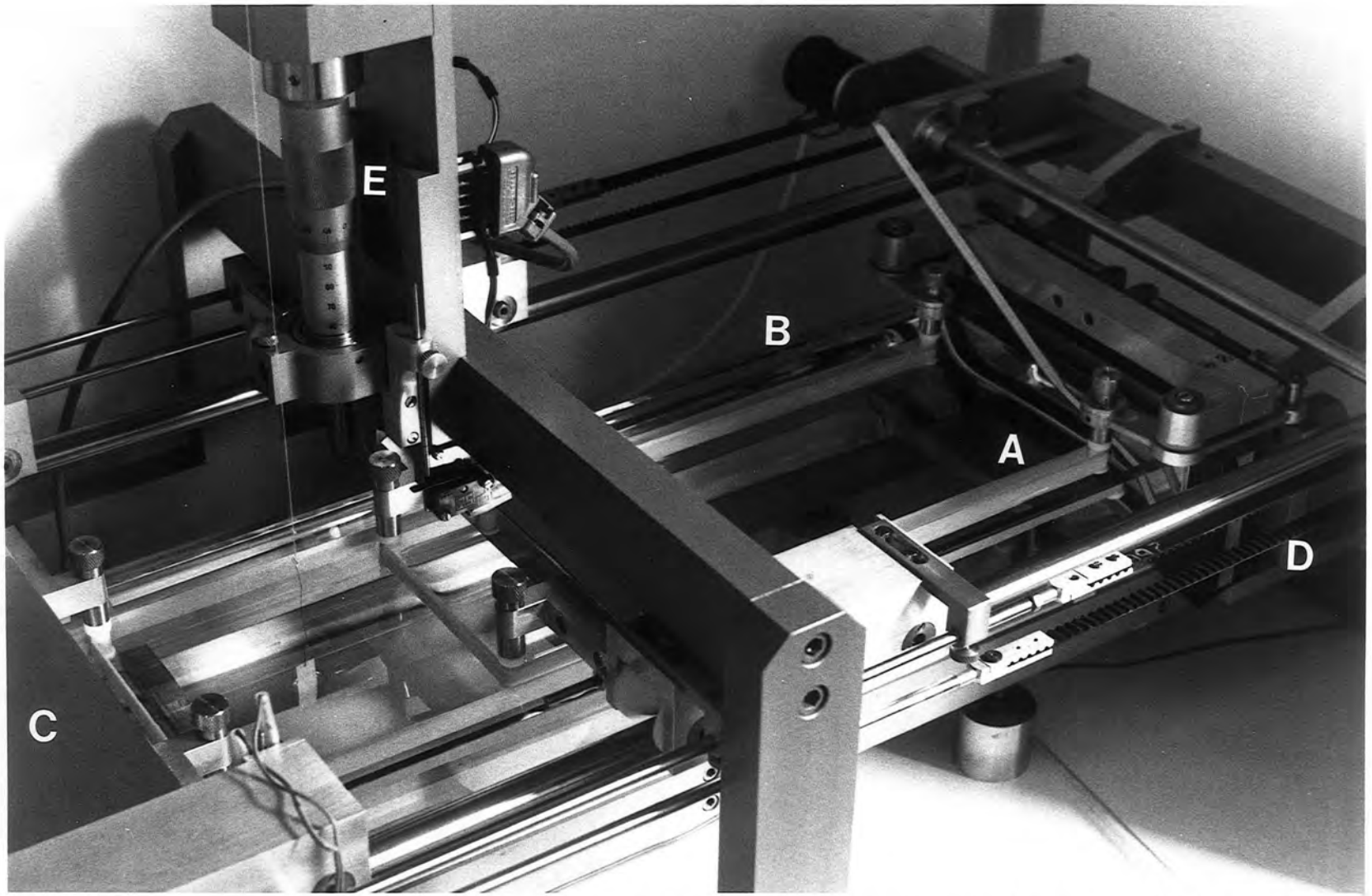

Fig. 4·1. One of the Langmuir Troughs used at Durham University.

H^+ ions in the polar group of two acid molecules thus forming the metal salt. Cadmium was used as the divalent metal in this study, and the cadmium salt of stearic acid (cadmium stearate, $CdSt_2$) is shown in fig. 4.2(b). The conversion of the acid monolayer to its metal salt is recognised to give greater lateral stability[11] and is usually necessary for the successful deposition of high quality films. It also prevents the slow collapse observed in stearic acid Langmuir films due to the dissolution of the film into the subphase. The degree of conversion of fatty acid to metal salt is chiefly dependent on the pH of the subphase. Usually the reaction is incomplete, resulting in a mixed film of acid and salt (see § 4.4.2). However, the amount of cadmium added to the subphase can affect the quality of the deposited films; too much can cause improper stacking resulting in poor quality multilayers. In common with most workers in the field, a 2×10^{-4} M solution was used in this study.

There are a range of other fatty acids which have been used to form LB films, e.g. arachidic acid has also been extensively studied. The materials are all very similar in structure and only differ in the length of the hydrocarbon chain, and hence the monomolecular dimension of the formed film. For example, stearic acid has 18 carbon atoms in the aliphatic chain compared to 20 carbons in arachidic acid. This results in molecular lengths of approximately 2.5 and 2.8 nm respectively. A number of other materials with structures very similar to these fatty acids have been used. These include a range of biologically important materials such as cholesterol[12], chlorophyll[13] and phospholipids[14] and a host of long chain polymeric materials such as diacetelyne[15] and ω-tricosenoic acid (ω-TA)[16]. This latter polymer is another of the materials used in this study and is therefore considered in some detail. The chemical structure of the molecule is shown in fig. 4.3. It has 23 carbons in the aliphatic chain, and only differs from the conventional fatty acids in having a

double vinyl bond, $CH = CH_2$, which replaces the CH_3 group. The material can be readily polymerized by an electron beam forming a linear polymer due to cross linking between the 'ω' double bonds. It may thus have important applications in the field of electron beam resists (see § 4.5) and in fact it was in this context that it was first considered. In addition, a recent study[17] has shown that it is possible to deposit multilayers at high speed and still retain a high degree of order - an obvious prerequisite for any electron beam resist material.

4.3.2 Novel Materials

In many instances, the LB technique provides an excellent method for the deposition and/or study of a material of interest. However, this material may not readily form a monolayer on the surface of the subphase and it must be modified in some way to render it suitable for use with the LB technique. The simplest method of achieving this is to mix the material with a conventional fatty acid in order to form a mixed Langmuir film[18] or alternatively to cause the material to be adsorbed onto a fatty acid film[19]. Recently a great deal of interest has been generated in the photoactive properties of materials in the form of LB films[20-23] (see § 4.5). In these cases the active molecule (usually a dye) is either incorporated in a conventional film or substituted with long hydrocarbon chains. However, even in this latter case, a mixed film is necessary to enable high quality films to be produced. In all of these cases the specific property of interest is necessarily diluted and the resulting films have limited mechanical and thermal stability. Recently some innovative chemistry has enabled a number of interesting materials to be studied in LB film form: Vincett et al[24] have shown that the aromatic material anthracene, substituted with short (C4) aliphatic side chains can be built up into multilayers. This was

expected to reveal the electrical properties of the conjugated π electron system to a much greater extent than with a conventional long chain substitution, and the layers were indeed found to exhibit some very interesting electrical (and optical) properties[25, 26]. Very recently, LB films of phthalocyanine (Pc) dye molecules without long chain substitutions have been reported[27, 28, 29]. The first films produced[27] were of metal-free, unsubstituted Pc and were definitely not monomolecular, although they were of reproducible thickness. Since then, lightly substituted Pc has been used[28][29] and successful deposition of at least bilayer, if not monolayer, films has been achieved. This is expected to prove an extremely important development for several reasons. The phthalocyanines are well known to be extremely stable, in particular their melting points (greater than 400°C) are far higher than that of any other LB film material. Furthermore, the layers have been found to adhere strongly to both substrates and each other, and to resist mechanical abrasion and the action of many solvents. Early reports suggest that the films possess insulating properties[27], although there exists the possibility of producing LB films of Pc with semiconducting properties, since the phthalocyanines are a well established group of organic semiconductors. In addition to these important properties, Pc is also recognised as an important photovoltaic pigment[30], although its use has been hindered by difficulties experienced in producing it in thin film form by other techniques. The phthalocyanines may well prove to be an important step towards the production of commercially viable LB film-based devices which to date has been prevented largely by the instability of the more conventional materials. For this reason Pc was also used in this study and fig. 4.4. shows the chemical structure of the particular Pc derivative used. It is a lightly substituted, copper Pc and the thickness of the deposited film is approximately 0.8 nm[28].

4.4 LANGMUIR-BLODGETT FILM DEPOSITION

The LB film materials used in this study were all synthesised to a high degree of purity and the spreading solvents used were all of Aristar (BDH) grade. Usually, the material was dissolved in the solvent (invariably chloroform) to a concentration of approximately 1 mg cm^{-3} and fresh solutions were made up at regular intervals to eliminate possible ageing problems. The further precaution of storing the ω-TA in the dark was taken to eliminate the possibility of UV-polymerisation.

The deposition procedure can be divided into three distinct procedures; i.e. monolayer spreading, monolayer compression (and isotherm measurement), and actual film deposition. These are now discussed in sequence.

4.4.1 Monolayer Spreading

Prior to spreading the monolayer, the surface of the subphase had to be cleaned. This was achieved by closing the barrier to its minimum area and 'vacuuming' the surface with the previously-described vacuum nozzle. It was found that the cleanest surface could be achieved by the spreading and subsequent removal of a Langmuir film. This was thought to be due to the adherence of surface particles to the film. The amount of contamination on the surface could be deduced from the residual surface pressure as the barrier was closed to minimum area. With care, this could be reduced to $\lesssim 0.05$ mN m^{-1} and under these circumstances good isotherms and high quality monolayers could be expected. After cleaning the surface of the subphase, the material (in solution in the solvent) was spread using the following technique: A known amount of solution was deposited, one drop at a time using a micrometer syringe system. The film was spread from the centre of the trough so that any surfactant material, remaining after the cleaning procedure, was forced to the perimeter of the dipping area. This reduced the possibility of any residual material being deposited onto the substrate. The solvent was then allowed about five minutes in which to evaporate with the extractor fan aiding the process.

4.4.2 Film Compression and Isotherm Recording

As a matter of routine, a surface pressure - area plot (a 'compression isotherm') was recorded each time a film was spread. Fig. 4.5 (a) shows such an isotherm for stearic acid, where the area axis has been calibrated in terms of the average area occupied by each molecule. It is convenient to draw an analogy between the compression of a monolayer on the surface of the trough and the compression of a gas - the main difference being that the the monolayer is essentially two dimensional and hence surface pressure replaces bulk pressure and surface area replaces volume. Before compression, the stearic acid molecules are well spaced out with the polar groups immersed in the water and the aliphatic chains oriented at random away from the water surface. The monolayer is said to be in the gas phase. On compressing the film, the average area occupied by each molecule reduces but there is little change in the surface pressure until at approximately 24Å^2/molecule, the monolayer undergoes a phase change. The molecules begin to interact and further compression results in a gradual increase in surface pressure. This is termed the liquid or expanded phase. The molecules can be envisaged as being relatively closely spaced and almost vertically aligned. A further phase change occurs at about 20Å^2/molecule and the film is in the solid or condensed phase. The molecules are fully aligned and tightly packed. With the film in this condensed phase, a small compression of the monolayer results in a large increase in the surface pressure. However, in practice the situation is not quite so simple since the conversion of stearic acid to cadmium stearate is often promoted and, since this reaction is pH dependent, the pH of the subphase has a marked effect on the shape of the isotherm. Fig. 4.5(b) shows isotherms for a stearic acid/cadmium stearate film at two different pH levels. At low pH the curve is very similar to the stearic acid isotherm and the film consists largely of stearic acid. However, at higher pH the extent of the liquid region is

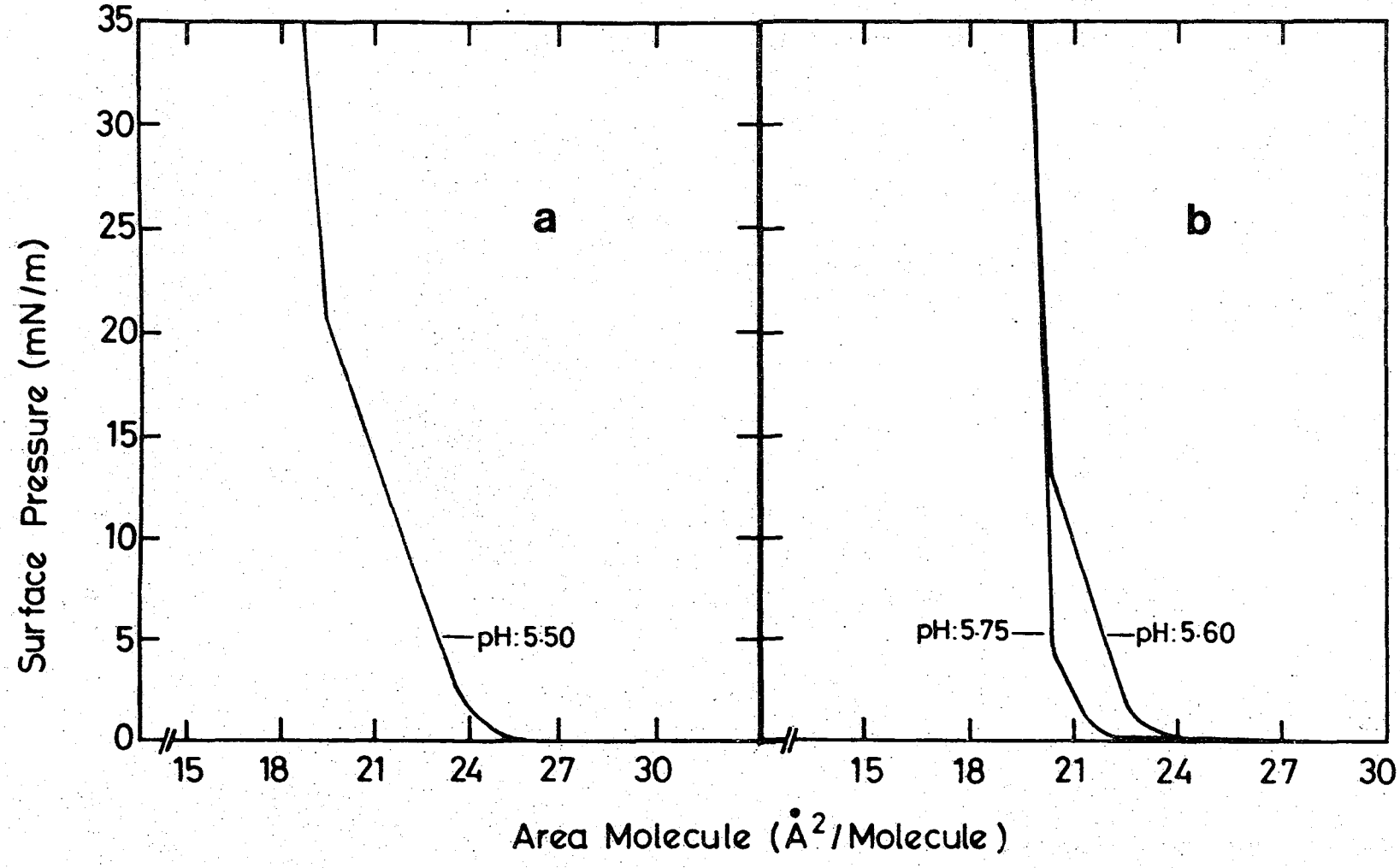

Figure 4.5 Typical compression isotherms for (a) stearic acid and (b) a mixed $CdSt_2$/stearic acid film at two different pH levels.

reduced and the liquid-solid 'break' point occurs at a substantially lower surface pressure. These two effects are indicative of the enhanced stability of the film which now is a mixed film of acid and salt. At still higher pH levels, the liquid phase is virtually non-existent and at a pH of 6.5 the monolayer is largely $CdSt_2$. It should be stressed that isotherms obtained for fatty acids and their divalent metal salts are nearly ideal. Many other films, including ω-TA and Pc, do not exhibit such well-defined phase changes and the isotherms are, in general, much more rounded and featureless. (Typical isotherms for ω-TA and Pc films are presented in chapter 5.) The control of pH was much less crucial in the deposition of these latter materials since cadmium was not incorporated into the subphase. Good quality multilayers could be deposited without the use of cadmium and, in fact, there was some evidence to suggest it may be detrimental. In practice, irregularities in the isotherms, such as additional features or poorly-defined breakpoints, were sometimes observed. These were almost certainly due to contamination and a thorough clean of the subphase surface, or in rare cases the entire trough, always resolved the problem.

After recording a satisfactory isotherm, the required surface pressure was preset and the trough was put into control mode. The monolayer was compressed to the preset surface pressure and usually left for about 10 minutes to allow any final rearrangement of the molecular packing before dipping commenced.

4.4.3 Film Deposition

In order to achieve successful deposition of high quality films in a repeatable fashion, the film must be transferred onto the substrate whilst in the condensed phase. This ensures that the deposited film is essentially homogeneous and slight variations in surface pressure have a relatively small effect on the film structure.

Classically, three deposition modes are recognised, namely the X, Y and Z modes. These deposition types are illustrated schematically in fig. 4.6 (a), (b) and (c) respectively. X-type deposition is used to describe the situation when deposition occurs only on the downstroke, Z-type on the upstroke only, and Y-type (often termed normal deposition) when pick-up occurs in both directions. The type observed in practice depends on factors such as the pH of the subphase and the substrate preparation. Although Y-type is by far the most often observed mode, X-type is sometimes encountered at extreme pH levels. When Langmuir and Blodgett[31] first discussed the different modes, Z-type deposition had not been observed and its definition was merely speculative. Since then, however, this mode has been observed[32] and was also encountered in this work when depositing lightly substituted Pc films. However, the actual stacking arrangement predicted from the deposition mode has been shown to be an oversimplification[33, 34] and the exact stacking sequence is much more complex. In particular, studies of both X and Y-type deposited films[35, 36], have shown that the separation of the acid groups is invariably twice the molecular length, suggesting that deposited films always stack 'Y-type'. Several authors[37, 33] have invoked the idea of overturning of the molecules during X-type deposition to explain this discrepancy. More recently, another deposition mode (XY-type) has been observed[34] and an elegant model, based on the formation of two distinct forms of salt, was used to explain both this, and X-type deposition without invoking the idea of overturning. The structure of deposited multilayers is obviously a complex problem which has yet to be conclusively resolved. At present, only Y-type films are known to possess a uniform, bilayer structure. In most of the devices prepared for this study, the deposition was Y-type - the substrate surface being sufficiently hydrophilic to prevent deposition on the first downstroke.

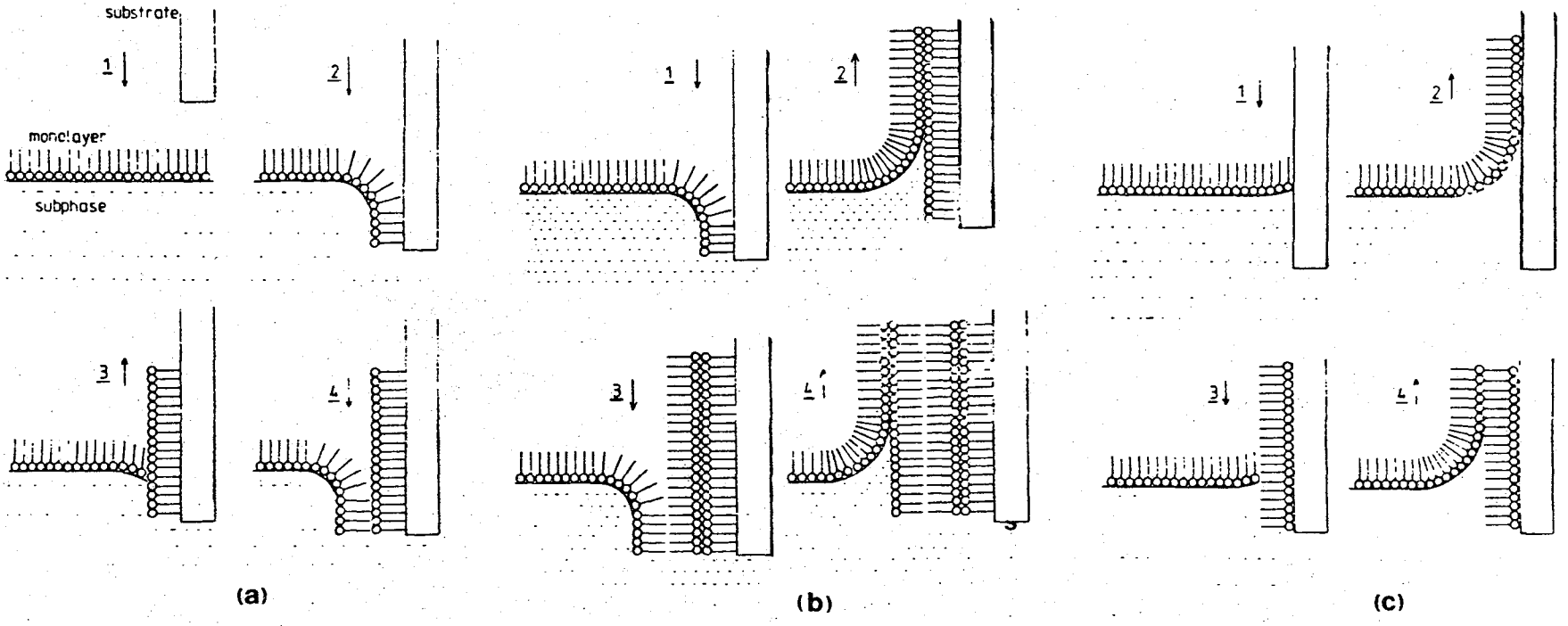

Figure 4.6 Depicting the three types of LB film deposition, (a) X-type, (b) Y-type and (c) Z-type.

The quality of the first deposited layer is of paramount importance to the quality of the eventual multilayer. This is due to the fact that any faults or inclusions are likely to be duplicated or to persist in subsequent layers. Furthermore, the bonding of the first layer is fundamentally different to the 'head to head, tail to tail' bonding of subsequent layers. For these reasons extreme care was taken to ensure a high quality first layer and this was achieved by depositing the first layer very slowly ($\sim$ 1 mm/min.) immediately after the substrate had been etched. The deposition of subsequent layers is more straightforward and can, in general, be performed at much greater speeds. The details of the deposition conditions used and the procedures adopted are given in § 5.2.

During the deposition procedure a 2 channel Y-t chart recorder continuously monitored both the surface pressure and the change in the area enclosed by the barrier, thus providing a record of the operation. A typical example is shown in fig. 4.7. From this it can be seen that, as the film is removed, the barrier area decreases in response to the feedback mechanism, thereby maintaining the surface pressure constant. A knowledge of the sample surface area enables the deposition ratio to be calculated which, for good quality films is very close to 100%. This is discussed in more detail in § 5.2 when the effect of surface preparation on this deposition ratio is studied.

The deposition of Pc LB films is more complex than that used for more conventional films. Briefly the main complications are as follows: The unsubstituted Pc is not soluble in the common organic solvents. This necessitates either a metal substitution[27] and/or a peripheral substitution such as that shown in fig. 4.4. The latter of these enables chloroform to be used as the solvent. However, since the molecules do not possess the classical hydrophilic - hydrophobic structure, transfer onto

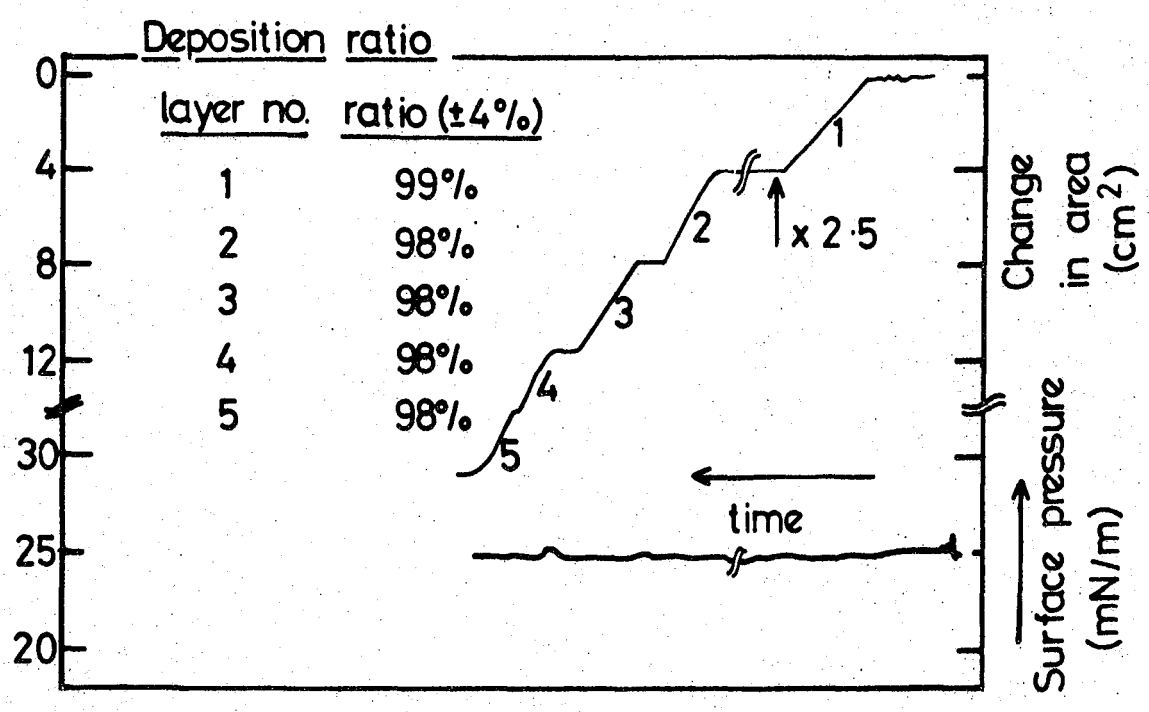

Figure 4.7 Typical deposition record for $CdSt_2$ onto GaP.

a substrate occurs only on the upstroke, i.e. Z-type deposition. Simple precautions are necessary to ensure that no transfer occurs on the down-stroke[28].

4.4.4 Quality Assessment

Langmuir-Blodgett films, especially those of the fatty acids or other similar aliphatic materials are generally good insulators with high breakdown strengths (> 10^6 V/cm) and dielectric constants which are almost independent of frequency, for frequencies $\lesssim 10^6$ Hz. The electrical properties of these films are usually studied by incorporating them into MIM or MIS structures and a number of such studies have been made (see for example, ref. (46)). Poole-Frenkel conduction between neutral traps is thought to be the dominant conduction mechanism in multilayered LB films although other mechanisms have been observed under certain circumstances. For example, in MIS devices fabricated on n-type semiconductors, electron injection into the insulator, resulting in space-charge-limited characteristics, has been observed[46].

A convenient measurement, which can be used to assess the general quality of an LB film is a reciprocal capacitance plot. This is usually achieved by depositing a stepped thickness LB film onto a metal substrate and producing MIM structures with a variety of insulator thicknesses. The total capacitance C_t, (per unit area) of such a structure is given by

$$\frac{1}{C_t} = \frac{Nd}{\varepsilon_{lb}} + \frac{\delta_{ox}}{\varepsilon_{ox}} \qquad 4.1$$

where δ_{ox} is the thickness of the interfacial metal-oxide film, ε_{ox} is its permittivity, ε_{lb} is the permittivity of the LB film, d is the single monolayer thickness and N is the number of monolayers incorporated into

the structure. Thus, a graph of C_t^{-1} against N should be linear with a slope equal to d/ε_{1b} for a good quality film. The intercept on the C_t^{-1} axis can be used to determine the mean thickness of the interfacial layer. Such a plot is used in §5.2 to assess the effect of electrode evaporation on the LB film quality.

4.5 APPLICATIONS OF LB FILMS

Although the LB technique was developed in the early twentieth century and LB films have been studied for well over fifty years, it is only recently that widespread interest has led to the demonstration of their potential for use in electronic and optical devices. This section provides a brief review of some of the more important applications for which LB films have been considered. A more detailed discussion can be found in ref. (10).

The insulating properties of these films have been utilised in many devices. For example, they have been used as the dielectric in low-loss capacitors[38] (an area which is enjoying renewed interest) an in capacitive hygrometers[38]. In addition, several electronic devices, based mainly on the MIS structure, have been fabricated: Tanguy et al[39, 40] studied MIS capacitors formed on silicon and demonstrated near-ideal behaviour. The Durham group have fabricated MIS field effect transistors based on InP[41] and amorphous silicon[42]. The same group has used LB films to investigate the properties of MIS solar cells based on CdTe[43] and have achieved a significant improvement in efficiency over the corresponding Schottky barrier cells. MIS devices have been fabricated on the narrow bandgap materials[44] InSb and HgCdTe with a view to producing improved infra-red detectors. Recently, considerable interest has been generated in the production of ion and gas detecting FETs using an LB film[45] or the LB film - semiconductor interface[46] as the active region.

A great advantage of the LB technique is that, within reason, the physical size of the application is of little importance. The technique is particularly suitable for large-area applications but also, because of the high degree of film perfection possible, microscopic applications can be contemplated. An important example of this is the use of polymerizable LB films as electron beam resists for microlithography[51, 17]. Of the materials studied to date, ω-TA appears to be the most promising and a resolution of better than 60 nm has been achieved[52]. Other applications which have been convincingly demonstrated include Josephson tunnel junctions[47], ultrasonic transducers[49] and the use of LB films as optical waveguides[50, 11] which makes possible a range of applications in the field of integrated optics. Applications in the field of electro-optics have also been envisaged where it is hoped that control over the precise molecular arrangement may enable the production of asymmetrical structures with large non-linear optical coefficients[57].

In addition to the mainly 'passive' applications discussed above, a variety of possibilities exist for the use of LB films as 'active' layers. Kuhn et al[53, 54] have demonstrated optical and energy transfer experiments with the possibility of fabricating light-driven 'molecular pumps' to convert light into chemical energy. The use of LB layers incorporating dyes to study dye-sensitization effects (the transfer of charge from photo-excited dyes to substrates, usually semiconductors) has also been demonstrated[55]. Dye sensitization is already a standard technique in the photographic industry and the use of LB films in this area is being actively pursued. A range of biologically important materials have been used in LB film form, both to model complex biological systems and to develop novel active membranes for filtration purposes such as reverse osmosis[56]. A particularly interesting area of research is concerned with the formation of LB films from organic semiconducting materials.

For example, films of lightly substituted anthracene have been prepared and shown to exhibit electroluminescent and photoconductive properties[26]. Phthalocyanine is also a well-known organic semiconductor and it is hoped that LB films of this material will possess some interesting properties. In particular, it may be possible to produce films exhibiting either n- or p-type conductivity by using suitable metal substitutions. Other 'active' applications include the use of magnetic atoms, periodically spaced in an LB film, to produce two dimensional magnetic arrays[48] and and also radioactive nuclides incorporated in a conventional film to produce a dilute radioactive source.

The range of potential applications is clearly vast and varied and, although much of the work is at an early stage, many are being actively pursued. In this study, the insulating properties of the conventional fatty acid films, allied to the control over insulator thickness which is possible using the LB technique, have been employed to study injection electroluminescence in MIS structures. In addition, diodes fabricated using films of phthalocyanine have also been studied in an attempt to benefit from the attractive properties possessed by this material.

CHAPTER 5

EXPERIMENTAL DETAILS

In this chapter a general description of the equipment and materials used in this work is given, together with an account of the experimental procedures adopted. In addition, the results of some of the basic, but nevertheless very important preliminary experiments concerned with device fabrication are presented and discussed.

5.1 SAMPLE DETAILS

(a) Gallium Phosphide

The GaP used in this investigation was n-type, single crystal material grown epitaxially onto large area ($\sim$ 10 cm^2) n^+ substrates. These substrates were doped with sulphur to give a carrier concentration of approximately 10^{18} cm^{-3}. The GaP epilayers were grown by vapour phase epitaxy to a thickness of about 40 μm. These layers were sulphur doped to give carrier concentrations in the range 10^{15} - 10^{17} cm^{-3}. Additionally, the final 10 microns were doped with nitrogen to a concentration of approximately 10^{18} - 10^{19} cm^{-3}. The slices were supplied highly polished and were optically very smooth and uniform. The internal quantum efficiency of the nitrogen activated EL from this material was of the order of 1%. The external quantum efficiency of unencapsulated, p-n junction LEDs, fabricated from GaP with very similar properties to that used here, is typically $\sim$0.05%.

(b) Zinc Selenide

The ZnSe samples were single crystal, n-type material grown epitaxially onto GaAs single crystal substrates. These substrates were either semi-insulating or in some cases were heavily doped to provide a sample suitable for a sandwich geometry. The ZnSe epilayers were grown[1],

using the recently-developed technique of organometallic chemical vapour deposition (OM-CVD), to a thickness of typically 3 μm and were intentionally doped with aluminium to yield carrier concentrations in the range 10^{16} - 10^{18} cm^{-3}. The cathodoluminescence spectra of the ZnSe material used here has been studied by Wight et al[2], and found to contain features in both the blue and yellow regions of the spectrum. The relative intensities of these emissions varied from one sample to another. The external quantum efficiency of material which emitted predominantly in the blue was measured to be 0.14% corresponding to an estimated internal efficiency of ∿30%[2]. A somewhat higher external efficiency (∿0.6) has been deduced for the yellow emission[3] due to the reduction in the effect of internal reabsorption. No previous EL measurements have been reported for conducting ZnSe grown by organometallic-CVD.

5.2 DEVICE FABRICATION

5.2.1 Ohmic Contacts

(a) Gallium Phosphide Samples

Since the active EL region of the GaP slices was only ∿ 10μm thick, extreme care was necessary, particularly from the viewpoint of etchants, to ensure that as little as possible of the surface material was removed during device fabrication. The following procedure was used to give reproducible, highly Ohmic, low resistance contacts without the need for an etching or chemical polishing process at this stage of the fabrication: The slices were thoroughly degreased by refluxing in isopropyl alcohol vapour for several hours. High quality (99.999%) indium wire was used to make two small, preformed contacts on the back face of each sample. These were then annealed in an inert atmosphere at 500°C for 10 minutes. The Ohmicity of the contacts was measured using a transistor curve tracer. The resistance thus measured was invariably of the order of a few Ohms and agreed well

with the expected value which was calculated from the resitivity of the bulk material.

(b) Zinc Selenide Samples

Two geometries were used for the ZnSe samples in this work, i.e. surface and sandwich geometries. For the surface arrangement, the Ohmic contacts were formed on the same sample surface as the barrier electrode, i.e. to the ZnSe material. In the sandwich structure, the Ohmic contact was formed, as usual, on the opposite face to the barrier electrode, i.e. to the GaAs material. In both instances the samples were degreased by refluxing in isopropyl alcohol vapour for several hours. Preformed contacts, made from indium wire for contacts to the ZnSe material and from an indium /5% tin alloy for contacts to GaAs, were annealed in an inert atmosphere for 10 minutes at 275°C.

5.2.2 Surface Preparation

The Langmuir-Blodgett technique is a room temperature, low energy technique which causes relatively little damage to the substrate surface when compared to other, more conventional techniques such as sputtering or evaporation. This means that the pre-LB film-deposition surface preparation is of paramount importance, as it can, in some instances, determine the nature of the LB film-substrate interface. This is particularly important when the substrate to be coated is a semiconductor; it has been shown for example, that the InP-LB film interface state density distribution can be significantly altered by suitable surface preparation[4]. From the viewpoint of this work, a particularly important consideration was the influence and extent of the inevitable interfacial layer which was present between the LB film and the semiconductor as a result of the surface preparation. A variety of etchants and chemical polishes were used in this study and these are discussed below.

(a) Gallium Phosphide

Three different chemical polishes, which have been reported as being suitable for GaP were investigated. Table 5.1 lists these polishes and some of their properties. Of these preparations, the peroxide treatment is the least useful from the viewpoint of this work. The resulting surface, as revealed microscopic examination, was generally good, although it did contain a number of gross defects which were the result of preferential etching. Moreover, the etch rate is quite large and this necessitated the use of a very brief etch in the case of EL material since the active region was only $\sim$10μm thick. This meant that it was less controllable than polishes with slower rates, and hence more likely to produce an uneven surface. It was not considered further in this work. The ferricyanide and Br_2/CH_3OH preparations exhibited more controllable, slower rates of action and this, coupled to their non-preferential polishing action, resulted in high-quality, polished surfaces. It was necessary to follow the Br_2/CH_3OH treatment with an HF, oxide-removal stage since devices fabricated without this invariably exhibited non-ideal characteristics. This was attributed to the presence of a significant interfacial layer (see § 6.3). The HF stage was not necessary in the case of samples prepared using the ferricyanide treatment, as such samples, although possessing a thin interfacial layer, still exhibited near-ideal characteristics (see § 6.2). In summary, both the ferricyanide and the Br_2/CH_3OH-HF polishes result in similar, high-quality semiconductor surfaces and both are suitable for use with the GaP EL material. However, the latter preparation is thought likely to result in a relatively oxide-free surface whereas the former is expected to possess some form of interfacial layer.

The etch rates listed in table 5.1 were determined by first protecting half of the semiconductor with 'Lacomit' and then polishing the sample for a known period of time, usually several minutes. Subsequent removal of the

Preparation	Concentrations	Abbreviation	'Etch' Rate	Comments
Bromine/Methanol	0.5% Bromine by volume	Br_2/CH_3OH	∿ 1μm/mm.	Mixture must be used fresh (ages rapidly). Results in polished, mirror-like surface
Hydrofluoric Acid	40% by Volume	HF	-	Oxide Removal. Used with Br_2/CH_3OH to produce high quality, oxide-free surface.
Potassium Ferricyanide/ Potassium Hydroxide In Water	3g $K_3Fe(CN)_6$ 0.24g KOH 10ccs H_2O	Ferricyanide	∿ 2.5μm/min.	Used at 80°C. Results in high quality polished surface.
Sulphuric Acid/ Hydrogen Peroxide In Water	$H_2SO_4:H_2O_2:H_2O$ 4 : 1 : 1 By Volume	Peroxide	∿ 8μm/min.	Known to leave oxidised surface. Surface quality good, although some preferentially etched regions.

Table 5.1 Listing the various surface preparations used for GaP and some of their properties

lacquer enabled the depth to which material had been removed to be measured using a microscope with a calibrated stage.

(b) Zinc Selenide

The scarcity of the organometallic-CVD ZnSe material used in this work meant that a comprehensive study of the effects of different surface preparations was not possible. Furthermore, the fact that the ZnSe epilayers were only $\sim$ 3μm thick meant that extreme care was necessary during surface preparation in order to prevent the ZnSe from being completely removed. The following technique was found to yield Schottky barriers with reasonably good characteristics and was therefore used to prepare all of the ZnSe devices: The samples were refluxed in isopropyl alcohol vapour for several hours and then polished, at room temperature using a mixture of bromine and methanol (0.5% bromine by volume) for 1 minute. This was followed by a carbon disulphide rinse in order to remove the surface bromine compounds which are a consequence of the polishing procedure[5].

5.2.3 LB Film Deposition

In all cases, the first monolayer was deposited as soon as possible after the semiconductor surface had been prepared. In practice this was invariably within 30 minutes. Similar deposition conditions were used each time a film was deposited so that, as far as possible, the structure and properties of the insulating films were reproducible.

(a) Cadmium Stearate

The following deposition conditions were used to deposit $CdSt_2$ LB films: The subphase pH was 5.75 ($\pm$ 0.05) and its temperature was 18 ($\pm$2)^{o}C. The surface pressure of the monolayer spread on the water surface was maintained at either 25 mN/m or 30 mN/m. Cadmium ions, in the form of

$CdCl_2$, were added to the subphase to give the required 2×10^{-4} M solution. It was shown in § 4.4 how a compression isotherm could be measured to give some indication of the quality of the monolayer, and this was routinely performed prior to each deposition procedure. A typical isotherm (pH = 5.75) is shown in fig. 5.1. (At this pH, the film consists largely of $CdSt_2$, although the conversion is not complete and there is still some stearic acid present.) The first monolayer was always deposited slowly, at a speed of $\sim$ 1-2 mm/min. Subsequent layers were found to deposit better (see later) if the samples were desiccated for $\sim$1-2 hours under a low pressure of dry nitrogen. These subsequent layers were deposited more quickly, at speeds of up to 10 mm/min.

(b) ω-Tricosenoic Acid

The deposition conditions were as follows: The subphase pH was 5.5 ($\pm$ 0.1) and the subphase temperature was 18 ($\pm$ 2)°C. The surface pressure of the monolayer was maintained at 35 mN/m. No cadmium was added to the subphase. A typical isotherm, obtained under these conditions, is shown in fig. 5.2. Since ω-TA is known to undergo an ageing process on the surface of the Langmuir trough[6], all depositions were completed in less than 1 hour using a freshly spread monolayer. Difficulty was experienced when attempting to deposit an aged film (i.e. more than four hours old) onto the semiconductors used in this work. The first monolayer was deposited at a speed of $\sim$ 1-2 mm/min and subsequent layers were deposited immediately at speeds of up to 50 mm/min. The post-first layer drying stage was found to be unnecessary when using ω-TA as the LB material.

(c) Substituted Phthalocyanine

The procedure used to deposit LB films of phthalocyanine is more complicated than that used for the more conventional films. This procedure was described briefly in chapter 4. The following deposition conditions

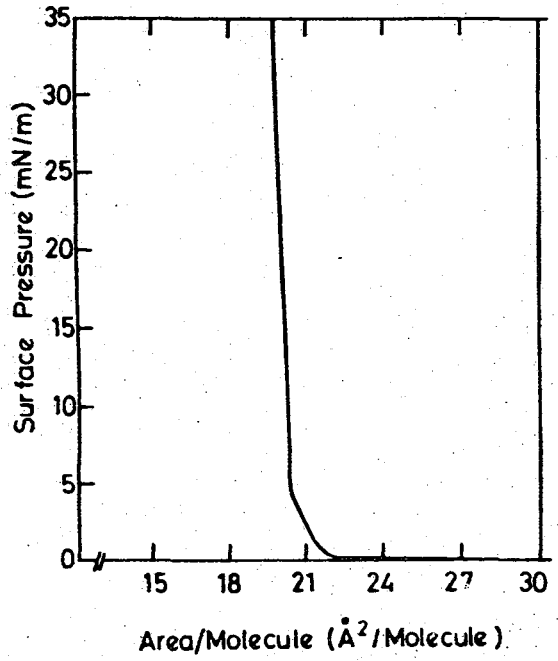

Figure 5.1 Typical $CdSt_2$ compression isotherm at pH 5.75.

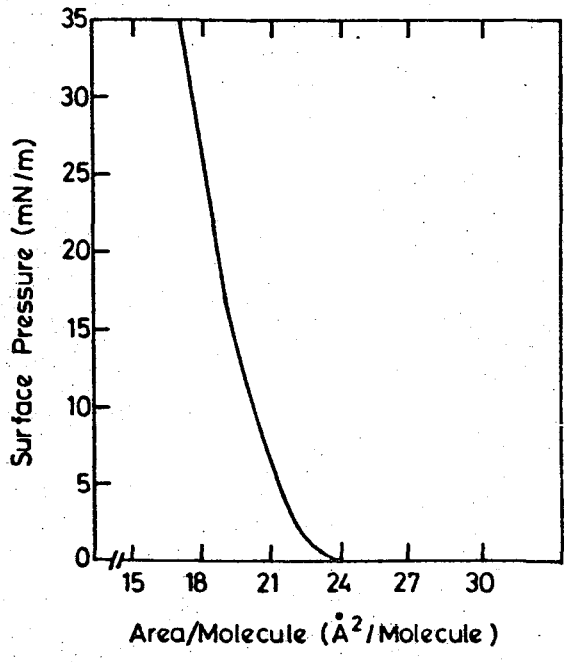

Figure 5.2 Typical ω-TA compression isotherm at pH 5.6.

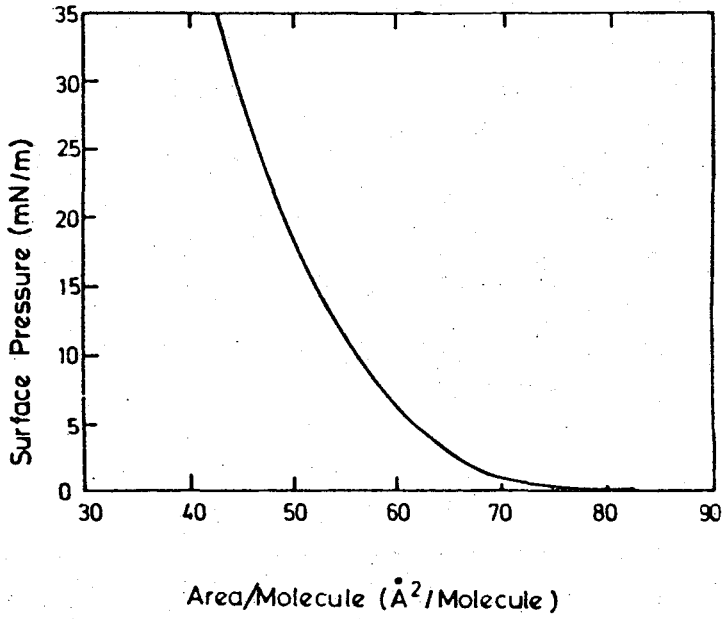

Figure 5.3 Typical Pc compression isotherm at pH 5.5.

were used: The subphase pH was adjusted to a value of 5.4 ($\pm$ 0.2) and its temperature was 18 ($\pm$ 2)°C. The surface pressure of the monolayer was maintained at 30 mN/m during the actual deposition. No cadmium was added to the subphase. A typical isotherm obtained under these conditions is shown in fig. 5.3. In this case all of the layers were deposited slowly, at a speed of $\sim$ 1-2 mm/min.

Irrespective of the material used to form the LB film, the samples were always desiccated, under a low pressure of dry nitrogen, for approximately 2 days prior to top electrode deposition. This is thought to improve the quality of the LB film and indeed, if this stage were omitted, then devices fabricated with insulators more than one monolayer thick invariably exhibited irreproducible characteristics.

Surface Preparation. In addition to being very important from the viewpoint of the interface properties, the sample surface preparation is also crucial with regard to LB film deposition. Usually this means that the surface must be either hydrophilic or hydrophobic in order to be conducive to pick-up. In the previous section, the properties of the GaP surface, as prepared by three different treatments, were discussed. One of these, the peroxide etch, was found to be unsuitable. It is convenient at this stage to consider the effect of the two remaining surface preparations on the success of the LB film deposition procedure. This will prove to be valuable in helping to choose the more suitable chemical polish with which to prepare the GaP for MIS diode fabrication. It was shown in §4.4 how a record of the dipping procedure could be made by monitoring the surface pressure and the surface area of the monolayer as a function of time. Fig. 5.4 shows such a record for a sample prepared using the ferricyanide treatment, onto which $CdSt_2$ was deposited. It can be seen that the surface pressure remains essentially constant (at $\sim$25 mN/m) as the material is removed from the surface of the water, thus causing the

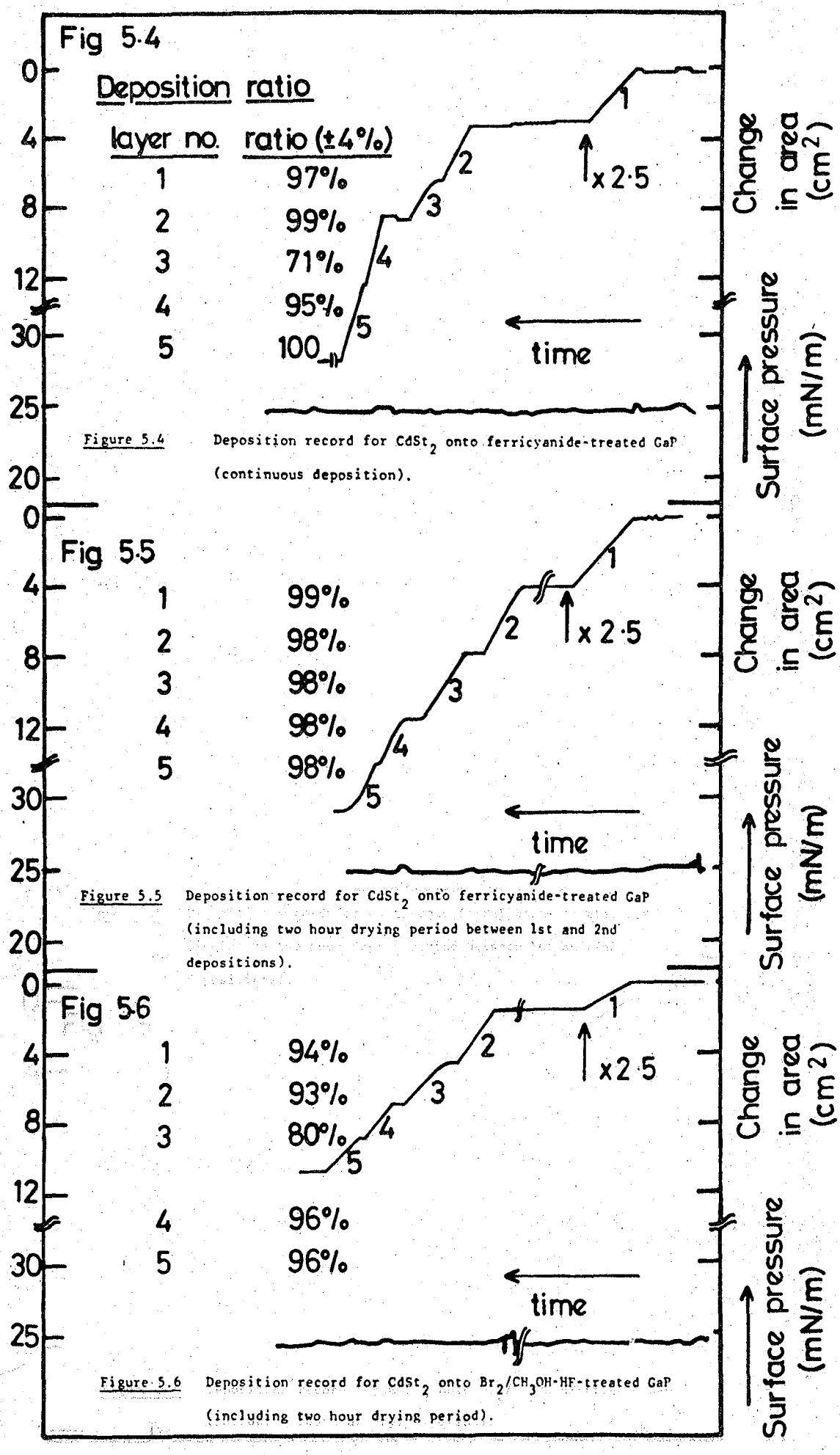

Figure 5.4 Deposition record for $CdSt_2$ onto ferricyanide-treated GaP (continuous deposition).

Figure 5.5 Deposition record for $CdSt_2$ onto ferricyanide-treated GaP (including two hour drying period between 1st and 2nd depositions).

Figure 5.6 Deposition record for $CdSt_2$ onto Br_2/CH_3OH-HF-treated GaP (including two hour drying period).

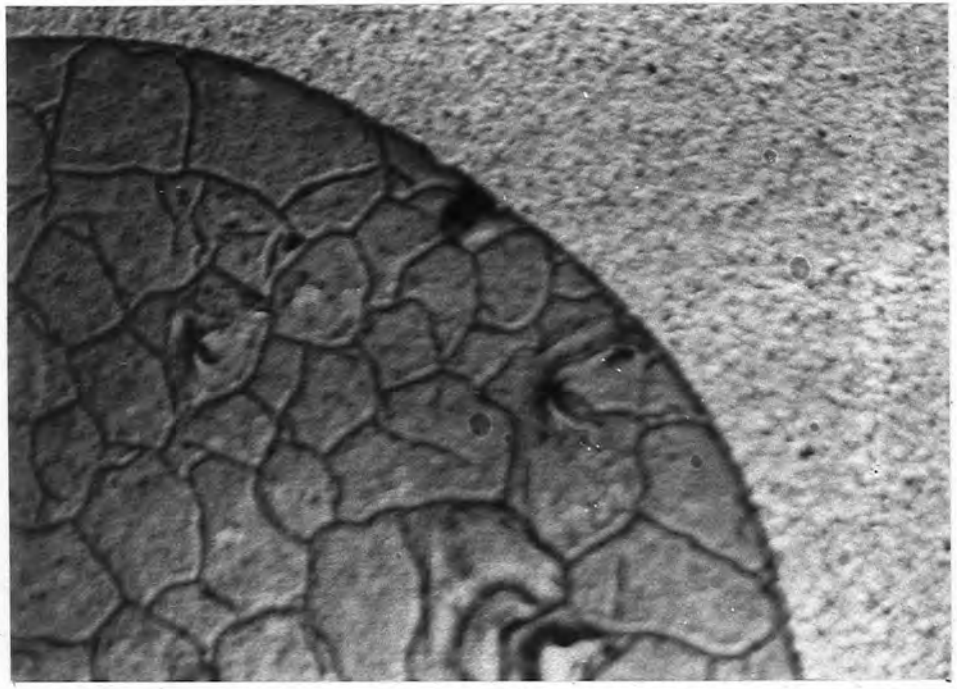

Figure 5.7 Photograph of a gold electrode on CaF exhibiting the 'crazed' appearance which is characteristic of thermal expansion problems.

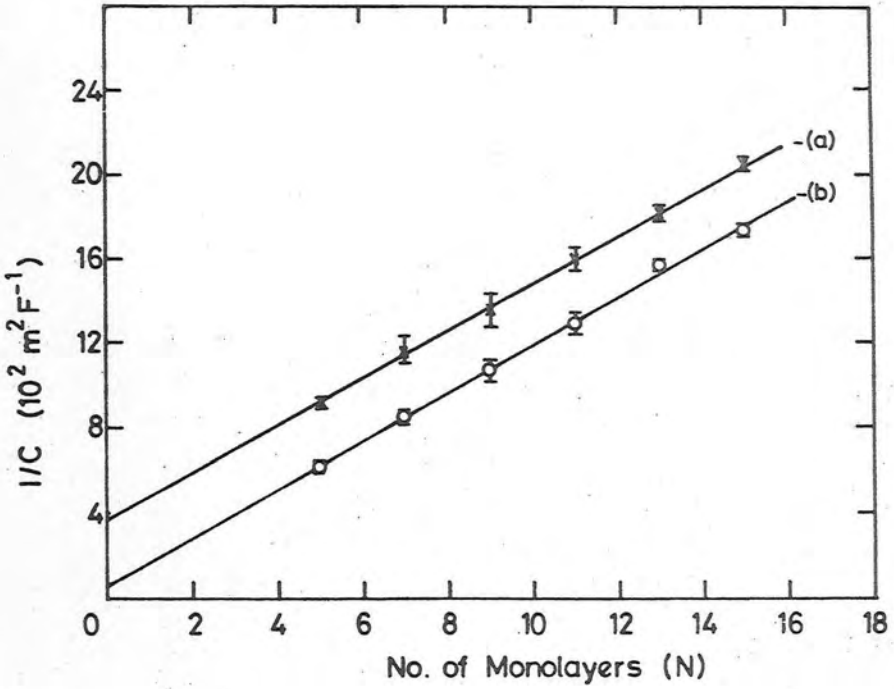

Figure 5.8 Reciprocal capacitance as a function of the number of monolayers, N, for two different MIM samples.

change in the area enclosed by the barrier. From this change in area, the deposition ratio was calculated by comparing it to the surface area of the sample which was measured using a microscope with a calibrated, moving stage. These deposition ratios are listed in fig. 5.4. (It should be noted that the LB film was deposited in a stepped-thickness manner which explains why the change in area is not the same in all cases.) The substrate in this instance was dipped continuously, i.e. with no drying time between the deposition of the 1st and 2nd layers. The ratios are largely very good (i.e. close to 100%) with an obvious exception relating to the pick-up of the third layer. This effect was unique to the deposition of $CdSt_2$ onto GaP, and was relatively independent of the mode of surface treatment. Its cause is uncertain, although it can be seen from the shape of the trace that the deposition gradually improves as the third layer is deposited. It was found that this effect could be eliminated, in the case of the ferricyanide treated substrates, by desiccating the sample for $\sim$1-2 hours after the first layer had been deposited. Fig. 5.5 shows another record where, in this case, the sample was desiccated for approximately 2 hours between the first and second depositions. It can be seen that the effect is no longer apparent and the deposition ratios are all close to 100%. This 'third layer' effect is clearly related to the properties of the 1st layer and this explains why it was never observed at any other stage in the procedure (e.g. during the deposition of the fifth layer). One possible explanation is that the crucial factor is the adherence of the second layer to the first. The unusual shape of the third trace in fig. 5.4 may be due to the partial removal of the second layer as the third deposition is attempted, rather than simply the incomplete deposition of the third layer. If this is the case, then the drying stage must render the first layer more conducive to pick-up.

The problem was not so easily overcome, however, in the case of a sample prepared using the Br_2/CH_3OH-HF treatment. Fig. 5.6 shows the dipping record for such a sample. Both the dipping conditions (pH, temperature and speed), and the drying period were identical to those used to obtain the record shown in fig. 5.5. In this case the third layer anomaly was still evident, although somewhat reduced in magnitude. However, it could usually be eliminated by the use of very slow dipping speeds (less than 1 mm/min.) although this was time-consuming and inconvenient. Another experimentally-observed trend can be seen in fig. 5.6, namely that the deposition ratios were, in general, lower than in the corresponding ferricyanide-treated samples. In concluding, it can be said that the ferricyanide treatment results in a somewhat better surface from the viewpoint of LB film deposition, although, with care, successful deposition is possible using either treatment. The difference between the two surfaces is likely to be due to the fact that the HF-prepared surface is expected to be essentially oxide-free, whereas the surface left by the ferricyanide preparation is expected to be uniformly coated with a thin 'oxide' layer. The extent of this layer, and its influence on device properties, is clearly an important issue and this is considered in §6.2.

5.2.4 Electrode Deposition

Since conventional LB film materials have, in general, low melting points, care must be exercised when evaporating metal electrodes. (For example, stearic acid has a bulk melting point of only $\sim 70^{\circ}C$ - although for $CdSt_2$ it is slightly higher than this and indeed, in monomolecular form it may well be higher still.) Previously, the method used to guard against thermal damage to the film has been to cool the substrate to a low temperature ($\sim -100^{\circ}C$) during the evaporating procedure. However, some authors[4] have experienced difficulty using this technique due to the mis-match of

the thermal expansion coefficients of the metal, insulator and substrate. This problem was found to be particularly acute when GaP was used as the substrate, and only a very low yield of reliable contacts was possible. Fig. 5.7 shows a photograph of a gold electrode (on GaP) exhibiting the 'crazed' appearance which is characteristic of this problem. Consequently, an alternative method for the evaporation of metal electrodes onto LB films was sought. It was found that, providing the evaporation was performed slowly, i.e. at a rate of about 0.5 nm/min in stages of $\sim$ 1nm at a time, the thermal damage caused to the film was minimal. This can be seen by considering fig. 5.8 which shows the reciprocal capacitance, plotted against the number of monolayers for two different metal-insulator-metal samples. These samples were identical, aluminized glass slides, which had been simultaneously coated with a stepped thickness, $CdSt_2$ LB film. The gold top electrodes were deposited (a) using the cooled substrate approach and (b) using the slow, staged technique. Each point represents an average value determined from several contacts on each region of the two samples. It can be seen that the two curves are very similar. Both are highly linear with almost identical slopes although the intercepts on the capacitance axis are somewhat different. These data can be analysed according to equation 4.1, i.e. $C^{-1} = Nd/\varepsilon_{1b}\varepsilon_o + \delta_i/\varepsilon_i\varepsilon_o$. This yields a value for d/ε_{1b} of 9.8 ($\pm$ 0.2) x 10^{-10}m which agrees well with previous results[4]. Assuming a molecular chain length of 2.5 nm, yields a value for the dielectric constant, ε_{1b}, of $\sim$2.5. The y-axis intercept can be used to deduce the thickness of the interfacial aluminium oxide layer. The intercept of curve (b) yields a value for δ_i of $\sim$4.5 nm (assuming a dielectric constant of 8.5 for the aluminium oxide). Again this value is consistent with that measured by other workers. However, the difference in the two intercepts is quite significant. It is not thought to be due to a difference in the thicknesses of the Al_2O_3 layer, since both samples

were fabricated in parallel under identical conditions (except for the method used to evaporate the top electrodes). The origin of this anomaly is unclear, it may be due to a reduction in the effective electrode area resulting from the cooling technique, or alternatively, it may be due to contamination of the LB film prior to electrode deposition (e.g. back-streaming diffusion pump oil condensing onto the cooled substrate). The slow staged technique is clearly the better of the two; it eliminates the problem of crazed contacts and also appears to result in better metal - insulator interfaces. This technique was used to evaporate top electrodes onto all of the samples used in this study. The evaporation procedure itself was shutter controlled and performed at a pressure of less than 10^{-6} torr to a final thickness of $\sim$ 15nm, as measured by a quartz-crystal oscillator, film thickness monitor. The contacts were delineated using a metal mask containing circular aperatures, typically 0.5 to 1.5 mm in diameter.

5.3 DEVICE CHARACTERISATION

Figure 5.9 shows a schematic diagram of the device geometry of a typical sample prepared using the procedures outlined in the previous section. It is shown specifically for devices fabricated on GaP but it is essentially the same for the ZnSe sandwich-type structures. For the ZnSe surface geometry samples, the Ohmic contact was made on the same surface as the gold electrode and was not coated with the LB film. Using reasonably large area substrates, it was possible to prepare samples with up to nine different regions of film thickness with approximately 15-25 contacts per region. This enabled a large number of diodes from each area to be sampled and representative ones chosen for full characterisation. In general, the reproducibility over a range of contacts from the same region was good. Samples which did not exhibit such reproducibility were not used further. The most reliable and convenient method of testing

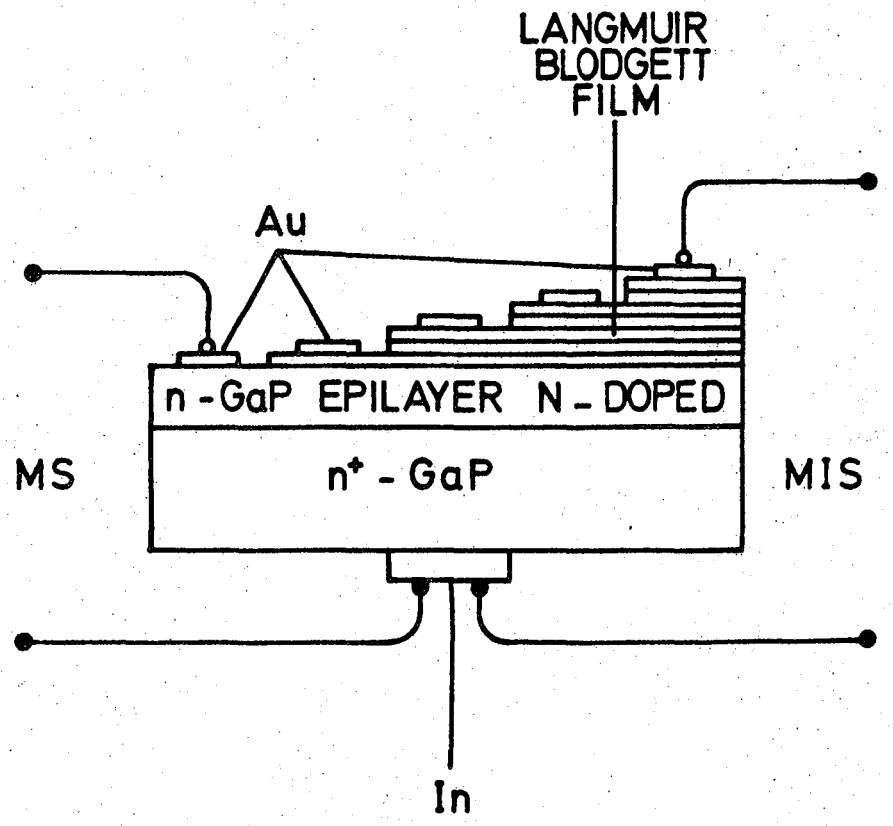

Figure 5.9 Schematic diagram of the device geometry.

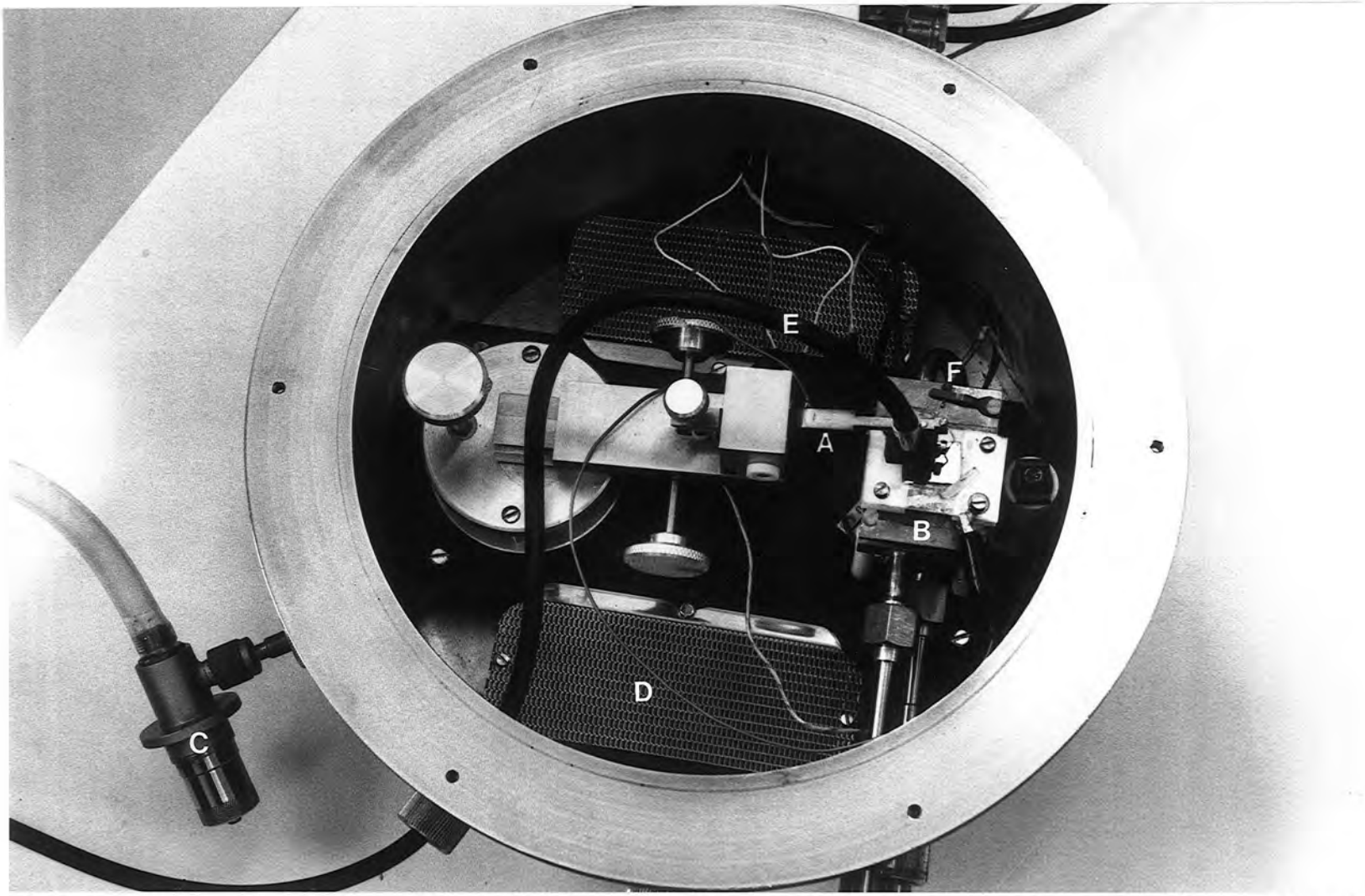

Fig. 5·10. Sample chamber used for both electrical and optical measurements.

this reproducibility was found to be by monitoring the current-voltage characteristics. In practice, the current taken by each device at a couple of preset voltage levels was measured and these data were used to choose typical contacts. This was found, in general, to be a more sensitive technique than, for example, measuring the diode capacitance, since the current taken by a diode is highly susceptible to defects or irregularities in the structure of the device.

Most of the experimental measurements were performed in a specially designed sample chamber. A photograph of this chamber is shown in fig. 5.10. Electrical contact was made using a gold ball ($\sim$ 0.5 mm in diameter) fastened to the end of the micromanipulator (A). A Peltier heater (B) placed beneath the sample mount, gave the chamber a limited cryogenic facility with a range of approximately -30°C to +60°C. A vacuum line connected to a rotary pump enabled the chamber to be evacuated, and a needle-valved gas inlet (C) allowed the atmosphere inside the chamber to be controlled. Furthermore, mesh covered metal trays containing silica gel desiccant (D) were used to provide a dry atmosphere. Illumination of the sample was possible through a glass window in the chamber lid. Alternatively, the optical fibre light pipe (E) could be positioned either directly over the electrode (as shown) or, by using an alternative sample base, directly underneath the electrode. This could also be used for collecting the light emitted from the diodes and guiding it to the detection equipment. A thermometer, placed inside the chamber, enabled the ambient temperature to be monitored and the thermocouple (F) was used to measure the sample temperature whenever the cryogenic facility was used.

5.3.1 Electrical Measurements

The current-voltage data were obtained using a Time Electronics type 2003S DC voltage calibrator and a Keithley 410A or 414 picoammeter. The analogue output from the picoammeter was monitored using a Y-t chart recorder so that the equilibrium current values could be taken. (The time taken for the current to reach equilibrium after a change in voltage was very much dependent on the particular substrate and LB film used. It was usually of the order of a few minutes although in some instances was as long as ∿30 minutes.) The capacitance-voltage measurements were made using a Boonton 72BD capacitance meter. This meter employs a 15mV(rms), 1MHz measuring signal and enables an external bias to be applied via the measuring terminals. The photoresponse data were obtained by coupling the sample to a Bausch and Lomb, high intensity (250W) grating monochromator by means of the optical fibre, and monitoring the short circuit photocurrent with a Keithley 410A picoammeter. Suitable filters, placed between the monochromator and the light pipe, were used to eliminate second order effects. The complete system was calibrated by replacing the sample with an Oriel 3810 thermopile, the output of which was measured using a Keithley 181 nanovoltmeter as a function of photon energy. This enabled the relative number of incident photons, and hence the photoresponse per incident photon to be calculated as a function of the photon energy.

5.3.2 Optical Measurements

The EL spectra were obtained by collecting the light emitted (through the back face of the diode for GaP devices, or through the gold electrode for ZnSe devices) using the optical fibre attachment and guiding it to a Hilger and Watts motor-driven grating monochromator coupled to an EMI type 9558QC photomultiplier tube. The output from the photomultiplier was

recorded on a Y-t chart recorder via the analogue output of a Keithley 414 picoammeter. The time axis of the chart recorder was calibrated in terms of the monochromator wavelength setting. A constant drive current density of ∿10A cm^{-2} was used to excite the EL. The efficiency measurements were made using a calibrated silicon photodiode. The sample was placed about 10 mm from the photodiode, in a specially constructed chamber. The active region of the photodiode was ∿5 mm square. In some instances, particularly in the case of less efficient diodes, it was necessary to use a larger drive current density. In these cases heating effects were eliminated by using a switching circuit to pulse the diodes with a constant current. A frequency of 500 Hz with a 2% duty cycle was used, providing a maximum current density of ∿25A cm^{-2}. The voltage developed across the diode, and the output from the silicon photocell were measured using a Telequipment D1011 oscilloscope. The external quantum efficiencies (in photons/electron) were measured using a calibrated, large area (∿ 7 cm^2) silicon photodiode. The photovoltaic measurements were made under approximate AM1 conditions which were provided using a Thorn OHS 1500W halogen lamp as a solar simulator.

5.4 GENERAL PROCEDURES

As in all aspects of semiconductor device fabrication, cleanliness was of paramount importance. Extreme care was taken to eliminate contamination of either the semiconductor substrates or the materials used at any stage of the device fabrication. Only the purest (Aristar grade) chemicals were used and all glassware was routinely cleaned with chromic acid, 'Decon 90' detergent and purified water prior to use. The semiconductor surface preparation was performed in a fume cupboard situated in a clean room in order to minimise contamination of the chemically prepared surface.

Each time a different semiconductor slice was used to fabricate MIS devices, a small piece was cut onto which near-ideal Schottky barriers were formed by evaporating the top electrodes soon after the surface preparation. Measurements made on these diodes were then used to characterise the slice and provide a standard by which the MIS diodes were judged. After fabrication, as a matter of routine, all samples were examined under an optical microscope. This revealed any gross defects or inclusions in the LB film and also any faults in the top electrodes. For device characterisation, the samples were usually mounted onto a PTFE base and a flying lead connection was made to the ohmic contact. The samples were stored, between measurements in an atmosphere of dry nitrogen at low pressure.

CHAPTER 6

RESULTS AND DISCUSSION : GaP SCHOTTKY BARRIER DEVICES

6.1 INTRODUCTION

In this chapter the characteristics of GaP Schottky barrier devices, fabricated using a variety of surface preparations, are presented and discussed. Diodes fabricated using the ferricyanide and Br_2/CH_3OH - HF treatments are shown to behave in a near-ideal fashion (as defined in §3.3). These diodes are fully characterised both electrically and optically in order to provide a standard by which the LB film MIS diodes can be judged. In addition, the theory described in § 3.3 is employed to deduce as much information as possible about the structure of the Schottky diodes, particularly with regard to the extent of the unintentional interfacial layer which is inevitably present. Devices prepared using a Br_2/CH_3OH surface treatment, without the HF oxide removal stage, are shown to exhibit non-ideal characteristics which are attributed to the presence of a significant interfacial layer. These devices are characterised and analysed in terms of the model described in §3.4, i.e. that pertaining to conventional MIS diodes. These diodes are essentially MIS structures incorporating a native 'oxide' layer as the insulator, and are therefore useful as a comparison for the LB film MIS data which are presented in chapter 7. Finally, the effect,on the Schottky diode characteristics, of exposing the semiconductor substrate to the conditions necessitated by the LB film deposition procedure is considered. This is used to obtain information on the extent and influence of the interfacial layer which will be present between the semiconductor surface and the LB film in the devices studied in chapter 7. This aspect is clearly very important since the elegance of the LB technique, from the viewpoint of this work, lies in

the ability to define the insulator thickness to a high degree of accuracy. This benefit would obviously be lost if the interfacial layer was completely uncharacterised.

6.2. NEAR-IDEAL SCHOTTKY BARRIERS

The characteristics of Schottky diodes fabricated using two different surface preparations are now considered. Diodes (a) were prepared using the ferricyanide treatment and diodes (b) using the Br_2/CH_3OH-HF preparation. Both samples were cut from the same crystal slice and the fabrication procedure, except for the surface preparation stage, was identical in both cases. The gold electrodes were deposited onto the two samples simultaneously using the slow, staged technique described previously.

6.2.1 Measurement of Barrier Height

The current density-voltage curves for typical diodes fabricated using the two different surfaces preparations are shown in fig. 6.1. Only that region of the characteristic which corresponds to the barrier limited regime is shown (for $J \gtrsim 10Am^{-2}$ the characteristics begin to be limited by the series resistance of the diode). The error bars represent the standard deviation of the experimental scatter measured over a large number of contacts on each slice. There is a small but definite difference evident between the two diodes, even when the experimental scatter is taken into account. The linear regions of the two curves are well described by eqs. (3.19) and (3.14) i.e. $J = J_o \exp(qV/nkT)$; where $J_o = A^*T^2 \exp(-q\phi_{bn}/kT)$. This is the thermionic emission theory ($V \gtrsim 3kT$) describing current transport in a Schottky barrier, and applying this to the data shown in fig. 6.1 yields an ideality factor very close to unity (~ 1.01) for both diodes but slightly different barrier heights in each case (1.37eV for diode (a) compared to 1.31eV for diode (b)). Fig. 6.2 shows an activation energy plot for a typical diode fabricated using the ferricyanide preparation. Here the

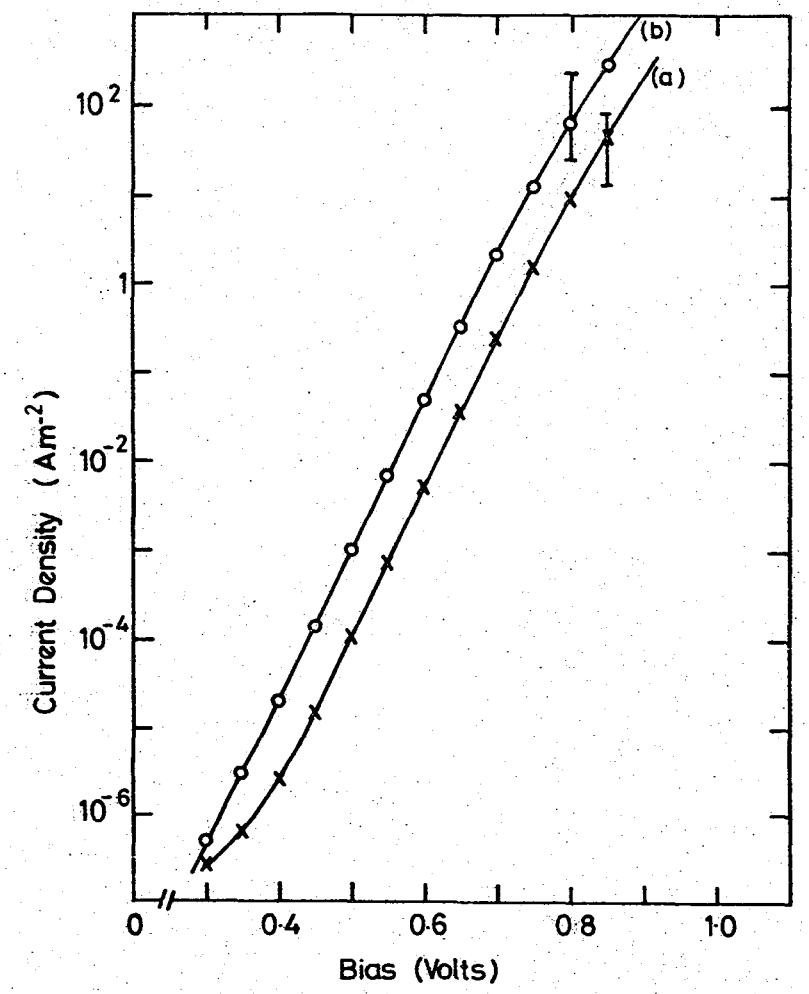

Figure 6.1 Current density as a function of forward bias for typical diodes prepared using (a) the ferricyanide treatment and (b) the Br_2/CH_3OH - HF treatment. (The reverse current was undetectable for an applied bias of -10V).

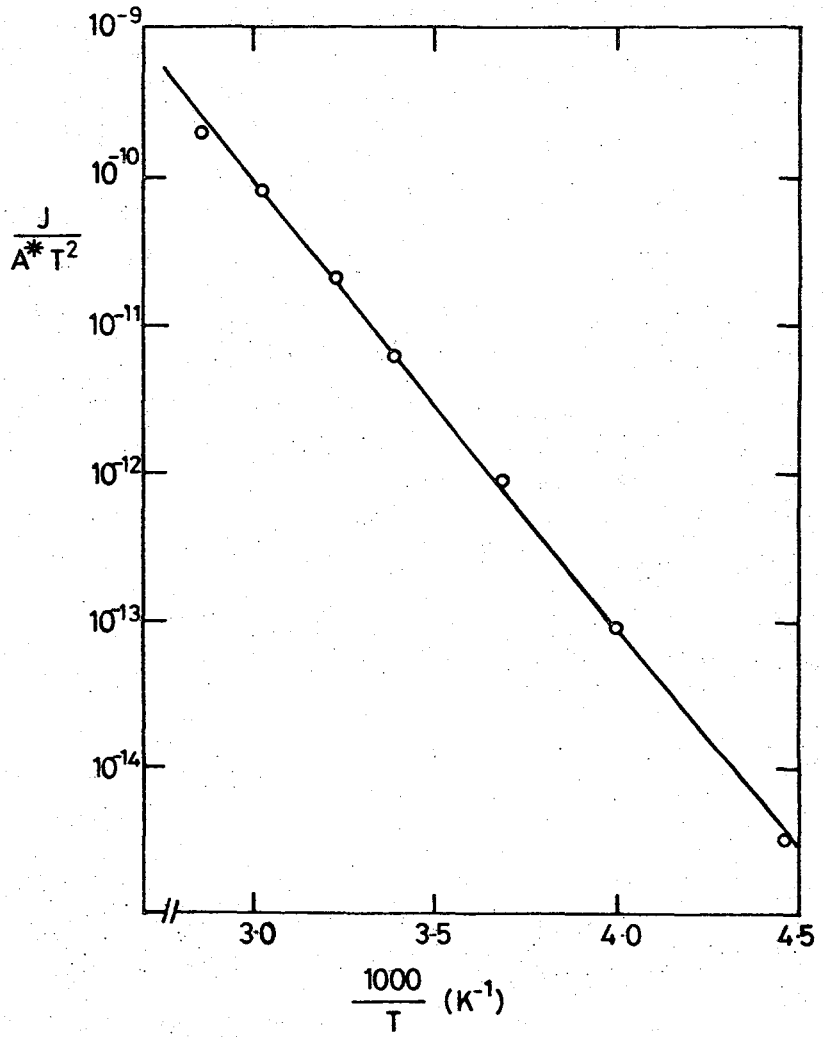

Figure 6.2 Activation energy plot for a near-ideal Schottky diode prepared using the ferricyanide treatment.

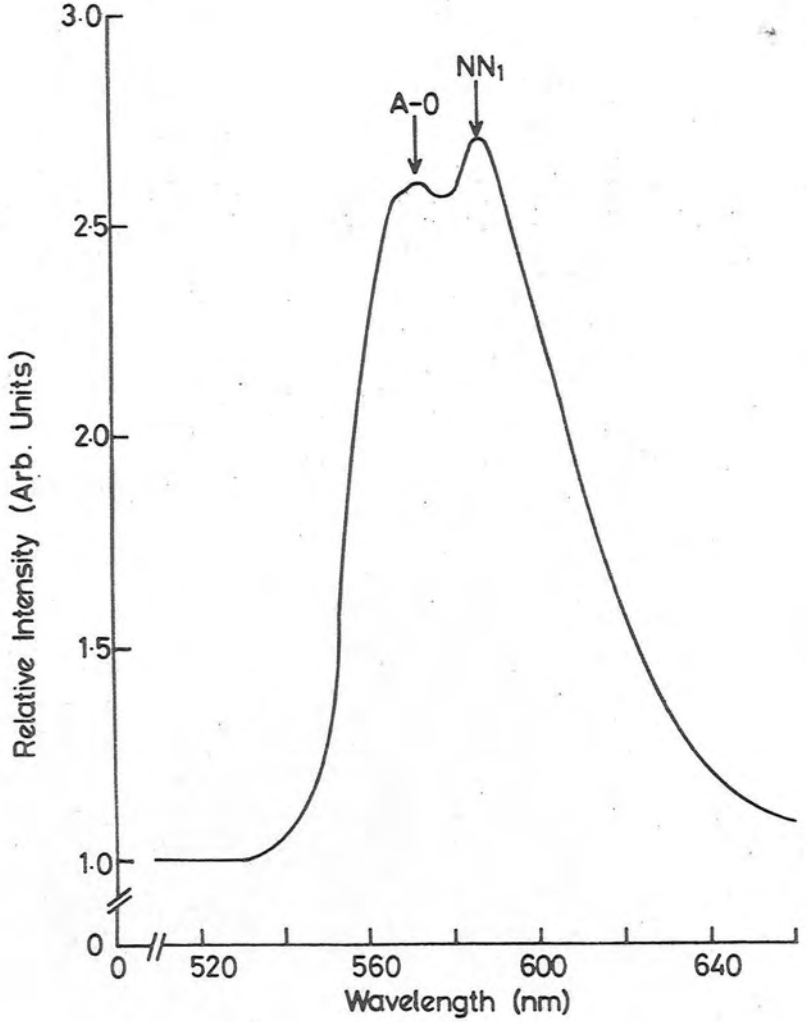

Figure 6.11 Spectral distribution of EL from a typical non-ideal Schottky diode.

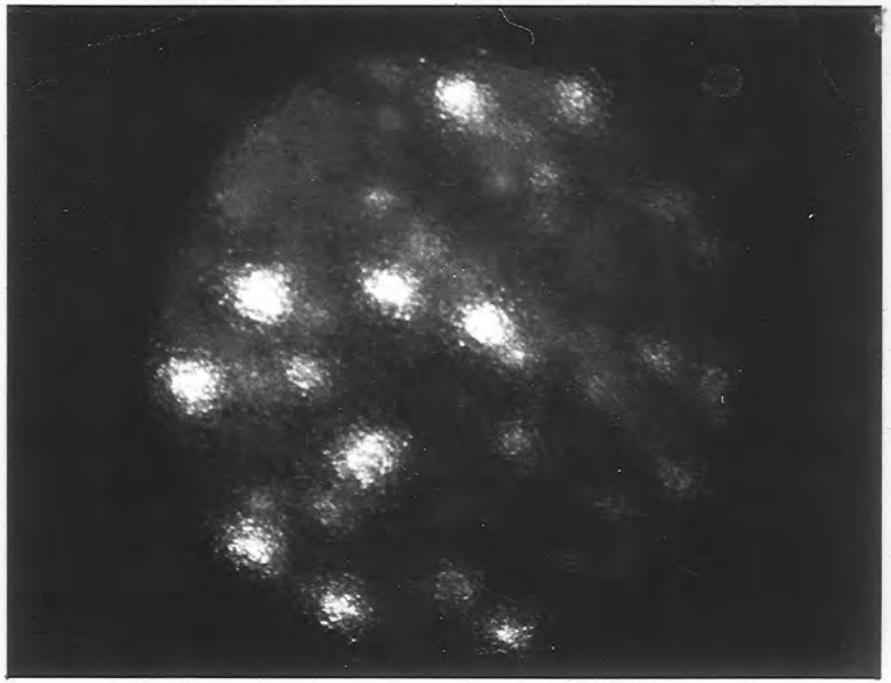

Figure 6.12 Photograph showing the irregular nature of the EL emission from a non-ideal Schottky diode.

current taken by the diode at a fixed value of forward bias (0.7V) over a range of different temperatures was measured and a graph of $\ln(J/A^*T^2)$ against $^1/T$ was plotted. According to the thermionic emission theory quoted above, such a graph should be linear, with a slope related to the barrier height and an intercept on the y axis of $\sim \ln(1)$, i.e. zero. The curve shown in fig. 6.2 is evidently highly linear, and analysing this data yields a barrier height of 1.30eV and an intercept of $\ln(9.3 \times 10^{-2})$. It will be shown in §6.2.3 how these results can be used to assess the extent of the interfacial layer which is present in these devices.

Fig. 6.3 shows the capacitance-voltage data, for the same two diodes, plotted as $^1/C^2$ against bias. Once again, the characteristics are slightly different in the two cases. Analysing these data according to the equation:

$$C^{-2} = (2/q\varepsilon_s Nd)(Vd-kT/q + Vr), \text{ i.e. eq. (3.31)}$$

yields barrier heights of 1.40eV and 1.35eV for diodes (a) and (b) respectively. This difference is small and much less significant than the corresponding difference in the conductivity data (see table 6.1 below). This arises from the fact that in the latter case, ϕ_{bn} is logarithmically dependent on the intercept (J_o) whereas in the former, it is linearly dependent on the intercept (Vd - kT/q). The change in slope, however, is not insignificant since the difference is clearly not accounted-for by experimental scatter. This disparity is attributed simply to different carrier concentrations in the two diodes since the slope was found to vary significantly between contacts even on the same sample. In fact the slope increased gradually as different diodes across the face of the individual samples were probed. The fact that the two semiconductor pieces were cut from opposite ends of the crystal slice accounts for the fact that the difference lies outside the limits defined by the experimental scatter.

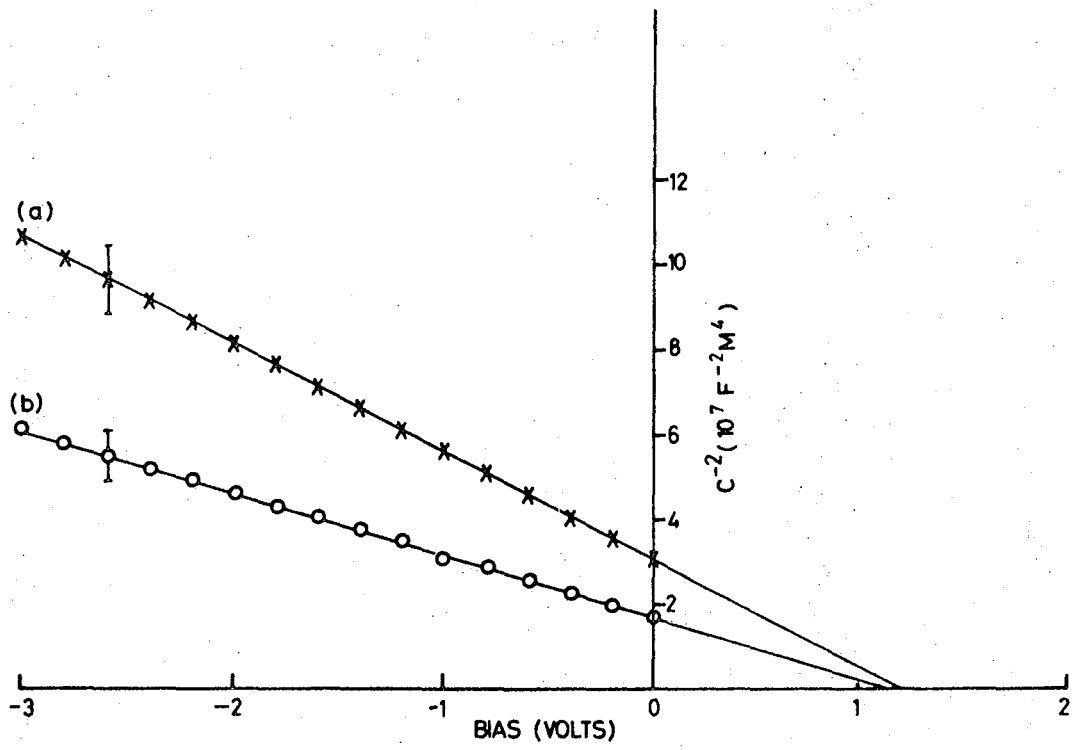

Figure 6.3 Reciprocal capacitance squared against bias for the two diodes used to obtain the data shown in fig. 6.1.

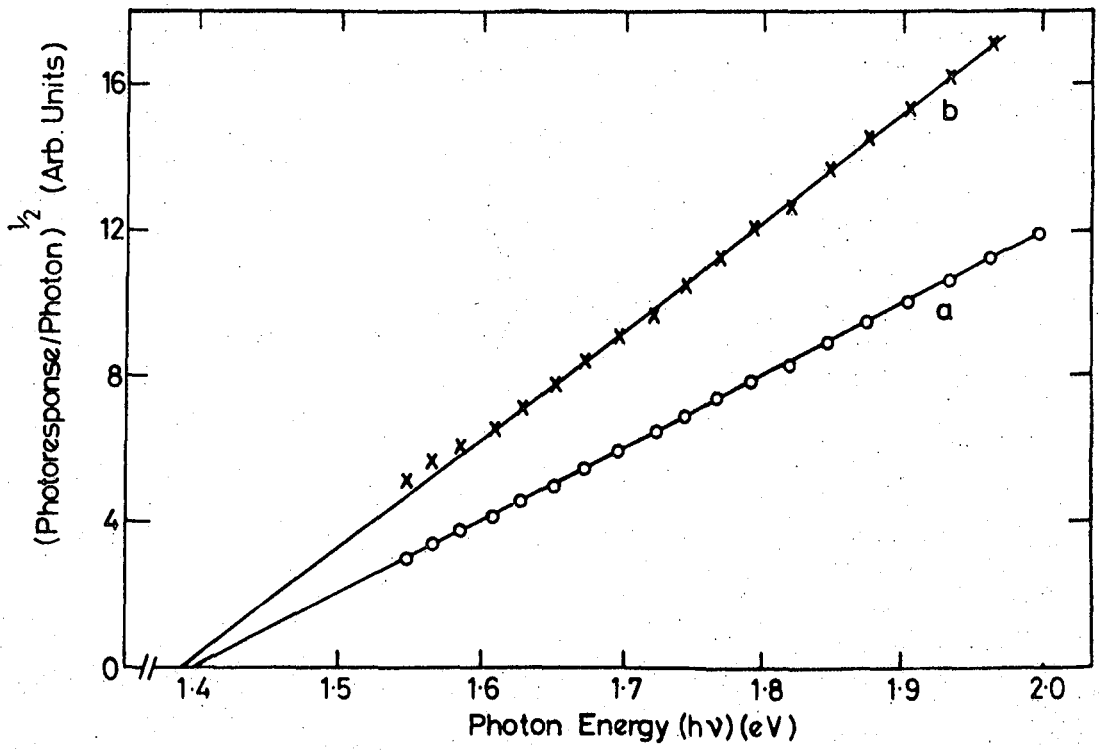

Figure 6.4 (Photoresponse per incident photon)$^{\frac{1}{2}}$ versus photon energy ('Fowler plots') for the two diodes used to obtain the data shown in fig. 6.1.

An approximate doubling of the doping concentration across the diameter of the semiconductor slice was noted.

The photoelectric data for the same two diodes are shown, in the form of Fowler plots, in fig. 6.4. Both diodes are well described by the relationship; $R = C(h\nu - h\nu_o)^2$ (i.e. eq.(3.30)) and extrapolating back to R = 0 yields barrier heights, $\phi_{bn} = h\nu_o$, which are very similar in each case ($\sim$1.39eV).

The information gathered from these three techniques is collated in table 6.1 below.

	J-V Data		$^1/C^2$ - V Data			Photoelectric Data
	Ideality factor	Barrier Height(eV)	Diffusion Voltage(eV)	Nd(cm^{-3})	Barrier Height(eV)	Barrier Height(eV)
Ferricyanide Preparation (Diode (a))	1.01	1.37($\pm$0.01)	1.23eV	5.0×10^{15}	1.40($\pm$0.03)	1.39($\pm$0.01)
Br_2/CH_3OH-HF Preparation (Diode (b))	1.02	1.31($\pm$0.01)	1.18eV	8.8×10^{15}	1.35($\pm$0.03)	1.39($\pm$0.01)

Table 6.1 . Information Deduced from figs. 6.1, 6.3 and 6.4

It can be seen from this data that there is a good agreement between the barrier heights measured by the various techniques, although those measured by the J-V technique are somewhat lower than the values determined from the other methods. Since the photoelectric technique gives the only direct measurement of this parameter, it can be assumed that the value of 1.39eV, measured for both diodes, is the most accurate. This means that the different values indicated by the J-V technique for the two diodes is not due to a real difference in barrier height. The only other possibility is that diode (a) possesses a more significant interfacial layer than

diode (b) and hence the J-V characteristics are affected by the $(\chi^{\frac{1}{2}}\delta)$ tunnelling transmission coefficient (§3.4.1). However, this layer is not of sufficient magnitude to cause a bias dependent barrier height since the ideality factor is still very close to unity. This interpretation is corroborated by the fact that the photoresponse, at any given photon energy, is smaller in the case of diode (a) (see fig. 6.4) which indicates an additional impediment to the current flow. This interfacial layer is considered in more detail in §6.2.3. It is interesting to note from fig. 6.1 how, at low bias, curve (a) tends towards curve (b). This can be explained if one assumes that the interfacial layer contains a significant pinhole density. At very low currents the conduction occurs via these pinholes and not by quantum mechanical tunnelling. However, at higher current densities this current path becomes saturated and the dominant mechanism is tunnelling which leads to the observed shift in the forward current characteristic.

6.2.2 Photovoltaic Properties

Gallium phosphide, with a bandgap of ∿2.25eV, is not a material which one would consider as suitable for solar cell applications since a large proportion of the solar spectrum would not be utilised by such a cell. However, the photovoltaic properties of the MIS devices will be shown to provide valuable information about the mechanism of minority carrier transport across the insulator. The photovoltaic characteristics of the near-ideal diodes are presented here, both for future reference, and to give additional information about the magnitude of the interfacial layer present in these devices. Fig. 6.5 shows the current density-voltage characteristics for a typical Schottky diode (type (b)) both in the dark and under illumination. For this particular diode, the open circuit voltage is ∿ 0.59V and the short circuit current is ∿ 0.18 Am^{-2}. Table 6.2

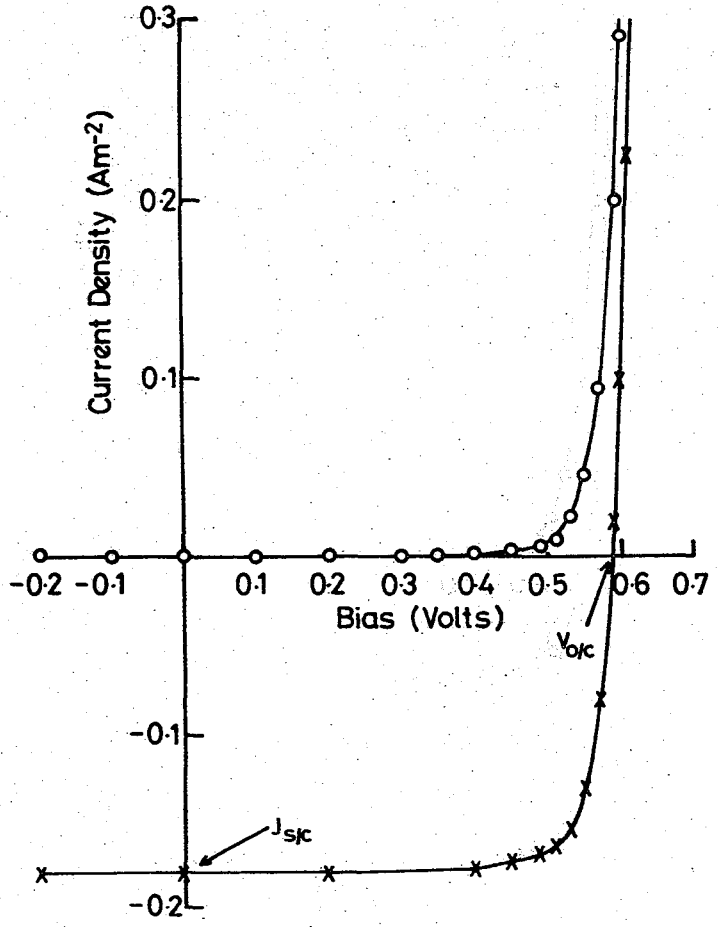

Figure 6.5 Current density versus bias for a typical Schottky diode (type (b)), both in the dark and under approximate AM1 illumination conditions.

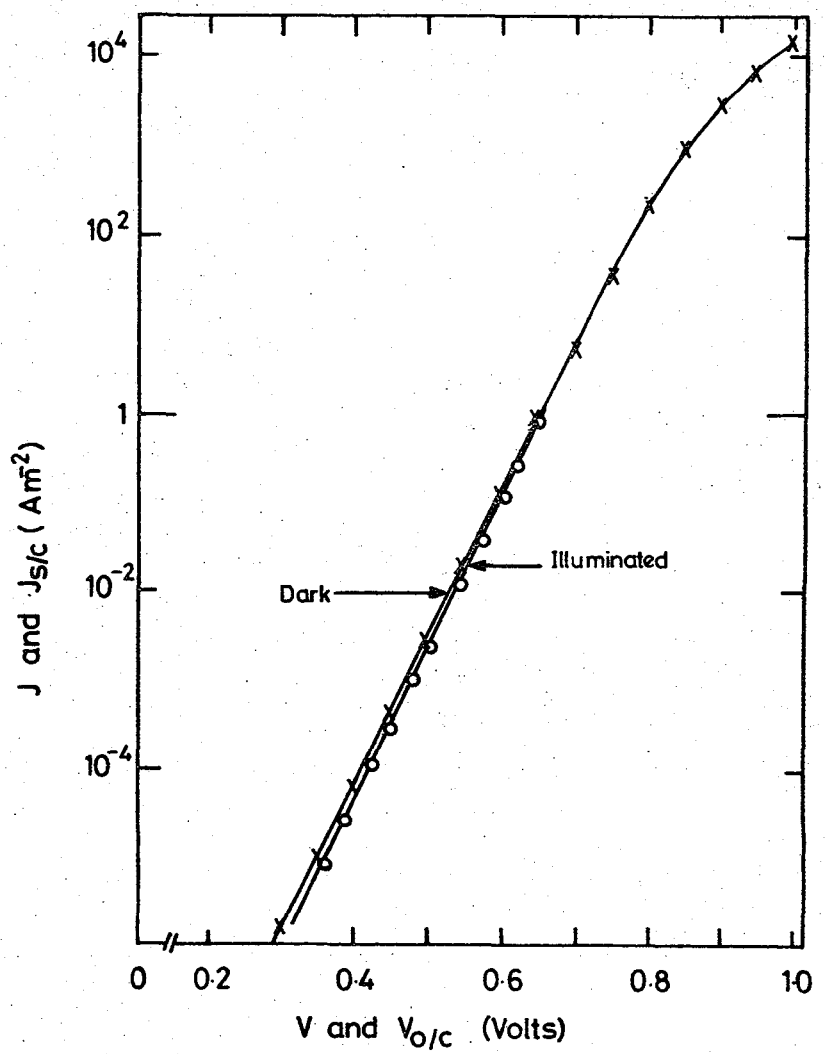

Figure 6.6 Showing dark J-V characteristic of a near-ideal Schottky diode (type (b)) and also the variation of $J_{s/c}$ against $V_{o/c}$ for the same diode.

shows these characteristics for diodes (a) (prepared using the ferricyanide treatment) and (b) (prepared using the Br_2/CH_3OH - HF treatment). They were determined from a number of contacts on each slice, the figures quoted being average values.

	$J_{s/c}$ (A/m^2)	$V_{o/c}$ (Volts)
Diodes (a)	0.19 ($\pm$0.02)	0.65 ($\pm$0.03)
Diodes (b)	0.19 ($\pm$0.04)	0.60 ($\pm$0.04)

Table 6.2 Photovoltaic properties of diodes fabricated using different surface preparations

The J-V characteristic of a Schottky diode under illumination can be written as:

$$J = J_o' \exp(qV/n'kT) - J_{s/c} \text{ for } V \gtrsim 3kT.$$

A relationship for the open circuit voltage can be found by equating J to zero. This yields:

$$V_{o/c} = n'\left(\frac{kT}{q}\right) \ln\left\{\frac{J_{s/c}}{J_o'}\right\}$$

where n' and J_o' represent the terms n and J_o under illumination. For the diodes used in this study, the values of n and J_o were almost unaffected by the illumination. This can be seen from fig. 6.6 which shows a plot of $J_{s/c}$ against $V_{o/c}$ for a range of illumination intensities in addition to a usual 'dark' J-V characteristic. The slopes, and hence ideality factors are similar in each case and there is only a slight change in J_o. If the

value of J_o' deduced from fig. 6.6 along with the short circuit current given in table 2 is used in the above relationship, $V_{o/c}$ is found to be equal to 0.61 volts. This is in excellent agreement with the figure quoted in table 2 for the diodes fabricated using the Br_2/CH_3OH - HF treatment and suggests that these diodes are particularly ideal, with a minimal interfacial layer. The slight increase in open circuit voltage observed in the case of diodes (a) is most likely due to the presence of an increased interfacial 'oxide' layer.

6.2.3 Assessment of Interfacial Layer

A number of conclusions can be drawn from the data presented in the previous two sections: Diodes (b), i.e. those fabricated using the Br_2/CH_3OH - HF treatment, exhibit the more ideal characteristics and are genuinely near-ideal since they agree well with the theory developed in §3.3. The photovoltaic data suggest that the interfacial layer in these devices is essentially 'transparent' to tunnelling electrons, i.e. the $(\chi^{\frac{1}{2}}\delta)$ tunnelling coefficient can be considered to be essentially zero. However, diodes fabricated using the ferricyanide preparation are not so ideal and this difference can be accounted-for by assuming the presence of a more significant interfacial layer. Nevertheless the diodes still behave largely according to the near-ideal model and they do not exhibit a bias-dependent barrier height. This is revealed by the fact that n is close to unity and that the barrier height measured by the capacitance technique agrees well with that calculated from the photoelectric technique. The thickness of this interfacial layer can be estimated indirectly from either the photoelectric or J-V data. Assuming that the difference in $V_{o/c}$ (shown in table 6.2) is due to the presence of an interfacial layer, then $V_{o/c}$ can be related to $J_{s/c}$ by eq. (3.63); i.e. $V_{o/c} = n'kT/q \{\ln(J_{s/c}/J_o') + \chi^{\frac{1}{2}}\delta\}$. This yields a value for $(\chi^{\frac{1}{2}}\delta)$ of approximately 2. As has been previously discussed, it is virtually impossible to assign a theoretical

value to χ (and hence deduce δ) for such thin interfacial layers since the band structure may be very different from that of bulk material. This has been shown to be the case in the Si : SiO_2 system where Card and Rhoderick[1] have fabricated MIS diodes with varying, known insulator thicknesses and have experimentally determined corresponding $(\chi^{\frac{1}{2}}\delta)$values. Assuming that the two systems are similar, it is possible to infer an approximate value for δ from the data published in ref. (1). This yields an interfacial layer thickness of $\sim$ 1 nm. The difference in the two J-V characteristics shown in fig. 6.1 can also be related to the $(\chi^{\frac{1}{2}}\delta)$ term by describing curve (a) in terms of eq. (3.39); i.e. $J = J_o \exp(-\chi^{\frac{1}{2}}\delta) \exp(qV/nkT)$. Assuming that $(\chi^{\frac{1}{2}}\delta) \sim 0$ in the case of diode (b), then a value for $(\chi^{\frac{1}{2}}\delta)$ of 2.4 is deduced for diode (a). Again, by relating this to the data in ref. (1), a value of $\sim$1.2 nm is inferred for δ. It is interesting to note that, although the interfacial layer probably contains pinholes, they do not affect the photovoltaic properties of the devices to any great extent since $V_{o/c}$ has increased in accordance with eq.(3.63). In fact it has been shown[5] that an MIS solar cell can tolerate a large pinhole density (up to 1000 cm^{-2}, $d \lesssim 1\mu m$) without significant degradation of the device properties.

Strictly speaking, the interfacial 'oxide' thickness deduced above is actually the difference between that possessed by the diodes fabricated by the two techniques, although the photovoltaic data (for diodes (b)) do give some justification for assuming that the $(\chi^{\frac{1}{2}}\delta)$ term is approximately zero in the devices fabricated using the Br_2/CH_3OH - HF treatment. However, the value of $(\chi^{\frac{1}{2}}\delta)$ can be deduced directly from the activation energy characteristic shown in fig. 6.2. Since the ferricyanide treated samples are best described by eq.(3.39)(see above) rather than the simple thermionic emission theory, then the intercept on the y axis should be equal to $\ln(-\chi^{\frac{1}{2}}\delta)$ and not $\ln(1)$. A value of $\sim$2.4 is thus deduced for $(\chi^{\frac{1}{2}}\delta)$ in

the ferricyanide treated samples which is in excellent agreement with that deduced earlier. Consequently, diodes fabricated using the Br_2/CH_3OH - HF treatment can be assumed to be free of any significant interfacial layer, whereas those fabricated using the ferricyanide preparation possess an interfacial layer, of the order of 1 nm thick, which has an appreciable tunnelling transmission coefficient but which does not result in a bias dependent barrier height. Such diodes will still be classed as near-ideal for the purposes of this work.

6.2.4 Energy Band Scheme

According to the simple Schottky - Mott theory (eq. (3.1)), the Schottky barrier height for the gold : (n) GaP system should be 1.1 eV. This is clearly not the case here where a value of 1.39eV has been measured. In fact, a wide range of barrier heights have been reported for this system and the exact value depends on both the surface preparation and the semiconductor properties. The Bardeen model of a Schottky barrier, i.e. the model used in the previous section to assess the extent of the interfacial layer, assumes that the Schottky barrier height is determined by the charge localised at the semiconductor surface in the interface states. Thus, by applying eq. (3.3), i.e. $\phi_{bn} = C_2 (\phi_m - \chi_s) + (1 - C_2)(Eg - \phi_o) - \Delta\phi_{bn}$, to this system assuming $\delta \sim 1nm$, $\varepsilon_i \sim 2\varepsilon_o$, $Eg - \phi_o = 1.6$ eV[2], and neglecting the image force barrier lowering, yields an interface state density of approximately 1.5×10^{13} cm^{-2} eV^{-1}. This value agrees well with the figures given in ref. (2) for a variety of Schottky diodes. This analysis will be extended in §6.3 when the effect of increasing δ is discussed and also in chapter 7 when the LB film MIS diodes are considered.

The proposed band diagram for the near-ideal Au : (n) GaP diodes described so far is shown in fig. 6.7. Dsa is the density of surface states and the subscript 'a' is used to denote the fact that their

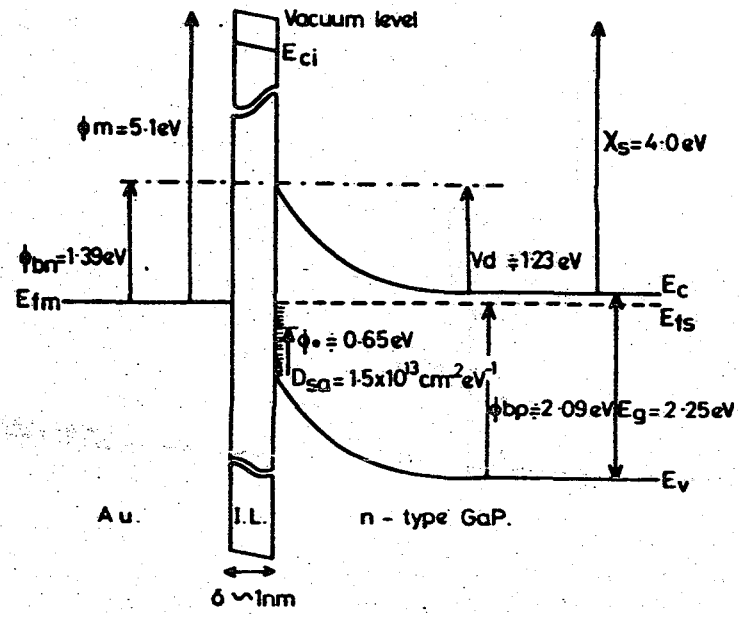

Figure 6.7 The proposed band diagram for the near-ideal Au : (n) GaP Schottky diodes.

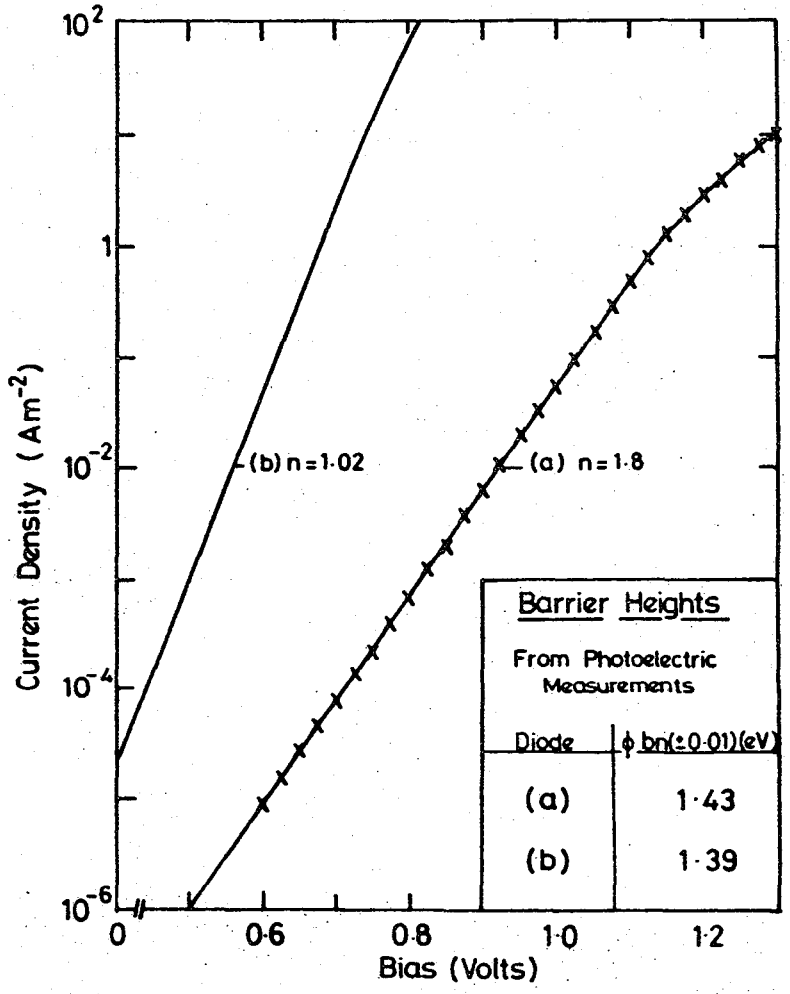

Figure 6.8 Current density-voltage data for a typical non-ideal diode (a). Also shown is a near-ideal characteristic (b). The inset shows the measured barrier heights. (The reverse current was undetectable for V = -10V).

population is governed by quantum mechanical tunnelling to and from the metal, i.e. they are populated according to the position of the metal Fermi-level. Since the interfacial layer is so thin, only a small fraction of any applied voltage is developed across the insulator. This means that the position of the Fermi level at the interface is essentially fixed relative to the band edges, and consequently the charge localised in the interface states does not vary with applied voltage, which explains the ideality of the diode characteristics. The band diagram under the application of a forward bias has been discussed previously and is shown in fig. 3.3.

6.2.5 Electroluminescent Properties

Irrespective of the method used to prepare the devices, none of the diodes discussed so far emitted any detectable EL, even for drive currents of up to 50 A cm^{-2} which is approximately an order of magnitude higher than that used in typical LEDs. The reason for this can be appreciated by considering fig. 6.7. The metal-semiconductor barrier which prevents holes from being injected into the semiconductor bulk (ϕ_{bp}) is $\sim$2.09eV high. This is much greater than the barrier presented to electrons (ϕ_{bn} = 1.39eV) crossing from the semiconductor into the metal. Therefore the bulk of the current, under the application of a forward bias, is due to electron flow and the minority carrier injection ratio , γ, is consequently very low. In fact by applying eq. (3.36) to the Au : (n)GaP system, γ can be estimated. This equation, which is known to be accurate for Au : (n) Si diodes, yields $\gamma \sim 10^{-14}$. This value is extremely small which is a consequence of the fact that $\gamma \alpha \exp\{-\frac{q}{kT}(\phi_{bp} - \phi_{bn})\}$ and is therefore acutely dependent on the value of $(\phi_{bp} - \phi_{bn})$. Since the EL efficiency is directly proportional to γ, it is not surprising that no EL could be detected from these near-ideal diodes. The scope for improvement, by

incorporating an insulator which enables a significant degree of band realignment to occur, is enormous since it should be possible to effectively reduce the height of ϕ_{bp} to zero by alignment of the metal Fermi level and insulator valence band edge (see fig. 2.8). Moreover, the control of insulator thickness afforded by the LB technique should enable diodes with the optimum thickness for EL efficiency to be fabricated.

6.3 NON-IDEAL SCHOTTKY DIODES

These diodes were prepared by polishing the sample for $\sim$ 2 mins. in a 0.5% Br_2/CH_3OH solution, and then exposing the semiconductor surface to atmospheric conditions for several hours before depositing the gold barrier electrodes. The HF oxide-removal stage was omitted. These devices are more accurately defined as MIS structures since the diode characteristics reveal the presence of a substantial interfacial layer which has a pronounced effect on the device properties. This layer is evidently a chemically prepared native 'oxide' and the diodes are termed 'non-ideal' in order to distinguish them from those containing the intentionally introduced, insulating layers (i.e. LB films).

6.3.1 Electrical Characterisation

The current density-voltage data for a typical diode is shown in fig. 6.8 (curve (a)). For comparison curve (b) shows the characteristic of a diode fabricated using the normal Br_2/CH_3OH - HF treatment. The corresponding barrier heights, as measured by the photoelectric technique, are also given in fig. 6.8. The $1/C^2$ against voltage curves for the same two devices are shown in fig. 6.9. It is immediately obvious that diode (a) is very different from the near-ideal diode (b). Both the increase in the ideality factor and the large voltage intercept on the $1/C^2$ - V plot are indicative of a bias - dependence of the barrier height

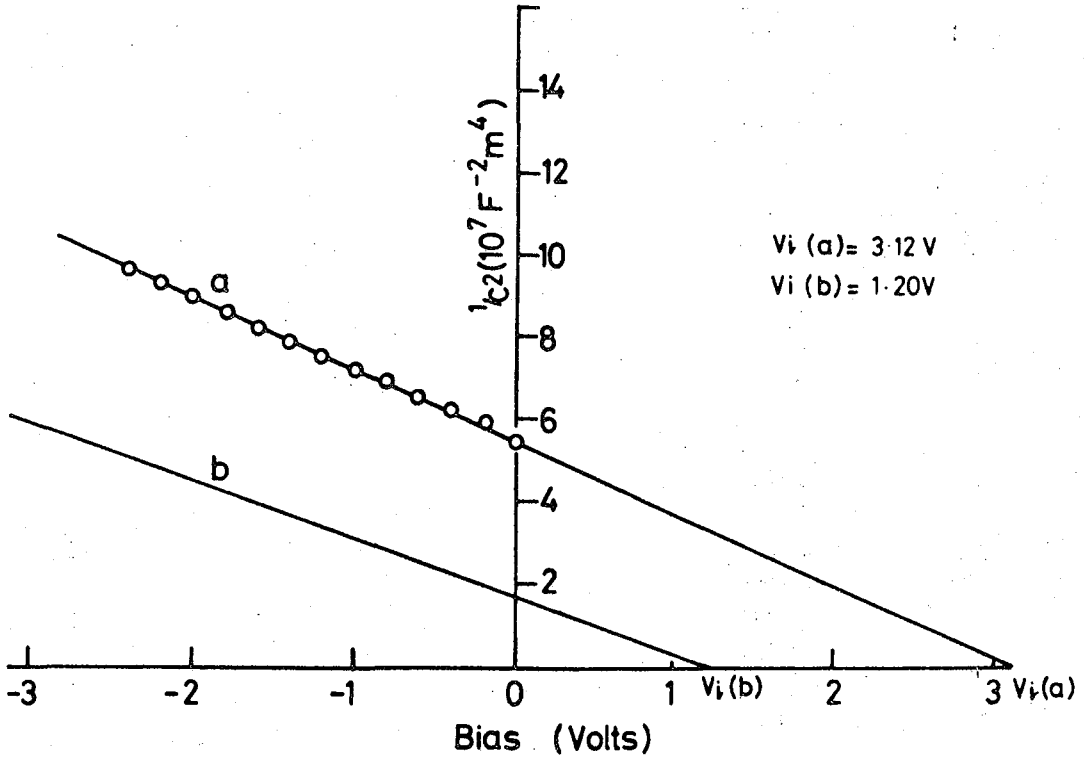

Figure 6.9 Reciprocal capacitance squared against voltage curve for a typical non-ideal diode. Also shown is a near-ideal characteristic (b).

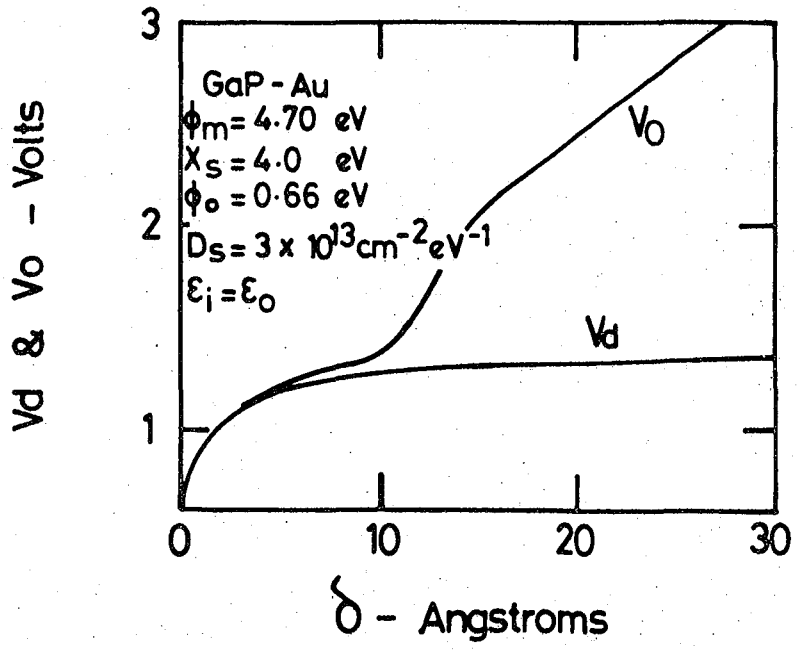

Figure 6.10 Variation of V_o with δ for non-ideal GaP Schottky diodes. (After Cowley[3]).

resulting from the presence of a substantial interfacial layer. The theory described by Cowley[3] (see §3.4.1), which was developed specifically to fit the Au : (n) GaP system, can be applied to the data in fig. 6.9. The main features of these data are that the slopes of the two curves are essentially the same whereas the intercepts are very different. These are precisely the features around which the Cowley theory[3] was developed. The model which was found to best describe this behaviour was one based on the presence of charged interface states and an interfacial layer significant enough to cause a degree of band realignment under the application of a bias. This results in a bias dependent interface charge density. The variation of V_o (the intercept on the voltage axis) with δ predicted by this model[3] is reproduced in fig. 6.10, from which an approximate value of δ can be deduced. This yields an insulator thickness of $\sim$ 3nm for diode (a) in fig. 6.9. However, this analysis must be considered as very approximate since the theory is rather complex and in order to produce the graph shown in fig. 6.10, a number of assumptions were made[3]. In particular, the dependency of the change in the interface charge on the degree of band realignment was chosen arbitrarily to provide a reasonable fit to the experimental data. In addition, an unknown fraction of the surface state charge may be governed by interactions with the semiconductor band structure rather than the metal. This latter problem is also encountered when attempting to relate the ideality factor of these diodes to δ using eq.(3.41). Nevertheless, the value of $\sim$ 3nm predicted from figure 6.10 for δ is not unreasonable since in the Si : SiO_2 system an insulator thickness of $\sim$ 2.2nm results in an ideality factor of 1.7[1]. The value of 1.8, calculated from fig. 6.8, for diode (a) agrees well with this.

6.3.2 Electroluminescence Measurements

A consequence of the voltage developed across the oxide under the application of a bias, is that an increase in the minority carrier injection ratio is achieved for a given value of forward bias. This effect has been discussed previously in § 2.4.3. and in more detail in § 3.4.1 and in fig. 2.8 the band realignment is clearly depicted. Since γ is an exponetial function of $q/kT\ (\phi_{bn} - \phi_{bp})$, even a small change in the relative positions of the metal Fermi level and semiconductor valence band will result in a dramatic increase in γ and possibly enable EL to be detected. This was indeed found to be the case. Under the application of a forward bias ($V \gtrsim 4.4\,V$) green/yellow light could be seen to be emitted from beneath the gold top electrode. The spectral distribution of this emission is shown in fig. 6.11. A drive current density of $10A\ cm^{-2}$ was used to excite the EL. At least two mechanisms can be distinguished in this spectrum and these can be identified, by their corresponding photon energies of 2.11 eV and 2.16eV, as the NN_1 and A-O processes respectively. The origins of these mechanisms were discussed in §2.6.2 and will therefore not be described here. However, the important aspect is that they are extremely characteristic of minority carrier recombination at nitrogen impurity centres. This confirms that the EL is a result of enhanced minority carrier injection due to the presence of the interfacial layer. The possibility of exciton formation due to impact ionization is ruled out since the turn on voltage for EL is known to be less than 4.4V, i.e. the lowest voltage at which EL could be detected. The electric fields necessary for impact ionization could not be achieved using such low voltages. The d.c. power conversion efficiency was measured to be at least $2.4\ (\pm\ 0.1) \times 10^{-4}\%$. Comparing this value to that of $\sim 5 \times 10^{-2}\%$, which is the efficiency of a typical, unencapsulated p-n junction diode

and assuming an injection ratio of 100% for the p-n junction, yields a value for γ of at least $\sim$0.5%. This represents a large increase over the value of 10^{-12}% predicted for the near-ideal diodes by eq. (3.36). However, the light emitted from the area beneath the gold electrode was not uniform. Fig. 6.12 shows a photograph of the emission as viewed through the back face of the semiconductor. The light can be seen to originate from numerous small regions. This is indicative of the irregular nature of the native 'oxide' layer with the bright spots being regions of high electric field. These diodes are clearly unacceptable as commercial devices although they are useful as a comparison for the MIS diodes fabricated using LB films. Since these films are highly uniform, both in thickness and in structure, a significant improvement in the uniformity of the light emitted should be possible. Furthermore, the fine control over the insulator thickness which is afforded by the LB technique will enable δ to be optimised and an improvement in the EL efficiency should be also possible. The results obtained for such diodes are discussed in chapter 7.

6.4 GaP/LB FILM INTERFACE : INTERFACIAL LAYER ASSESSMENT

Before proceeding to discuss the characteristics of LB film MIS diodes, it is useful at this stage to consider the question of the unintentional interfacial layer which must be present between the LB film and the semiconductor surface. It has already been demonstrated that in the case of the near-ideal Schottky diodes, this interfacial layer is of the order of $\sim$1 nm thick. However, in the LB film diodes this thickness may be somewhat different as a result of the device fabrication procedure. There are primarily three stages during the deposition of an LB film when an interfacial layer may grow on the semiconductor surface. These are: (i) the period during which the semiconductor is exposed to the aqueous environment of the Langmuir trough, (ii) during the 1-2 hour, post-1st

layer drying period and (iii) during the 2-3 day pre-electrode deposition period. (The two latter periods both involve storage under a low pressure of dry nitrogen.) It has previously been mentioned that the J-V characteristic is very sensitive to the presence of an interfacial layer, and the effect of each of the above stages on this characteristic is now considered in sequence. Fig. 6.13 shows three typical current-voltage characteristics: Curve (a) represents the control diode where the barrier electrode was deposited immediately after the ferricyanide surface preparation. Curve (b) represents a typical diode which was prepared in parallel with sample (a) but also dipped at usual speed into the Langmuir trough (without a film spread on the surface) prior to deposition of the barrier electrode. Curve (c) is the characteristic of a typical diode from a sample which was dipped with sample (b), but then desiccated for 2 hours before metal electrode deposition. The error bars are again indicative of the experimental scatter over a wide range of contacts. There is little difference between the three characteristics with all exhibiting ideality factors very close to unity ($\sim$1.01) and no significant change in the magnitude of the forward current. In all three cases the reverse current, for V_R = 10V, was less than 10^{-12}A i.e. below the sensitivity of the measuring equipment. The barrier heights (see inset to fig. 6.13), as measured by the photoelectric technique, were very similar for all three diodes. From these data it can be concluded that neither exposing the sample to the aqueous environment of the trough, nor storage under dry nitrogen for 2 hours increases the magnitude of the interfacial layer to any significant extent. However, this was found not to be the case for stage (iii). Exposure to a low pressure of dry nitrogen for 2-3 days was found to result in the growth of an appreciable 'oxide' layer on the semiconductor surface. The effect of this layer on the device characteristics can be seen in fig. 6.14 where curve (b) shows the characteristic of a

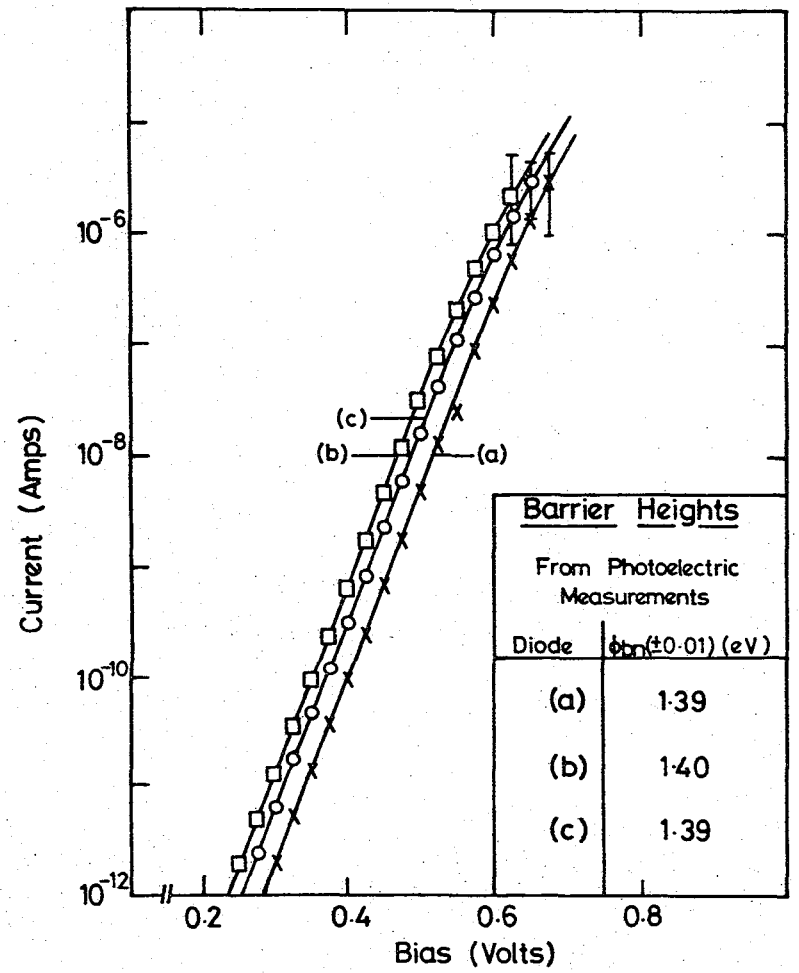

Figure 6.13 Three typical J-V characteristics for diodes fabricated using different techniques (refer to the text for a description). The corresponding barrier heights are listed in the inset.

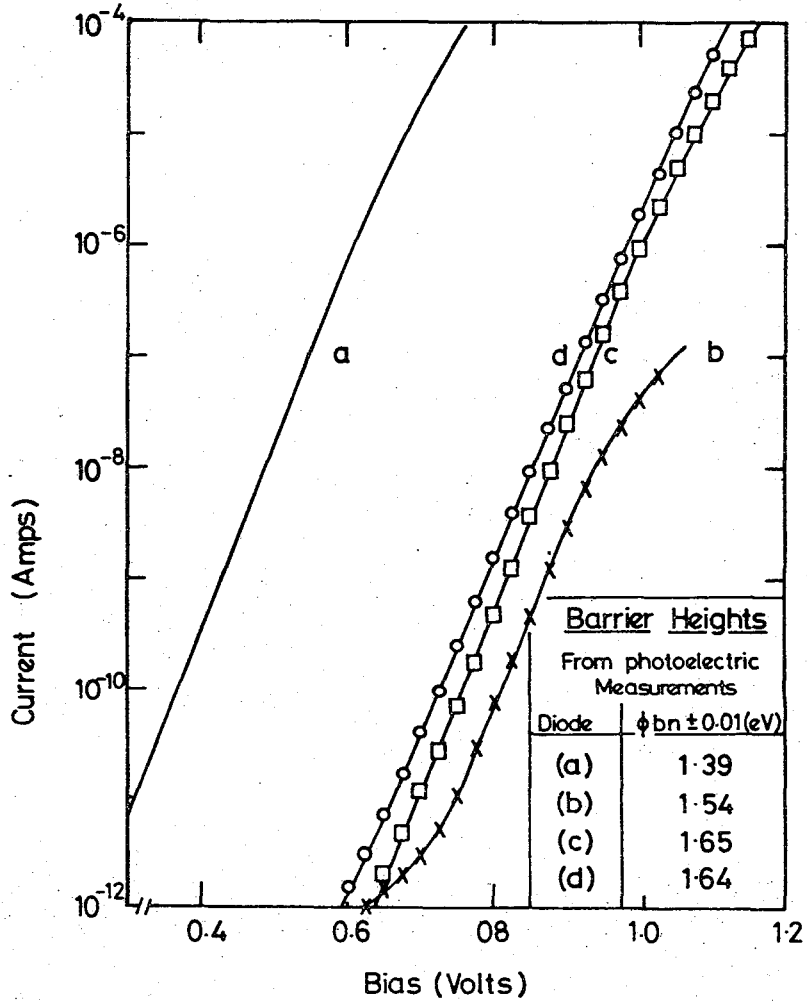

Figure 6.14 Showing typical J-V characteristics for four different diodes (refer to the text for a description). The corresponding barrier heights are listed in the inset.

typical diode fabricated by this method and (a), shown for comparison, is for a near ideal diode which had been desiccated for only 2 hours prior to electrode deposition. The barrier heights of the two devices are also listed in fig. 6.14. There is clearly a large difference between the characteristics of the two diodes. Although there has been little change in the ideality factor (from 1.01 to 1.05), there has been a dramatic decrease (of over six orders of magnitude) in the value of the forward current at a given voltage. In addition, the extent of the barrier limited regime has been reduced and the series resistance, associated with the diode has increased. All of these observations are indicative of a significant interfacial layer and although the ideality factor is still close to unity, these diodes cannot be considered as 'near-ideal'. The fact that the ideality factor remains largely unaltered indicates, that, although this layer may in fact be relatively thick, the majority of the interface states are populated according to the position of the metal Fermi level. This can be deduced from eq.(3.41); i.e. $n = 1 + (\delta/\epsilon_i)(\epsilon_s/W + qDsb)/(1 + (\delta/\epsilon_i)\, qDsa)$ where it is evident that interface states which equilibrate with the metal tend to maintain n at approximately unity whereas those which equilibrate with the semiconductor tend to increase n. The large decrease in the forward current can be explained, at least in part, by the increase in the Schottky barrier height, as revealed by the photoelectric measurement. This increase of 0.15 eV is predicted by the general expression for ϕbn derived by Cowley and Sze[2] (eq. (3.3)) as a consequence of an increase in δ. It accounts for a decrease in the current of over two orders of magnitude. The remaining decrease must be due to the $(\chi^{\frac{1}{2}}\delta)$ term in eq.(3.39) and by relating curve (b) to this equation, it is possible to deduce a value of $\sim$10 for $(\chi^{\frac{1}{2}}\delta)$. The thickness of the interfacial layer can be estimated (a) by comparing the value for $\chi^{\frac{1}{2}}\delta$ deduced here to data obtained using Si : SiO_2 diodes[1], or

(b) by relating the increase in barrier height to eq. (3.3). The former of these methods yields a value of ∿3nm whereas the latter gives ∿5nm, which is a reasonable agreement considering the approximations involved. It is interesting to compare the characteristics of these diodes with those discussed in §6.3.1. Although the effective thickness of the interfacial layer may, in fact, be quite similar in the two cases, their properties are clearly very different. This is understandable since the diodes discussed in §6.3 contained a chemically prepared interfacial layer whereas those discussed in this section possessed a 'grown' layer whose structure and properties may differ significantly. The former of these layers evidently possesses the better insulating properties, possibly due to a lower density of defects and pinholes. The effective 'resistance' of this layer is significant when compared to that of the semiconductor depletion region and this is manifest in the pronounced bias dependence of the barrier height. The intercept on the voltage axis in the C^{-2} -V data was much smaller in the case of the 'grown' layer (1.6V compared with 3.1V for devices incorporating the chemically prepared layer) which again indicates a much reduced bias-dependency of the barrier height.

The cause of the oxide growth during stage (c) is uncertain although it could be a result of impurities contained in the nitrogen gas or possibly residual oxygen in the desiccator, since diodes fabricated on samples exposed to the atmosphere for 2-3 days exhibited similar characteristics. Whatever the cause, an important question arises: Does this layer grow only in the exposed region of an LB film-coated sample, or is it also present beneath the LB film? This is of paramount importance since the elegance of the LB technique, from the viewpoint of this work, lies in the ability to accurately define the insulator thickness. Furthermore, it is important to distinguish between effects due to the

presence of the LB film and those due to the interfacial layer. The problem arises because it has been shown that some LB films are porous to certain gases[4], thus the insulator may not prevent the growth of such a layer. The question can be answered by again considering fig. 6.14. Curve (c) represents the current-voltage characteristic of an MIS diode fabricated with one monolayer (2.5 nm) of $CdSt_2$, which was desiccated for ∿2 hours before electrode deposition. Curve (d) corresponds to a diode fabricated on an identical substrate except that it was desiccated for ∿2 days prior to metallisation. The finer details of these curves will be discussed in chapter 7 together with the other MIS data and are therefore not discussed here. However, it can be seen that there is only a small difference in the magnitude of the forward current at a given voltage and that the barrier heights are approximately the same for the two diodes. This is in marked contrast to the difference between curves (a) and (b), and indicates that the deposition of a monolayer of the LB film prevents, or at least greatly retards, the growth of the interfacial layer. Hence the unintentional layer present in a metal LB film - (n) GaP device can be assumed to be of the order of 1 nm thick and not to significantly affect the device properties. It should be noted that once the barrier electrodes had been deposited, none of the characteristics shown in fig. 6.14 exhibited any ageing effects over a period of several weeks.

6.5 SUMMARY

In summarising the results presented in this chapter, the following conclusions can be drawn:

(a) Devices fabricated by either the ferricyanide or the Br_2/CH_3OH - HF methods can be said to exhibit near-ideal characteristics, although those prepared using the ferricyanide treatment posses a slightly more significant interfacial layer (∿1 nm thick). This interfacial layer

represents an additional barrier to the transport of electrons across the interface which manifests itself as a $(\chi^{\frac{1}{2}}\delta)$ term. It is not, however, sufficient to cause an appreciable realignment of the band structure under the application of a bias.

(b) No EL can be detected from any of these near-ideal diodes even for drive current densities of up to $\sim$50A cm^{-2}. This is a consequence of the extremely low value of γ in these devices.

(c) Diodes fabricated with a chemically prepared native 'oxide' layer exhibit non-ideal characteristics which can be described using the MIS diode model discussed in §3.4. The thickness of this interfacial layer is estimated to be $\sim$3 nm and is sufficient to cause a degree of band alignment under the application of a forward bias. This results in a dramatic increase in the minority carrier injection ratio and enables EL to be observed, although the emission is very irregular in nature and has a low measured external efficiency ($\sim 2 \times 10^{-4}$%).

(d) It has been demonstrated that it is possible to incorporate an interfacial layer which has a pronounced effect on the current-voltage characteristics without causing a significant increase in the ideality factor. This is interpreted as an indication that the majority of interface, states equilibrate with the metal. The criterion '$n \lesssim 1.2$' which is often assumed to justify the use of the simple Schottky barrier thermionic emission theory may therefore not always be valid.

(e) The interfacial layer present beneath the LB film in the MIS devices is not significantly different in extent or influence from that present in the near-ideal diodes, i.e. it is of the order of 1 nm thick and has only a small effect on the device properties. The characteristics of the LBfilm MIS diodes, which are described in the following chapter, can therefore be attributed to the presence of the LB film and are not a consequence of any unintentional interfacial layer.

CHAPTER 7

RESULTS AND DISCUSSION : GaP MIS STRUCTURES

7.1 INTRODUCTION

The results presented in this section can be roughly divided into two catagories. The first deals with the characterisation of the devices from the viewpoint of their band structure, electrical properties and mode of operation, and the second concerns the light-emitting properties of the devices. Some of the data which will be presented later in this chapter, together with the results of an independent, parallel study of the Au : LB film : (n) GaP system have been the subject of a number of recent publications[1-6]. It is clear from these reports that this system exhibits a number of very interesting properties. In particular, the insertion of an LB film into the Au : (n) GaP Schottky barrier structure has been demonstrated to significantly increase the effective barrier height in the device. However, the mechanism by which this is achieved is not understood, and more importantly, the actual mode of operation of the device remains uncertain. This increase in the (majority carrier) barrier height is very important from the viewpoint of this work since it would be expected to cause a significant improvement in the minority carrier injection ratio, and hence the EL efficiency. A thorough investigation of this phenomenon is made and a model is proposed to explain both the results presented here and previously published data. The EL properties are presented and interpreted in terms of the model. Measurements made on the devices under illumination are shown both to support the proposal and to provide some insight into the actual EL mechanism. The question of device lifetimes and degradation mechanisms is considered in §7.3.4, which concludes the work on fatty acid-based devices. In the final section the 'model' system is extended to incorporate LB films of phthalocyanine and the properties of these diodes are examined. The chapter concludes with an assessment of the future prospects for MIS LEDs based on LB technology.

7.2 GENERAL CHARACTERISATION OF THE MIS STRUCTURE

In this section, the results of probing the MIS diode barrier, in devices with a range of insulator thicknesses, are presented, analysed and discussed. The methods employed are the J-V, C-V and photoelectric techiques which were described in §3.3.5 and §3.4.1, and used in chapter 6 to study the near-ideal Schottky diodes. Most emphasis is placed on the Au : $CdSt_2$: (n) GaP system although some data are also presented for devices incorporating ω-TA as the insulator. The capacitance-voltage characteristics are discussed separately following the approach used first by Cowley[7] which was later modified by Fonash[8].

7.2.1 Measurement of Barrier Height

(a) Au : $CdSt_2$: (n) GaP Devices

Conductivity Data. The forward bias current density-voltage curves for a number of typical MIS diodes with varying insulator thickness are shown in fig. 7.1. Curve (b) corresponds to a diode fabricated with one monolayer of $CdSt_2$ (molecular length of ∿2.5 nm), curve (c) corresponds to a diode incorporating three monolayers, and (d) corresponds to five monolayers. Also shown (for comparison) is the characteristic of a near-ideal Schottky diode, fabricated in parallel with the MIS devices. There are a number of important features in these data: (i) All of the curves exhibit well-defined linear regions which can be described by the relation $J = J_o \exp(qV/nkT)$. Furthermore, the value of the ideality factor, n, is approximately the same in all cases and is very close to unity (n ∿1.05). (ii) The effect of incorporating one monolayer is very pronounced and represents a decrease of over four orders of magnitude in the value of the intercept, J_o. However, the effect of subsequent layers is much smaller and indeed a slight increase in J_o is observed in the case of curves (c) and (d) over that of (b). (iii) As the film thickness is increased, the extent of the linear region is decreased and the deviation from linearity at higher

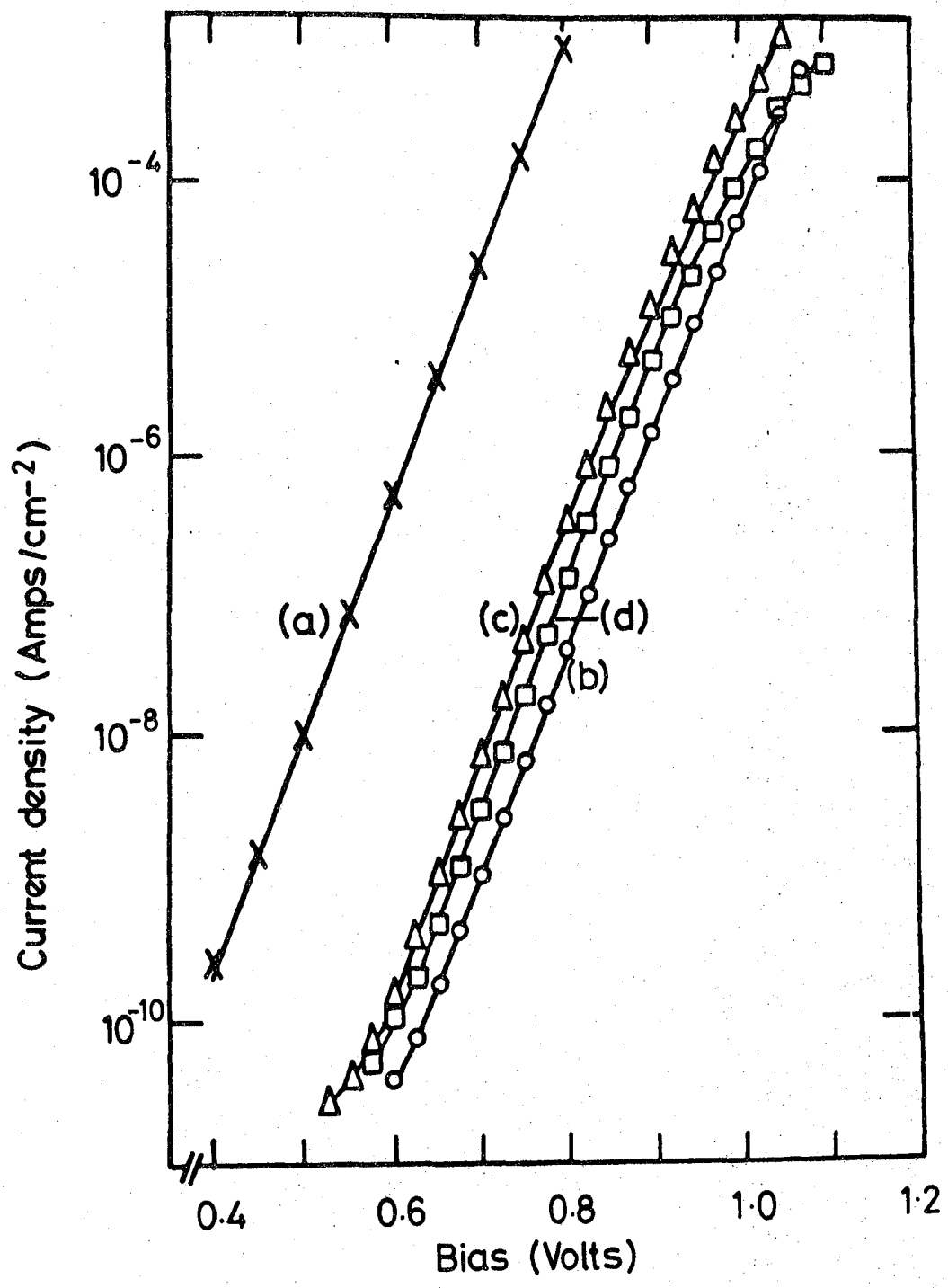

Figure 7.1 Current density versus forward bias for diodes incorporating a range of $CdSt_2$ insulator thicknesses; (a) no insulator (near-ideal curve), (b) one monolayer, (c) three monolayers and (d) five monolayers. (The reverse current was undetectable for V = -10V).

biases is more pronounced. This indicates that, although the addition of subsequent layers, after the first, have little effect on J_o, they do introduce an additional, series impediment to current flow in the same manner as the series resistance associated with the semiconductor bulk. The effect of the insulator can be seen more easily in fig. 7.2(a) which shows the J-V characteristic for a diode fabricated with 9 monolayers (22.5 nm) of $CdSt_2$. In this case a larger current range has been investigated and three distinct regions can be identified. The linear (barrier limited) region (a) is much reduced, as expected from the trend discussed in (iii) above. Region (c) is the usual, series limited régime and the characteristic is near-ohmic for $V \gtrsim 2.1V$. Region (b), which is completely absent from both the near-ideal and non-ideal Schottky characteristics, is evidently a consequence of the LB film. This, together with the feature marked by the arrow in fig. 7.2(a) will be discussed at a later stage.

(iv) The current carried by the diodes is much larger than that expected considering the insulating properties of the LB film. This is demonstrated by fig. 7.2(b) which shows a graph of log J against $V^{\frac{1}{2}}$ for a Au : $CdSt_2$: Al, MIM device incorporating five monolayers of $CdSt_2$. The curve is highly linear and characteristic of the Poole-Frenkel type hopping mechanism which is believed to be the dominant conduction mechanism in multilayered LB films. The characteristic exhibits only a slight dependence on the polarity of the applied bias and the value of the dielectric constant estimated from the slope of the curve is of the correct order of magnitude. Comparing this characteristic with curve (d) in fig. 7.1 reveals a clear anomaly between the currents measured in the MIM diode and those measured in an MIS diode incorporating an identical insulating film. This aspect must be explained by any model which is proposed to explain the other diode characteristics.

Photoresponse Data. The photoelectric technique is generally regarded to give the definitive measurement of the metal-semiconductor barrier height,

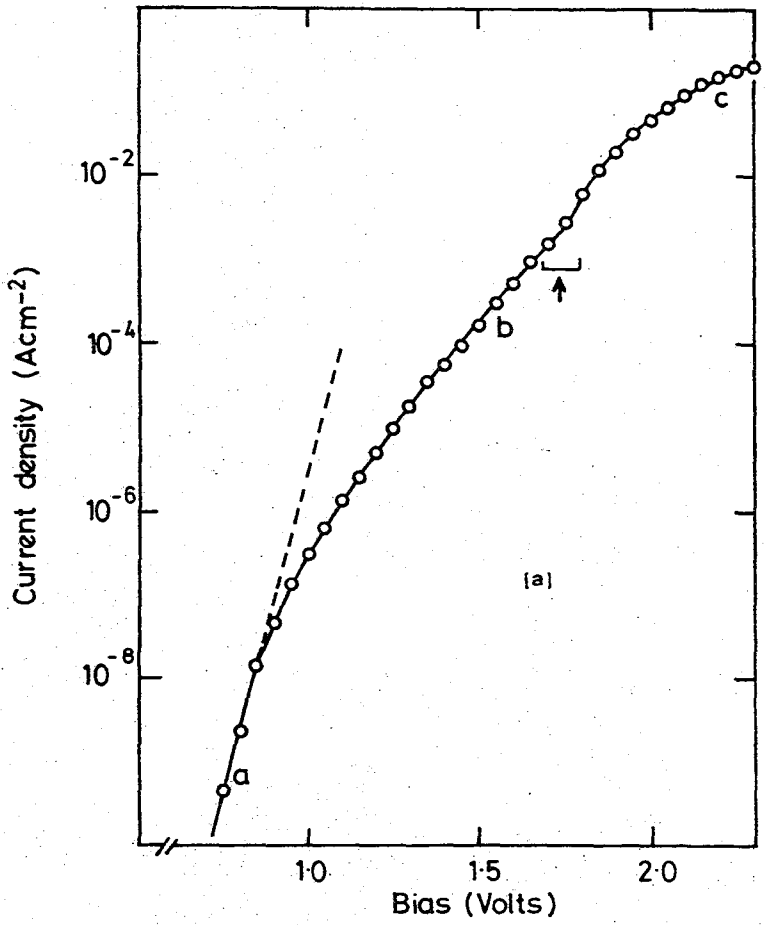

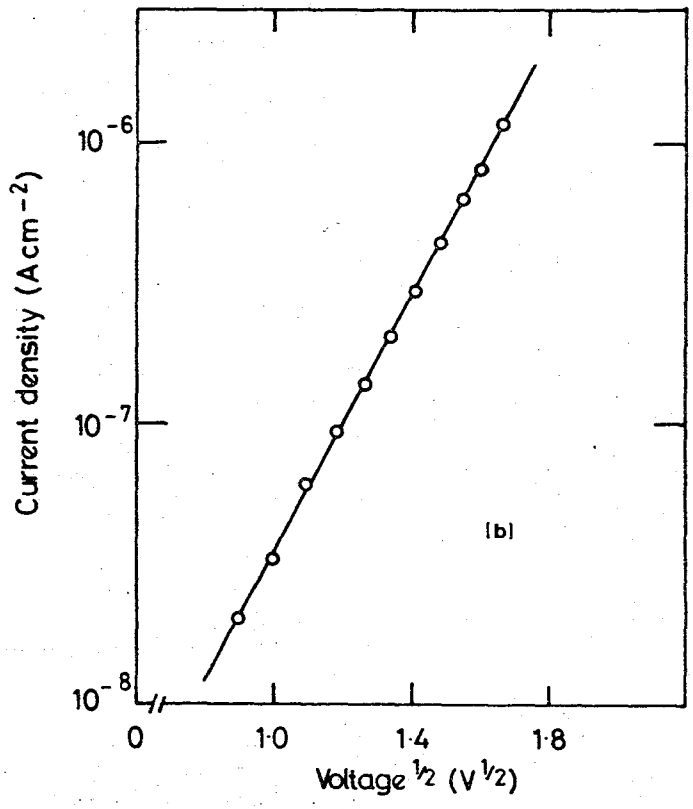

Figure 7.2 (a) Current density versus forward bias for a diode incorporating nine monolayers (22.5 nm) of $CdSt_2$.

(b) Current density versus $V^{\frac{1}{2}}$ for an MIM device incorporating five monolayers (12.5 nm) of $CdSt_2$.

ϕ_{bn}. However, a more accurate assessment of the technique is that the Fowler plot gives a direct measurement of the height of the barrier which is surmounted by photoexcited electrons in order to enter the semiconductor conduction band. Fig. 7.3 shows the Fowler plots for the same four diodes used to obtain the J-V data shown in fig. 7.1, with curves (a) to (d) representing devices fabricated with 0, 1, 3 and 5 monolayers, respectively. These data confirm the implications of the J-V results, i.e. that the effect of the insulator is to increase the height of the actual barrier presented to majority carriers, and that this increase is relatively independent of the film thickness. An increase of $\sim$ 0.25eV is revealed due to the incorporation of one monolayer of $CdSt_2$ and a subsequent slight decrease of $\sim$ 0.05eV is measured due to the incorporation of additional layers. There are two important features in these data : Firstly, the curves are all reasonably linear - even for diode (d) where the insulator thickness is at least 12.5 nm; and secondly, the barrier heights measured directly using the photoelectric technique agree remarkably well with those calculated from the J-V data (fig. 7.1) using the simple Schottky barrier theory

$$\text{i.e } J = A^{*}T^{2} \exp(-q\phi_{bn}/kT) \exp(qV/nkT)$$

The barrier heights measured by the two techniques are shown in table 7.1 below.

Diode	Measured Barrier Height (±0.01) (eV)	
	J-V Data	Photoelectric Data
(a)	1.31	1.39
(b)	1.58	1.64
(c)	1.54	1.59
(d)	1.55	1.59

Table 7.1

Barrier Heights Measured by J-V and Photoelectric Techniques

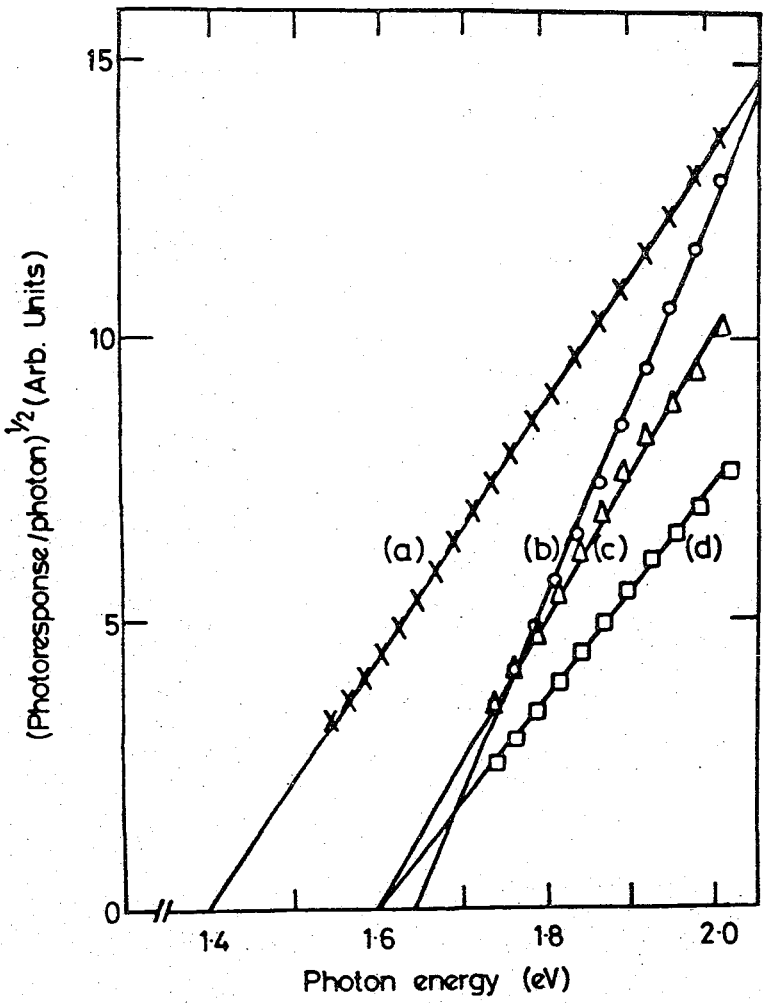

Figure 7.3 Photoresponse data (Fowler plots) for the same four diodes used to obtain the data shown in fig. 7.1.

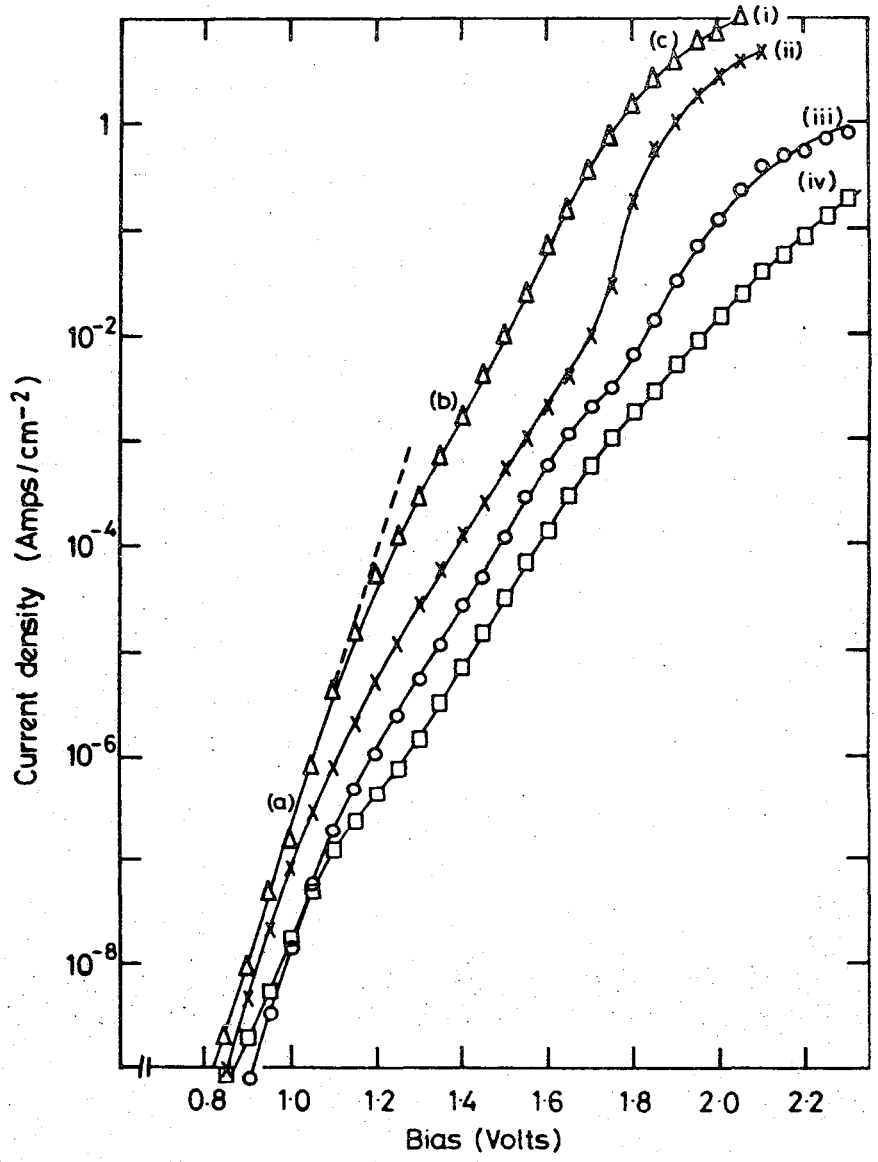

Figure 7.4 Conductivity data for diodes incorporating a range of (ω-TA) insulator thicknesses; (i) one monolayer, (ii) seven monolayers, (iii) nine monolayers, (iv) eleven monolayers.

This implies that there is no tunnelling transmission ($\chi^{\frac{1}{2}}\delta$) term in the expression for the current and presents another anomaly which must be resolved.

(b) Devices Incorporating ω-TA LB Films

These devices displayed characteristics which were very similar to those described in the previous section. Fig. 7.4 shows the J-V characteristics for diodes fabricated with a range of insulator thicknesses, and it is clear that they exhibit the same features as the $CdSt_2$ devices. The only difference is that the extent of the barrier limited régime is reduced, which indicates that the effect of the insulator at higher biases is more pronounced in the case of the ω-TA diodes. The barrier heights, as measured by the photoelectric technique, in diodes incorporating one and three monolayers of ω-TA were very similar (1.60 and 1.61 (± 0.01) eV respectively). These too agree well with the values measured in the corresponding cadmium stearate devices, and also with the barrier heights reported for a range of gold : LB film : (n) GaP devices[1]. However, the slight decrease in the barrier height, observed in the $CdSt_2$ devices due to the incorporation of subsequent layers (after the first), was not detected in the ω-TA diodes. This may be an effect of incorporating excess cadmium ions in the $CdSt_2$ films and hence producing an effective dipole in the interface region. (The ω-TA films were deposited without the use of cadmium ions in the subphase.) However, in view of the other similarities between the two types of devices (it will subsequently become evident that the optical properties are also very similar) the discussion from this point will be concerned with the more general gold : fatty acid LB film : (n) GaP system.

Discussion

There are at least two possible explanations for the results presented so far : The measured increase in the height of the barrier may be a 'real' effect, i.e. an increase in the actual degree of band-bending in the

semiconductor, or it could be an 'apparent' increase which is related in some way to the barrier presented by the insulator.

Consider first the possibility that the increase is a real increase in the diffusion potential. There has been much interest in recent years in the modification of the Schottky barrier height by interfacial, insulating layers (see for example ref. (9) and the references contained therein). This is because of the fact that such an increase would be highly desirable in a number of electronic devices (for example in MESFETs, IMPATTs and MIS solar cells). Many of the reports concerning barrier height modification have been the result of incorporating native 'oxides' into the device structure and these have been explained using the Bardeen model discussed in chapter 3. For example, Pruniaux and Adams[10] have demonstrated a linear variation of ϕ_{bn} with δ, approximately in accordance with the general expression for the barrier height derived by Cowley and Sze[11] (i.e. eq. (3.3)). (An increase due to the presence of a native 'oxide' was also observed in this work (see §6.4) where an increase from 1.39eV to 1.54 eV was measured.) In some cases[12], however, the barrier height has been measured only by the J-V and C-V techniques and not directly by the photoelectric technique. The results from such studies may not always be conclusive, a point demonstrated by Morgan and Frey[9], due to the susceptibility of these techniques to the presence of an interfacial layer. The first report of an apparent increase in ϕ_{bn} due to the presence of an LB film, concerned diodes fabricated on CdTe[13]. In these devices the beneficial effect on the photovoltaic properties was studied, although the authors stressed that an independent measurement of ϕ_{bn} (by the photoelectric technique) would be necessary to distinguish between a real change in ϕ_{bn} and an effect due to the $(\chi^{\frac{1}{2}}\delta)$ transmission coefficient for the insulator bandgap. Tredgold and Jones[1] first reported an effect on GaP devices when studying the photovoltaic properties of GaP MIS diodes.

They showed that incorporating a single monolayer of stearic acid into the Au : (n) GaP system almost doubled the open circuit voltage of the devices and they demonstrated that this was due to an effective increase in the barrier height. In their case the near-ideal Schottky barrier height was $\sim$ 1.1eV and this increased to $\sim$ 1.6eV due to the presence of the monolayer. They demonstrated the phenomenon for a range of LB film materials, although the effect of thicker insulators was not studied in any detail. They used the fact that good agreement was obtained between the J-V and photoelectric measurement of barrier height, and that the ideality factors were close to unity, to interpret their data in terms of a real increase in barrier height, assuming that the LB monolayer was 'transparent' to tunnelling electrons (i.e $(\chi^{\frac{1}{2}}\delta) \sim 0$). The expression derived by Cowley and Sze (eq. (3.3)) was used to explain the increase in ϕ_{bn}. However, this model predicts a further increase in ϕ_{bn} on increasing the film thickness and the data shown in fig. 7.3 clearly show that this is not the case. If the increase in the measured barrier height is a real increase in ϕ_{bn}, then the effect is evidently related to the properties of the first monolayer (or the interface) and models based on the thickness of the LB film must be rejected. A possible explanation was proposed by Batey et al[3], who suggested that a chemical reaction, similar to that observed on aluminium substrates[14], could occur between the surface of the semiconductor and the LB film. Such a reaction could have an effect on ϕ_{bn} analogous to that recognised to occur in a variety of metal-semiconductor systems (e.g. in metal- silicide - silicon diodes as discussed in § 3.2.3). If this were the case, then the addition of subsequent layers might not be expected to substantially change ϕ_{bn}. Winter and Tredgold[6], having presented further experimental evidence to refute their earlier model (based on interface states) have extended the idea of an interfacial chemical reaction. They studied the effect of incorporating polymeric

monolayers into Au : (n) GaP diodes which could be modified in various ways to produce monolayers with differing headgroups, but with the same monomolecular thickness. They demonstrated a limited control over the barrier height (as measured by the J-V, C-V and photoelectric techniques) by depositing various modified versions of the polymer. Again, only the effect of single monolayers was reported and the results were interpreted as a real increase in barrier height.

However, the data presented here, for diodes incorporating thicker LB films reveal some inconsistencies in any model based on a conventional MIS diode with an increased barrier height.

(i) The ideality factor of a thin-MIS structure is given by eq.(3.41) as

$$n = 1 + \frac{(\delta/\varepsilon_i)\,(\varepsilon_s/_w + qDsb)}{1 + (\delta/\varepsilon_i)\,qDsa}$$

It can be seen from this equation that, in order that n should be close to unity, Dsa >> Dsb, i.e. the majority of the interface states must communicate more easily with the metal than with the semiconductor. This is clearly not a reasonable assumption when the insulator is greater than five monolayers (12.5 nm) thick.

(ii) The barrier heights determined from the J-V characteristics using the simple thermionic emission theory agree reasonably well with the values measured by the photoelectric technique (see table 7.1).

This too is inconsistent with the idea of a conventional MIS diode with a real change in ϕ_{bn}, since no account has been made of the additional barrier due to the insulating layer. That is, no $(\chi^{\frac{1}{2}}\delta)$ tunnelling transmission coefficient was invoked in the analysis and it is clearly unreasonable to suppose that this might be zero for such thick insulators. Moreover, the greatest insulator thicknesses are known to be in excess of the direct quantum mechanical tunnelling regime ($\gtrsim$ 10nm) and this conduction mechanism cannot be used to explain the experimental observations.

(iii) The currents passed by the diodes are much too high to be explained by conduction through the bulk of the $CdSt_2$ film. This can be seen by comparing the conductivity data in fig. 7.1 with those in fig. 7.2(b)(which show the log $J-V^{\frac{1}{2}}$ characteristic of an MIM diode fabricated with 5 monolayers of $CdSt_2$). It can be seen that in this latter case a voltage of 1V causes a current density of $\sim 3 \times 10^{-8}$ Acm^{-2} to flow, whereas in the corresponding MIS case, the current density is approximately four orders of magnitude greater than this.

There is clearly good reason to look for an alternative explanation of the results. Batey et al[5] have recently proposed that the barrier measured by the J-V and photoelectric techniques involves the metal - insulator interface rather than the conventional barrier due to the depletion region of the semiconductor. In the following sections further evidence will be presented to support this view and the model is discussed in some detail. The model essentially proposes that the measured increase in the barrier height is not a real increase, i.e. that the diffusion potential is not increased by the presence of the LB film. An independent measurement of the diffusion potential is an obvious test for this theory.

7.2.2. Capacitance Data

The C^{-2} -V characteristics are most often used to measure the diffusion voltage, Vd. These characteristics, for the same four diodes used to obtain the data shown in figs. 7.1 and 7.3, are presented in fig. 7.5. It can be seen from these data that the effect of incorporating an LB film is, in general, to increase both the slope and the intercept of the curves. At first sight, the data seem to suggest that the barrier height increase is real, and that the metal-semiconductor barrier height, calculated from the intercept, is $\sim$ 1.66eV in all cases where an LB film is present. However, the change in slope is a certain indication that interface states, separated

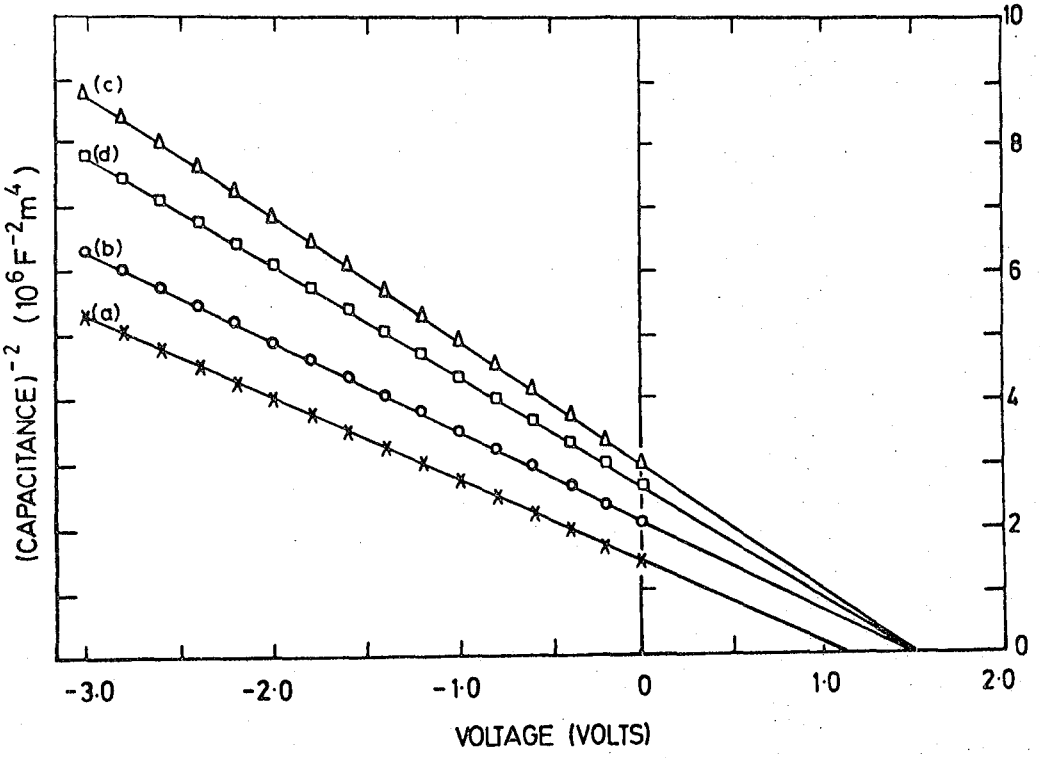

Figure 7.5 Reciprocal capacitance squared against voltage for the same four diodes used to obtain the data shown in fig. 7.1.

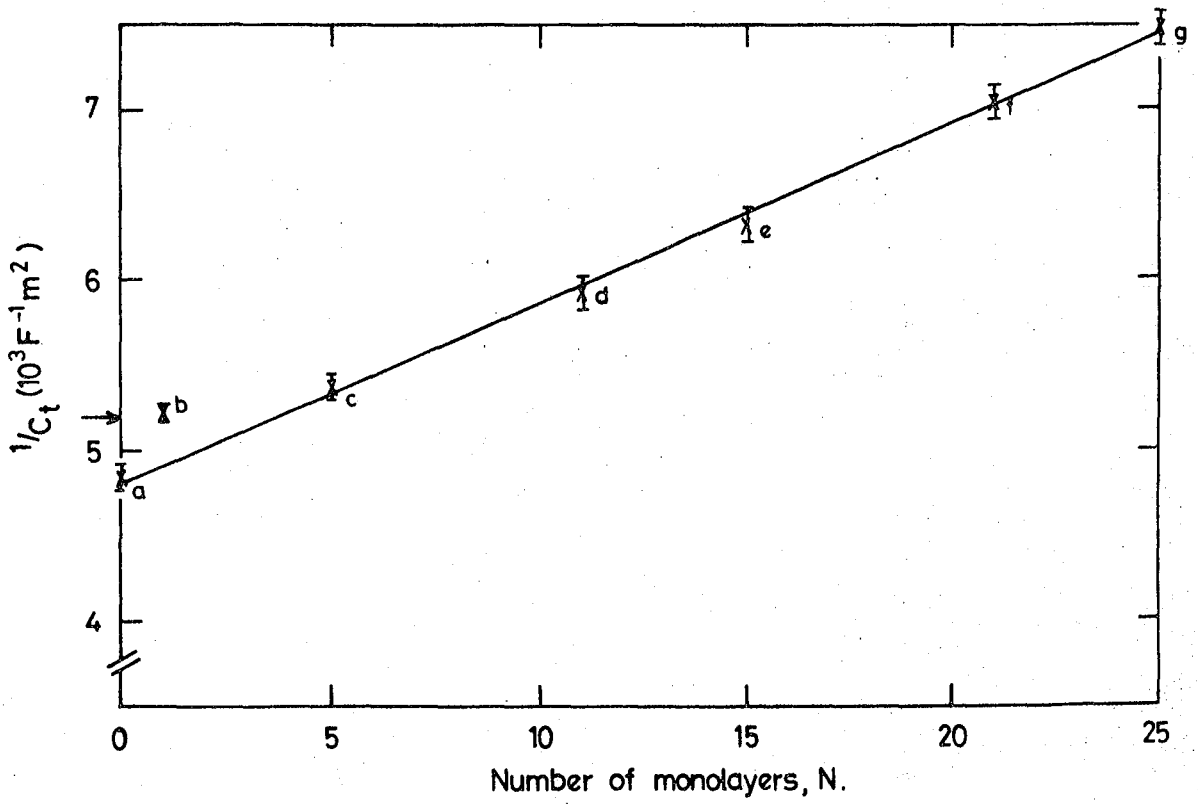

Figure 7.6 Reciprocal capacitance against the number of monolayers for MIS diodes incorporating a wide range of insulator ($CdSt_2$) thicknesses.

from the metal by the insulating layer are affecting the characteristics. Thus, the interpretation of the curve is more complex, and the value of 1.66eV, calculated for Vd cannot be considered as accurate. In fact, it will be argued here that the variation of zero bias capacitance with insulator thickness can be used, in this case, to demonstrate that there is no change in the diffusion voltage due to the presence of the LB film. The technique is essentially that used for the quality assessment of LB films (see § 4.4.4), i.e. the C^{-1} -N technique. In this case, however, the device is modelled by three capacitances in series; that due to the LB film (C_{lb}), that due to the unintentional interfacial layer (C_i) and that due to the semiconductor depletion region (C_d). This last term, C_d, is, of course, voltage dependent but, because the measurements are all made at zero bias, this is not important. The total capacitance (C_t) is therefore given by the relation

$$\frac{1}{C_t} = \frac{1}{C_{lb}} + \frac{1}{C_i} + \frac{1}{C_d} = \frac{dN}{\varepsilon_{lb}} + \frac{\delta_i}{\varepsilon_i} + \frac{1}{C_d} \quad .... \qquad (7.1)$$

where N is the number of monolayers, δ_i and ε_i are the thickness and permittivity of the interfacial layer, d is the monomolecular thickness and ε_{lb} is the permittivity of the LB film. (All capacitances are per unit area.) Fig. 7.6 shows a graph of $1/C$ against N for MIS diodes fabricated using a wide range of insulator ($CdSt_2$) thicknesses. Each point represents an average value determined from ten contacts on each region of the slice and the experimental scatter can be seen to be small. Neglecting, for the time being, point (b) which corresponds to diodes incorporating one monolayer, the remarkable feature of the plot is that it is highly linear. The line which has been fitted to the data is the result of a linear regression using points (c) to (g) and the correlation coefficient is 0.998. From this it can be concluded that C_d^{-1} is either

constant or varies linearly with N. The latter can be disproved by calculating the slope of the curve, the value of which (106 (±8) $m^2\ F^{-1}$ per monolayer) corresponds closely to the value of 110 (±2) $m^2\ F^{-1}$ per monolayer measured for the term (d/ε_{1b}) from the MIM data shown in fig. 5.7. The capacitance associated with the depletion region, and hence the diffusion voltage, must therefore remain constant over the insulator thickness range investigated. This is unexpected but can be explained using precisely the same argument as that used to explain Fermi level pinning in the Bardeen model of Schottky barrier formation : Since the interface state density is known to be high (from Schottky barrier measurements), then the charge associated with the potential drop in the insulator (at zero bias) can easily be accommodated by the large density of interface states, without a significant change in the position of the Fermi level. Consequently, the diffusion voltage remains virtually unchanged. It can be seen from eq. (7.1) that the value of C_d is related to the intercept, C_o^{-1}, by the relation $C_o^{-1} = C_i^{-1} + C_d^{-1}$. However, δ_i is small (∿1nm) and hence $C_d^{-1} >> C_i^{-1}$ and thus $C_d \simeq C_o$. The value of the diffusion voltage can therefore be computed using eq. (3.23), i.e. $C_d = (q\ \varepsilon_s\ Nd/2Vd)^{\frac{1}{2}}$. However, this is not necessary as it can be seen from fig. 7.6 that the value is, within experimental error, equal to the diffusion voltage in the near-ideal Schottky diodes (point (a)). It is therefore concluded that there is no change in Vd due to the presence of the LB film and consequently, the increase in ϕ_{bn} is not 'real' according to the definition given earlier. A real increase of the magnitude indicated by the photoelectric measurements would certainly have been detected in the C^{-1} -N plot since this would have given an intercept of ∿ $5.2 \times 10^3\ m^2\ F^{-1}$, as indicated by the arrow in fig. 7.6.

One detail in this figure remains to be explained, namely the fact that point (b) does not fit the theory. The argument that this anomaly is actually indicative of an increase in Vd is rejected, since diodes fabricated with thicker insulators display an increase in the measured barrier height but no anomalous capacitance behaviour. In fact the effect is thought to be completely unrelated to the semiconductor depletion capacitance since the same anomaly is sometimes observed, albeit to a lesser extent, when studying the C^{-1} -N characteristics of MIM structures[15]. The effect is not fully understood, although it is evidently a consequence of the single monolayer or its interface. It is conceivable that the properties of the first deposited layer are somewhat different in single monolayer form than those exhibited by the first of a multilayer, and this could affect the device capacitance. However, a more likely explanation is that the interfacial layer beneath the thin LB film differs in some way to that beneath the thicker films. This could result from a modification due to gases permeating the thin LB film, but which are prevented from reaching the interface by the thicker films. To test this theory, three identical samples were prepared in parallel and a single monolayer of $CdSt_2$ was simultaneously deposited onto each. Gold barrier electrodes were evaporated, onto sample (a) immediately, onto sample (b) after a two hour drying period and onto (c) after a two day drying period. The J-V and C^{-2} -V characteristics of typical contacts from each sample were studied. Table 7.2 below summarizes the results obtained from these measurements.

It can then be seen from these data that the J-V characteristics are very similar in all cases. (The only significant difference, which is not evident from the data in table 7.2, is a slightly more pronounced deviation from linearity at high biases in the case of diode (c)). This is consistent with the data presented in § 6.4. However, there is a

Diode	Conductivity Data		Capacitance Data	
	Ideality Factor	J_o(Amps m^{-2})	$d(C^{-2})/dV(F^{-2}m^4V^{-1})$	Intercept, V_o (Volts)
(a)	1.04	1.85×10^{-16}	$2.6\ (\pm 0.1) \times 10^6$	1.36 (±0.02)
(b)	1.07	3.29×10^{-16}	$2.9\ (\pm 0.1) \times 10^6$	1.40 (±0.02)
(c)	1.06	2.09×10^{-16}	$2.7\ (\pm 0.1) \times 10^6$	1.48 (±0.02)

Table 7.2

Results obtained from Conductivity and Capacitance Measurements

definite trend evident from the capacitance data of an intercept, V_o, which increases with the pre-electrode-deposition drying period. This tends to support the interpretation of a post-LB film-deposition modification. The effect is possibly due to a change in the relative permittivity of the interfacial layer. Assuming that the interpretation is correct, then five monolayers is evidently sufficiently thick to retard the process to such an extent that it does not significantly affect the characteristics.

It should be stressed that the C^{-1} -N technique was only successful in this instance because Vd remained approximately constant, even for diodes incorporating relatively thick insulators. It did not, in this case, suffer from the problems which complicate the analysis in the C^{-2} -V technique. Nevertheless, the C^{-2} -V characteristics, corresponding to typical diodes chosen from the sample used to obtain the data in fig. 7.6, are shown in fig. 7.7. These will be referred to in § 7.2.4 when a semi-quantitative analysis of the C^{-2} -V data is given.

It has been demonstrated that any model based on a real increase in the barrier height is inconsistent with much of the experimental evidence and an alternative explanation must be sought. Such an alternative is now proposed.

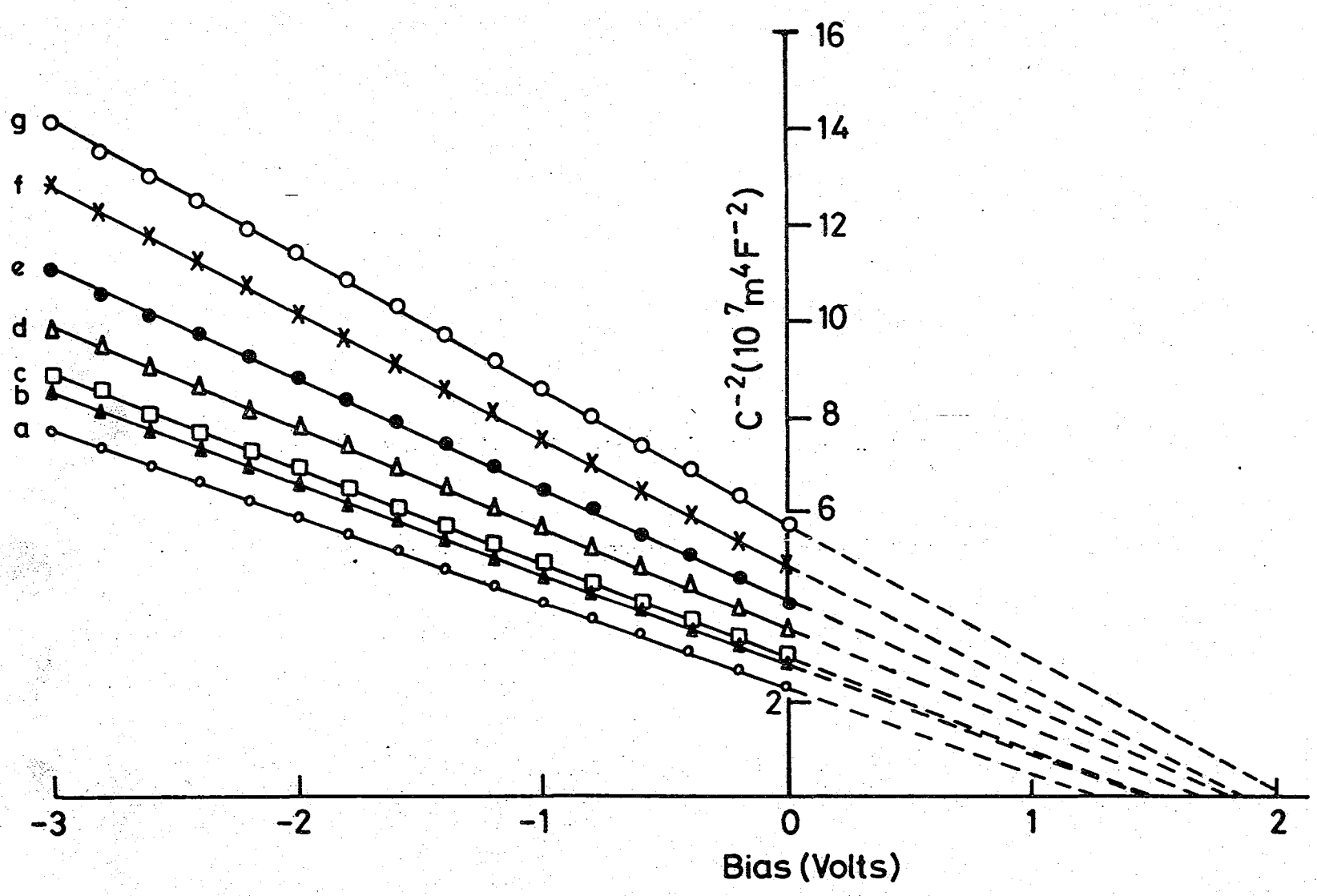

Figure 7.7 Reciprocal capacitance squared against voltage for typical MIS diodes incorporating a range of insulator ($CdSt_2$) thicknesses.

7.2.3 Proposed Model

A number of authors[7][4] have expressed concern that the barrier height measured by the photoelectric technique might be that associated with the bandgap of the insulator rather than the depletion region of the semiconductor. Cowley[7] argued that this was inconsistent with his experimental results: He argued that the mechanism of current flow in his diodes was thermionic emission over a parabolic (Schottky) barrier. However, this argument is not valid. In fact, the shape of the barrier is irrelevant since the theory is based on the flux of carriers, incident on the interface, with sufficient energy to surmount the barrier (see § 3.3.3). Tredgold and Winter[4] invoked the idea of photoexcitation over the insulator barrier to interpret photoelectric measurements on GaP MIS diodes incorporating polymeric LB monolayers (although the devices were still discussed in terms of a real change in barrier height). A model is now presented, based on the effect of the insulator bandgap, which can explain much of the available experimental data for Au : (n) GaP diodes incorporating both monolayer and multilayer fatty acid LB films. Fig. 7.8 shows an approximate energy level diagram which is proposed for the Au : LB film : (n) GaP diodes. It was deduced on the following basis: It is evident from fig. 7.6 that Vd, even in the presence of an LB film, is $\sim$ 1.4eV. The barrier height of $\sim$ 1.6eV, measured by the photoelectric technique, is interpreted to be that presented by the bandgap of the insulator. The validity of drawing such a well-defined insulator band structure must be questionable, even though an LB film is essentially an ordered sheet of molecules and there is some evidence to suppose that consecutive layers are deposited partially epitaxially. In such a molecular material, conduction occurs via defects which are associated with the precise molecular arrangement in the material. In an LB film, it is possible to envisage defects originating, for example, from the bonding between successive layers. Such defects, having specific origins, are likely to give rise to levels at certain energies and possibly to a psuedo

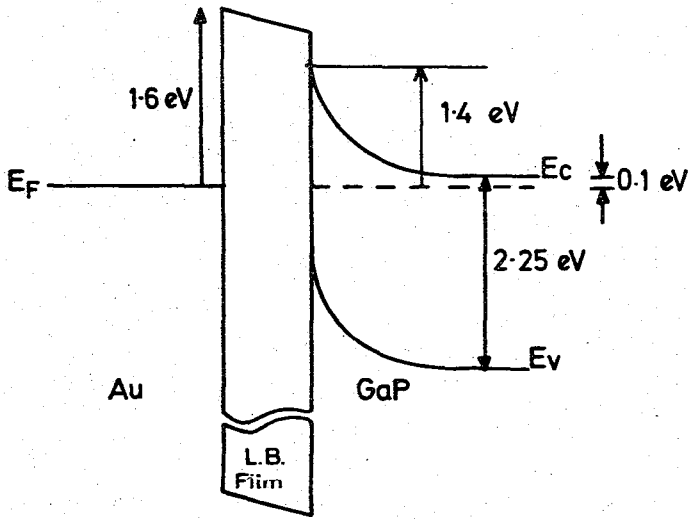

Figure 7.8 Approximate energy level diagram proposed for the Au:fatty-acid LB film : (n) GaP system.

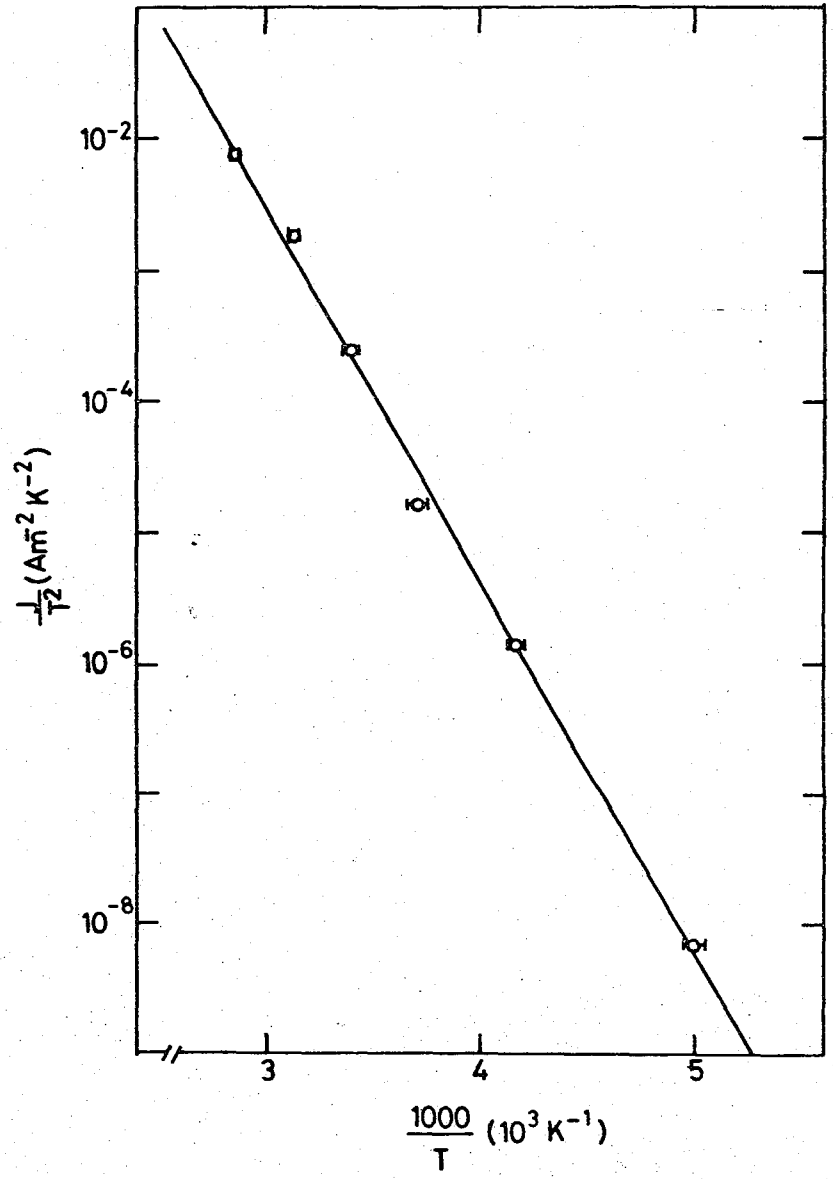

Figure 7.9 Activation energy plot for an MIS diode incorporating one monolayer of $CdSt_2$.

conduction band. This is envisaged as the origin of the conduction level located at ∿(Ef + 1.6eV). This level is, perhaps, best considered as an energy, above which electrons may traverse the insulator by a mechanism, other than the normal Poole-Frenkel process, which is not necessarily ohmic (as would be the case in a semiconductor). Unfortunately, there are few reports concerning the band structure in LB films, and the only published data is related to the measurement of metal-insulator barrier heights in MIM structures[16-18]. However, it is possible to estimate χ_i, the electron affinity of the insulator, from such data by assuming that the simple Schottky-Mott relation, $\phi_{bi} = \phi_m - \chi_i$, is valid, where ϕ_{bi} is the metal-insulator barrier height. A number of systems have been studied including tin, aluminium and mercury electrode MIM structures. The tin - LB film system is expected to yield the most reliable value of χ_i, since tin oxide is relatively conducting and therefore less likely to complicate the measurement than, say aluminium oxide. Indeed the values reported for ϕ_{bi} in the Sn : LB film system are very consistent[16,17] and yield an approximate value of 3.5eV for χ_i. However, it should be noted that the value obtained using a number of other metals[18] was slightly different (2.3 (±0.7)eV). Again, applying the simple Schottky-Mott theory to the Au : LB film interface yields an expected barrier height of ∿ 1.6eV which is in excellent agreement with the actual measured value. Unfortunately, no other information is available on the band structure in LB films and, in particular, the size of the bandgap is unknown, although it is expected to be large (of the order of several eV).

Discussion

All of the experimental results presented so far can be interpreted using this model. For example, it explains both the increase in the barrier height and also its relative insensitivity to insulator thickness,

as measured by the photoelectric technique. Indeed, it explains how this measurement was even possible in the case of the thicker insulators (i.e $\delta \gtrsim$ 10nm) when other authors have experienced difficulty using insulators much thinner than this[19]. (The photoelectric technique was used successfully in this work for diodes with up to 15nm of $CdSt_2$ as the insulator.) The decrease in the slope of the Fowler plot with increasing film thickness is indicative of the increased impediment to electron transport by the conduction mechanism in the insulator 'conduction band'. The unusual features of the J-V data (figs. 7.1 and 7.2(a)) can also be explained, by proposing that the forward current is limited, not by thermionic emission over the depletion region barrier in series with a transport process across the insulator, but by thermionic emission over a composite barrier comprised of the semiconductor depletion region and the insulator bandgap. The height of this composite barrier is equal to ϕ_{bi}, the height of the metal-insulator barrier. Over a limited range of bias, at least until the semiconductor bands are flattened, the characteristic will resemble that of a Schottky barrier with an increased barrier height (1.6eV). Furthermore, since the insulator is an integral part of the barrier, then any bias-dependence of the barrier height will result only from image force lowering effects and the characteristic will be near-ideal with an ideality factor close to unity, as observed in practice. This mechanism also explains why the J-V data can be analysed so successfully using the simple Schottky barrier thermionic emission theory,

$$\text{i.e} \quad J = A^{*}T^{2} \exp(-q\,\phi_{bi}/kT) \exp(qV/nkT) \qquad (7.2)$$

and also explains the large current densities passed by the diodes (via the insulator 'conduction band'). This proposal is also supported by the data in fig. 7.9 which shows an activation energy plot for an MIS diode incorporating one monolayer of $CdSt_2$. In this case, $\ln(J/T^2)$

has been plotted as a function of $10^3/T$, where J is the measured current density at a fixed bias (1.1 volts in this case). The curve shown in fig. 7.9 is highly linear, and the value of ϕ_{bi}, calculated from the slope according to the above relationship, is 1.67 (±0.02) eV. This is in excellent agreement with the value of 1.64 (±0.01) eV measured by the photoelectric technique. Moreover, the value of A^* calculated from the intercept on the y axis is 1.09 (±0.05) x 10^6 Am^{-2} K^{-2} which is very close to the expected value. This indicates that there is no $(\chi^{\frac{1}{2}}\delta)$ term in the expression for J, thus supporting the model. It will be remembered that the interfacial layer in even the near-ideal diodes was significant enough to manifest itself in the activation energy plot (see §6.2.1).

The full J-V characteristic shown in figs. 7.2(a) and 7.4 can now be interpreted. In the linear region (a) the current is limited by thermionic emission over the composite barrier, according to eq. (7.2). Region (c) is the normal series resistance limited region where the characteristic becomes approximately ohmic due to the resistance associated with the semiconductor bulk. Region (b), which is evidently a consequence of the LB film, is interpreted as representing an additional, series impediment to current flow resulting from the conduction mechanism in the insulator 'conduction band'. The origin of the feature marked by the arrow in fig. 7.2(a) is unclear. It corresponds quite closely to the voltage at which EL is first detected from the diodes. However, it is not thought to be an increase in J due solely to the injection of minority carriers since the effect, particularly in the case of the ω-TA diodes (fig. 7.4) is too large. Rather, it is believed to correspond to the bias at which the field in the insulator becomes reversed, from the direction shown in fig. 7.8, and thereby enhances the transport mechanism in the LB film. The fact that this necessarily indicates that a degree of band realignment has occured, explains the simultaneous emission of light.

That the dominant current mechanism should be emission over the top of the composite barrier (J_e) rather than the conventional tunnel-assisted emission (J_t) can be seen from the following simplified calculation : Assuming that J_e is given by

$$J_e \simeq A^* T^2 \exp(-q\,\phi_{bi}/kT) \exp(qV/kT)$$

and that J_t is given by

$$J_t = A^* T^2 \exp(-q\,\phi_{bn}/kT) \exp(-\chi^{\frac{1}{2}}\delta) \exp(qV/kT),$$

then the ratio J_t/J_c is given by

$$J_t/J_c \simeq \exp\{q/kT\,(\phi_{bi} - \phi_{bn}) - \chi^{\frac{1}{2}}\delta\} \qquad (7.3)$$

Inserting ϕ_{bn} = 1.39eV, ϕ_{bi} = 1.64eV, and using χ = 0.25eV and δ = 25 (angstroms), yields $J_t/J_c \simeq 0.05$ and J_e is the dominant component, even in the case of diodes incorporating only one monolayer. In addition, the fact that MIS devices incorporating $CdSt_2$ LB films fabricated on CdTe[20] are well-described by the conventional MIS tunnel diode can also be explained. In these devices, the barrier height, ϕ_{bn}, is much smaller ($\sim$ 0.7eV) and in this case eq. (7.3) predicts $J_t/J_e \sim 10^5$ and the dominant current mechanism is J_t. The same argument provides a possible explanation for the non-ideal nature of the J-V characteristics measured by Tredgold and Jones[1] for Au : LB film : (n) GaP diodes. In their case, the Schottky barrier height was significantly less than the 1.39eV measured here ($\sim$ 1.12eV in fact) and their increased barrier height was $\sim$ 1.58eV. Inserting these values into eq.(7.3) yields $J_t/J_e \simeq 2$ and both mechanisms would be expected to contribute.

The only experimental evidence which does not fit the model is the apparent control of ϕ_{bn} reported for diodes incorporating various polymeric films[4][6]. It is possible that these systems behave quite differently to the fatty acid system although it should be noted that the conclusions were drawn largely from the C^{-2} -V data, and the effects of the insulator, coupled to interface states were neglected.

7.2.4 Analysis of C^{-2} -V Characteristics

Two sets of experimental C^{-2} -V curves have been presented. In fig.7.5, the effect of incorporating relatively thin films was considered and in fig. 7.7 a much wider range was investigated. In this section the data in fig. 7.7 will be discussed. In view of the evidence (§ 7.2.2) which suggests that the single monolayer : semiconductor interface may be modified in some way, it is reasonable to assume that the same may be true for thin multilayers of LB films. This is thought to be the effect observed in fig. 7.5 where the curve corresponding to devices incorporating three monolayers has a larger slope than that corresponding to five. This implies that five monolayers retards the modification to a much greater extent than three does, and this is consistent with the data in fig. 7.6.

The effect of an interfacial layer and interface states on the C^{-2} -V characteristic was considered in some detail in § 3.4.1 following the theory developed first by Cowley[7] which was then modified by Fonash[8]. The models considered by Fonash will be discussed first since they were analysed using the correct, differential variation of Vd (see § 3.4.1). The features of the data shown in fig. 7.7 are; (a) the curves are all highly linear, (b) an increase in insulator thickness causes an increase in the slope of the curve, and (c) increasing the insulator thickness also increases the magnitude of the intercept, V_o. Fonash[8] considered several different models. Here the assumption is made that both the surface states which communicate with the metal, Dsa, and those which communicate with

the semiconductor, Dsb, have a uniform density over the energy range traversed by the Fermi level. Fonash considered nine possible models using such an assumption. Of these, only two predict that the curve should be linear; i.e. the simple case of Dsa = Dsb = 0, and the case considered in § 3.4.1 (eq.(3.55)). However, in both of these instances the slope of the curve is not predicted to vary with insulator thickness and neither model is therefore suitable. It is possible that one of the other models correctly describes the data in fig. 7.7, and that the degree of non linearity predicted is small. However, careful analysis of the various models has shown that, even making substantial simplifying assumptions, none can be used easily to analyse the C^{-2} -V data. The purpose of this section is to try and demonstrate that surface states together with an interfacial layer can give at least a qualitative explanation of the experimental results. In fact, the theory developed by Cowley[7], which has been used extensively in the past to analyse C^{-2} -V data, can demonstrate this quite nicely. This is now used to analyse the data in fig. 7.7, although it is acknowledged that there is a slight error in the theory. According to the Cowley theory, eq. (3.54) describes the C^{-2} -V relationship. It can be seen from this equation that interface states in equilibrium with the metal (which determine α_1) tend to maintain the slope and intercept of the C^{-2} -V characteristic close to the simple Schottky barrier values, whereas those which equilibrate with the semiconductor (and hence determine α_2) tend to increase both the slope and the intercept. The diodes used to obtain the data shown in fig. 7.7 were chosen as typical, solely from the viewpoint of their capacitance characteristics and are therefore expected to accurately display the variation of the C^{-2} -V characteristic with thickness. It is evident from the increase in slope with film thickness that a significant proportion of the interface states equilibrate with the semiconductor rather than with the

metal. This is to be expected when the insulator thickness is large. However, a quick numerical check reveals that, even in the case of curve (g) ($\delta \simeq 62.5$ nm), the interface states cannot be considered to communicate solely with the semiconductor : The interface state density, Dsb, determined by setting α_1 to zero in eq.(3.54),and comparing the slopes of the two curves (a) and (g), is approximately 1×10^{-11} cm^{-2} eV^{-1}. This is two orders of magnitude less than that calculated for the near-ideal Schottky diode interface. Moreover, the value of V_o, the intercept on the voltage axis, predicted using this value for Dsb in eq.(3.54)is $\sim$ 4.23V which is much greater than the actual value of 2.04V. Thus, Dsa is significant compared to Dsb, even for the diodes incorporating the thickest insulators. In fact, eq. (3.54) can be used to obtain two simultaneous equations which can be solved for α_1 and α_2 : If the term $(1 + \alpha_1 + \alpha_2)/(1 + \alpha_1)$ is denoted by x then the two equations are

$$\frac{1 + \alpha_1 + \alpha_2}{1 + \alpha_1} = x \qquad (7.4)$$

and

$$\frac{V_1}{4(1+\alpha_1+\alpha_2)} + \frac{V_1^{\frac{1}{2}} Vd^{\frac{1}{2}}}{(1 + \alpha_1)} + \frac{Vd\ (1 + \alpha_1 + \alpha_2)}{(1 + \alpha_1)} = V_o \qquad (7.5)$$

Substitution from 7.4 into 7.5 yields

$$\frac{V_1}{4x\ (1 + \alpha_1)^2} + \frac{V_1^{\frac{1}{2}} Vd^{\frac{1}{2}}}{1 + \alpha_1} + Vdx = V_o$$

The general solution for this quatratic in $1/(1 + \alpha_1)$ is

$$\frac{1}{1 + \alpha_1} = \frac{-V_1^{\frac{1}{2}} Vd^{\frac{1}{2}} \pm (V_1 Vd + V_1(V_o - Vd\, x)/x)^{\frac{1}{2}}}{V_1/2x} \qquad (7.6)$$

The results obtained by analysing the data in fig. 7.7 using eq.(7.6) are shown in table 7.3 below. Curve (a), the near-ideal characteristic, is assumed to give the correct values of V_d ($\sim$ 1.24V) and Nd ($\sim 7.1 \times 10^{21}$ m^{-3}).

Curve	Number of Monolayers	x	V_o (Volts)	V_1 (Volts)	α_1	α_2	Dsa ($cm^{-2}eV^{-1}$)	Dsb ($cm^{-2}eV^{-1}$)	$\frac{Dsa}{Dsb}$
(c)	5	1.09	1.48	0.11	1.9	0.3	2.2×10^{12}	3.6×10^{11}	6.1
(d)	11	1.17	1.68	0.54	2.7	0.6	1.5×10^{12}	3.3×10^{11}	4.5
(e)	15	1.28	1.78	1.00	4.9	1.7	1.9×10^{12}	6.8×10^{11}	2.8
(f)	21	1.45	1.88	1.96	18.2	8.6	5.2×10^{12}	2.4×10^{12}	2.2
(g)	25	1.56	2.04	2.77	16.8	10.0	4.0×10^{12}	2.4×10^{12}	1.7

Table 7.3

Interface State Densities Deduced from C^{-2} -V Data

It should be noted that the errors involved in calculting α_1 and α_2 are quite large. This arises from the fact that the term $V_1(V_o - Vdx)/x$ is relatively small and thus the value $(1 + \alpha_1)^{-1}$ is also small, especially for curves (f) and (g). This means that the value of α_1, and hence α_2, Dsa and Dsb, are very sensitive to a slight change in the slope of C^{-2} -V plot. The maximum error involved in calculating α_1 from curves (f) and (g) has been estimated at approximately 500%. This is large but only represents half of an order of magnitude in the corresponding interface state densities.

The error involved in the other cases is substantially less than this ($\sim$ 20% in the case of curve (a)). However, the ratio of Dsa : Dsb for a given insulator thickness should be reasonably accurate since $\alpha_2 \propto 1 + \alpha_1$. It can be seen from table 7.3 that this ratio decreases with increasing film thickness which is precisely as expected. However, the relatively high value of Dsa is somewhat surprising. In an ideal insulator, communication between the metal and the semiconductor is by quantum mechanical tunnelling and Dsa can be assumed to be zero for $\delta \gtrsim 10$ nm. However, in a real insulator, other processes (such as Poole-Frenkel conduction in LB films) can give rise to an additional degree of metal-semiconductor communication. When this is considered (together with the fact that in a large bandgap material interactions between the surface states and the semiconductor bands are less likely) it is not surprising that, even when $\delta \sim 62.5$ nm, Dsa is still comparable with Dsb. The total interface state density ($\sim 2 \times 10^{12}$ cm^{-2} eV^{-1}) is reasonably consistent with the value ($\sim 1.5 \times 10^{13}$ cm^{-2} eV^{-1}) estimated for the near-ideal interface.

A combination of the two groups of interface states can therefore give a reasonable interpretation of the experimental data. Furthermore, the variation of Dsa and Dsb with insulator thickness is qualitatively as expected.

7.3 OPTICAL CHARACTERISATION

The main part of this section is concerned with the EL characteristics of the MIS devices; the photovoltaic properties are also described and the section concludes with a discussion comparing the EL and photovoltaic characteristics.

7.3.1 Experimental Results

(a) EL Measurements

The incorporation of an LB film into the Schottky barrier structure results in a yellow-green light emission from beneath the gold electrode

when the device is operated under forward bias. The emission is of uniform brightness across the area of the contact and this can be seen from the photograph shown in fig. 7.10. This represents a marked improvement over the emission achieved using a 'native oxide' as the insulator which was shown in the photograph in fig. 6.12. The intensity of the EL was found to be highly dependent on the insulator thickness. This is clearly illustrated in fig. 7.11, which shows the spectral distribution of the emission from typical MIS diodes fabricated with different insulator thicknesses. In all cases, the EL was excited using a constant drive current of $\sim$ 10A cm^{-2} and the effect of increasing the film thickness is pronounced. Fig. 7.12 shows both the current density and the relative EL intensity as a function of the applied voltage for a device incorporating five monolayers of $CdSt_2$ as the insulator. It can be seen that the shape of the two curves are very similar, and indeed, the inset to fig. 7.12, which shows the EL intensity as a function of current density, demonstrates that the variation of these two parameters is approximately linear for $J \gtrsim 10^{-1}$ A cm^{-2}, i.e. $V \gtrsim 1.8V$. The voltage at which EL was first detected was $\sim$ 1.7 volts in this case, which indicates that the 'turn-on' voltage for EL emission was somewhat less than this. The general trend observed throughout this work was a decrease in the 'detection voltage' with increasing film thickness. This is not thought to represent a decrease in the actual turn-on voltage, rather it is thought to be a consequence of the increasing intensity enabling the EL to be detected at lower voltages. The EL data presented so far have been described in terms of the EL intensity. A more important parameter is the actual EL efficiency and, in particular, its dependency on the insulator thickness. This variation is shown in fig. 7.13, where the d.c. power conversion efficiency is plotted as a function of insulator thickness. The error bars arise from the fact that each point represents an average value determined from measurements made on several diodes. The

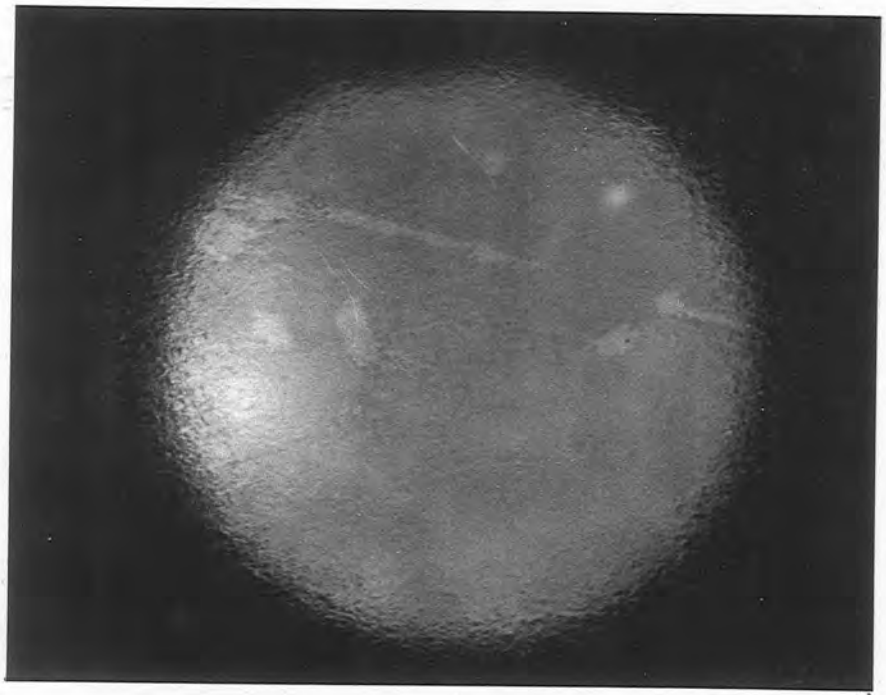

Figure 7.10 Photograph showing EL emission from a typical MIS diode (taken through the back face of the semiconductor).

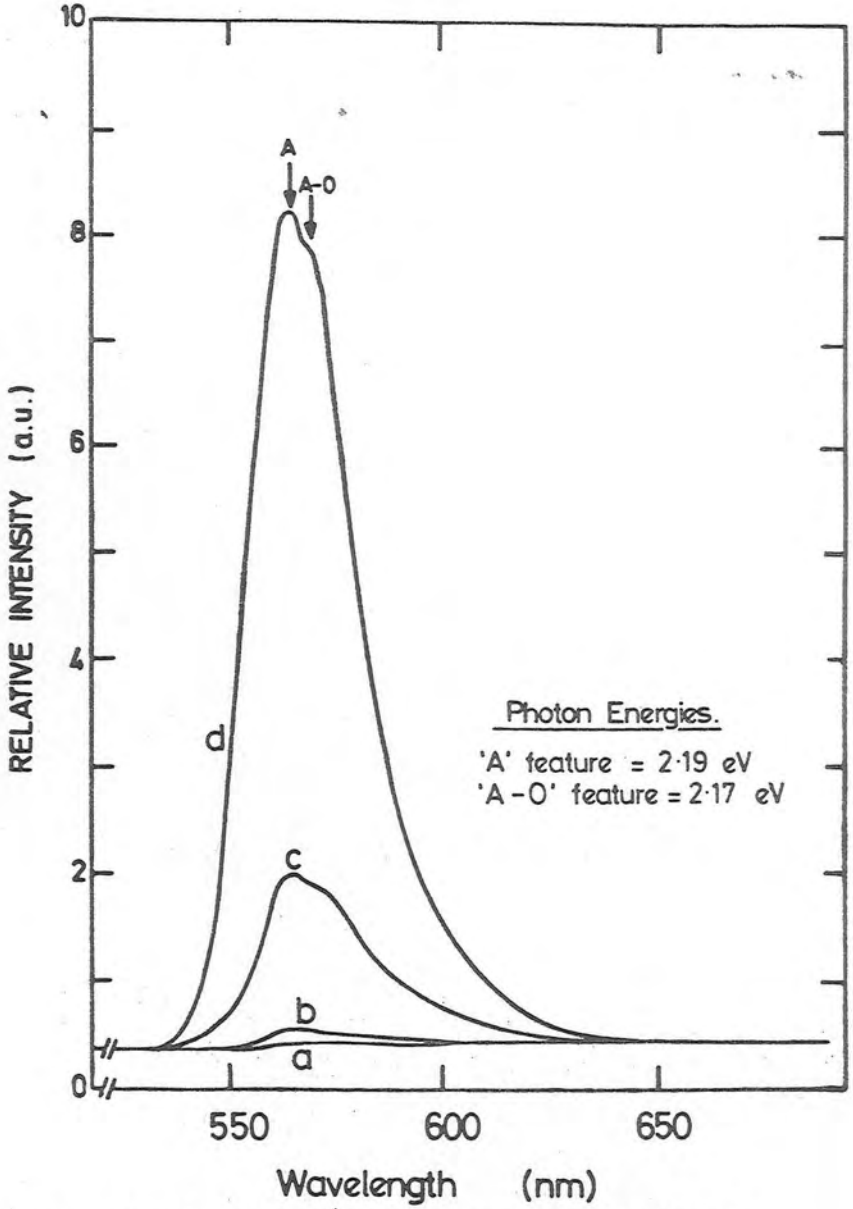

Figure 7.11 Spectral distribution of the EL emitted from typical MIS diodes incorporating (a) one monolayer, (b) three monolayers, (c) five monolayers and (d) seven monolayers of $CdSt_2$.

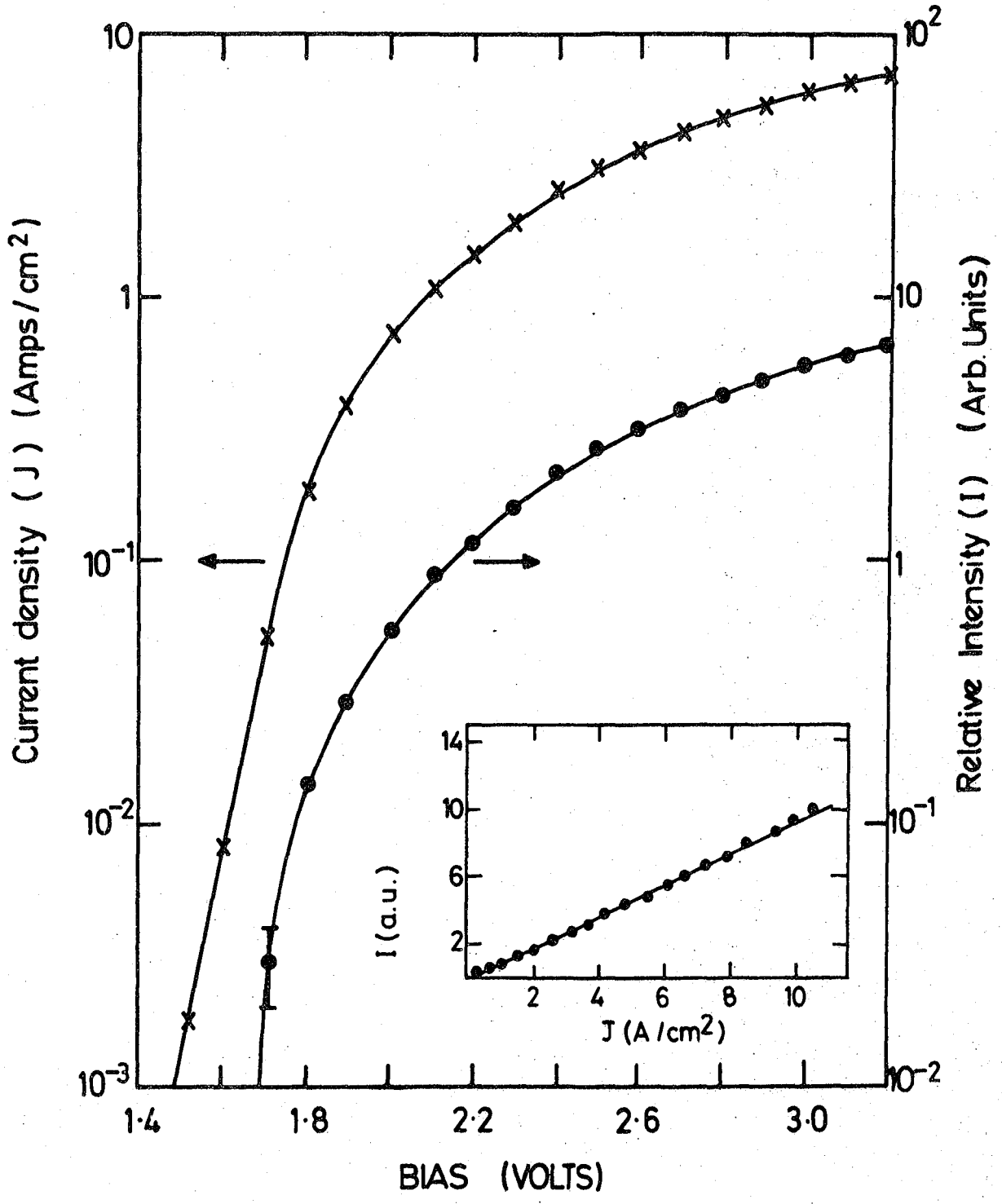

Figure 7.12 Current density and relative EL intensity as a function of bias for a device incorporating five monolayers of $CdSt_2$. (Inset shows the intensity as a function of J).

variation is clearly depicted; after an initial, gradual increase the efficiency peaks sharply at an insulator thickness of $\sim$ 27 nm, at which the actual EL efficiency is $\sim 3.8 \times 10^{-3}$%. Repeating the experiment using ω-TA as the insulator gives almost exactly the same optimum thickness (as shown by the dotted curve in fig. 7.13) but a higher maximum efficiency ($\sim 6 \times 10^{-3}$%). The agreement between the two is really quite remarkable, especially so in view of the fact that the monomolecular dimensions of the two materials are different (the optimum thickness is $\sim$ 9 monolayers for ω-TA diodes compared with $\sim$ 11 monolayers for $CdSt_2$ devices). This aptly demonstrates the importance of an accurately defined insulator thickness. It is important to consider the effect of much thicker insulators on the EL efficiency since this may provide some information about the actual EL mechanism. This is illustrated in fig. 7.14 which shows a similar optimum curve but for a much wider range of insulator ($CdSt_2$) thicknesses. Once again, the optimum thickness is consistent with that shown previously, but it is evident that, even in the case of insulators $\sim$ 62.5 nm thick, the EL can still be detected and, furthermore, it is still highly uniform in appearance. This aspect, together with all of the other EL data, will be discussed at length in the following section once the evidence from the photovoltaic measurements has been presented.

(b) Photovoltaic Properties

Figure 7.15 (a) shows the current-voltage characteristics, both in the dark and under approximate AM1 conditions, for an MIS diode fabricated with one monolayer of ω-TA. Comparing these with those for the near-ideal Schottky diode (fig. 6.5) reveals that, although the short circuit current density is approximately the same in both instances, a large increase in the open circuit voltage has been achieved. Furthermore, the fill-factors are similar in both cases and a significant improvement in conversion efficiency has been obtained over the Schottky barrier structure. This has been reported previously

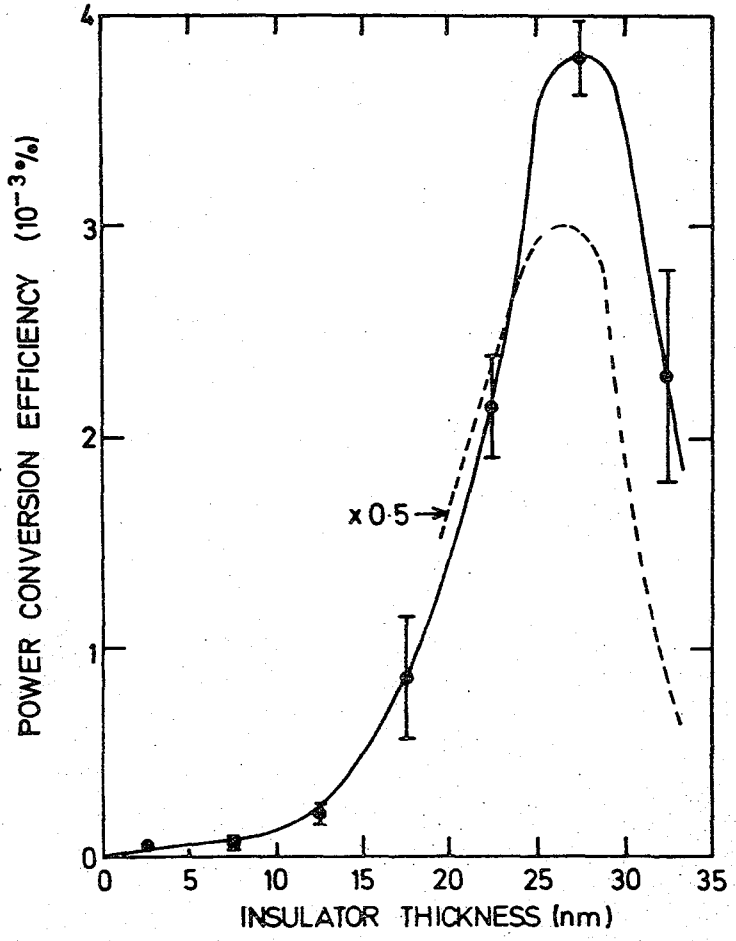

Figure 7.13 D.C. power conversion efficiency as a function of insulator ($CdSt_2$) thickness (the dotted curve shows the same variation for diodes incorporating ω-TA).

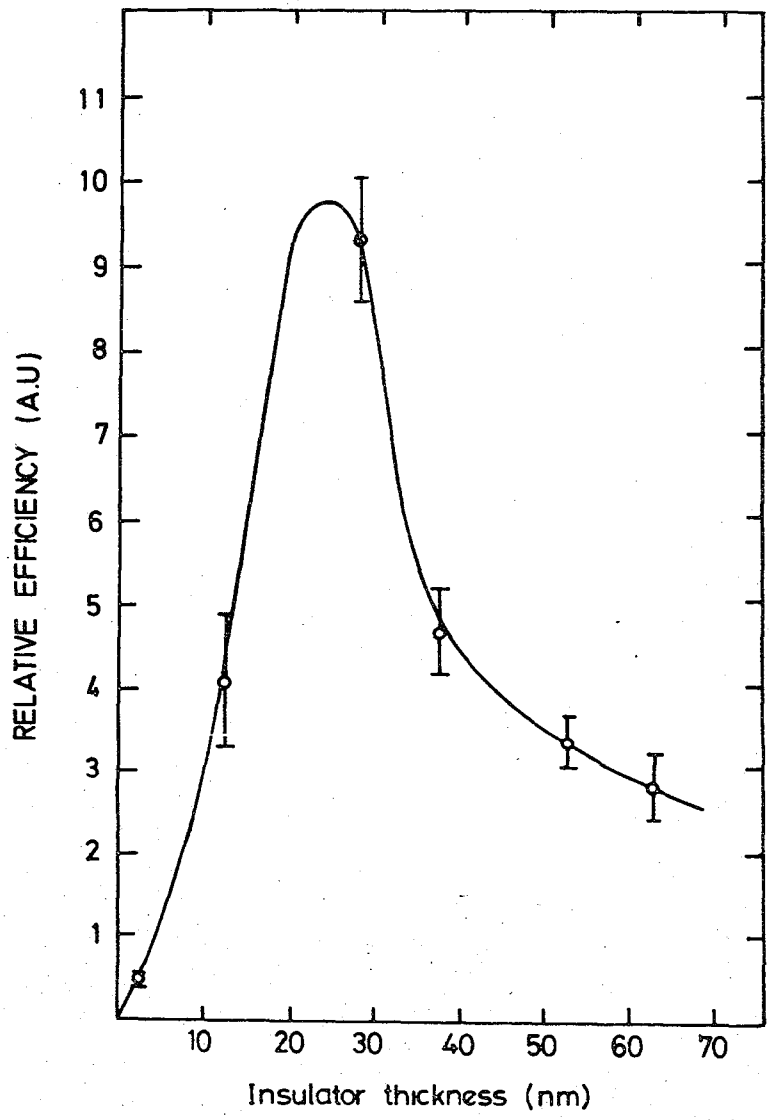

Figure 7.14 D.C. power conversion efficiency as a function of insulator ($CdSt_2$) thickness.

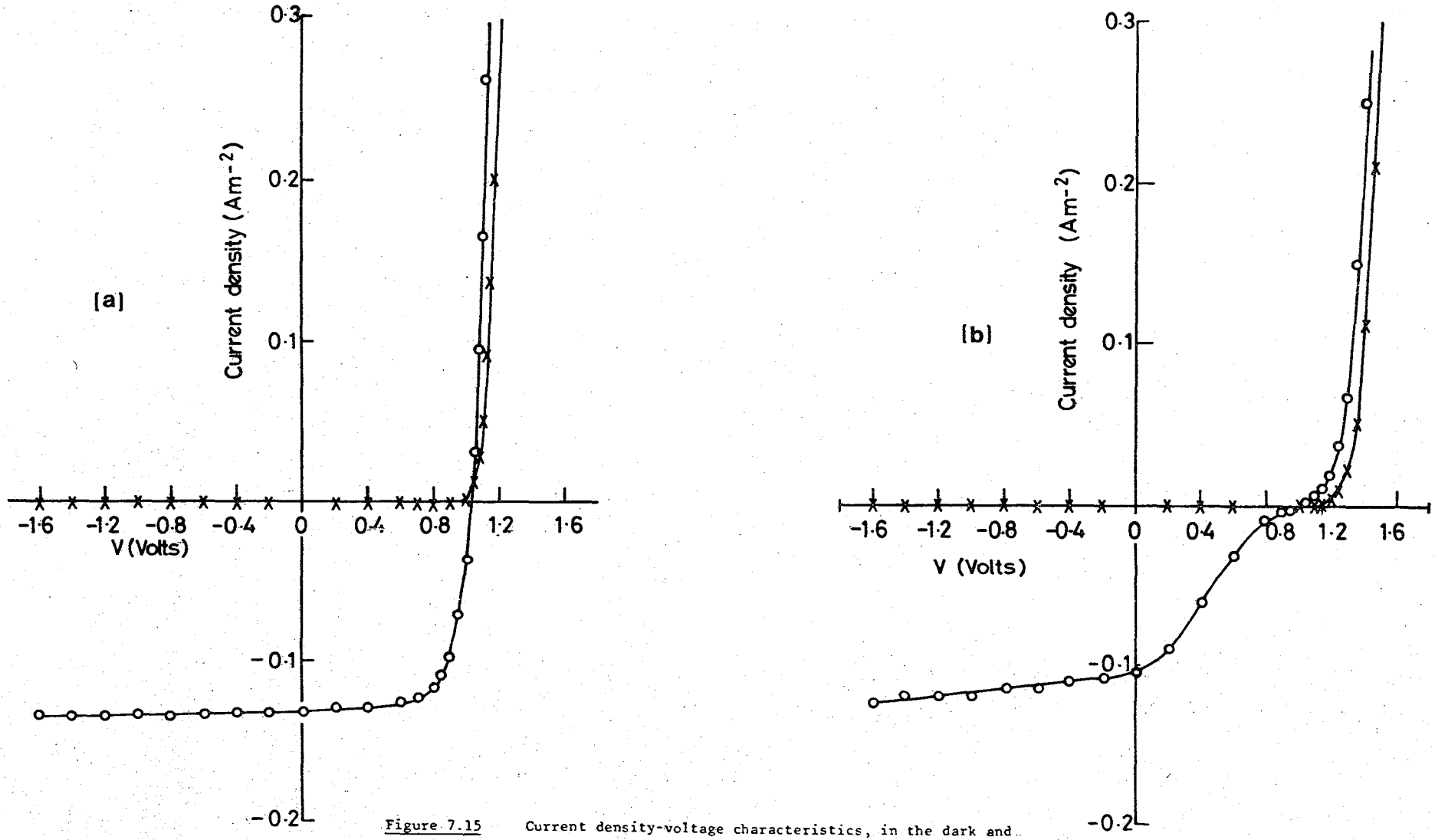

Figure 7.15 Current density-voltage characteristics, in the dark and under illumination, for an MIS diode fabricated with (a) one monolayer and (b) seven monolayers of ω-TA.

for single monolayer MIS devices on GaP[1] and, prior to that, for a range of LB insulator thicknesses on CdTe[13]. In this latter case, the value of $J_{s/c}$ was shown to be unaffected by the presence of the LB film until the insulator thickness was $\sim$ 3.6 nm, in accordance with the tunnelling MIS theory described in § 3.4.4. However, the GaP diodes behaved very differently. For example, fig. 7.15 (b) shows the J-V characteristic, both in the dark and under illumination, for a diode fabricated with 7 monolayers ($\sim$ 21 nm) of ω-TA. Although there is a significant decrease in the fill factor, the values of $J_{s/c}$ and $V_{o/c}$ are only slightly affected. The full variation of these two parameters with insulator thickness is shown in fig. 7.16. Again, each point represents an average over a number of contacts from each region of the slice. The value of $J_{s/c}$ remains approximately constant for thicknesses of up to $\sim$ 21 nm, after which it decreases until, at $\sim$ 45 nm, it is $\sim$ 40% of its maximum value. The value of $V_{o/c}$, however, remains relatively unaffected by the film thickness after the initial large increase, and in fact only decreases by $\sim$ 15% over the range 3-45 nm.

7.3.2 Discussion

The uniformity of the EL emission is indicative of the homogeneity of both the structure and thickness of the LB film. The electrode shown in the photograph in fig. 7.10 is $\sim$ 1.1 mm in diameter which is really quite large compared with commercial LEDs (typically $\sim$ 0.3 mm x 0.3 mm), and there are no obvious irregularities in the emission. This demonstrates the suitability of the LB technique in a study such as this. However, before proceeding further with the results, it is important to elucidate, as far as possible, the operation of the device, and in particular the mechanism by which the EL is excited.

The spectra shown in fig. 7.11 reveal that two dominant radiative recombination processes govern the emission. These are marked A and A-O and are identified by their respective photon energies (given in fig. 7.11);

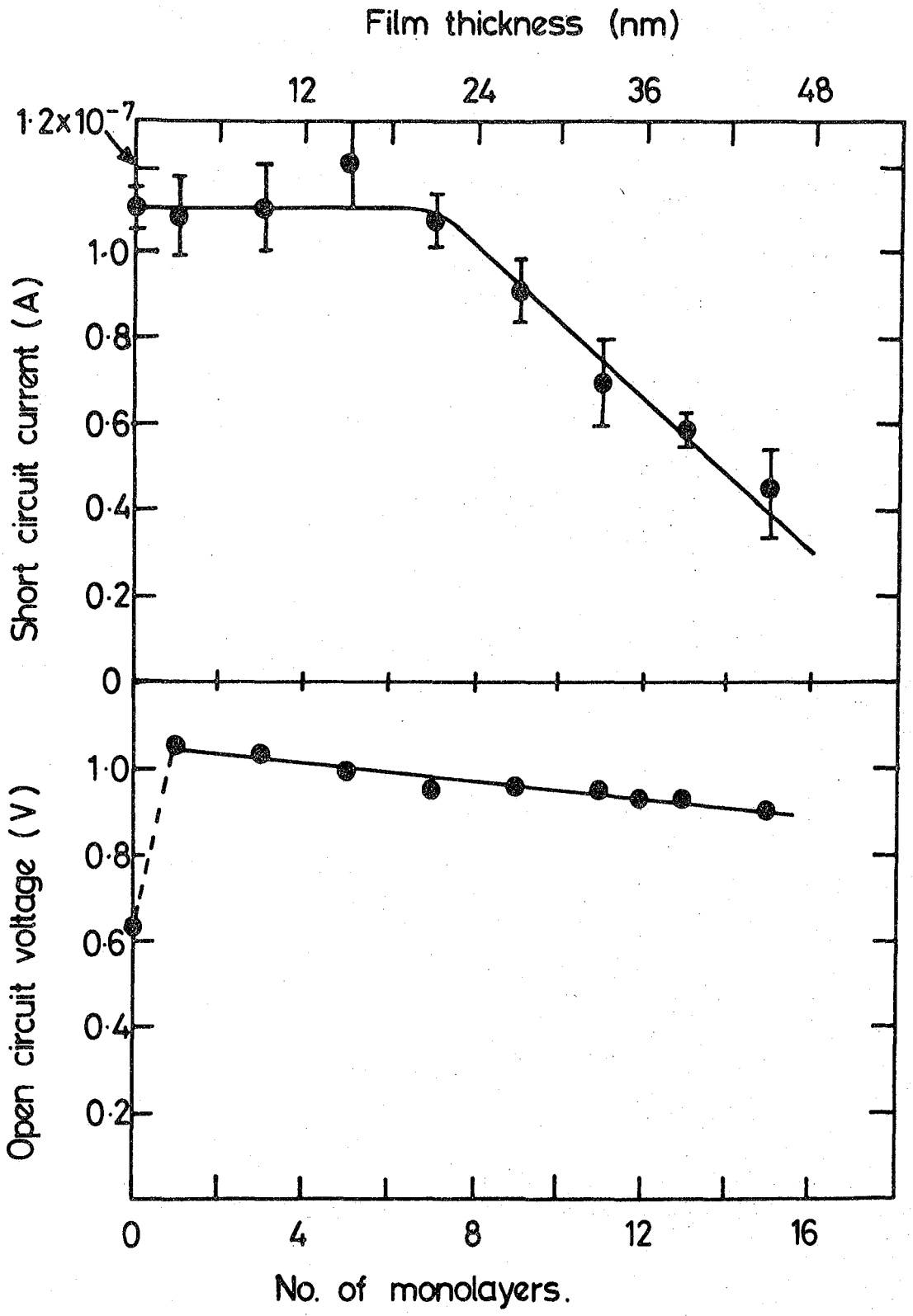

Figure 7.16 Variation of open circuit voltage and short circuit current with the number of monolayers of ω-TA.

they arise from the recombination of excitons bound to isolated impurity atoms (see § 2.6.2) and are highly characteristic of minority carrier injection EL. Furthermore, the very low turn-on voltage for EL ($\lesssim$ 1.7V) eliminates virtually all but minority carrier injection as the excitation mechanism. The spectra are somewhat different to those obtained for the 'non-ideal' Schottky diodes, one of which was shown in fig. 6.11. This is merely a consequence of the lower concentration of nitrogen activation centres in the substrates used to fabricate the LB film MIS diodes and does not indicate different excitation mechanisms in the two devices. Having established minority carrier injection as the excitation mechanism, it is clear that the effect of increasing the film thickness (up to $\sim$ 27 nm) is to enhance the minority carrier injection ratio, γ, and hence the EL efficiency. The mechanism by which this enhancement is achieved must now be discussed.

Previous MIS LED Theories

There are two theories which have been used extensively to explain enhanced minority carrier injection in MIS devices under forward bias, both of which were discussed in chapter 3. These are (i) the tunnel-injection theory (§ 3.4.2), and (ii) the two-stage Auger recombination theory (§ 3.4.3.). The applicability of these two theories to the data presented here will now be discussed.

Direct quantum mechanical tunnelling of minority carriers into the semiconductor is clearly an unreasonable explanation for the minority carrier injection mechanism. The insulator thicknesses involved ($\sim$ 27 nm in the optimum case) are well in excess of the tunnelling regime ($\lesssim$ 10 nm). These relatively large dimensions suggest a possible similarity between these results and those obtained using II-VI materials which are often interpreted in terms of the theory (ii) above. For example, the results of Livingstone et al, which were reproduced in fig. 3.8, are fairly typical

and show that an 'optimum' exists for insulators $\sim$ 50 nm thick, although for $\delta \gtrsim$ 50 nm, the efficiency is relatively independent of the thickness. However, for two reasons, this mechanism is not thought to be responsible for the injection of minority carriers in the GaP diodes. Firstly, such a mechanism, whereby both minority and majority carriers surmount the barrier presented by the insulator bandgap, is expected to result in an efficiency which is relatively independent of insulator thickness. This is observed in the case of the II-VI diodes (at least for $\delta \gtrsim$ 50 nm), but not in the data presented here where the efficiency - thickness curve is much more acute (e.g. fig. 7.14). The sharp decrease observed in the case of insulators greater than the optimum, indicates that the impediment to minority carrier transport increases rapidly as the insulator thickness is increased beyond the optimum value. This is not consistent with the Auger mechanism. The second reason is that the bandgap of $CdSt_2$ is expected to be large ($\sim$ several eV) and the Auger process is thought to be inherently inefficient. The efficiencies measured in this work are believed to be too high to be explained using this mechanism. This may explain why the efficiencies achieved to date using II-VI materials fall disappointingly short of the theoretical maximum.

Proposed Mechanism for Minority Carrier Enhancement

Before proceeding to discuss the mechanism, it is instructive to consider the evidence from the photovoltaic measurements: It is clear from the variation of $J_{s/c}$ with δ that the impediment to the (minority carrier) photocurrent due to the insulator is insignificant, when compared to the processes in the semiconductor bulk, for thicknesses less than $\sim$ 21 nm. This reveals the existence of a relatively 'easy' current path for minority carriers through the insulator bulk and provides an explanation as to how, in the case of the EL measurements, the minority carriers can be injected

into the semiconductor even though the insulator thickness is beyond tunnelling dimensions. The possible origins of this mechanism are discussed at a later stage, but for the present discussion it is sufficient to assume that such a mechanism exists.

In view of this evidence, the most obvious explanation is one based on the essential principles of the tunnel-injection theory, but employing an alternative minority carrier transport mechanism. These are the principles of band realignment and ease of hole transport across the insulator, when compared to the processes in the semiconductor bulk. In this interpretation, the degree of band realignment achieved under forward bias, for a given current density, increases with insulator thickness and consequently, γ also increases. Once the impediment to hole current due to the transport process in the insulator becomes appreciable, then γ is reduced. An optimum is achieved and the thickness at which it is obtained depends on the ease with which holes can traverse the insulator. However, there is an inconsistency between this explanation and some of the experimental results : Consider again fig. 7.12, which shows the variation of current density and relative EL intensity with the applied bias. For $V \gtrsim 1.8V$, the J-V characteristic approaches Ohmic behaviour and the EL intensity varies linearly with J. This has the important implication that, for $V \gtrsim 1.8V$, further band realignment has relatively little effect on the EL efficiency, and indeed in this voltage region the efficiency was found to be virtually independent of bias. This was true for all of the diodes, irrespective of their insulator thickness. This is an important piece of evidence since it shows that at a voltage of $\sim 1.8V$, the semiconductor valence band edge must be adjacent to empty states in the metal, i.e. in the vicinity of the metal Fermi level. Figure 7.17(a) shows the simplified band diagrams of the MIS diode (i) in equilibrium and (ii) under the application of a forward bias of $\sim$ 1.8V. From this figure, it is

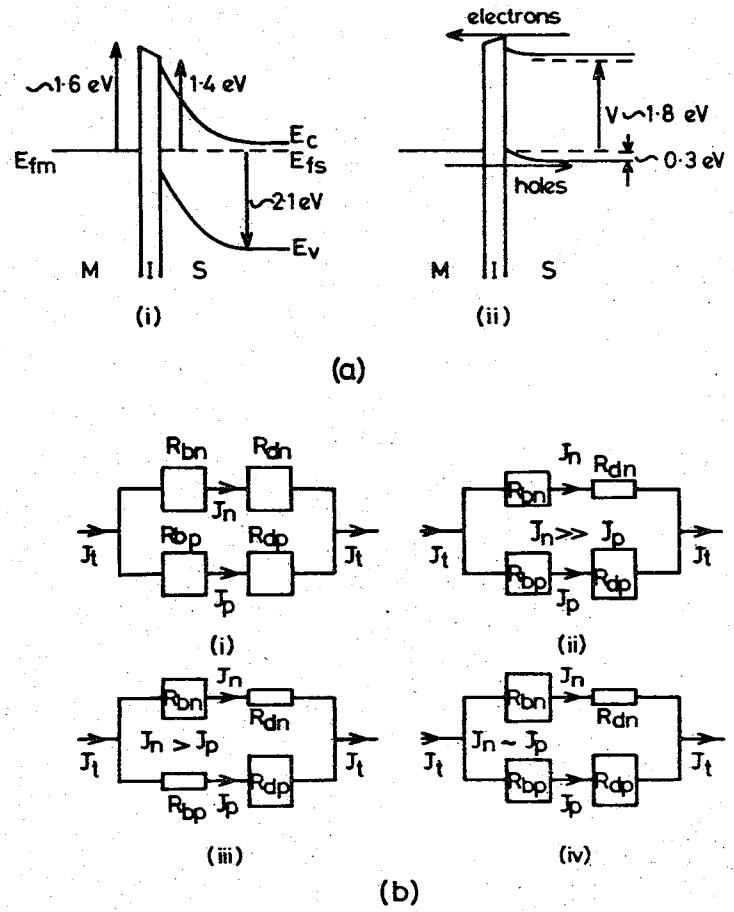

Figure 7.17 (a) Simplified energy band diagram of an MIS diode (i) in equilibrium and (ii) under a forward bias of ~ 1.8V. (b) Simplified equivalent circuits depicting the various impediments to current flow in MIS diodes (refer to text for an explanation).

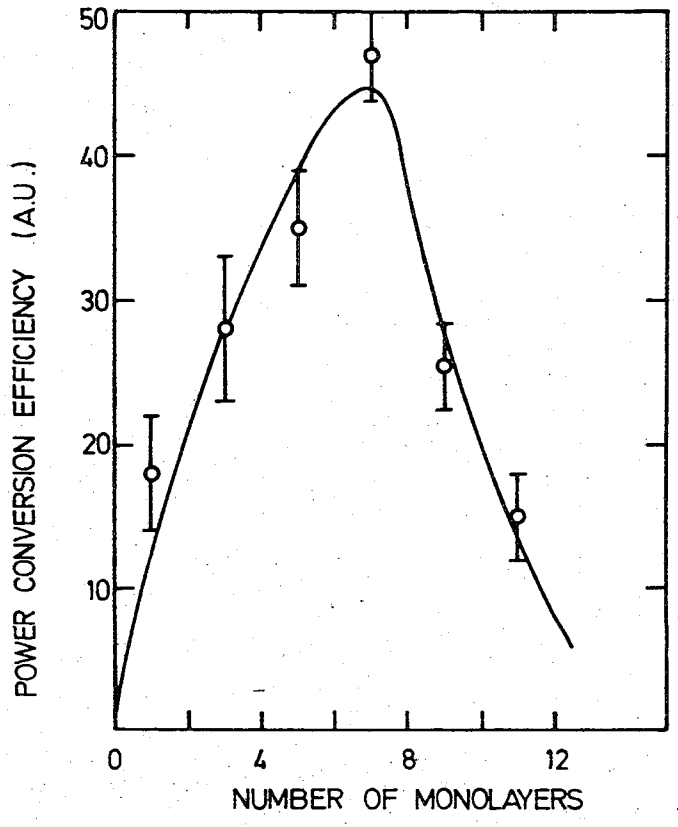

Figure 7.18 EL efficiency as a function of the number of monolayers of ω-TA. (From the same sample used to obtain the data in fig. 7.16)

clear that this voltage is almost sufficient to align the metal Fermi level and the semiconductor valence band edge. The implication of the experimental data that, at this voltage, Ev is adjacent to empty states in the metal, can be explained by invoking the concept of an Auger type recombination of hot electrons in the metal (as in the II-VI MIS LEDs). However, in this instance, the excess energy required is only $\sim$ 0.3eV, which is quite feasible in view of the energy with which the electrons enter the metal ($\sim$ Efm + 1.6eV). It is proposed that this degree of band realignment is achieved in all diodes, irrespective of the insulator thickness - certainly the bias required to pass the excitation current of $\sim$ 10 A/cm^2 was always in excess of 2V. Since total band realignment is therefore achieved even in diodes incorporating only one monolayer, the increase in γ obtained by incorporating subsequent layers must now be explained.

To do this, it is convenient to separate, completely, the majority and minority carrier currents and to think of the various impediments to each current as effective resistances. Then a simple equivalent circuit can be drawn, as in situation (i) in fig. 7.17(b). The total current taken by the diode, J_t, is comprised of a minority carrier component, J_p, and a majority carrier component, Jn. there are two mechanisms which can limit either current; the emission over the barrier at the metal-semiconductor interface, and the process of drift and diffusion in the semiconductor bulk. These have been assigned the 'effective resistances' Rb and Rd respectively and the subscripts 'n' and 'p' in fig. 7.17(b) refer to electrons and holes respectively. However, it must be remembered that both Rbn and Rbp themselves represent two mechanisms in series; the actual thermionic emission over the barrier and the transport process in the insulator. In an ideal Schottky barrier, Rbn >> Rdn and Rdp > Rbp, however the total impediment to majority

carriers is much less than that presented to minority carriers and Jn >> Jp, i.e. γ is small. On increasing the forward bias, the situation is barely affected and γ is still very small. This is situation (ii) in fig. 7.17 (b) where the size of each block is intended to represent the magnitude of the impediment. The inclusion of one monolayer into the structure alters the picture quite dramatically (situation (iii)); Rbn is increased (due to the increase in the height of the barrier) but, under the application of a forward bias, Rbp is much reduced (due to band realignment). In this situation, the electrons are still limited by Rbn and the holes by Rdp. However, since Rdp is still greater than Rbn, then the inequality Jn > Jp is still valid, although much reduced in magnitude. A significant increase in γ has been achieved. Increasing the insulator thickness has two effects; it increases both Rbn and Rbp by increasing the impediment due to the transport across the insulator. However, the effect on the electrons is much more significant since the holes are limited, not by Rbp, but by Rdp. The result is a further increase in γ with δ until the optimum thickness is reached. At this optimum, Rbp just becomes appreciable when compared with Rdp; the maximum value of γ has been achieved and Jp may be comparable to Jn (situation (iv)). Further increases in δ increase both Rbn and Rbp by virtue of the series impediment due to the insulator; however, Rbp increases more rapidly than Rbn which results in the observed decrease in γ.

The experimental observations can therefore be explained using the essential principles of the tunnel injection theory but assuming different mechanisms for the transport of holes and electrons. The factor which determines the maximum EL efficiency is essentially the extent to which the mechanism in the insulator 'conduction band' impedes the electron current. This may explain why the diodes fabricated using ω-TA as the insulator exhibit an optimum $\sim$ 50% greater than those fabricated with $CdSt_2$. It is clear from

a comparison of the data shown in figs. 7.1 and 7.4, that this impediment is greater in the case of the ω-TA diodes.

One aspect has yet to be explained, and that is the actual process by which the holes are transported across the insulator. The exact mechanism remains unclear although certain possibilities can be eliminated. For example, it has already been argued that excitation over the hole barrier presented by the insulator is not consistent with the experimental observations. Also, the possibility of conduction via pinholes in the film is thought unlikely. Although it is known that a large pinhole density can be tolerated without degradation of the photovoltaic properties[22], a density significant enough to allow a photocurrent of ~ 0.14 A m^{-2} to flow would surely have manifest itself as a deviation from ideal in the (majority carrier) J-V characteristics presented earlier. The fact that the process appears to be limited only to hole transport suggests that conduction via energy levels located in the insulator bandgap, and conveniently situated with respect to the semiconductor band structure, may provide an accurate explanation. Such levels could arise from the 'amorphous' nature of the insulator or from specific structural defects. In fact, such an alternative for the photocurrent transport mechanism has been observed previously[23] where oxide traps, conveniently situated adjacent to the minority carrier band edge, enabled insulators much thicker than tunnelling dimensions to be used effectively in MIS solar cells. These traps had no detrimental effect on the open circuit voltage of the devices since they did not affect the majority carrier current. Such results are very similar to those observed here. A measurement of the type made by Yu and Snow[24] where a transistor structure was used to separately study the minority and majority carrier currents, would undoubtedly prove useful in determining the precise nature of the process. Unfortunately, such a measurement was not possible in this work.

7.3.3 Comparison between EL and Photovoltaic Properties

It is interesting to compare the photovoltaic and EL properties of the MIS diodes since this has not previously been done. It has already been mentioned that the similarity in the operation of the two devices lies in the fact that, in both cases, holes are required to traverse the insulator. However, the direction of hole transport is different in the two devices and the minority carrier current levels involved are also very different ($\sim 10^{-5}$ A cm^{-2} in the photocell compared with $\sim$ 1 A cm^{-2} in the EL diode). Furthermore, the behaviour of the hole quasi-Fermi level is also somewhat different in the two cases (see figs. 3.7(b) and 3.11). Despite these differences, the optimum thickness for EL efficiency corresponds almost exactly to the value at which the photocurrent begins to be reduced by the insulating layer. This can be seen by comparing the data shown in fig. 7.16 to the EL optimum curve in fig. 7.18. Both sets of data were obtained from the same sample and the optimum insulator thickness for EL efficiency is precisely the value at which the photocurrent begins to be affected. This is additional confirmation that the hole transport process is the same in both instances. Further, it is evident that the process is bi-directional suggesting that the mechanism is, indeed, a bulk process through the LB film, although the exact nature of the process remains uncertain.

Before proceeding to discuss the lifetimes of the LEDs, it is interesting to note how the photovoltaic measurements are consistent with the model which was proposed in § 7.2.3. The variation of $J_{s/c}$ with δ has been discussed previously; consider now the variation of $V_{o/c}$ with δ (fig. 7.16). The feature of this curve is that the increase obtained by incorporating an LB film into the Schottky diode structure is relatively independent of its thickness. The characteristic does not conform to equation (3.63), i.e.

$$V_{o/c} = n' \left(\frac{kT}{q}\right) (\ln (J_{s/c}/J_o') + \chi^{\frac{1}{2}}\delta)$$

since this predicts an optimum in $V_{o/c}$ for an insulator thickness of the order of tunnelling dimensions. This has been observed experimentally in Si : SiO_2 diodes[21]. (It should be noted that the full expression for $V_{o/c}$ contains a contribution due to the incorporation of fixed charge, either in the insulator, or at the interface, which may or may not be significant. For the purposes of this discussion it has been omitted.) In fact, the data in fig. 7.16 support the model proposed earlier. According to this model, the majority carrier barrier height is that of the insulator barrier, ϕ_{bi}, and the dominant current mechanism is thermionic emission. The data should then conform to the equation

$$V_{o/c} = n' (kT/q) \ln (J_{s/c}/J_{no}')$$

where, in this case, $J_{no}' = A^*T^2 \exp (-q \phi_{bi}'/kT)$.

The barrier height predicted by inserting the relevant values of $V_{o/c}$ and $J_{s/c}$ for the single monolayer diode into the above equation is $\sim$ 1.67 eV which agrees well with the measured value of 1.64eV. For the five monolayer devices, the predicted value is $\sim$ 1.63eV and for the diodes incorporating 15 monolayers, $\phi_{bi} \sim$ 1.56eV. The barrier heights are predicted to be relatively independent of the insulator thickness and the results are, at least qualitatively, consistent with the proposed model.

7.3.5 LED Degradation

(a) Device Lifetimes

All of the diodes fabricated using either $CdSt_2$ or ω-TA as the insulator exhibited relatively poor lifetimes, although those incorporating ω-TA were somewhat better in this respect. Fig. 7.19 shows the relative EL intensity as a function of time (a) for a diode fabricated with ∿ 27 nm (11 monolayers) of $CdSt_2$ and (b) for a diode fabricated with a similar thickness (9 monolayers) of ω-TA. The curves have been normalized to show the same initial intensities. The same (constant) drive current of ∿ 7 A cm^{-2} was used to excite the EL. It can be seen that the decay is much more rapid in the case of the $CdSt_2$ diode. There is little doubt that the ω-TA is the more stable material; it forms a much more ordered, closely packed film and also appears to have better mechanical properties and these attributes are thought to be reflected in the increased lifetime of the device. In general, the device lifetime was found to be a function of the current density used to drive the device and diodes driven with high current densities, i.e. ∿ 25 A cm^{-2} (under pulsed conditions in order to eliminate heating problems) lasted only a few hours. Under continuous long term operation the EL gradually diminished until it was eventually undetectable (by eye) for normal drive currents. This degradation is most likely to be a consequence of the LB film properties rather than those of the semiconductor substrate. However, it is important at this stage to establish the origin of the degradation mechanism so that the prospects for significant improvements by incorporating even more stable insulators, can be assessed.

(b) Degradation Mechanisms

The failure of these devices appears to be a consequence of the relatively large current densities (by LB film standards) which are necessary to excite the EL. This is confirmed by considering fig. 7.20 which shows the current-voltage characteristic of an MIS diode incorporating five monolayers of $CdSt_2$

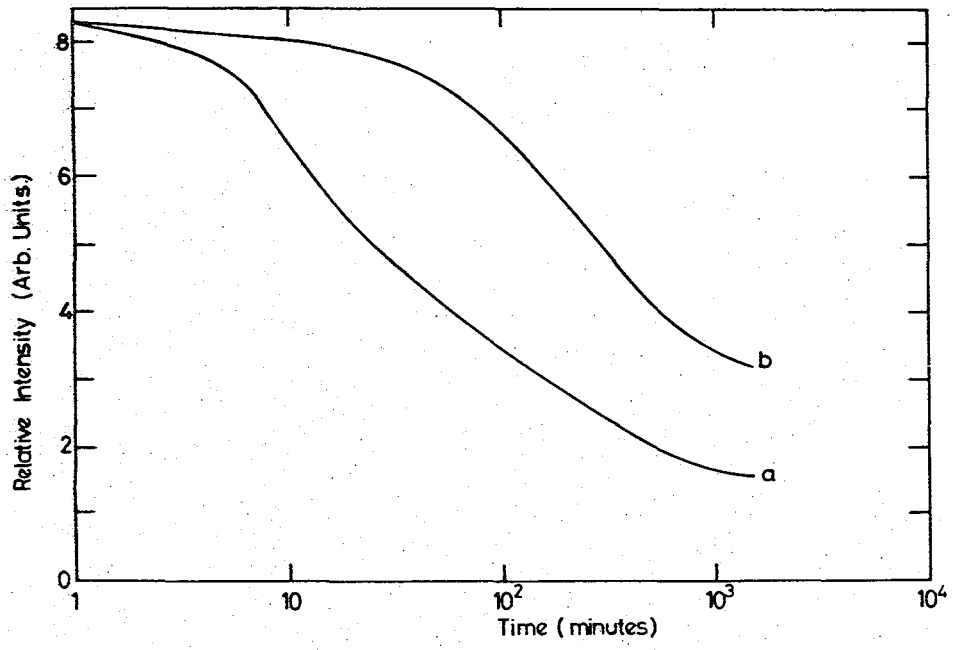

Figure 7.19 Relative EL intensity as a function of time for a diode incorporating (a) 11 monolayers (∿ 27 nm) of $CdSt_2$ and (b) 9 monolayers (∿ 27nm) of ω-TA.

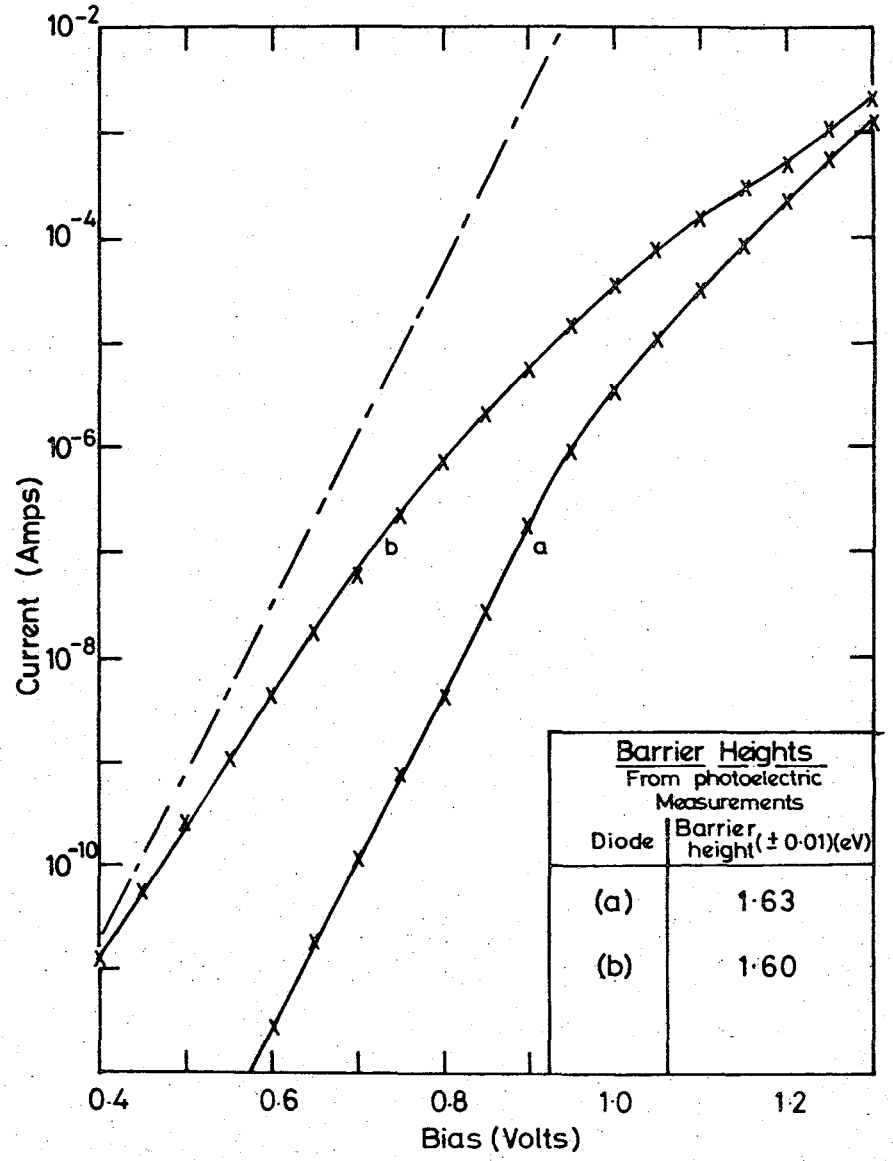

Figure 7.20 Conductivity data for a diode fabricated with five monolayers of $CdSt_2$ (a) before, and (b) after, 15 hours of continuous operation.

(a) before, and (b) after, 15 hours of continuous operation at $\sim$ 7 A cm^{-2}. Also shown (as the dashed line) is the characteristic of a typical near-ideal Schottky barrier. At high bias, i.e. when the curve begins to be limited by the series resistance of the diode, the two curves (a) and (b) are reasonably similar. However, at low bias the curves differ greatly, and for a given applied voltage a much larger current (by up to 3 orders of magnitude) is taken by the diode after 15 hours of continuous operation. In fact, at very low bias, the curve (b) approaches that of the near-ideal Schottky diode. However, although the low bias current-voltage characteristic has been greatly affected, the majority carrier barrier height, as measured by the photoelectric technique, (see inset to fig. 7.20) remains approximately constant. This suggest that an alternative current path has been formed through the insulator which electrons in the semiconductor find 'easier' than emission over the top of the barrier but in the photoelectric measurement, excitation over the insulator is still dominant. This indicates that the insulating properties of the film are not completely destroyed. The extent to which curve (b) deviates from (a) is, in general, dependent on the drive current density and duration. Thus it is concluded that the effect of passing this large current is to cause a deterioration in the insulating properties of the LB film resulting in the formation of alternative current paths in parallel to the normal thermionic emission process. At low current densities, the current can easily flow through the insulator (via these alternative paths) and the characteristic approaches that corresponding to thermionic emission over the semiconductor depletion region (i.e. the near ideal characteristic). At higher current densities these paths become 'saturated' and the curve approaches the normal curve (a). This interpretation is supported by the fact that the open circuit voltage developed by the diode under illumination had decreased from $\sim$ 1.05V (in this case) to $\sim$ 0.64V, i.e. to approximately that observed

in near-ideal Schottky diodes. The insulator, now 'leaky' to majority carriers after 15 hours continuous operation, does not present any significant additional impediment to the loss mechanism associated with the thermionic emission of majority carriers from the semiconductor into the metal.

It is clear that LEDs fabricated from fatty acid LB films display little potential from the viewpoint of commercial devices. This was not unexpected in view of their poor mechanical and thermal properties. However, it has been shown that a significant increase in device lifetime can be achieved by using a more stable LB film (i.e. ω-TA) and it is clear that a further improvement will be possible by incorporating still more stable films. An ideal candidate is the phthalocyanine material which has only very recently been deposited in LB film form[25-27]. Measurements made on devices fabricated using this material are presented in the following section.

7.4 DEVICES INCORPORATING PHTHALOCYANINE LB FILMS

The phthalocyanines are one of a number of groups of organic materials which are known to possess semiconducting properties. However, because of the almost total insolubility of the common phthalocyanine (Pc) derivatives in most solvents, they have received little attention as possible LB film materials. Recently, however, as a result of collaboration between the University of Durham and ICI Ltd., these problems have been circumvented and LB films of a number of Pc derivatives have been successfully deposited. In view of their excellent stability, both thermally and structurally, and the fact that these films adhere tenaciously to substrates and resist the action of many organic solvents, the Pc material is an obvious choice for the extension of the 'model' system towards a more commercially viable device. Unfortunately, the research on phthalocyanine in LB film form is in its early stages and such films have yet to be fully characterised. In

particular, the conduction processes have yet to be fully investigated and, although preliminary results reveal that they are fairly insulating, the possibility exists that they may exhibit semiconducting properties[27]. This in itself is sufficient reason to study LEDs incorporating Pc since most of the phthalocyanines exhibit p-type conductivity when prepared in other forms, and this introduces the possibility of enhanced hole injection into the n-type substrate.

7.4.1 Electrical Characterisation

The diode characteristics were, in general, very different from diodes fabricated using fatty acid LB films. For example, fig. 7.21 shows the current density-voltage curves for diodes incorporating a range of different thicknesses of Pc LB films. Curve (a) represents the characteristic of a diode fabricated with one layer, curve (b) corresponds to the incorporation of five layers and curve (c) represents twenty layers. The thickness of each deposited layer is believed to be $\sim$ 0.8 nm[26]. Also shown in fig. 7.21, for comparison, is the curve for a near-ideal Schottky barrier. The characteristics are very different from those observed for the fatty acid diodes and they do not exhibit the distinct regions shown in figs. 7.1 or 7.4. The effect of the film is much more noticeable in the Pc-based diodes. Even the effect of a single monolayer is very pronounced, although it is only $\sim$ 0.8 nm thick, and increasing the film thickness affects the characteristics markedly. The conduction mechanism is clearly not the thermionic emission process which was proposed for the fatty acid diodes, but the lack of information on the film properties makes these data difficult to interpret. The 'step-like' feature in the characteristic, which is most evident in curve (b) may provide some insight into the conduction mechanism. Similar features have been observed many times in more conventional MIS diodes and have usually been attributed to interface states. However, an alternative possibility is the charging of states in the film itself giving rise to a

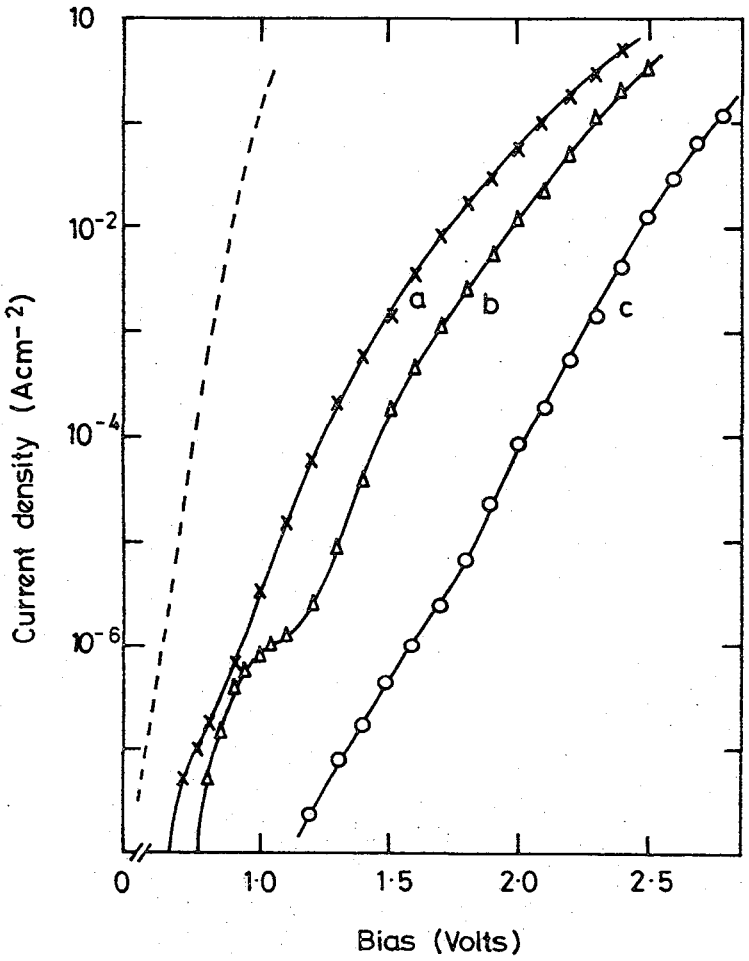

Figure 7.21 Current density-voltage curves for diodes incorporating (a) one layer, (b) five layers and (c) twenty layers of Pc. (Also shown is a near-ideal Schottky diode characteristic.)

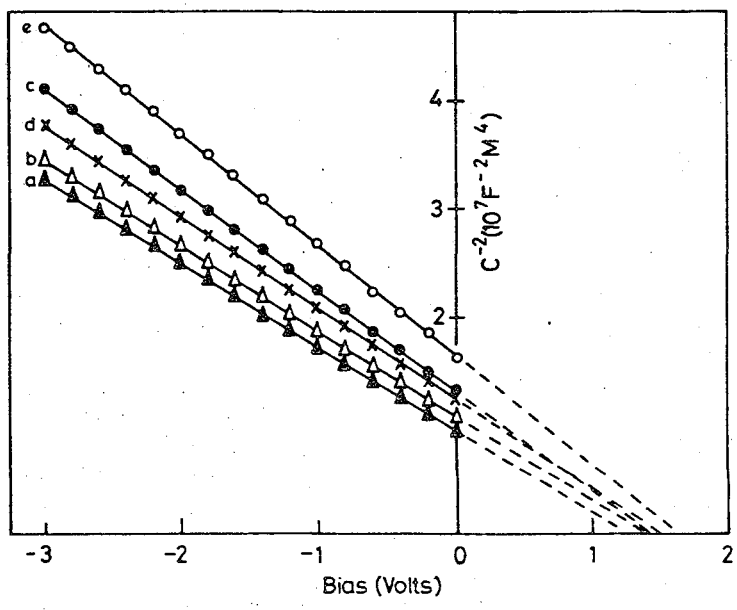

Figure 7.22 Reciprocal capacitance squared against voltage curves for diodes incorporating a range of different thickness of Pc. Curves (a) to (e) correspond to diodes incorporating 0, 1, 5, 10 and 30 layers respectively.

space charge effect. Certainly the time taken for the current to reach equilibrium, after a change in bias, was very long (in some instances several hours) which would appear to indicate a trapping mechanism.

Attempts to directly measure the barrier heights of the diodes were unsuccessful; even in the case of a diode fabricated with one layer, the metal-semiconductor photoresponse could not be detected. This could be interpreted as an indication that the metal-insulator barrier height, ϕ_{bi}, is significantly greater than the 1.64eV measured in the case of diodes fabricated using $CdSt_2$, since in a diode with $\phi_{bi} \gtrsim 1.8$eV, the relevant photoresponse would be obscured by photoexcitation processes in the semiconductor bulk. Since the photovoltaic measurements of the fatty acid diodes could be used to predict the barrier height quite successfully, the photovoltaic properties of the Pc MIS diodes were also studied. In fact, the devices were found to exhibit interestingly unusual photovoltaic action. For example, when a short circuited diode was illuminated, it initially gave rise to a photocurrent of the same order of magnitude as that measured in the fatty acid diodes. However, this gradually decayed with time over a period of several tens of minutes until a new, lower value was established. The magnitude of this decay decreased with decreasing light intensity and, in fact, under normal room illumination it was virtually absent. This could be further evidence for a large trapping effect in the Pc films. Alternatively it could be a result of (opposing) photovoltaic action at the Au : Pc interface or even a photoconductive effect in the Pc film itself. This latter interpretation was corroborated by the fact that the magnitude of the photocurrent was unusually dependent on both bias and ambient conditions, (the conductivity of the Pc is known to be affected by certain ambients). If this interpretation is correct, then the p-type conductivity exhibited by the Pc films should provide some interesting EL properties. These are described in § 7.4.2.

In view of the above discussion, it is somewhat surprising that the C^{-2} -V characteristics of the Pc MIS diodes were very similar to those

observed in fatty acid diodes. These characteristics, for a range of Pc film thickness, are shown in fig. 7.22. Curves (a) to (e) correspond to diodes incorporating 0, 1, 5, 10 and 30 layers respectively. As in the case of the fatty acid diodes, the general trend evident in this figure is an increase in both the slope and the intercept of the curve with film thickness. This suggests that the metal and semiconductor are capacitively coupled in the same manner in both cases (at least in the absence of illumination) and with regard to the capacitance measurements, the film acts as an insulator.

7.4.2 EL Measurements

Under the application of a forward bias ($V \gtrsim 2.4V$), all of the diodes emitted yellow/green EL from beneath the gold top electrode. The spectrum of the emission was identical to that shown in fig. 7.11 for the $CdSt_2$ - based devices. No additional features were detected as a result of incorporating phthalocyanine LB films. Fig. 7.23 shows a graph of the dc power conversion efficiency against the number of layers of Pc. The measurements were made using a drive current density of approximately 7 A/cm^2. There are a number of important features in this graph : Although the general shape of the optimum curve is very similar to that achieved with the other LB films, the insulator thicknesses involved are somewhat different. In particular, the optimum ($\sim$ 5.6 nm) is much less than that measured in the case of the fatty acid devices and, in fact, is close to the value which would be expected from conventional tunnel injection theory. It corresponds closely to the value of $\sim$ 4.0 nm measured by Card and Smith [28] for GaP devices incorporating SiO_2 as the insulator. It is interesting to note that an increase of only $\sim$ 100% is achieved in increasing the insulator thickness from one layer to the optimum number of seven. This is much less than the corresponding increase (of almost two orders of magnitude)

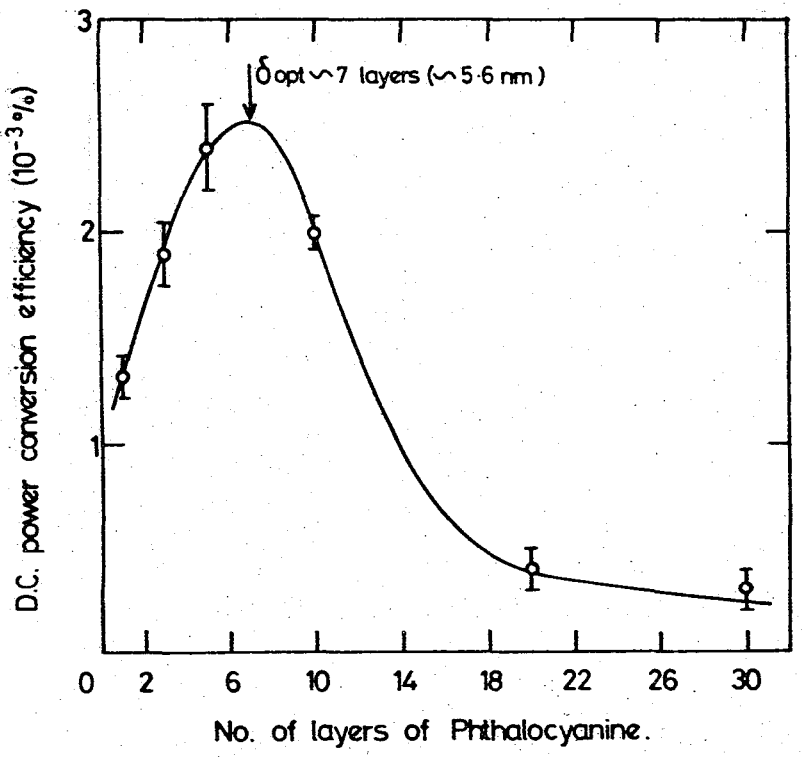

Figure 7.23 D.C. power conversion efficiency against the number of layers of Pc.

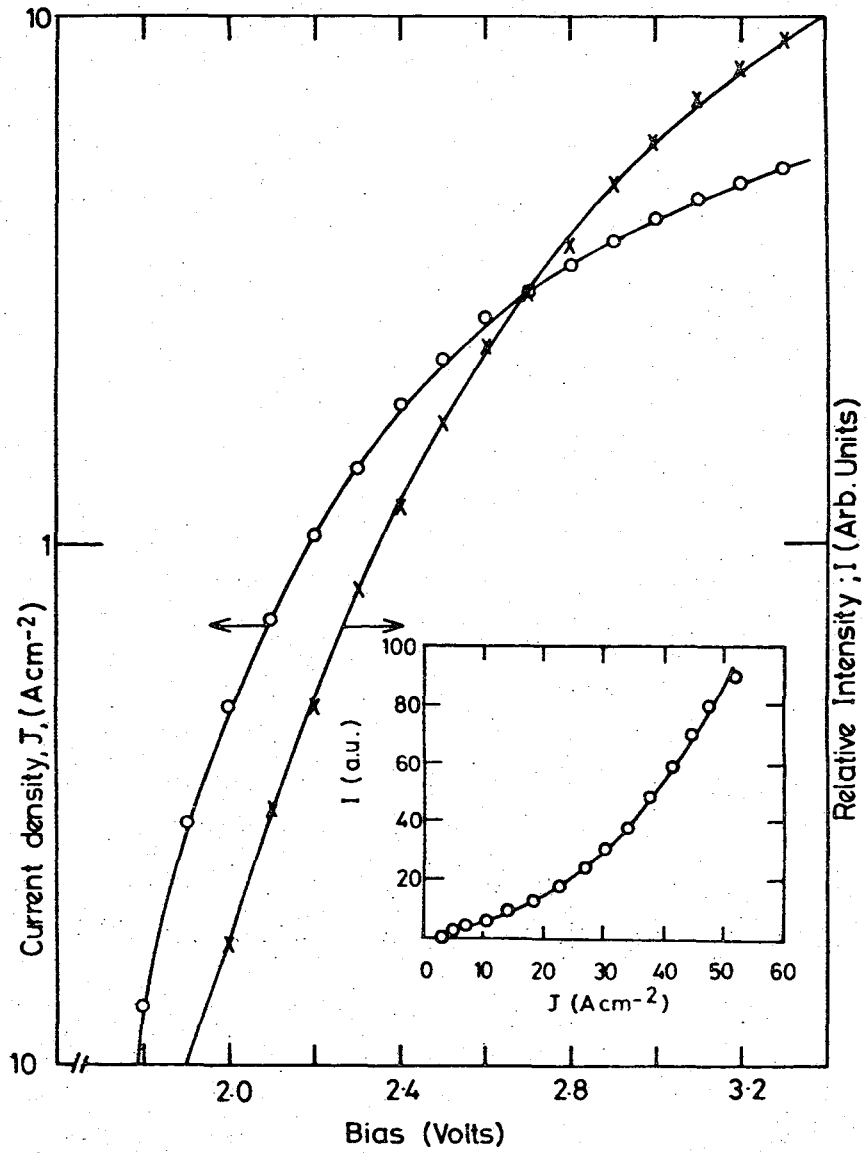

Figure 7.24 Current density and relative EL intensity against bias for a device incorporating 5 layers of Pc. (Inset shows intensity as a function of J).

in the fatty acid diodes (although the maximum measured efficiencies are similar). It is clear that the mechanism by which the EL is excited is very different in the two cases. Again, however, without a detailed knowledge of the Pc LB film properties it is difficult to draw any conclusions about the actual mechanism. There are essentially two possibilities : Either the film acts as a conventional insulator and the tunnel - injection theory is applicable, or the film acts as a p-type semiconductor and the diode is essentially a p-n junction. In view of the clear dependence of the efficiency on the Pc film thickness, the former of these possibilities is thought to be more likely, although the latter cannot be ruled out. Another piece of evidence which supports this view is the fact that the EL emitted from diodes fabricated with 20 or 30 layers was very uneven in appearance and originated from numerous regions of high electric field. This was due to electrical breakdown in the film and demonstrated that the current mechanism was different in those diodes where the film thickness was greater than approximately 8.0 nm (i.e. tunnelling dimensions). The maximum efficiency shown in fig. 7.23 is $\sim 2.4 \times 10^{-3}\%$. This was typical of that measured over a number of GaP substrates, although the maximum measured efficiency was $\sim 8.6 \times 10^{-3}\%$ and corresponded to a diode fabricated with 5 layers of Pc. These efficiencies will be discussed in more detail in § 7.4.3 when the commercial viability of the devices is considered.

Fig. 7.24 shows graphs of current density and relative EL intensity against bias for a device fabricated with 5 layers of Pc; the inset shows the relative intensity as a function of current density. These data also indicate that the mechanism present in the Pc diodes is rather different to that present in the fatty acid diodes, since in this latter case the variation of relative intensity with current is linear. In fact the super-linear characteristic shown in the inset to fig. 7.24 is consistent with the tunnel injection theory since it implies that an increase in bias

results in an increase in γ, which in turn suggests that total band realignment has not been achieved. It will be remembered that, according to this theory, the optimum shown in fig. 7.23 is the result of improved band realignment competing with an increased impediment to tunnelling minority carriers as the film thickness is increased.

Device Degradation

In view of the fact that Pc was used primarily because of its potential from a commercial viewpoint, the device degradation is clearly an important issue. Fig. 7.25 shows a graph of EL intensity as a function of time for a device fabricated with 10 layers of Pc and excited using a constant current density of $5A/cm^2$. There are a number of important features in this curve: After a small initial increase, the EL intensity decreased gradually with time over a period of several hours, as in the case of the fatty acid diodes. However, there is an important difference; in the Pc diodes the intensity approached, asymptotically, a certain intensity level I_o and even after several days of continuous operation, this intensity had remained at approximately this level. This is in marked contrast to the fatty acid-based diodes where the intensity diminished gradually to zero with time. Another important difference is the fact that the effect was, to a certain extent, reversible. The dotted trace in fig. 7.25 shows the variation for the same diode, after allowing $\sim$ 1 hour for the device to recover. It is clear from these measurements that the degradation is very different from that observed in the fatty acid diodes, although the actual mechanism remains unclear. It is certainly a function of the phthalocyanine layer since the degradation is accompanied by a significant increase in the conductivity of the film. This can be seen from fig. 7.26 which shows the J-V characteristic of a device incorporating five layers of Pc (a) before and (b) after 46 hours continuous operation. For a given bias, a significant increase in the conductivity of the film is evident. In fact, although the intensity of

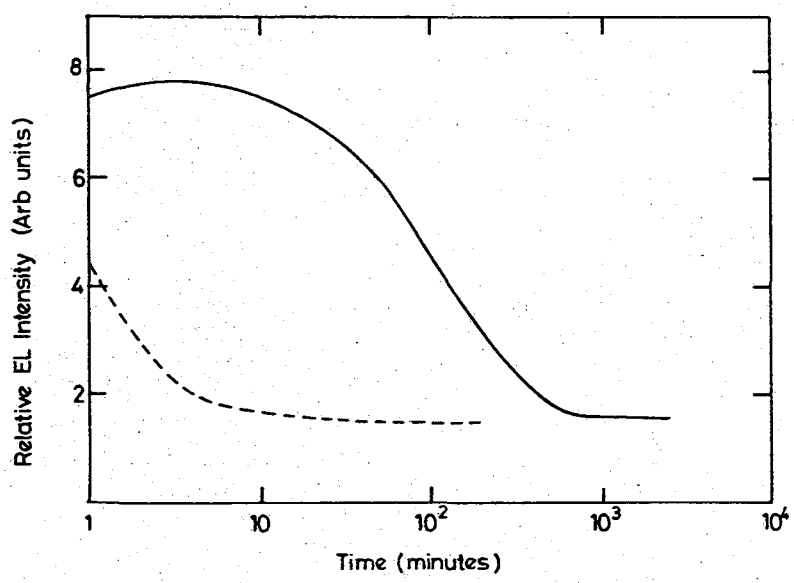

Figure 7.25 Relative EL intensity as a function of time for a device fabricated with 10 layers of Pc.

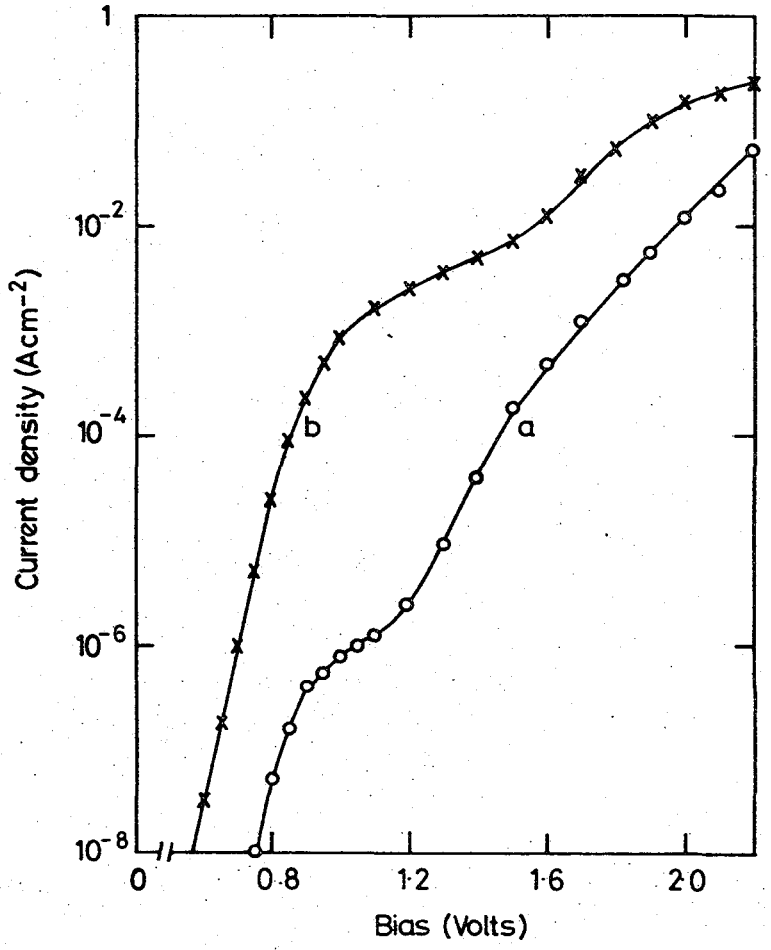

Figure 7.26 Conductivity data for a device incorporating 5 layers of Pc (a) before, and (b) after, 46 hours of continuous operation.

the EL has decreased considerably in going from (a) to (b), the actual conversion efficiency has not been so greatly reduced: A decrease from 3×10^{-3}% to 9.5×10^{-4}% was noted in this case over the time period of $\sim$ 46 hours. The fact that the degradation effect is, to a certain extent, reversible may indicate that a charge trapping effect is responsible for the increased conductivity, alternatively it may be an effect due to the heating of the sample resulting from the passage of a relatively large current. One piece of experimental evidence which appears to confirm this latter interpretation was that a low temperature anneal ($\sim 100^{o}$C for $\sim$ 3 hours) appeared to remove the reversible property of the degradation and the intensity remained at the value I_o. In addition to these effects, the conductivity of the Pc films is known to change in response to certain gases[26] and hence ambient conditions may be an important factor. There is clearly much to be gained by a program of research aimed at elucidating the mechanisms responsible for both the operation and degradation of Pc-based LEDs.

7.4.3 Assessment of Future Prospects

Before proceeding to discuss the prospects for commercial viability, it is useful to consider the device efficiencies that have been achieved. The maximum power conversion efficiency measured in this work corresponded to diodes fabricated with 5 layers of phthalocyanine. This value, of 8.6×10^{-3}%, compares very favourably with the efficiencies measured by other workers for MIS devices on GaP[28][29]. However, it is difficult to draw meaningful comparisons between figures quoted in the literature since many factors affect the measured efficiency. For example, some measurements will have been made in an integrating sphere so that most of the generated light is detected, whereas some efficiencies are calculated simply from that fraction of light which is incident on a photodetector.

In some instances, the latter method is used and an integrating calculation is performed to account for the light which is not detected. Furthermore, the device can be arranged so that the light is emitted either predominantly through the top electrode or the semiconductor substrate. A much more effective assessment can be made by directly comparing the performance of the devices with those commercially available, or better still, unencapsulated p-n junction diodes made from similar materials. Both of these comparisons were made in this work simply by replacing the research diode with the commercial ones in the measuring equipment and calculating their efficiencies. The commercially available, encapsulated diodes had a measured power conversion efficiency of $\sim$ 0.3%. This is quite high considering that the GaP material has a luminescence efficiency of only $\sim$ 1% and is well over an order of magnitude better than that measured in the best Pc-based diode. However, it must be remembered that the encapsulant is designed not only to increase the light extraction efficiency but also to directionalize the light output. In fact the viewing angle of such diodes is quite small (30^{o}) which indicates that most of the light is emitted normally in the forward direction, in contrast to the research diodes where much of the light may be trapped or emitted in directions away from the detector. The comparison is therefore unfair and a more reasonable one is achieved using the unencapsulated diodes. Such devices, operated at drive current densities of between 6 and 25 A cm^{-2} were found to have measured efficiencies in the range 5.5×10^{-3}% to 1×10^{-2}%. It is remarkable that the MIS diodes should be, on average, about half as efficient as p-n junction devices made from similar material, and implies that the minority carrier injection ratio achieved in the MIS devices approaches that of the p-n junction. These preliminary, comparative experiments are extremely encouraging, but further measurements, such as comparisons with a wider range of unencapsulated devices and with

encapsulated Pc-based diodes are required to confirm them. However, if the implications of these preliminary comparisons are correct, then the prospects for the MIS diodes are very promising. If the same level of injection in the GaP diodes can be achieved in II-VI based diodes, then very efficient LEDs should be possible.

However, producing devices with a promising initial efficiency is a long way from producing a commercially viable device. The next important consideration is the device lifetime. The preliminary results for the Pc-based diodes are encouraging and a program of research in this area would certainly prove useful.

In the following chapter, the results of preliminary experiments aimed at extending the system to incorporate zinc selenide as the luminescent material will be discussed.

7.5 SUMMARY

In summarizing the results presented in this chapter, it can be said that the Au : LB film : (n) GaP system exhibits some very interesting electrical and optical characteristics. The following conclusions can be drawn:

(a) The introduction of a fatty acid monolayer into the Au : (n) GaP Schottky barrier structure results in an increase in the height of the barrier presented to majority carriers from 1.39eV to 1.64eV. The addition of subsequent layers has relatively little effect on the height of this barrier.

(b) Capacitance measurements show that this is not due to an increase in the actual diffusion potential and a model is presented which is argued to explain most of the available experimental data. This model is based on the explanation that the barrier probed in both the J-V and photoelectric techniques is the metal - insulator barrier rather than that presented by the semiconductor depletion region.

(c) The introduction of the LB film also enables EL to be emitted when the devices are operated under forward bias. The spectrum of this EL indicates that enhanced minority carrier injection is the mechanism responsible for the excitation of EL.

(d) In contrast to the increase in barrier height, the efficiency of the MIS LEDs is acutely dependent on the insulator thickness. The optimum thickness is $\sim$ 27 nm for diodes fabricated with either ω-TA or $CdSt_2$. The maximum efficiency was measured to be $\sim 6 \times 10^{-3}$% for a device incorporating nine monolayers (27 nm) of ω-TA.

(e) Measurements made on the devices under illumination are shown both to support the proposed model and to reveal the presence of a current path through the insulator for minority carriers. This explains the fact that, for insulator thicknesses well in excess of tunnelling dimensions, minority carrier enhancement is still achieved.

(f) The EL measurements are explained using a modified version of the conventional tunnel injection theory. The exact mechanism by which the minority carriers traverse the insulator remains uncertain although it may be conduction via defect levels conveniently situated in the insulator bandgap.

(g) Devices incorporating Pc films behave very differently. It is difficult to draw conclusions about the operation of such devices due to a lack of information on the properties of Pc LB films. Nevertheless, the optimum insulator thickness for EL efficiency ($\sim$ 5.6 nm) suggests that the diodes may conform to the conventional tunnel injection theory, although the possibility of the Pc exhibiting p-type conductivity, and hence forming a p-n junction on the GaP, cannot be ruled out. The maximum efficiency measured was $\sim 8.6 \times 10^{-3}$%.

(h) Comparisons between the Pc-based devices and the performance of p-n junction LEDs fabricated from similar material indicates that, subject to an in-depth study of the device degradation properties, the Pc MIS

structure may prove to be attractive from a commercial viewpoint. This is particularly true if the system can be successfully extended to incorporate a II-VI material as the luminescent material since the minority carrier injection ratio achieved in these devices appears to be comparable with that achieved in a p-n junction.

CHAPTER 8

PRELIMINARY STUDIES OF LB FILM DEVICE STRUCTURES ON OTHER SEMICONDUCTORS

8.1 INTRODUCTION

This chapter presents the experimental results of investigations into a number of potential applications for LB film materials in MIS structures. The first section represents the culmination of the MIS LED work, in that it describes the results of an attempt to extend the research to incorporate ZnSe as the luminescent material. This semiconductor is one of the important materials for blue electroluminescent devices; it has a wide, direct bandgap ($\sim$ 2.72 eV) and is a very efficient phosphor. However, it is difficult to prepare in p-type form due to the phenomenon of self-compensation[1] and consequently p-n junctions cannot easily be formed. It is therefore an ideal material with which to extend the GaP-based MIS system which was discussed in the previous chapter.

Also presented in this chapter are the results of preliminary investigations into two other potential applications of LB films in MIS structures. The first of these concerns an attempt to benefit from the low temperature deposition features of the LB techniuqe in varying the GaAs : LB film interface properties, with a view to inverting the surface of p-type GaAs material. This is an essential prerequisite for the production of an n-channel field effect transistor based on GaAs. The final section describes the results of incorporating novel LB films in double dielectric structures, in particular the metal : LB film : SiO_2 : Si system. Both phthalocyanine and anthracene LB films are used to achieve very different effects which give rise to a range of possible applications.

The introductions given to these latter topics are necessarily brief and therefore rather superficial. However, in both instances a number of recent references are quoted which will enable the interested reader to obtain an up-to-date appraisal of the subject.

8.2 ZnSe : LB FILM MIS EL DEVICES

Zinc selenide, like most II-VI semiconductors is a difficult material to grow, particularly in low resistivity, large area, single crystal form, which is the ideal for a study such as this. However, recent advances in crystal growth techniques have enabled single crystal ZnSe films to be grown epitaxially onto GaAs substrates using techniques such as molecular beam epitaxy (MBE) and organometallic CVD, The material used in this work was grown by the organometallic CVD technique and has been described in chapter 5.

Two sample geometries were used, A surface arrangement was employed when the GaAs substrate was semi-insulating and a sandwich structure in the case of conducting GaAs substrates.

8.2.1 Electrical Characterisation

(a) Surface Geometry Structures. Figure 8.1 shows the current density-voltage curves for (a) a gold-ZnSe (carrier concentration $\simeq 10^{17}$ cm^{-3}) Schottky barrier structure and (b) an MIS device incorporating one monolayer of $CdSt_2$; also shown are the device barrier heights (measured using the photoelectric technique). Consider first the Schottky barrier curve. This is clearly non-ideal; the poor ideality factor indicates the presence of a significant interfacial layer and there is also a large series resistance associated with the thin ($\sim$ 3μm) ZnSe layer. The value of this resistance ($\sim$1KΩ), agrees well with that expected from the resistivity of the material. The effect of incorporating one monolayer into the device is to cause a significant drop in the value of the forward current at a given bias and also to increase the ideality factor, This increase in n is contrary to the effect observed in the near-ideal GaP diodes where the n-value remained close to unity. However, incorporating an LB film into the non-ideal GaP Schottky barrier structure (i.e, that including a significant native 'oxide').

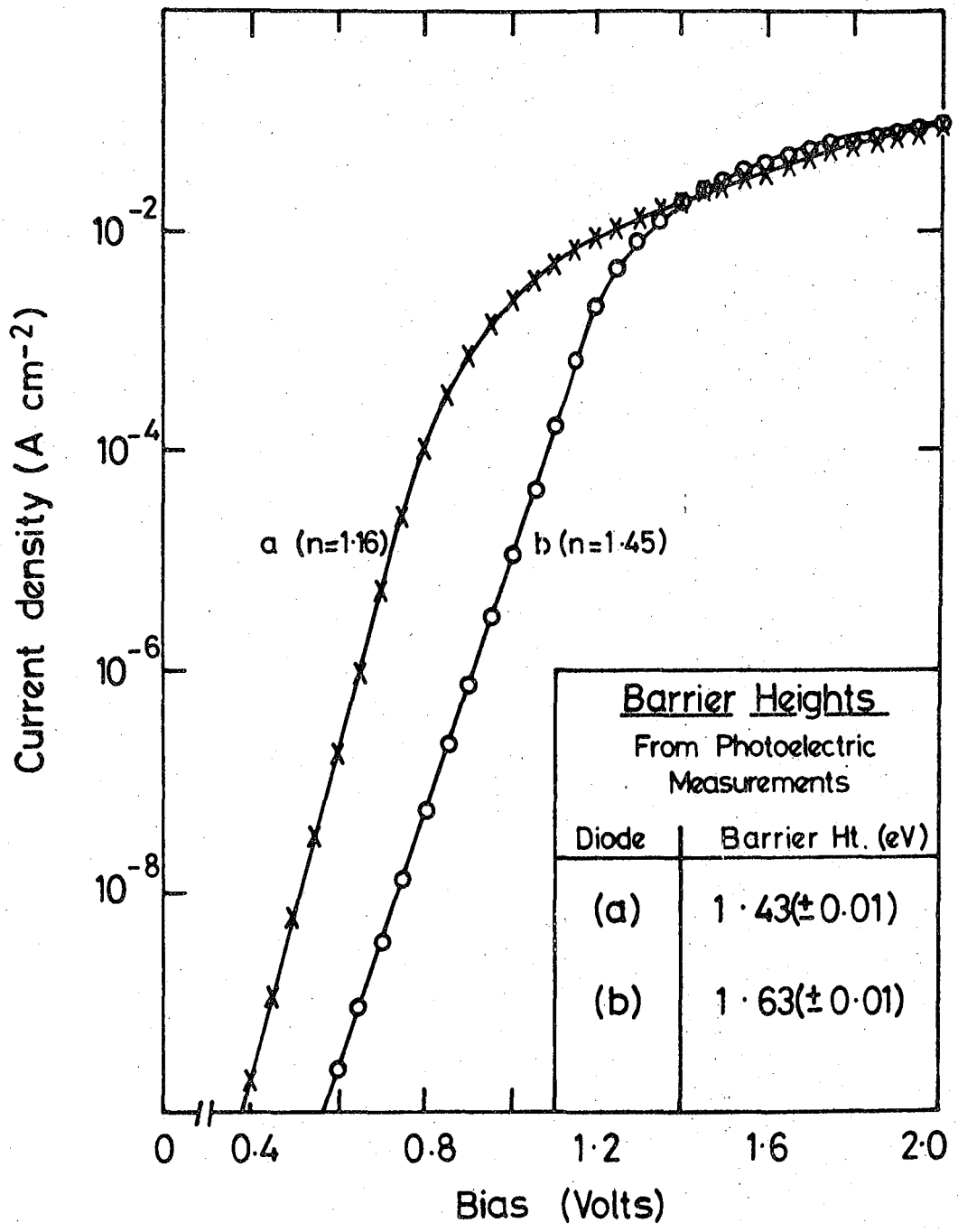

Figure 8.1 Conductivity data for (a) an Au:ZnSe (surface geometry) Schottky barrier and (b) an MIS diode incorporating one monolayer of $CdSt_2$. (The inset shows the corresponding barrier heights.)

also has the effect of causing a drop in the forward current and an increase in the ideality factor. This, together with the similarities in the measured barrier heights in the two different systems, suggest they may, in fact, be very similar. If this is the case, then it may be possible to emulate the success achieved with GaP LEDs using ZnSe as the semiconductor. Unfortunately, the series resistance associated with these diodes prevented the EL properties from being properly investigated since a bias of several tens of volts was required to produce a current of $\sim$ 1 A cm^{-2}, at which level the power dissipation in the diode was too great. Attempts to pulse-drive the devices were equally unsuccessful.

(b) Sandwich Geometry Structures. In an attempt to eliminate the large series resistance assoicated with the thin film of ZnSe, a sandwich geometry was employed. Highly conducting GaAs substrates were used and an Ohmic contact was made to this material. Unfortunately, the J-V characteristics of these diodes were initially even less ideal than those achieved with the surface geometry. Figure 8.2(a) shows a typical characteristic. In this case the curve exhibits a barrier limited regime at low bias (region (i)), but the current is severely limited at a relatively low value by an alternative mechanism (region (ii)). This latter region of the characteristic can be described by the approximate relationship $J \simeq Jri \exp(qV/nkT)$, where in this case $n \sim 8$. The mechanism responsible is thought to be recombination at the ZnSe : GaAs interface, possibly via interface states. This view is supported by the fact that strong illumination largely eliminates the current limitation, presumably due to photoexcitation effects at this interface. The effect of light on the characteristic is clearly demonstrated in fig. 8.2(b) which shows J-V curves measured both in the dark and under illumination. It is clear from these data that a large current can be made to flow through the devices, provided the limitation at the interface is reduced (by illumination in this case).

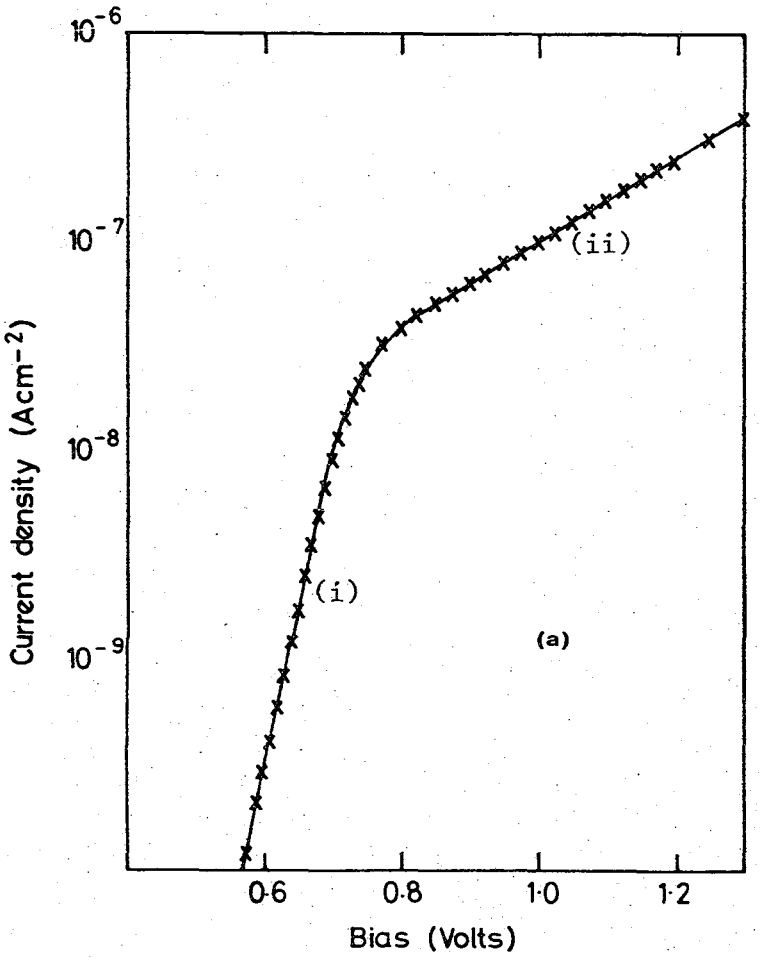

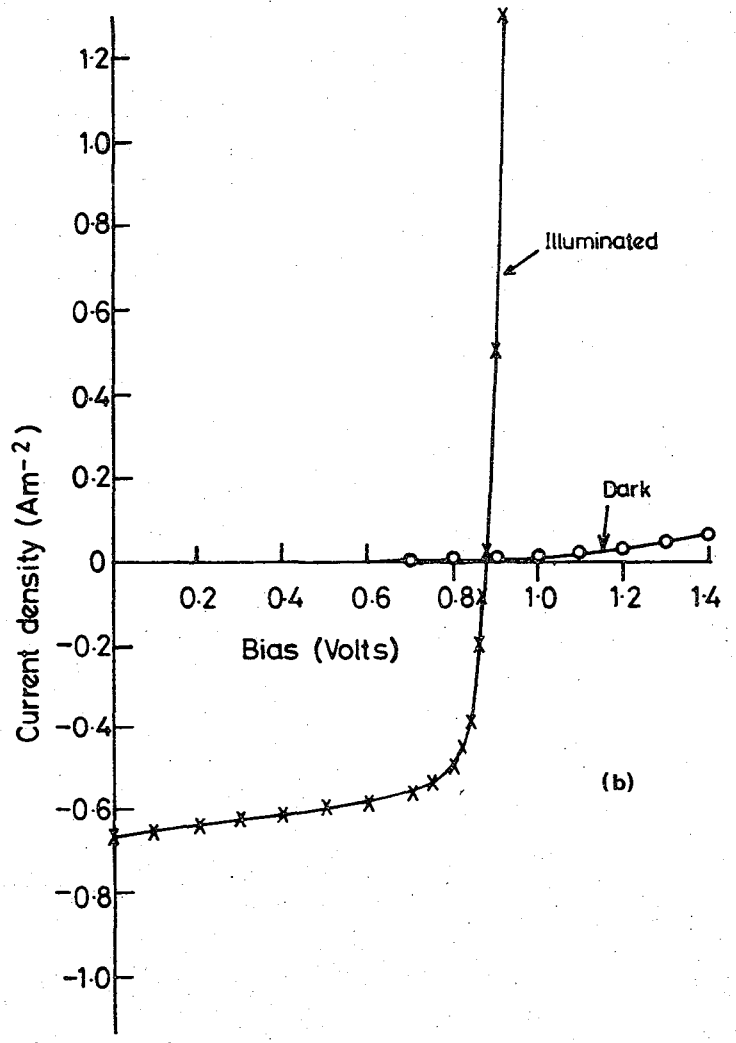

Figure 8.2 (a) Conductivity data for an Au:ZnSe (sandwich geometry) Schottky diode.

(b) Conductivity Data, both in the dark and under illumination for the same diode.

Fortunately, the situation could be improved quite considerably by annealing the substrate. However, annealing also had the effect of reducing the carrier concentration in the sample - an effect verified by monitoring the resistance between two surface ohmic contacts in-between the annealing stages. A reasonable compromise was found to be an anneal at approximately 275°C for twenty minutes. Two small samples were prepared in parallel. Schottky barrier structures were formed onto one, and MIS diodes incorporating five layers of Pc were fabricated on the other. The structures were found to be sufficiently conducting to enable a suitable current (from an EL viewpoint) to be carried for biases of approximately 20V.

8.2.2 EL Measurements

Under an applied voltage of ∿20V, corresponding to a drive current density of ∿ 5 A cm^{-2}, blue EL could be detected from the region of the gold electrode. The light, however, escaped from around the edges of the electrode rather than through it, which is indicative of the problems concerned with light extraction in the direct bandgap ZnSe material (see § 2.6.3). No EL could be detected from the Schottky barrier structures using the same measuring equipment and similar drive conditions.

The spectral response of the emitted light is shown in fig. 8.3. It consists of a single dominant mechanism corresponding to a photon energy of ∿ 2.64 eV. In this particular case there is no evidence of the deep centre luminescence which has been detected previously[2] in cathodoluminescence studies of similar material. The photon energy of the emitted light is very close to the bandgap energy (∿ 2.72 eV) and can be correlated, using previously reported cathodoluminescence spectra[2], with the recombination of free excitons.

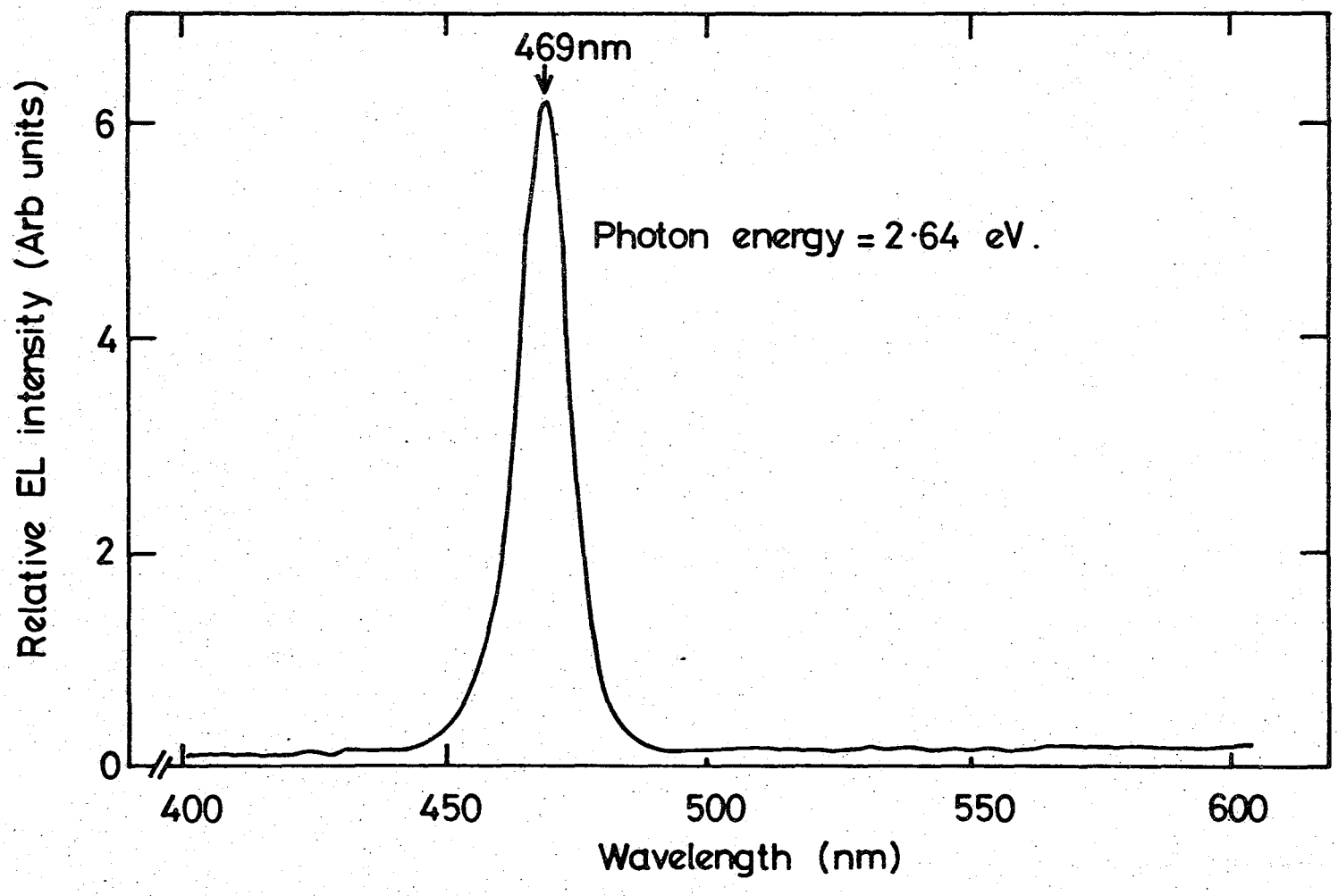

Figure 8.3 Spectral distribution of EL emission from an MIS (ZnSe) diode incorporating five layers of Pc.

The power conversion efficiency of the MIS diodes was very low ($\sim 1.2 \times 10^{-7}$); there are a number of possible explanations for this. For example, the light extraction efficiency is likely to be very low in the structures used here and the large voltage required to pass a suitable current reduces the measured power conversion efficiency. In addition, the high resistance associated with the ZnSe : GaAs interface is likely to support a substantial proportion of the applied voltage and complete band realignment at the Au : LB film : ZnSe interface may not be achieved.

Nevertheless, these preliminary results are very encouraging and there is clearly much research still to be done in this field. Some suggestions as to the direction of future research are made in the concluding chapter.

8.3 GaAs : LB FILM MIS STRUCTURES

In the early 1970s the increased demand for faster electronic devices revealed some of the fundamental limitations of the Si : SiO_2 system. The III-V compounds, such as InP and GaAs, were obvious materials with which to attempt to produce devices with superior performances to silicon-based ones. The combination of high mobilities and reasonably well-advanced growth technologies led to the assessment of these semiconductors as potential materials. Most of the early research concentrated on GaAs because of its better (at that time) prospects, although it is now recognised that InP has much more controllable interface properties and it is currently favoured as much as GaAs. (A 'state of the art' review of InP MIS technology can be found in ref. (3)). However, the research on GaAs remains intense and many believe that, if the shortcomings concerning the GaAs : insulator interface can be overcome, then this will prove to be the better material. A full account of the GaAs technology (up to 1981) can be found in the book by Croydon and Parker[4].

The motivation for this work on GaAs was the realization that the use of the (low temperature) LB technique to deposit a dielectric onto InP substrates[5] results in very different interface properties to those achieved using other, high temperature methods. Furthermore, these properties can be significantly altered by the pre-deposition surface preparation in the LB film devices[5], since this, and not the damage caused by the dielectric deposition, can determine the interface properties. In view of the (limited) success achieved using GaAs MIS devices incorporating native oxides[4], it was hoped that the GaAs interface properties would be controllable in the same manner as that achieved with InP.

A convenient method of examining the properties of an MIS structure is to study its admittance characteristics. Fig. 8.4 shows the variation of the measured capacitance and conductance of an Au : SiO_2 : (p) Si MOS structure. These experimental data show most of the features required for transistor action: Under a sufficiently large forward bias, a high concentration of majority carriers accumulate at the semiconductor surface, the device capacitance is approximately the geometric capacitance associated with the oxide, and the device is said to be 'in accumulation'(A). Altering the applied voltage towards reverse bias, gradually depletes the semiconductor surface of majority carriers (B) until eventually the surface begins to invert. Strong inversion (C) occurs when the depletion region becomes 'screened' by the minority carrier inversion layer and is thus prevented from extending further. The capacitance in the inversion region is determined by the ability of the minority carriers to follow the measuring signal and at very low frequencies the accumulation and inversion values should be equal. The conductance data exhibit a small peak (D) which can be attributed to losses due to interface states[6] and a larger peak, which is often observed in p-type material and results from lateral conduction in the surface inversion layer[7]. This lateral conduction also

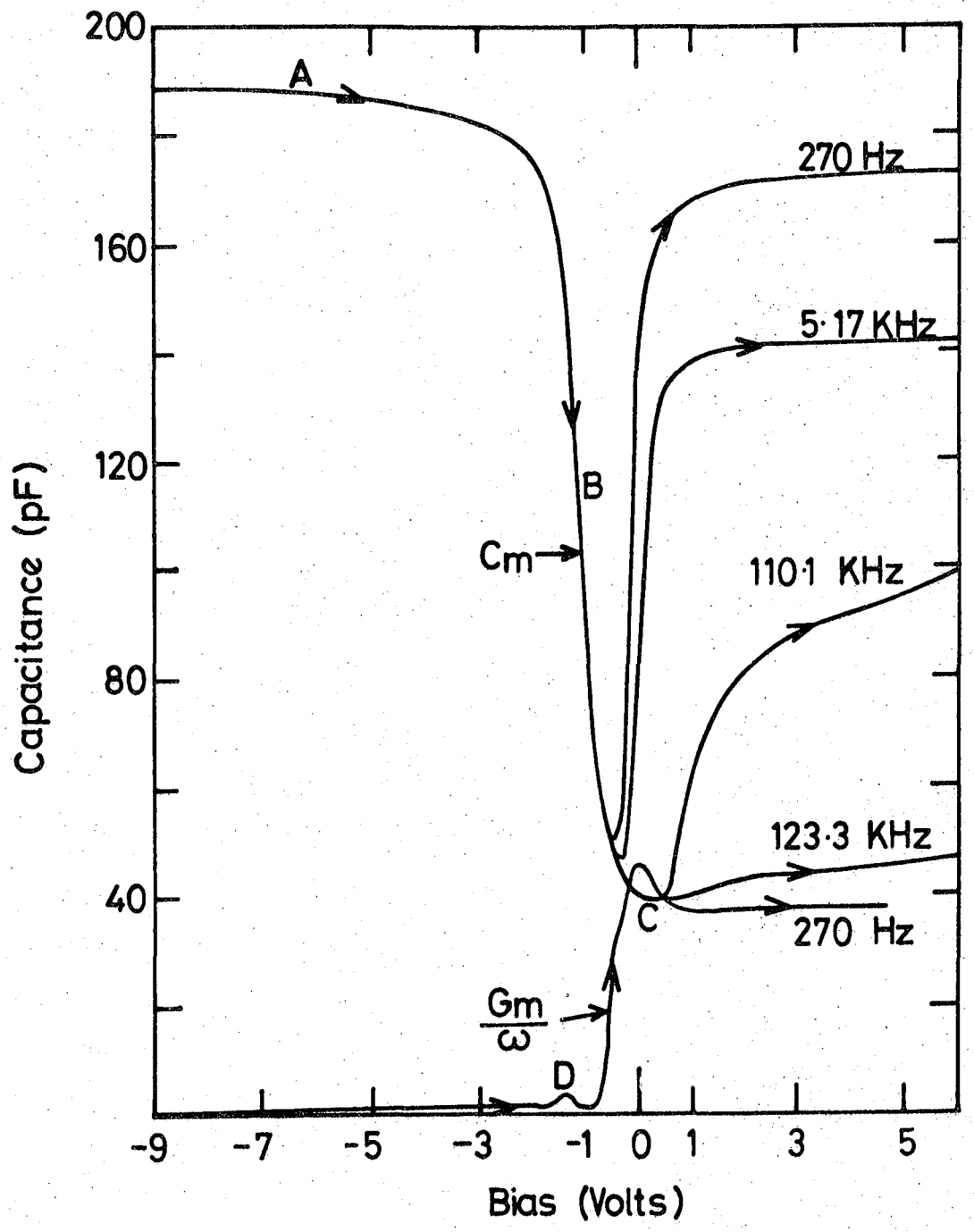

Figure 8.4 Admittance data at various frequencies for an Au:SiO_2 (p) Si MOS device.

explains the rise in the capacitance in inversion, even though the measuring frequency is relatively high[7]. From the viewpoint of this work, it is the inversion characteristics of the capacitance data that are important, since they give a first indication of the suitability of the material for producing inversion mode FETs.

In this study a wide range of surface preparations were used prior to LB film deposition and they were found to result in a range of different admittance characteristics. Only two will be described here as they demonstrate effectively the degree of variation that is possible. Two identical (p) GaAs samples were fabricated in parallel under identical conditions, except for the method used to prepare the surface prior to insulator deposition: Both samples were chemically polished with a 0.2% Br_2/CH_3OH mixture for two minutes and then refluxed for several hours in alcohol. (This treatment was believed, from previous experience, to result in an 'oxidised' surface.) However, immediately prior to film deposition, sample (b) was given an HF oxide-removal treatment which was expected to leave a relatively clean, oxide-free surface. Sample (a) was not otherwise treated. Diacetylene polymer was the LB material used as the dielectric and 31 layers (∿93 nm) were deposited onto each sample. The film was polymerized, by exposure to UV light, and then desiccated for ∿ 2 days before the Au electrodes were deposited. Figure 8.5(a) and (b) show the admittance data (at ∿ 5KHz) obtained from two contacts; one each from samples (a) and (b) respectively. There is clearly a large difference between the two sets of data. Both of the capacitance characteristics exhibit apparent accumulation (A) (although the accumulation capacitance is slightly less than the expected value of ∿ 200 pf), and depletion (B), and both of the conductance curves contain peaks (D) which can be attributed to interface states. In addition, both conductance characteristics exhibit a sharp increase in forward bias (E). This has been observed previously in LB film-based MIS devices (see, for

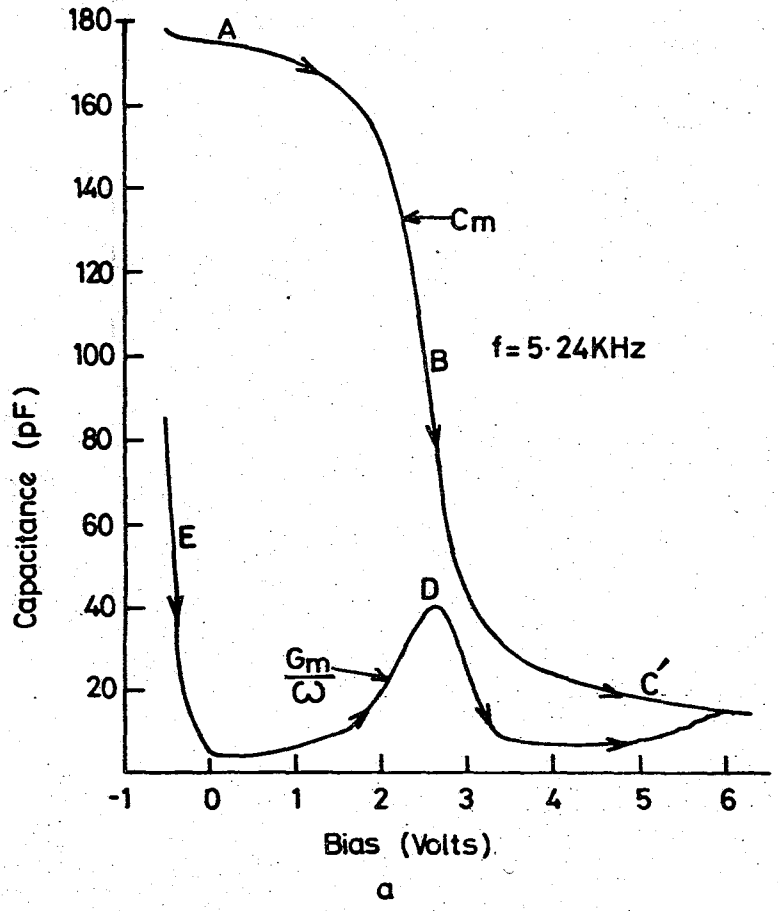

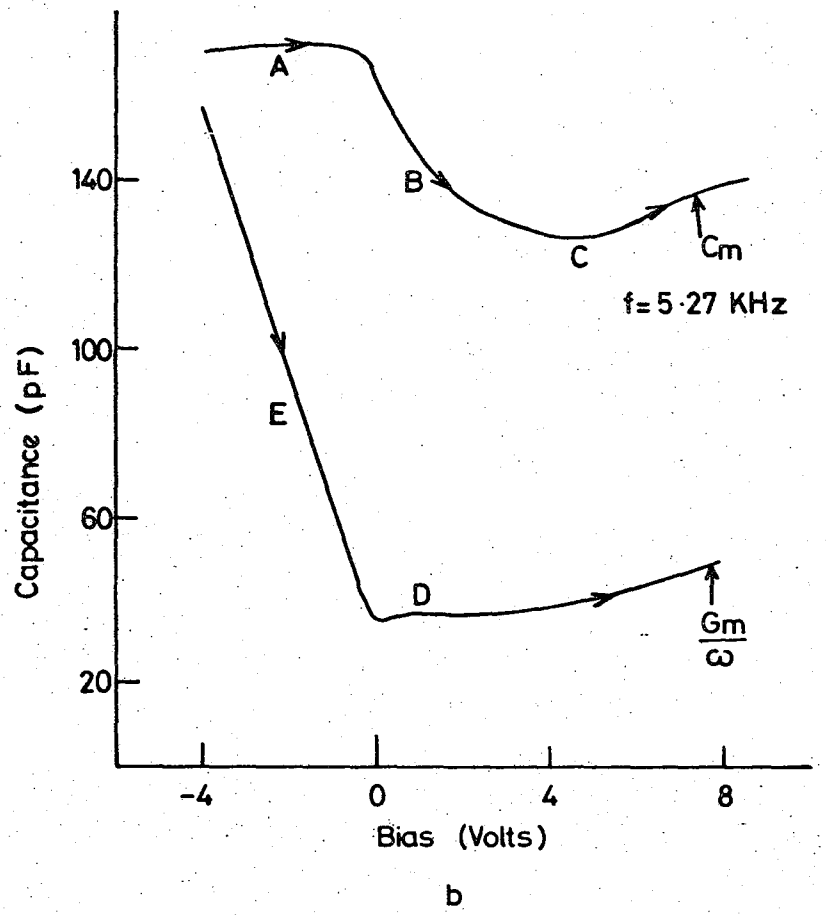

Figure 8.5 Admittance data for Au:LB film: (p) GaAs MIS structures fabricated using two different surface preparations. (Refer to text for a description.)

example, ref. (5)) and is interpreted to represent charge injection into the insulator. The major difference in the two sets of data is in the reverse bias regime. In sample (a) there is no evidence for an inversion layer and the capacitance characteristic exhibits 'deep depletion'. The semiconductor bulk is not screened from the metal and, hence, the depletion layer grows continuously with reverse bias ((c') in fig. 8.5 (a)). The capacitance characteristic in sample (b), however, is very different. The extent of the depletion part of the characteristic is much reduced, and in the region marked 'c' the capacitance levels off and then begins to increase again. One possible explanation for this is that inversion has been achieved and the increase is due to the response of minority carriers. However, it should be noted that additional data obtained from sample (b) were highly non-ideal. For example, a large amount of both hysteresis and frequency dispersion were observed, and the data shown in fig. 8.5 (b) cannot be considered as conclusive evidence that inversion has been achieved.

Nevertheless, the data presented demonstrate the large variation in the device characteristics that can be achieved by varying the pre-LB film deposition treatment, and are encouraging in this respect. Work is currently in progress to explore the effect of other surface preparations in detail, and to fabricate FET structures for lateral conductivity measurements, which should give an unambiguous indication of whether inversion is achieved.

8.4 DOUBLE DIELECTRIC STRUCTURES : LB FILMS ON SiO_2

Preliminary investigations of two potential applications for LB films on SiO_2 have been made. The first of these concerns the use of Pc LB films to improve the breakdown characteristics of metal : SiO_2 : Si MOS capacitors. The second investigation concerns the incorporation of anthracene LB films into the silicon MOS structure with a view to obtaining enhanced current injection into the SiO_2 at low voltages.

8.4.1 Improved Electrical Breakdown using Pc LB Films

Low voltage breakdown (i.e. electrical breakdown at applied electric fields which are less than the intrinsic breakdown strength) is a serious problem in the production of large area MOS capacitor structures. It is usually associated with structural defects, iregularities or pinholes at the SiO_2 : metal interface leading to a local enhancement of the electric field which initiates breakdown. The study of the breakdown mechanisms in insulators (particularly SiO_2) is currently a much studied topic (see for example, ref. (8) and the references contained therein), and numerous methods for controlling this breakdown have been employed. For example, electron traps in the oxide have been demonstrated to be effective[9]; such traps are filled by injected electrons, causing the build-up of a space charge which retards the growth of localized electric fields and prevents premature breakdown. More recently[10] it has been demonstrated that the presence of a silicon-rich SiO_2 layer on top of the SiO_2 region causes a similar reduction in the occurrence of low voltage breakdown and this too is believed to be due to the build up of a space charge in the Si rich SiO_2 layer which opposes the breakdown.

In this work LB films of Pc have been deposited onto Si : SiO_2 substrates in an attempt to similarly control the breakdown of the SiO_2 and also to benefit from the highly uniform nature of the LB film.

A large area p-type Si : (50 nm) SiO_2 sample was half coated with six layers of Pc, and gold top electrodes ($\sim$ 1 mm in diameter) were subsequently deposited. (It should be noted that the material used in this application was metal-free unsubstituted Pc[11] and the thickness of each deposited layer is belived to be $\sim$ 40 nm.) To test the device breakdown characteristics in this preliminary investigation, a voltage ramp ($\sim$ 0.5 V/sec) was applied to each device and the J-V characteristic was monitored directly on an X-Y chart recorder. Figure 8.6 shows four typical characteristics, two from

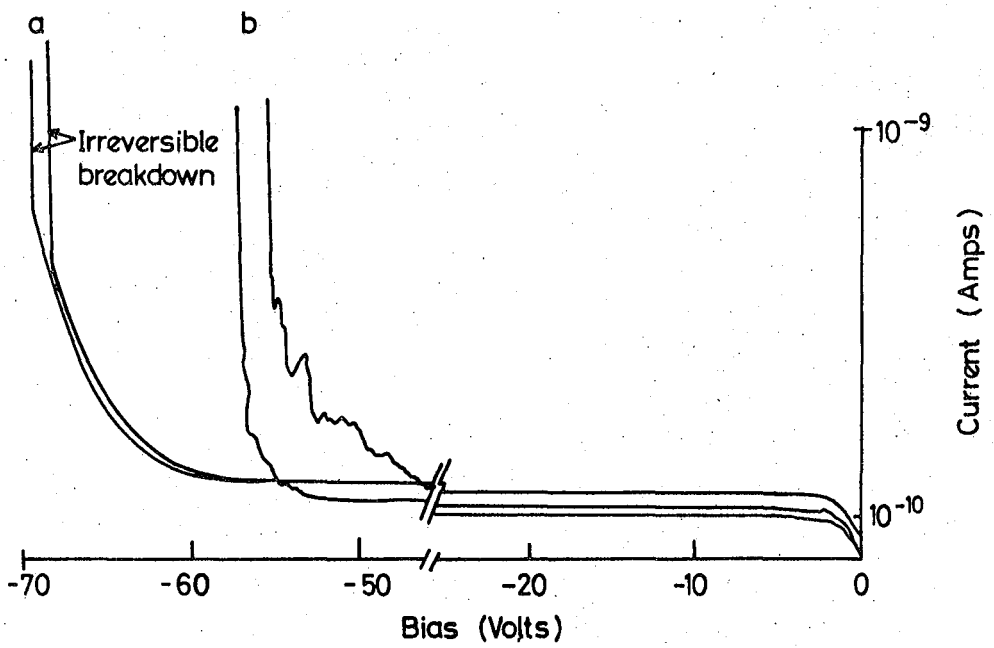

Figure 8.6 Ramped current-voltage characteristics corresponding to MIS devices (a) with, and (b) without, six layers of Pc.

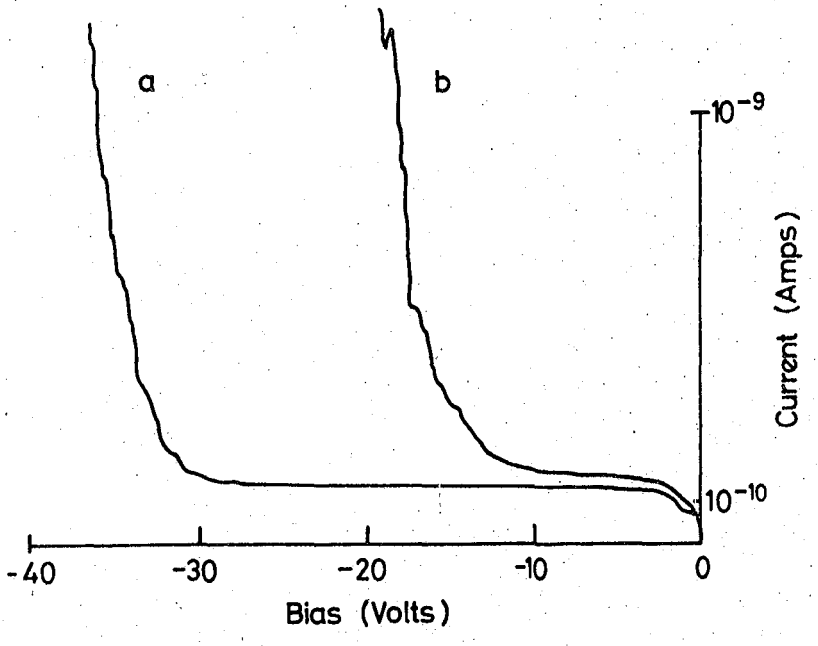

Figure 8.7 Ramped current-voltage characteristics corresponding to MIS devices (a) without, and (b) with, a Si-rich SiO_2 injector layer.

each region of the slice. Usually, in a study such as this, a large number of contacts from each region must be measured and statistical analyses performed. However, the effect of incorporating the Pc film is very pronounced and is aptly demonstrated by the four curves shown in fig. 8.6. The two curves marked (b) correspond to contacts on the uncoated region of the slice. At a voltage of about -55V (corresponding to an electric field of $\sim 1 \times 10^7$ V cm^{-2}) the current increases rapidly, probably due to intrinsic breakdown in the SiO_2. However the breakdown characteristic is very irregular and the additional, lower voltage features are interpreted in terms of localized breakdown in the SiO_2 at regions of high electric field (at defects etc.). However, in contrast, the contacts incorporating the Pc film exhibited a very smooth, controlled breakdown at approximately the same value of electric field ($\sim$ 10 MV/cm). The mechanism by which this effect is obtained is not yet clear. The Pc film evidently opposes the onset of premature breakdown mechanisms, and in view of the evidence for space charge effects in Pc LB films (which was mentioned in the previous chapter), it is possible that the mechanism is similar to that achieved using Si-rich SiO_2 layers[10]. In addition, the effect of the very uniform LB film in physically 'sealing off' pinholes and defects etc. in the SiO_2 may also be important. This latter effect has been used successfully to help study interface states by the electron spin resonance technique[12] where it is necessary to use very large area contacts in order to obtain a strong signal. Attempts to use the basic metal/thin-SiO_2/Si system were unsuccessful, due to the large leakage currents obtained. However, the incorporation of only a few monolayers (of ω-TA) into the structure reduced the leakage dramatically and enabled the technique to be used effectively. It should prove interesting to study the effects of incorporating LB films of the (much thinner) unsubstituted Pc material (see chapter 4) since it was shown in the previous chapter how just a single monolayer can have a pronounced effect on the conductivity characteristic of the Schottky barrier structure.

8.4.2 High Current injection into SiO_2 using Anthracence LB Films

There are a number of applications where the injection of current into silicon dioxide might be desirable. For example, the operation of the electrically alterable read only memory device (EAROM) depends, for its operation, on such an injection mechanism. However, SiO_2 has a large energy gap ($\sim$ 9eV) and therefore forms very large energy barriers with all metals and semiconductors. This makes current injection (by Fowler-Nordheim tunnelling, for example) very difficult to achieve and in conventional planar structures, many tens of volts are required for device operation. The problem is purely one of the injection of carriers into the SiO_2, since once this has been achieved, the electrons have a relatively high mobility ($\sim$ 30 cm^2/V-sec) in the SiO_2. There have been many recent reports concerning the enhancement of injection into the SiO_2; at low voltages; for example, very thin insulators[13] or asperities on polysilicon surfaces[14] have been used. Another technique which has been reported recently[10] is the use of Si-rich SiO_2, deposited on top of the normal SiO_2 layer. This material is composed of two distinct phases with regions of amorphous silicon dispersed in a (mainly SiO_2) oxide matrix. High temperature annealing causes small crystalline 'islands' of silicon to form, typically $\lesssim$ 10 nm in diameter. The conductivity of this material increases rapidly with the applied field and at moderate fields it is much more conducting then normal SiO_2. Enhanced electron injection into SiO_2 is believed to be achieved[10] by a local enhancement of the electric field at the Si-rich SiO_2: SiO_2 crystallites. Fowler-Nordheim tunnelling has been established as the mechanism by which the electrons are injected[15]. Various applications of this phenomenon have been demonstrated: For example, it has been used to produce a non-volatile memory device[10] capable of being 'written' with low voltages (as low as -13V) in the space of a few milliseconds. Also the 'ramped' current-voltage characteristics

of this injector device have been used to study trapping centres in SiO_2 layers[15].

The anthracene material used in this investigation, although not described fully in previous chapters, is a well-characterised LB film material[16, 17]. The molecule is essentially an anthrance moiety, onto which two short aliphatic side chains have been substituted[17]. One of these provides the hydrophobic end to the molecule ($C_n H_{n+1}$) and the other, consisting of an acid (C_2H_4COOH) grouping, provides the hydrophilic end. It has been shown[16] that, in LB film form, the molecules are almost certainly arranged as layers of tilted anthracene nuclei, which are separated by alternating layers of interleaving aliphatic chains and polar end groups.

In view of the similarity between the physical model of the Si-rich SiO_2 material and the microscopic model of the anthracene LB film (an alternating array of conducting and insulating regions), an attempt has been made to emulate the work described above by replacing the Si-rich SiO_2 with an anthracene LB film.

The sample used to obtain the results which will be presented in this seciton, was a p-type Si substrate, covered with $\sim$ 50 nm of SiO_2, and subsequently coated with 6 monolayers of C4 anthracene (molecular length $\sim$ 1.22 nm[16]). The top electrode was gold ($\sim$ 15 nm thick, $\sim$ 1 nm in diameter). To perform this preliminary investigation, numerous contacts from both regions of the sample were studied; each one was ramped with an increasing negative voltage (-0.5 V/sec) and the current was monitored as a function of applied bias on an X-Y chart recorder. Control samples (identical to those described above, but incorporating 20 nm of Si-rich SiO_2 instead of the anthracene, and with Al top electrodes instead of Au) were also studied.

Figure 8.7 shows the current voltage characteristic of two contacts from these control samples; (a) corresponds to the conventional Al:SiO_2:Si sample and at a bias of $\sim$ -35V, the current increases rapidly. This is thought to represent charge injection into the SiO_2, by Fowler-Norheim tunnelling from the Al electrode, rather than intrinsic electrical breakdown. The incorporation of the Si-rich layer (b) produces a marked decrease in the voltage (and hence the average electric field) which is required to initiate injection. The voltage required for this particular contact was relatively low, $\sim$ -17v, which is in accordance with previous reports for similar structures[15].

The results from the anthracene-coated sample are shown in fig. 8.8. The four curves marked '(a)' are typical characteristics corresponding to contacts on the uncoated region, whereas those marked '(b)' are typical characteristics from the coated region of the slice. In this case, the increase in current observed in the curves marked '(a)' is most likely to result from breakdown (the average electric field is of the order of 10 MV/cm). The difference between these characteristics and the corresponding curve in fig. 8.7 is merely a consequence of the high work function of the gold top electrode and is not relevant to this study. However, the devices incorporating the anthracene LB film exhibited injection characteristics at very low values of applied voltage ($\lesssim$ 5V in most cases). The inset to fig. 8.8 shows the characteristic of a typical contact over a much larger current range and demonstrates that high current injection can be achieved in these devices without catastrophic failure. The origin of the injection mechanism remains unresolved; the data shown in the inset to fig. 8,8 do not conform to any obvious power law. However, if the operation is analogous to that observed in the Si-rich SiO_2 work (as it was hoped) then it is possible to envisage an ordered array of injection sites (anthracene nuclei)

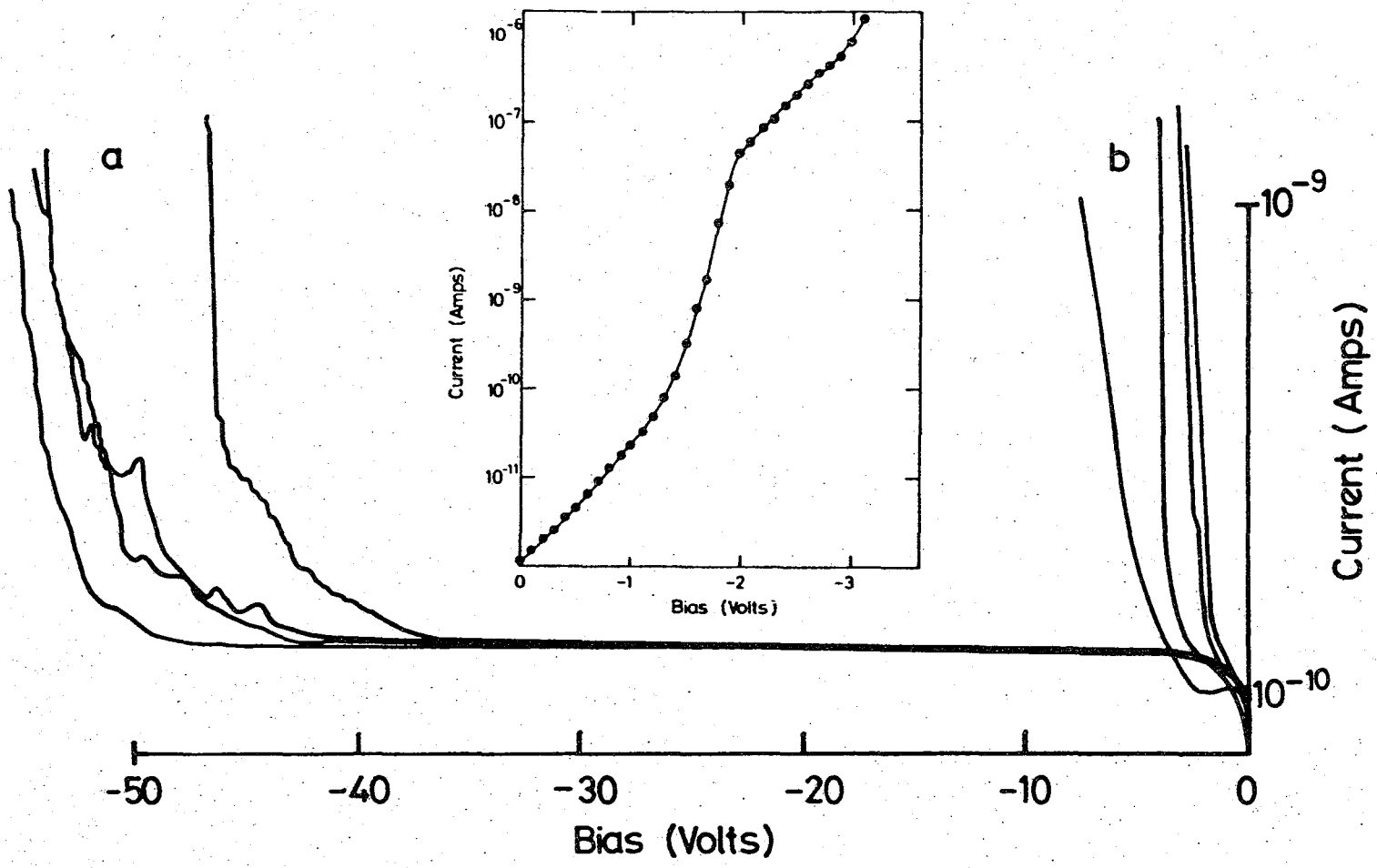

Figure 8.8 Ramped current-voltage characteristics corresponding to MIS devices (a) without, and (b) with, six layers of anthracene. (The inset shows the current voltage-characteristic of a typical contact over a large current range)

in very close proximity to the SiO_2 interface. This could explain the very low voltage required for injection.

These preliminary data are very encouraging; high current injection into SiO_2 has been achieved at very low values of applied voltage ($\lesssim$ 5V), and, hence, the potential for applications in the area of low voltage programmable memories has been demonstrated.

CHAPTER 9

CONCLUSIONS AND SUGGESTIONS FOR FUTURE WORK

CONCLUSIONS

The aim of the research reported in this thesis was to investigate the feasibility of using insulating films, formed by the LB technique, as the dielectric in MIS light emitting diodes. A model system, based on well-characterised materials, was studied first and this was subsequently extended to incorporate more stable LB films and an efficient II-VI phosphor (ZnSe) as the luminescent material.

Gold : (n) GaP Schottky diodes, fabricated so as to minimise the extent of the interfacial layer, are shown to behave in a near-ideal fashion. The interfacial layer, which must inevitably be present, has little effect on the diode characteristics. Such diodes do not emit any detectable EL. The introduction of a fatty-acid monolayer into the 'near-ideal' structure produces a substantial change in the height of the effective barrier presented to majority carriers and also enables EL to be detected. The addition of subsequent monolayers has relatively little effect on the effective barrier height but causes a further increase in the EL efficiency. This increase is due to an enhancement of the minority carrier injection ratio , γ. An optimum thickness for EL efficiency exists which is $\sim$ 27 nm in the case of diodes incorporating either ω-TA or $CdSt_2$ as the insulator. This value is much greater than that predicted on the basis of direct quantum mechanical tunnelling. Measurements made on the diodes under illumination reveal the presence of a current path across the insulator for minority carriers, even in relatively thick ($\gtrsim$ 20 nm) insulators and this can explain the relatively large, optimum thickness for EL. The essential principles of the minority carrier tunnel injection theory are used to explain the EL results although the carriers traverse the insulator by processes other than quantum mechanical tunnelling.

The increase in the effective barrier height, due to the incorporation of an LB film is shown not to result from an increase in the degree of band bending in the semiconductor, and a model is proposed which accounts for most of the experimental results.

Devices incorporating LB films of phthalocyanine (Pc) behave very differently to the fatty acid-based ones. In this case the optimum thickness for EL efficiency is $\sim$ 5.6 nm which suggests that the diodes conform to the tunnel injection theory, although the possibility of the Pc exhibiting p-type conductivity, and hence enabling enhanced hole injection into the GaP, cannot be ruled out. The maximum EL efficiency of these devices (measured to be $\sim 8.6 \times 10^{-3}$%) is about half of that measured in unencapsulated p-n junction devices fabricated from similar material. This implies that a high injection ratio has been achieved in the LB film MIS devices. Preliminary investigations into the reliability of the devices are encouraging although a more detailed investigation is required before an accurate assessment of the commercial viability can be made.

The system has been extended to incorporate ZnSe as the luminescent material. In this case the presence of a Pc LB film enables near-gap (blue) EL to be observed. Although the measured efficiency is low ($\sim 10^{-5}$%), these early results are very encouraging since the ZnSe substrates used to date are far from ideal. Significant improvements should be possible using more suitable semiconductor substrates. Indeed, if the injection ratios obtained in the GaP devices can be achieved using ZnSe, then a very efficient blue LED will be produced. If this is the case, then Pc-based MIS devices could well form the basis of a commercial device.

In addition to the LED work, a number of other potential applications for LB films in MIS structures are demonstrated in this research. For example, the incorporation of a Pc LB film into the Si : SiO_2 MOS structure is shown to improve the electrical breakdown characteristics of

the device. The incorporation of an anthracene LB film, on the other hand, is shown to enhance electron injection into the SiO_2 at low voltages which has potential applications in the field of semiconductor memory devices. Also, the influence of the sample surface preparation on the admittance characteristics of GaAs MIS structures incorporating thicker LB films is shown to be very pronounced. This gives a degree of control over the interface properties of the MIS device which may enable n-channel, inversion-mode FETs to be fabricated on p-type GaAs.

SUGGESTIONS FOR FUTURE WORK

A number of areas which would benefit from further study have been identified. Future work on LB film-based MIS LEDs should concentrate on the use of stable LB films such as phthalocyanine. There are essentially three areas where further research should prove fruitful. First, it is important to fully characterise the Pc : (n) GaP system, so that the mechanism of operation can be established. An in-depth study of the degradation mechanisms, which may require the encapsulation of some devices, would also be very useful and would enable the commercial viability of MIS LEDs, based on LB technology to be accurately assessed. Finally, the extension of the research to date on ZnSe-based diodes, perhaps using single crystal (bulk) material in the first instance, should prove interesting and, hopefully, rewarding.

Other areas where further study could prove rewarding include a detailed investigation into the effect of other surface preparations on the LB film : (p) GaAs interface and the fabrication of FET structures on such material so that lateral conductivity experiments can be used to give an unambiguous indication of whether or not inversion has been achieved. (A related application is the potential for fabricating very high speed Schottky gate FETs from ternary and quaternary alloys (e.g. the GaInAs system) where the

carrier mobilities can be very high (in excess of 10,000 $cm^2\ V^{-1}$ -sec.). The presence of an LB film between the gate and the semiconductor could increase the effective barrier height of the device, thereby reducing the reverse leakage current which is so detrimental in these devices.)

It should prove interesting to study the effect of very thin LB films, in particular films of the substituted Pc material, on the electrical breakdown characteristics of MOS structures. It may be possible to achieve results, similar to those described here, using ultra-thin LB films which would have potential applications in the field of low-loss or high-strength capacitors. The final area which would benefit from further research is the work on charge injection into SiO_2. The very low voltages required for injection which have been demonstrated in this work give rise to an important potential application in the fabrication of low voltage EAROM devices. In this study, the effect has merely been demonstrated and there is much to be gained from an investigation into the injection mechanism, and in attempting to benefit from the versatility of the LB technique.

APPENDIX A

THE QUASI FERMI LEVEL

In many instances, it is convenient to retain the concept of the Fermi level and to draw energy band diagrams even under non-equilibrium conditions. To do this one invokes the concept of quasi Fermi levels (one each for electrons and holes) which are defined as those quantities which, when substituted into the place of the Fermi level, give the concentration of each carrier under non-equilibrium conditions. Consequently, they are also defined by the expressions

$$n = N_c \exp (\phi_n - E_c)/kT = n_i \exp (\phi_n - E_i)/kT \qquad (A.1)$$

$$\text{and} \quad p = N_v \exp (E_v - \phi_p)/kT = n_i \exp (E_i - \phi_p)/kT \qquad (A.2)$$

where ϕ_p and ϕ_n represent the hole and electron quasi Fermi levels respectively and E_i is the position of the intrinsic Fermi level.

The general expression for current flow in a depletion region is given by eq. (3.15) as

$$J_n = q\, n\, \mu_n\, E + q\, D_n \left(\frac{dn}{dx}\right)$$

$$\text{or} \quad J_n = q\, \mu_n\, n \left(\frac{d\phi_n}{dx}\right) \qquad \left(\text{using } D_n = \frac{kT}{q}\, \mu_n\right) \qquad (A.3)$$

A similar relation holds for holes, i.e,

$$J_p = q\, \mu_p\, p \left(\frac{d\phi_p}{dx}\right) \qquad (A.4)$$

It is evident that the electron and hole current densities are proportional to the gradients of their respective quasi Fermi levels. Thus, this gradient can be considered as a 'driving force' for the respective current components.

In a forward biased p-n junction it is usually assumed that quasi equilibrium holds, i.e. that the product 'p x n' is constant throughout the depletion region (although it is greater than the equilibrium value of n_i^2). This has the important implication that both, ϕ_p and ϕ_n remain flat throughout the space charge region. Furthermore, if the applied voltage is assumed to be dropped predominantly across this region, then the separation of ϕ_n and ϕ_p is given by the applied voltage, V_f, i.e.

$$\phi_n - \phi_p \simeq qV_f \qquad (A.5)$$

A number of authors[1][2] have considered the behaviour of the quasi Fermi levels in Schottky diodes under various biasing conditions. Crowell and Beguwala[1] performed theoretical calculations to show that, at least in silicon Schottky diodes, the electron quasi Fermi level remains essentially flat throughout the depletion region. This indicates that the processes of drift and diffusion in the semiconductor are insignificant when compared with the emission process over the barrier and hence confirms the thermionic emission theory of current transport. Rhoderick[2] subsequently analysed published data for a range of different Schottky diodes and confirmed these theoretical predictions. Furthermore, he demonstrated[2] that the hole quasi Fermi level could also be considered as flat throughout the depletion region (under forward bias) as in a p-n junction.

The concept of the quasi Fermi level is very useful; it can be used both as a diagrammatical representation and as a mathematical formalism.

FIGURE CAPTIONS

Figure 2.1 Internal field emission in a reverse-biased Schottky diode

Figure 2.2 Energy band diagram of a p-n junction (a) in equilibrium and (b) under a small forward bias.

Figure 2.3 Radiative recombination processes (refer to text for description).

Figure 2.4 Simplified E-k diagrams, depicting recombination (a) in a direct bandgap material and (b) in an indirect bandgap material.

Figure 2.5 Schematic diagram of a p-n junction (a) in equilibrium, (b) under reverse bias and (c) under forward bias.

Figure 2.6 Simplified energy band diagrams depicting the formation of an ideal Schottky barrier (a) before, and (b) after, contact has been made.

Figure 2.7 Energy band diagram of Schottky diode (a) under forward bias and (b) under reverse bias.

Figure 2.8 Exaggerated, idealised band diagram of a thin-MIS diode (a) in equilibrium and (b) under forward bias.

Figure 2.9 Schematic diagrams depicting various structures used in large area display devices; (a) A.C. driven device, (b) D.C, driven 'composite' device and (c) D.C. driven powder device.

Figure 2.10 Cathodoluminescence spectra obtained from nitrogen-doped ($\sim 10^{18}$ cm^{-3}) GaP material. (after Wight et al[28]).

Figure 3.1 Depicting variation of (a) charge density, (b) electric field strength, and (c) electrostatic potential with distance for an ideal Schottky barrier.

Figure 3.2 Sequence of energy band diagrams depicting Schottky barrier formation in the presence of a high density of surface states. (NB. The interfacial layer has been omitted for simplicity.)

Figure 3.3 Energy band diagram of a Schottky barrier incorporating an interfacial layer of atomic dimensions (a) in equilibrium and (b) under the application of a forward bias.

Figure 3.4 Image force lowering in a Schottky barrier. The inset illustrates the effect on both the conduction and valence bands.

Figure 3.5 Schematic diagram depicting basic current transport processes in an MIS diode under forward bias.

Figure 3.6 Field and thermionic field emission in a degenerately doped Schottky barrier structure.

Figure 3.7 Energy band diagram of an MIS diode, (a) in equilibrium and (b) under forward bias showing the behaviour of the quasi-Fermi levels.

Figure 3.8 Variation of EL quantum efficiency with insulator thickness in ZnSe MIS diodes (after Livingstone et al[54]).

Figure 3.9 Minority carrier injection by two stage Auger recombination process (refer to text for explanation).

Figure 5.5 Deposition record for $CdSt_2$ onto ferricyanide-treated GaP (including two hour drying period between 1st and 2nd depositions).

Figure 5.6 Deposition record for $CdSt_2$ onto Br_2/CH_3OH-HF-treated GaP (including two hour drying period).

Figure 5.7 Photograph of a gold electrode on GaP exhibiting the 'crazed' appearance which is characteristic of thermal expansion problems.

Figure 5.8 Reciprocal capacitance as a function of the number of monolayers, N, for two different MIM samples.

Figure 5.9 Schematic diagram of the device geometry.

Figure 5.10 Photograph of the sample chamber used for both electrical and optical measurements.

Figure 6.1 Current density as a function of forward bias for typical diodes prepared using (a) the ferricyanide treatment and (b) the Br_2/CH_3OH - HF treatment. (The reverse current was undetectable for an applied bias of -10V).

Figure 6.2 Activation energy plot for a near-ideal Schottky diode prepared using the ferricyanide treatment.

Figure 6.3 Reciprocal capacitance squared against bias for the two diodes used to obtain the data shown in fig. 6.1.

Figure 6.4 (Photoresponse per incident photon)$^{\frac{1}{2}}$ versus photon energy ('Fowler plots') for the two diodes used to obtain the data shown in fig. 6.1.

Figure 6.5 Current density versus bias for a typical Schottky diode (type (b)), both in the dark and under approximate AM1 illumination conditions.

Figure 6.6 Showing dark J-V characteristic of a near-ideal Schottky diode (type (b)) and also the variation of $J_{s/c}$ against $V_{o/c}$ for the same diode.

Figure 6.7 The proposed band diagram for the near-ideal Au : (n) GaP Schottky diodes.

Figure 6.8 Current density-voltage data for a typical non-ideal diode (a). Also shown is a near-ideal characteristic (b). The inset shows the measured barrier heights. (The reverse current was undetectable for V = -10V).

Figure 6.9 Reciprocal capacitance squared against voltage curve for a typical non-ideal diode. Also shown is a near-ideal characteristic (b).

Figure 6.10 Variation of V_o with δ for non-ideal GaP Schottky diodes. (After Cowley[3]).

Figure 6.11 Spectral distribution of EL from a typical non-ideal Schottky diode.

Figure 6.12 Photograph showing the irregular nature of the EL emission from a non-ideal Schottky diode.

Figure 6.13 Three typical J-V characteristics for diodes fabricated using different techniques (refer to the text for a description). The corresponding barrier heights are listed in the inset.

Figure 6.14 Showing typical J-V characteristics for four different diodes (refer to the text for a description). The corresponding barrier heights are listed in the inset.

Figure 7.1 Current density versus forward bias for diodes incorporating a range of $CdSt_2$ insulator thicknesses; (a) no insulator (near-ideal curve), (b) one monolayer, (c) three monolayers and (d) five monolayers. (The reverse current was undetectable for V = -10V).

Figure 7.2 (a) Current density versus forward bias for a diode incorporating nine monolayers (22.5 nm) of $CdSt_2$.

(b) Current density versus $V^{\frac{1}{2}}$ for an MIM device incorporating five monolayers (12.5 nm) of $CdSt_2$.

Figure 7.3 Photoresponse data (Fowler plots) for the same four diodes used to obtain the data shown in fig. 7.1.

Figure 7.4 Conductivity data for diodes incorporating a range of (ω-TA) insulator thicknesses; (i) one monolayer, (ii) seven monolayers, (iii) nine monolayers, (iv) eleven monolayers.

Figure 7.5 Reciprocal capacitance squared against voltage for the same four diodes used to obtain the data shown in fig. 7.1.

Figure 7.6 Reciprocal capacitance against the number of monolayers for MIS diodes incorporating a wide range of insulator ($CdSt_2$) thicknesses.

Figure 7.7 Reciprocal capacitance squared against voltage for typical MIS diodes incorporating a range of insulator ($CdSt_2$) thicknesses.

Figure 7.8 Approximate energy level diagram proposed for the Au;fatty-acid LB film : (n) GaP system.

Figure 7.9 Activation energy plot for an MIS diode incorporating one monolayer of $CdSt_2$.

Figure 7.10 Photograph showing EL emission from a typical MIS diode (taken through the back face of the semiconductor).

Figure 7.11 Spectral distribution of the EL emitted from typical MIS diodes incorporating (a) one monolayer, (b) three monolayers, (c) five monolayers and (d) seven monolayers of $CdSt_2$.

Figure 7.12 Current density and relative EL intensity as a function of bias for a device incorporating five monolayers of $CdSt_2$. (Inset shows the intensity as a function of J).

Figure 7.13 D.C. power conversion efficiency as a function of insulator ($CdSt_2$) thickness (the dotted curve shows the same variation for diodes incorporating ω-TA).

Figure 7.14 D.C. power conversion efficiency as a function of insulator ($CdSt_2$) thickness.

Figure 7.15 Current density-voltage characteristics, in the dark and under illumination, for an MIS diode fabricated with (a) one monolayer and (b) seven monolayers of ω-TA.

Figure 7.16 Variation of open circuit voltage and short circuit current with the number of monolayers of ω-TA.

Figure 7.17 (a) Simplified energy band diagram of an MIS diode (i) in equilibrium and (ii) under a forward bias of $\sim$ 1.8V. (b) Simplified equivalent circuits depicting the various impediments to current flow in MIS diodes (refer to text for an explanation).

Figure 7.18 EL efficiency as a function of the number of monolayers of ω-TA. (From the same sample used to obtain the data in fig. 7.16)

Figure 7.19 Relative EL intensity as a function of time for a diode incorporating (a) 11 monolayers ($\sim$ 27 nm) of $CdSt_2$ and (b) 9 monolayers ($\sim$ 27nm) of ω-TA.

Figure 7.20 Conductivity data for a diode fabricated with five monolayers of $CdSt_2$ (a) before, and (b) after, 15 hours of continuous operation.

Figure 7.21 Current density-voltage curves for diodes incorporating (a) one layer, (b) five layers and (c) twenty layers of Pc. (Also shown is a near-ideal Schottky diode characteristic.)

Figure 7.22 Reciprocal capacitance squared against voltage curves for diodes incorporating a range of different thickness of Pc. Curves (a) to (e) correspond to diodes incorporating 0, 1, 5, 10 and 30 layers respectively.

Figure 7.23 D.C. power conversion efficiency against the number of layers of Pc.

Figure 7.24 Current density and relative EL intensity against bias for a device incorporating 5 layers of Pc. (Inset shows intensity as a function of J).

Figure 7.25 Relative EL intensity as a function of time for a device fabricated with 10 layers of Pc.

Figure 7.26 Conductivity data for a device incorporating 5 layers of Pc (a) before, and (b) after, 46 hours of continuous operation.

Figure 8.1 Conductivity data for (a) an Au:ZnSe (surface geometry) Schottky barrier and (b) an MIS diode incorporating one monolayer of $CdSt_2$. (The inset shows the corresponding barrier heights.)

Figure 8.2 (a) Conductivity data for an Au:ZnSe (sandwich geometry) Schottky diode.

(b) Conductivity Data, both in the dark and under illumination for the same diode.

Figure 8.3 Spectral distribution of EL emission from an MIS (ZnSe) diode incorporating five layers of Pc.

Figure 8.4 Admittance data at various frequencies for an Au:SiO_2 (p) Si MOS device.

Figure 8.5 Admittance data for Au:LB film: (p) GaAs MIS structures fabricated using two different surface preparations. (Refer to text for a description.)

Figure 8.6 Ramped current-voltage characteristics corresponding to MIS devices (a) with, and (b) without, six layers of Pc.

Figure 8.7 Ramped current-voltage characteristics corresponding to MIS devices (a) without, and (b) with, a Si-rich SiO_2 injector layer.

Figure 8.8 Ramped current-voltage characteristics corresponding to MIS devices (a) without, and (b) with, six layers of anthracene. (The inset shows the current voltage-characteristic of a typical contact over a large current range)

REFERENCES : CHAPTER 2

1. A. A. Bergh and P. J. Dean, "Light Emitting Diodes", Oxford Univ. Press (1976).

2. J. Shah and R. C. C. Leite, Phys. Rev. Lett., 22 (1969) 1304.

3. R. A. Smith, "Semiconductors", Camb, Univ. Press (1959).

4. P. D. Dapkus, W. H. Hackett, Jr., O. G. Lorimor and R. Z. Bachrach, J. Appl. Phys., 45 (1974) 4920.

5. M. Lax, Phys. Rev., 119 (1960) 1502.

6. For Example, N. T. Gordon, M. D. Ryall and J. W. Allen, Appl. Phys. Lett., 35 (1979) 691.

7. M. Yoshida, K. Tanaka, K. Taniguchi, Y. Yamashita, Y. Kakihara and T. Inogughi, SID Symp. Tech. Dig., (1980) 106.

8. C. N. Berglund, Appl. Phys. Lett., 9 (1966) 441.

9. F. E. Harper and W. J. Bertram, IEEE Trans. Elect. Dev., 16 (1969) 641.

10. S. Fujita, S. Arai, K. Itoh and T. Sakaguchi, J. Appl. Phys., 46 (1975) 3070.

11. H. J. Lozykowski, H. L. Oczkowski and F. Firszt, J. Luminesc., 11 (1975) 75.

12. M. Aven and D. A. Cusano, J. Appl. Phys., 35 (1964) 606.

13. T. Ota, K. Kobayashi and K. Takahashi, Solid State Electron., 15 (1972) 1387.

14. G. Destriau, J. Chem. Phys., 33 (1936) 620.

15. W. E. Howard, J. Luminesc., 24/25 (1981) 835.

16. R. Mach and G. O. Müller, Phys. Stat. Sol. (a), 69 (1982) 11.

17. A. Vecht, J. Cryst. Growth, 59 (1982) 81.

18. J. J. Hanak, Jap. J. Appl. Phys., Suppl. 2 (1974) 809.

19. C. J. Alder, A. F. Fray, C. Hilsum and P. Lloyd, Displays, 1 (1980) 191.

20. K. Okamoto, Y. Nasu and Y. Namakawa, IEEE Trans. Elect. Dev., 28 (1981) 698.

21. T. Mishima, W. Quan-Kun and T. Takahashi, J. Appl. Phys., 52 (1981) 5797.

22. G. G. Roberts, M. McGinnity, W. A. Barlow and P. S. Vincett, Solid State Commun., 32 (1979) 683.

23. A. C. Aten and J. H.Haanstra, Phys. Lett., 11 (1964) 97.

24. D. G. Thomas, J. J. Hopfield and C. J. Frosch, Phys. Rev. Lett, 15 (1965) 857.

25. D. G. Thomas and J. J. Hopfield, Phys. Rev., 150 (1966) 680.

26. J. J. Hopfield, D. G. Thomas and R. T. Lynch, Phys. Rev. Lett., 17 (1966) 312.

27. D. R. Wight, J. Phys. C., 1 (1968) 1759.

28. E. C. Lightowlers, J. C. North and O. G. Lorimor, J. Appl. Phys., 45 (1974) 2191.

29. R. Nicklin, C. D. Mobsby, G. Lidgard and P. B. Hart, J. Phys. C, 4 (1973) L344.

30. D. R. Wight, J. C. H. Birbeck, J. W. A. Trussler and M. L. Young, J. Phys. D., 6 (1973) 1622.

31. M. L. Young and D. R. Wight, J. Phys. D, 7 (1974) 1824.

32. Annual Report on DCVD Contract R.U. 19-5, 'Deep States in Semiconductors', (1980).

33. P. J. Dean, J. D. Cuthbert, D. G. Thomas and R. T. Lynch, Phys. Rev. Lett., 18 (1967) 122.

34. D. R. Wight, J. Phys. D., 10 (1977) 431.

35. D. R. Wight, P. J. Wright, and B. Cockayne, Electronics Lett., 18 (1982) 594.

36. P. J. Dean, A. D. Pitt, M. S. Skolnick, P. J. Wright and B. Cockayne, J. Cryst. Growth, 59 (1982) 301.

REFERENCES : CHAPTER 3

1. F. Braun, Ann. Phy. Chem., 153 (1874) 556.

2. N. F. Mott, Proc. Cambridge Phil. Soc., 34 (1938) 568.

3. W. Schottky, Naturwiss., 26 (1938) 843.

4. W. Schottky and E. Spenke, Wiss. Veroff Siemens-Werken, 18 (1939) 225.

5. For example, E. H. Rhoderick, IEE Proc., 129 (1982) 1.

6. J. Bardeen, Phys. Rev., 71 (1947) 717.

7. For example, D. A. Davies, 'Waves Atoms and Solids', Longman (1978).

8. A. M. Cowley and S. M. Sze, J. Appl. Phys., 36 (1965) 3212.

9. For example, B. R. Pruniaux and A. C. Adams, J. Appl. Phys. 43 (1972) 1980.

10. V. Heine, Phys. Rev. A, 138 (1965) 1689.

11. J. M. Andrews and J. C. Phillips, Phys. Rev. Letts., 35 (1975) 56.

12. L. J. Brillson, Phys. Rev. B, 18 (1978) 2431.

13. L. J. Brillson, R. Z. Bachrach, R. S. Bauer and J. McMenamin, Phys. Rev. Letts., 42 (1979) 397.

14. W. E. Spicer, I. Lindau, P. Skeath, C. Y. Su and P. Chye, Phys. Rev. Letts. 44 (1980) 420.

15. R. E. Allen and J. D. Dow, J. Vac. SciTechnol., 19 (1981) 383.

16. R. H. Williams, R. R. Varma and V. Montgomery, J. Vac. Sci. Technol., 16 (1979) 1418.

17. W. E. Spicer, I. Lindau, P. Skeath and C. Y. Su, J. Vac. Sci. Technol., 17 (1980) 1019.

18. J. L. Freeouf, Appl. Phys. Lett., 41 (1982) 285.

19. J. M. Woodall and J. L. Freeouf, J. Vac. Sci. Technol., 21 (1982) 574.

20. B. W. Lee, D. C. Wang, R. K. Ni, G. Xu and M. Rowe, J. Vac. Sci. Technol., 21 (1982) 577.

21. D. L.Scharfetter, Solid State Electronics, 8 (1965) 299.

22. C. Wagner, Phys. Z., 32 (1931) 641.

23. H. A. Bethe, M.I.T. Rad. Lab. Rep., 43-12 (1942).

24. C. R. Crowell and S. M. Sze, Solid State Electronics, 9 (1966) 1035.

25. For example, E.H. Rhoderick, 'Metal-Semiconductor Contacts', Oxf. Univ. Press (1978).

26. C. R. Crowell and M. Beguwala, Solid State Electronics, 14 (1971) 1149.

27. A. Padovani and R. Stratton, Solid State Electronics, 9 (1966) 695.

28. C. R. Crowell and V. L. Rideout, Solid State Electronics, 12 (1969) 89.

29. A. Y. C. Yu and E. H. Snow, Solid State Electronics, 12 (1969) 155.

30. M. A. Green, Solid State Electronics, 19 (1976) 421.

31. P. Bräulich (Ed.), 'Thermally Stimulated Relaxation in Solids' Springer-Verlag (1979).

32. A. M. Goodman, J. Appl. Phys., 35 (1964) 573.

33. T. Chot, Phys. Stat. Sol. (a), 66 (1981) K43.

34. R. H. Fowler, Phys. Rev., 38 (1931) 45.

35. W. G. Spitzer, C. R. Crowell, and M. M. Atalla, Phys. Rev. Lett., 8 (1962) 57.

36. B. M. Arora, A. K. Srivastava and S. Guha, J. Appl. Phys., 53 (1982) 1820.

37. A. M. Cowley, J. Appl. Phys. 37 (1966) 3024.

38. E. H. Rhoderick, J. Phys. D., 5 (1972) 1920.

39. M. A. Green and J. Shewchun, Solid State Electronics, 16 (1973) 1141.

40. H. C. Card and E. H. Rhoderick, J. Phys. D., 4 (1971) 1589.

41. A. M. Goodman, J. Appl. Phys., 34 (1963) 329.

42. C. L. Chen and K. D. Wise, IEEE Trans. Electron Devices, 29 (1982) 1522.

43. S. J. Fonash, J. Appl. Phys., 54 (1983) 1966.

44. H. C. Card and E. H. Rhoderick, Solid State Electronics, 16 (1973) 365.

45. A. G. Fischer and H. I. Moss, J. Appl. Phys., 34 (1963) 2112.

46. R. C. Jaklevic, D. K. Donald, J. Lambe and W. C. Vassell, Appl. Phys. Letts., 2 (1963) 7.

47. H. C. Card and B. L. Smith, J. Appl. Phys., 42 (1971) 5863.

48. S. Y. Haeri and E. H. Rhoderick, Inst. Phys. Conf. Ser., 22 (1974) 84.

49. M. Chybicki, Acta. Phys. Pol., A48 (1975) 575.

50. L. G. Walker and G. W. Pratt Jr., J. Appl. Phys., 47 (1976) 2129.

51. E. H. Nicollian, B. Schwartz, D. J. Coleman Jr., R. M. Ryder and J. R. Brews, J. Vac. Sci. Technol., 13 (1976) 1047.

52. J. I. Pankove, IEEE Trans. Electron Devices, ED-22 (1975) 721.

53. O. Lagerstedt, B. Manemar and H. Gilslason, J. Appl. Phys., 49 (1978) 2953.

54. A. W. Livingstone, K. Turvey and J. W. Allen, Solid State Electronics, 16 (1973) 351.

55. C. Lawther and J. Woods, Phys. Stat. Sol., 50 (1978) 491.

56. C. Lawther and J. Woods, Phys. Stat. Sol. (a), 44 (1977) 693.

57. N. B. Lukyanchikova, G. S. Pekar, N. N. Tranchenko, Hoang Mi Shin, M. K. Sheinkman, Phys. Stat. Sol. (a), 41 (1977) 299.

58. A. G. Fischer, Phys. Letts., 12 (1964) 313.

59. H. Watanabe, T. Chikamura and M. Wada, Jap. J. Appl. Phys., 13 (1974) 357.

60. A. E. Thomas, J. Woods and Z. V. Hauptman, J. Phys. D., 16 1123.

61. S. J. Fonash, 'Solar Cell Device Physics', Academic Press, (1981).

62. See For Example, D. R. Lillington and W. G. Townsend, Appl. Phys. Letts., 28 (1976) 97.

63. H. C. Card, Solid State Electronics, 20 (1977) 971.

REFERENCES : CHAPTER 4

1. See For Example, V. J. Bigelow, "The Complete Works of Benjamin Franklin", 5 p. 253.

2. A. Pockels, Nature, 43 (1891) 437.

3. Lord Rayleigh, Phil. Mag., 48 (1899) 321.

4. I. Langmuir, J. Am. Chem. Soc., 39 (1917) 1848.

5. K. B. Blodgett and I. Langmuir, Phys. Rev., 51 (1937) 964.

6. J. Jaffe, G. Bricman and A. Gelbecke, J. Chem. Phys., 64 (1967) 942.

7. G. L. Gaines, Jnr., 'Insoluble Monolayers at Liquid-Gas Interfaces', Wiley (1966).

8. H. Bucher, K. H. Drexhage, M. Fleck, H. Kuhn, D. Möbius, F. P. Schafer, J. Sondermann, W. Sperling, P. Tillman and J. Wiegand, Mol. Cryst., 2 (1967) 199.

9. G. G. Roberts, P. S. Vincett, W. A. Barlow, Phys. Technol., 12 (1981) 69.

10. P. S. Vincett and G. G. Roberts, Thin Solid Films, 68 (1980) 135.

11. For Example, C. W. Pitt and L. M. Walpita, Thin Solid Films, 68 (1980) 101.

12. L. Y. Wei and B. Y. Woo, Biophys. J., 13 (1973) 215.

13. W. H. Simpson and P. J. Reucroft, Thin Solid Films, 6 (1970) 167.

14. W. L. Procarione and J. W. Kaufman, Chem. Phys. Lipids, 12 (1974) 251.

15. B. Tieke, G. Wegner, D. Naegele and H. Ringsdorf, Angew. Chem. Int. Ed. Engl., 15 (1976) 764.

16. A. Barraud, C. Rosilio and A. Ruaudel-Teixier, J. Coll. Interface Sci., 62 (1977) 509.

17. I. R. Peterson, G. J. Russell and G. G. Roberts, To be published in Thin Solid Films.

18. T. Ohnishi, M. Hatakeyama, N. Yamamoto and H. Tsubomura, Bull. Chem. Soc. Jpn., 51 (1978) 1714.

19. A. Sen and G. S. Singhal, J. Coll. Interface Sci., 68 (1979) 471.

20. H. Kuhn, J. Photochem., 10 (1979) 111.

21. H. Kuhn, Pure Appl. Chem., 51 (1979) 341.

22. M. Sugi, K. Nembach and D. Mobius, Thin Solid Films, 27 (1975) 205.

23. H. Killersreiter, Z. Naturforsch, Teil A, 34 (1979) 737.

24. P. S. Vincett, W. A. Barlow, F. T. Boyle, J. A. Finney and G. G. Roberts, Thin Solid Films, 60 (1979) 265.

25. G. G. Roberts, T. M. McGinnity, W. A. Barlow and P. S. Vincett, Thin Solid Films, 68 (1980) 223.

26. G. G. Roberts, T. M. McGinnity, W. A. Barlow and P. S. Vincett, Solid State Commun., 32 (1979) 683.

27. S. Baker, M. C. Petty, G. G. Roberts and M. V. Twigg, Thin Solid Films, 99 (1983) 53.

28. S. Baker, G. G. Roberts and M. C. Petty, IEE. Proc. Accepted for Publication (1983).

29. R. A. Hann, W. A. Barlow, J. H. Steven and B. L. Eyers, M. V. Twigg, G. G. Roberts, Paper presented at 2nd International Workshop on Molecular Electron. Devices, Washington (1983).

30. S. Grammatic and J. Mort, Appl. Phys. Lett., 38 (1981) 445.

31. K. B. Blodgett, J. Am. Chem. Soc., 57 (1935) 1007.

32. See For Example, reference (24).

33. For Example, E. P. Honig, J. Colloid. Int. Sci., 43 (1973) 65.

34. H. Hasmonay, M. Vincent and M. Dupeyrat, Thin Solid Films, 68 (1980) 21.

35. C. Holley and S. Bernstein, Phys. Rev., 52 (1937) 525.

36. I. Fanteuchen, Phys. Rev., 53 (1938) 909.

37. G. L. Gaines, Jnr., Nature, 186 (1960) 384.

38. Electronics, Nov, 23 (1978).

39. A. Barraud, J. Messier, A. Rosilio and J. Tanguy, Colloqu. AVISEM, Versailles, 1971 Soc. Fr. Ing. Tech. Vide, Paris (1971) p.341.

40. J. Tanguy, Thin Solid Films, 13 (1972) 33.

41. G. G. Roberts, K. P. Pande and W. A. Barlow, Solid State Electron. Dev., 2 (1978) 169.

42. J. P. Lloyd, M. C. Petty, G. G. Roberts, P. G. LeComber and W. E. Spear, Thin Solid Films, 99 (1983) 297.

43. G. G. Roberts, M. C. Petty and I. M. Dharmadasa, IEE Proc., 128 (1981) 197.

44. K. K. Kan, G. G. Roberts and M. C. Petty, Thin Solid Films, 99 (1983) 291.

45. A. D. Brown, Ph.D. Thesis, Univ. of Southampton (1981).

46. R. W. Sykes, Ph.D. Thesis, Univ. of Durham (1980).

47. G. L. Larkens, Jnr., E. D. Thompson, E. Ortiz, C. W. Burkhart and J. B. Lando, Thin Solid Films, 99 (1983) 277.

48. For Example, I. A. Asaolu, B. H. Blott, W. I. Khan and D. Melville, Thin Solid Films, 99 (1983) 263.

49. J. R. Drabble and S. M. Al-Khowaildi, Thin Solid Films, 99 (1983) 271.

50. C. W. Pitt and L. M. Walpita, Electrocomp. Sci. Technol., 3 (1977) 191.

51. A. Barraud, Thin Solid Films, 99 (1983) 317.

52. G. Fariss, J. B. Lando and S. Rickert, Thin Solid Films, 99 (1983) 305.

53. H. Kuhn, D. Möbius and H. Bucher, 'Spectroscopy of Monolayer Assemblies', In A. Weissberger and B. Rossiter (eds.), Physical Methods of Chemistry, Vol. 1, Part 3B, Wiley, New York (1972).

54. E. E. Polymeropoulos, D. Möbius and H. Kuhn, Thin Solid Films, 68 (1980) 173.

55. M. Sugi, T. Fukui, S. Iizima and R. Iriyama, Bull. Electrotech. Lab., 43 (1979) 625.

56. K. Heckmann, Ch. Strobl and S. Bauer, Thin Solid Films, 99 (1983) 265.

57. A. F. Garito and K. D. Singer, J. Opt. Society, 70 (1980) 1399.

REFERENCES - CHAPTER 5

1. P. J. Wright and B. Cockayne, J. Cryst. Growth, 59 (1982) 148.

2. D. R. Wight, P. J. Wright and B. Cockayne, Electronics Lett., 18 (1982) 594.

3. D. R. Wight, Private Communication.

4. R. W. Sykes, Ph.D. Thesis, Univ. of Durham (1980).

5. A. Sagar, W. Lehmann and J. Faust, J. Appl. Phys., 39 (1968) 5336.

6. I. R. Peterson, G. J. Russell and G. G. Roberts, To be published in Thin Solid Films.

REFERENCES - CHAPTER 6

1. H. C. Card and E. H. Rhoderick, J. Phys. D., 4 (1971) 1589.

2. A. M. Cowley and S. M. Sze, J. Appl. Phys., 36 (1965) 3212.

3. A. M. Cowley, J. Appl. Phys., 37 (1966) 3024.

4. R. W. Sykes, Ph.D. Thesis, Univ. of Durham (1980).

5. M. A. Green, Appl. Phys. Lett., 33 (1978) 178.

REFERENCES : CHAPTER 7

1. R. H. Tredgold and R. Jones, IEE Proc., 128 (1981) 202.

2. R. H. Tredgold and G. W. Smith, IEE Proc., 129 (1982) 137.

3. J. Batey, G. G. Roberts and M. C. Petty, Thin Solid Films, 99 (1983) 283.

4. R. H. Tredgold and C. S. Winter, Thin Solid Films, 99 (1983) 81.

5. J. Batey, M. C. Petty and G. G. Roberts, Proc. INFOS Conf., Eindhoven (1983), To be Published.

6. C. S. Winter and R. H. Tredgold, IEE Proc., (1983), To be Published.

7. A. M. Cowley, J. Appl. Phys., 37 (1966) 3024.

8. S. J. Fonash, J. Appl. Phys., 54 (1983) 1966.

9. D. V. Morgan and J. Frey, Phys. Stat. Sol. (a), 51 (1979) K29.

10. B. R. Pruniaux and A. C. Adams, J. Appl. Phys., 43 (1972) 1980.

11. A. M. Cowley and S. M. Sze, J. Appl. Phys., 36 (1965) 3212.

12. O. Wada and A. Majerfeld, Electronics Lett., 14 (1978) 125.

13. G. G. Roberts, M. C. Petty and I. M. Dharmadasa, IEE Proc., 128 (1981) 197.

14. A. Barraud, C. Rosilio and A. Ruaudel-Teixier, Thin Solid Films, 68 (1980) 7.

15. R. W. Sykes, Ph.D. Thesis, Univ. of Durham (1980).

16. S. Horiuchi, J. Yamaguchi and K. Naito, J. Electrochem Soc : Sol. State Sci., 115 (1968) 634.

17. T. D. Clark, Mullard Res. Rept. No. 512 (1964).

18. E. E. Polymeropoulos, J. Appl. Phys., 48 (1977) 2404.

19. B. M. Arora, A. K. Srivastava and S. Guha, J. Appl. Phys., 53 (1982) 1820.

20. I. M. Dharmadasa, G. G. Roberts and M. C. Petty, Electronics Letts., 16 (1980) 201.

21. D. R. Lillington and W. G. Townsend, Appl. Phys. Letts., 28 (1976) 97.

22. M. A. Green, Appl. Phys. Letts., 33 (1978) 178.

23. A. H. M. Kepperman, S. C. M. Kackerra, H. J. Maaskanip and R. J. C. van Zolingen, Proc. Photovoltaic Solar Energy Conf., Luxembourg (1977), Reidel Amsterdam.

24. A . Y. C. Yu and E. H. Snow, Solid State Electronics, 12 (1969) 155.

25. S. Baker, M. C. Petty, G. G. Roberts and M. V. Twigg, Thin Solid Films, 99 (1983) 53.

26. S. Baker, G. G. Roberts and M. C. Petty, IEE. Proc., Accepted for Publication.

27. R. A. Hann, W. A. Barlow, J. H. Steven and B. L. Eyers, M. V. Twigg, G. G. Roberts, Paper presented at 2nd Int. Workshop on Mol. Electron. Dev., Washington (1983).

28. H. C. Card and B. L. Smith, J. Appl. Phys., 42 (1971) 5863.

29. S. Y. Naeri and E. H. Rhoderick, Inst. Phys. Conf. Ser., 22 (1974) 84.

REFERENCES : CHAPTER 8

1. G. Mandel, Phys. Rev., 134 (1964) A1073.

2. D. R. Wight, P. J. Wright and B. Cockayne, Electronics Lett., 18 (1982) 594.

3. J. J. Simonne, Proc. INFOS Conf., Eindhoven (1983), to be published.

4. W. F. Croydon and E. H. C. Parker, 'Dielectric Films on GaAs', Gordon and Breach (1981).

5. R. W. Sykes, Ph.D. Thesis, Univ. of Durham (1980).

6. A. Goetzberger, E. Klausmann, M. J. Schulz, CRC Critical Rev. in Sol. St. Sci., 6 (1976) 1.

7. E. H. Nicollian and A. Goetzberger, IEEE Trans. Elec. Dev. ED-12 (1965) 108.

8. J. M. Gibson, D. W. Dong, and R. J. Zeto, J. Electrochem. Soc., 127 (1980) 2722.

9. D. J. DiMaria, D. R. Young, D. W. Ormond, Appl. Phys. Lett., 31 (1977) 680.

10. D. J. DiMaria, K. M. De Meyer, C. M. Serrano, and D. W. Dong, J. Appl. Phys., 52 (1981) 4825.

11. S. Baker, M. C. Petty, G. G. Roberts and M. V. Twigg, Thin Solid Films, 99 (1983) 53.

12. G. G. Roberts, M. C. Petty, P. J. Caplan and E. H. Poindexter, Proc. INFOS Conf., Eindhoven (1983), To be published.

13. M. Horiuchi and H. Katto, IEEE Trans. on Electron Dev., ED-26 (1979) 914.

14. R. Klein, W. H. Owen, R. T. Simko, W. E. Tchon, Electronics, 52 (1979) 111.

15. D. J. DiMaria, R. Ghez and D. W. Dong, J. Appl. Phys., 51 (1980) 4830.

16. P. S. Vincett and W. A. Barlow, Thin Solid Films, 71 (1980) 305.

17. P. S. Vincett, W. A. Barlow, F. T. Boyle, J. A. Finney and G. G. Roberts, Thin Solid Films, 60 (1979) 265.

APPENDIX A - REFERENCES

1. C. R. Crowell and M. Beguwala, Solid State Electron., 14 (1971) 1149.

2. E. H. Rhoderick, J. Phys. D., 5 (1972) 1920.